THE UNIVERSITY OF ADELAIDE

Department of Geology and Geophysics
South Australia

Tertiary Uplift and its Implications for the Tectonic Evolution of Sedimentary Basins, Offshore South-West United Kingdom.

Robert John Menpes

B.Sc. Hons (Adelaide 1992)

Submitted in fulfilment of the requirement
for the degree of Doctor of Philosophy

September 1997

Contents

Abstract

Sonic velocities from the Danian Chalk, Upper Cretaceous Chalk, Lower Cretaceous Greensand/Gault Clay, Lower Cretaceous Wealden, Upper Jurassic mudstones, Triassic Mercia Mudstone (above and below salt), and Triassic Sherwood Sandstone have been used to quantify apparent exhumation (i.e. amount of missing section) in the Celtic Sea/South-Western Approaches. The recognised structural inversion axes of the Brittany, South-West Channel, North Celtic Sea, Caernarvon, Cardigan Bay, and Kish Bank basins are highs in apparent exhumation of up to 2 kilometres. However apparent exhumation of approximately one kilometre also occurred in the uninverted St. Mary's and Plymouth Bay basins, and on the margins of the Armorican and Cornubian Platforms and the Pembroke Ridge. Hence Tertiary exhumation was regional, and not restricted to inversion axes, and thus it must have had a thick-skinned origin.

When corrected for exhumation, the Upper Cretaceous-Tertiary post-rift sequence in the Celtic Sea/South-Western Approaches shows relatively little localisation over the syn-rift Upper Jurassic-Lower Cretaceous depocentres. Therefore thinning of the lower lithosphere, thermal re-equilibration of which controls post-rift subsidence, was widespread and not restricted to the areas where syn-rift depocentres have been generated by (upper) crustal thinning.

The subsidence/uplift history of the Celtic Sea/ South-Western Approaches has been modelled by a two-layer, heterogeneous deformation model. Two-dimensional, multiple-event modelling of the tectonic history has shown a distinct difference in the nature of both crustal and subcrustal deformation between the internal basins closest to the Cornubian Platform (St. Mary's, Plymouth Bay, and South Celtic Sea basins), and the external basins further away from the Cornubian Platform (North Celtic Sea, Fastnet, Brittany, and South-West Channel basins). The latter basins are best modelled by localised crustal deformation, with minimal associated subcrustal deformation. In contrast, the St. Mary's, Plymouth Bay, and South Celtic Sea basins, as well as the Cornubian Platform, are best modelled by significant subcrustal deformation, with little or no associated crustal deformation. The amount of crustal deformation in the external basins is not sufficient to balance the excess subcrustal deformation in the internal basins and Cornubian Platform, hence the modelling suggests a regional strain imbalance between deformation in the crust and subcrust is necessary during both Late Jurassic-Early Cretaceous rifting and Tertiary compression. It is speculated that the excess subcrustal deformation may have been related to thermal perturbation of the lithosphere due to the high heat production granites of the Cornubian Batholith. A similar excess of subcrustal deformation has previously been documented for the conjugate Canadian North Atlantic margin.

Acknowledgments

First thanks are due to my supervisor, Richard Hillis, for his support, guidance, understanding, and ability to challenge me time and time again. In addition, I also thank Richard for his friendship over the years, in spite of the potential for conflict inherent in such a situation. For technical support, my thanks to Andy Mitchell and Peter Tingate of the National Centre of Petroleum Geology and Geophysics, and to the numerous computer services personnel who have passed through the Geology Department at Adelaide University, and all of the other general staff who have helped me along the way. Academically, the entire department are thanked for showing me the joys of Geology and Geophysics, however special mention to John Foden, Mike Sandiford, Pat James, and Thomas Flottmann for numerous enlightening discussions over the years.

Thanks to the University of Adelaide for the financial support of a University of Adelaide scholarship, and to Chevron UK and ARCO UK, who supplied me with much of my data, and through their interest in the results of my work became the source of funding to purchase further data.

I wish to thank all the friends I have made during my years at Adelaide. In particular, I am deeply indebted to Nicola, Susie, Tim, Kylie, Scotty, Lisa, and Bruce, for getting me through the most difficult time of my life, and for being there when I needed to unwind. Thanks as well to an old friend and house mate rediscovered, Tania, whose abilities as a chiropractor as well as a close friend have been much appreciated after long hours at a computer terminal. A warm thank you to my fellow students both past and present; along the way all of you have inspired me, helped me, or simply given me a fantastic group to celebrate the highs and lows of a university life with.

Finally, I wish to thank my family, in particular my parents, for their patience, love, and understanding. I hope they consider it all to have been worth it, as I do.

Declaration

This work contains no material which has been accepted for the award of any other degree or diploma in any university or other Tertiary institution and, to the best of my knowledge and belief, contains no material previously published or written by another person, except where due reference has been made in the text.

I give consent to this copy of my thesis, when deposited in the University Library, being available for loan and photocopying.

Robert J. Menpes

22 September 1997

Chapter 1
Introduction

1.1 Project Rationale

It is relatively easy to recognise basin inversion from stratigraphic and structural evidence (Williams *et al.*, 1989). However, quantifying the amount of section removed as a result of inversion is more problematic. Of the numerous methods available for quantifying the amount of section removed, comparison of the degree of compaction of a given rock unit with a normal or undisturbed compaction trend is one of the more accurate and readily applied techniques (Skagen, 1992). This project uses the compaction methodology to quantify the amount of missing section in the Celtic Sea/South-Western Approaches, where Tertiary basin inversion has been identified.

It has recently become apparent that the structural inversion of relatively localised basins in and around the United Kingdom is superimposed on more regional Tertiary uplift (e.g. Green, 1989; Bray *et al.*, 1992; Green *et al.*, 1993; Brodie & White, 1994; Hillis, 1995*a*). This thesis aims to quantify both basin inversion and the regional component of Tertiary uplift.

In addition to quantifying basin inversion and regional uplift, this thesis aims to formulate and test a tectonic model that can account for both the distribution of basin inversion and uplift in the Celtic Sea/South-Western Approaches, and the extension and subsidence history of the area prior to inversion. The tectonic origin of basin subsidence has been extensively modelled by many authors, often based on McKenzie's (1978) model of basin formation. However, few authors have modelled the mechanisms of inversion and regional uplift. This project attempts to redress the imbalance by addressing basin inversion and uplift as well as prior subsidence.

The majority of refinements to McKenzie's (1978) pure shear model of basin formation have been concerned with single rifting events (e.g. Royden & Keen, 1980; Hellinger & Sclater, 1983; White & McKenzie, 1988). Relatively few authors have modelled multiple tectonic events with boundary conditions inherited from previous events (e.g. Hellinger *et al.*, 1989; Odling, 1992; Lippard & Liu, 1992). In order to model basin inversion and uplift it is necessary to investigate the nature of the lithosphere, in particular its thermal state, that existed prior to uplift. Basin formation and prior subsidence are modelled in this thesis in order to set appropriate initial boundary conditions upon the models of inversion and regional uplift.

1.2 The Celtic Sea/South-Western Approaches

It has been widely recognised that many of the Mesozoic sedimentary basins of the North Atlantic margin have been inverted and exhumed from their maximum burial-depth during Late Cretaceous-Tertiary times (e.g. references in Ziegler, 1987*a* and Cooper & Williams, 1989). The geological history of the Celtic Sea/South-Western Approaches has been well documented in the last decade (e.g. Evans, 1990; Tappin *et al.*, 1994; and references in Ziegler, 1987*a*; Cooper & Williams, 1989; Buchanan & Buchanan, 1995; Croker & Shannon, 1995). However, unlike other regions of the North Atlantic margin such as the North Sea basins, at the time of commencement of this project there was only limited published material

quantifying the exhumation associated with Tertiary inversion in the region (e.g. Cornford, 1986; Tucker & Arter, 1987; Roberts, 1989; Evans, 1990; Hillis, 1991). With a large number of wells that give a good regional spread (Fig. 1.1), the Celtic Sea/South-Western Approaches is ideal for quantifying exhumation using the compaction methodology.

Although the Celtic Sea/South-Western Approaches is recognised as an area of basin inversion, not all of the basins of the region have been structurally inverted (Chapter 2). The complex history of the region, where adjacent basins respond differently to imposed stresses, both during basin development and inversion, makes the region an interesting one in which to investigate the potential mechanisms involved in basin inversion. Furthermore, the recognition and quantification of regional exhumation in the Celtic Sea/South-Western Approaches (e.g. Cornford, 1986; Roberts, 1989; Evans, 1990; Hillis, 1991; Hillis, 1992*a*; Tappin *et al.*, 1994), upon which basin inversion is superimposed, also has important consequences for the tectonic controls on basin development.

In the Celtic Sea/South-Western Approaches, the areas of maximum subsidence during rifting events are also the areas of maximum Tertiary uplift and inversion (Chapter 2). The observed subsidence and uplift patterns of the Celtic Sea/South-Western Approaches thus have important consequences for the understanding of the mechanisms of continental lithospheric deformation on the North Atlantic margin.

1.3 The Scope of this Thesis

This thesis summarises the geological history of the Celtic Sea/South-Western Approaches (Chapter 2), addresses the quantification of exhumation using the compaction methodology (Chapters 3 & 4), and presents an extension of the compaction methodology using outcrop samples (Chapter 5). The implications of exhumation for reconstructing tectonic histories are then addressed (Chapter 6). The multiple subsidence and uplift events of the Celtic Sea/South-Western Approaches are modelled incorporating the exhumation results from the compaction methodology (Chapters 7 & 8), and finally the potential mechanisms controlling the subsidence/uplift history of the Celtic Sea/South-Western Approaches are investigated and discussed (Chapter 8).

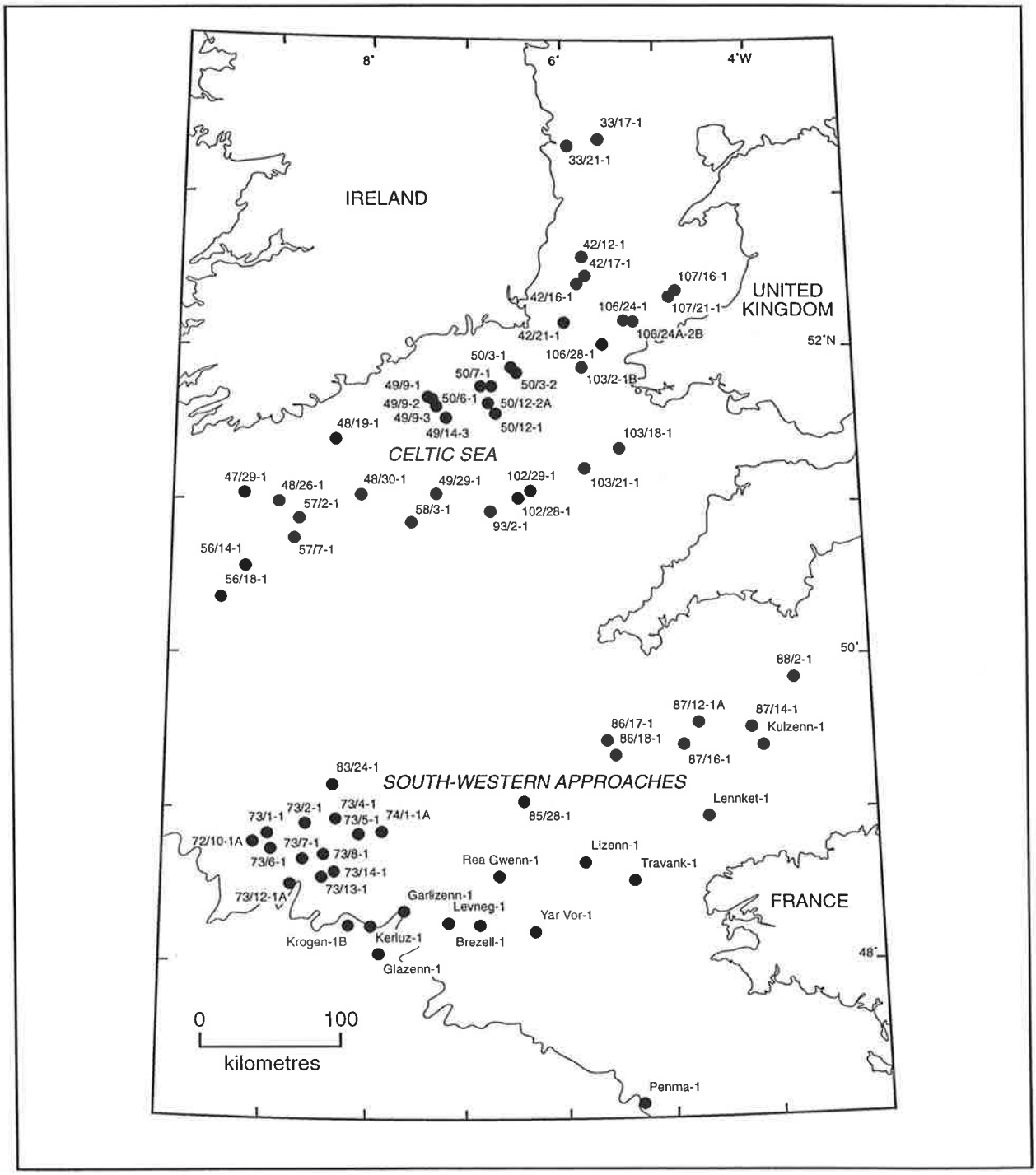

Fig. 1.1. Well locality map of the Celtic Sea/South Western Approaches area. Continental shelf edge (200m contour) is shown.

Chapter 2

Geological History of the Celtic Sea/South-Western Approaches

2.1 Introduction

The Mesozoic basins of the Celtic Sea/South-Western Approaches are a series of failed-rift basins whose formation is related to rifting and wrenching during the early stages of the opening of the North Atlantic, and hence they form part of the multi-directional Arctic-North Atlantic rift system (Petrie *et al.*, 1989). The basins have had protracted histories of subsidence and uplift since they came into existence during Permian to Early Triassic times, with the Triassic, Jurassic and Early Cretaceous evolution of the graben and wrench systems intimately linked with the development of the Bay of Biscay rift-wrench basin to the southwest and the Rockall Trough to the northeast (Ziegler, 1987*b*).

The locations of the Mesozoic basins of the Celtic Sea/South-Western Approaches are shown in Figure 2.1, and representative sections through the basins are presented in Figure 2.2. The major basins are:

- the complex Fastnet-North Celtic Sea rift basins, which bifurcate to the northeast into the half-grabens of the Cardigan Bay and Caernarvon basins;
- the South Celtic Sea Basin and Bristol Channel Basin, which are separated from the North Celtic Sea basins by the Pembroke Ridge;
- the composite Western Approaches Trough, which comprises the Plymouth Bay, St. Mary's, Melville, Brittany, and South-West Channel basins, and is separated from the South Celtic Sea-Bristol Channel basins by the Cornubian Platform, and;
- the relatively shallow Haig Fras graben, which is enclosed within the Cornubian Platform.

The Mesozoic basins of the Celtic Sea/South-Western Approaches terminate to the northeast along a complex set of wrench faults and associated pull-apart basins. The Kish Bank Basin (Fig. 2.1) can be interpreted as forming part of this complex wrench and pull-apart system which compensated for crustal dilation taking place in the Celtic Sea/South-Western Approaches rift basins (Ziegler, 1987*b*). The basins of the Celtic Sea/South-Western Approaches are truncated to the southwest by the almost orthogonally-trending Amorican passive margin (Fig. 2.3) of the oceanic Bay of Biscay (Ziegler, 1987*b*).

Interplay between pre-existing structural trends and the stress regimes related to the various stages in the opening of the North Atlantic has led to the basins within the Celtic Sea/South-Western Approaches exhibiting contrasting Mesozoic-Tertiary structural and stratigraphic histories. This chapter briefly outlines the pre-existing structural framework which controlled basin orientation and formation, summarises the geological history of the region through late Palaeozoic, Mesozoic, and Tertiary times, and investigates the similarities and differences between the basins within the Celtic Sea/South-Western Approaches. The lithostratigraphic nomenclature pertaining to this thesis for the Celtic Sea/South-Western Approaches has been compiled from various sources (Shannon, 1995; Tappin *et al.*, 1994; Evans, 1990), and is shown in Figure 2.4.

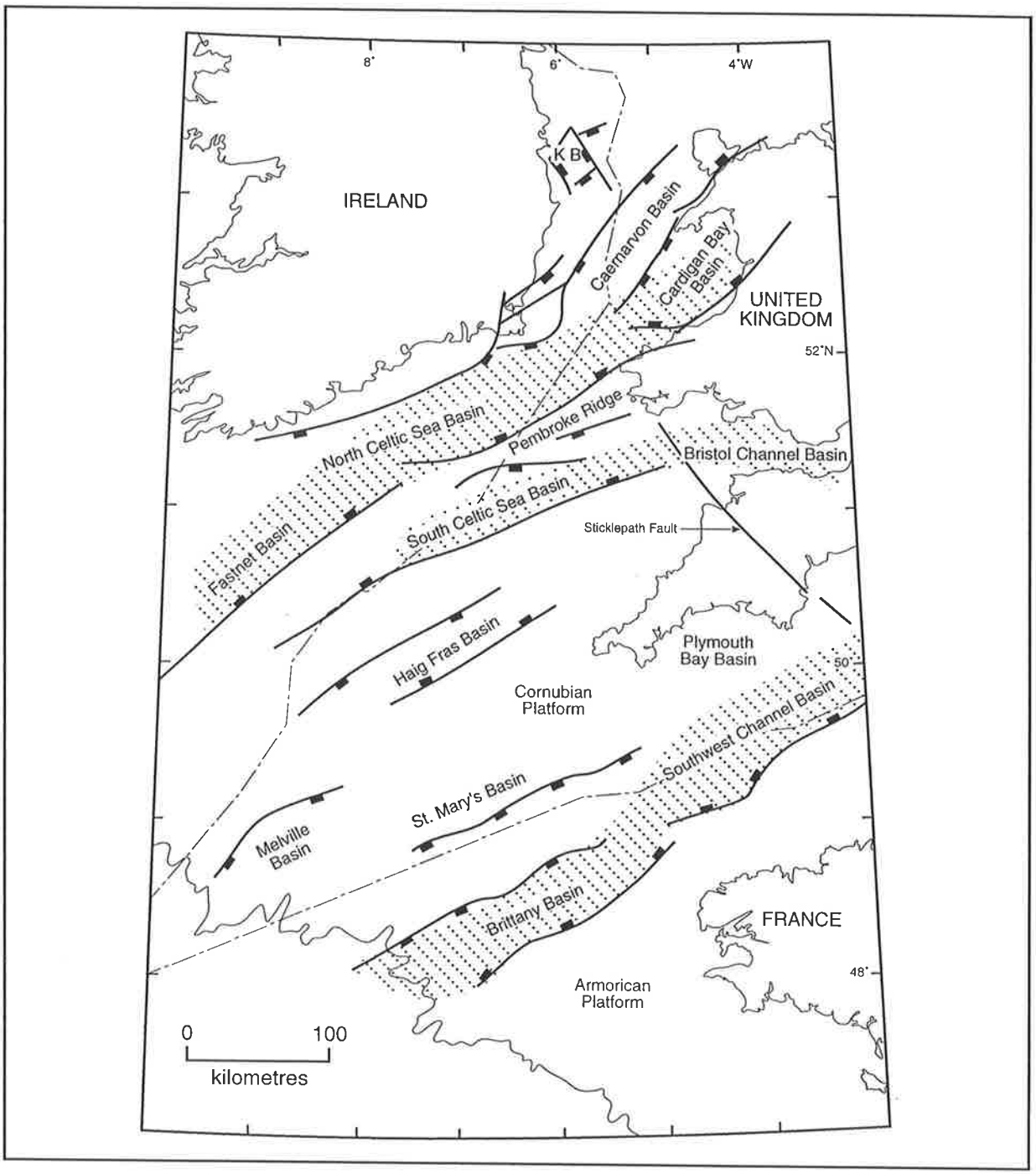

Fig. 2.1. Major structural elements map of the Celtic Sea/South Western Approaches area. Inverted regions are dotted, KB = Kish Bank, continental shelf edge (200m contour) is also shown.

2.2 Structural Framework of the Celtic Sea/South-Western Approaches

Two distinct Palaeozoic structural trends are present in the Celtic Sea/South-Western Approaches area, related to the Late Silurian-Early Devonian Caledonian orogeny and the Devonian-Carboniferous Variscan orogeny. These two distinct orogenic events were the result of convergence of the Avalonian, Laurentian, and Gondwanan continental masses during the Palaeozoic (Tappin *et al.*, 1994). The Mesozoic basins of the region have formed on these

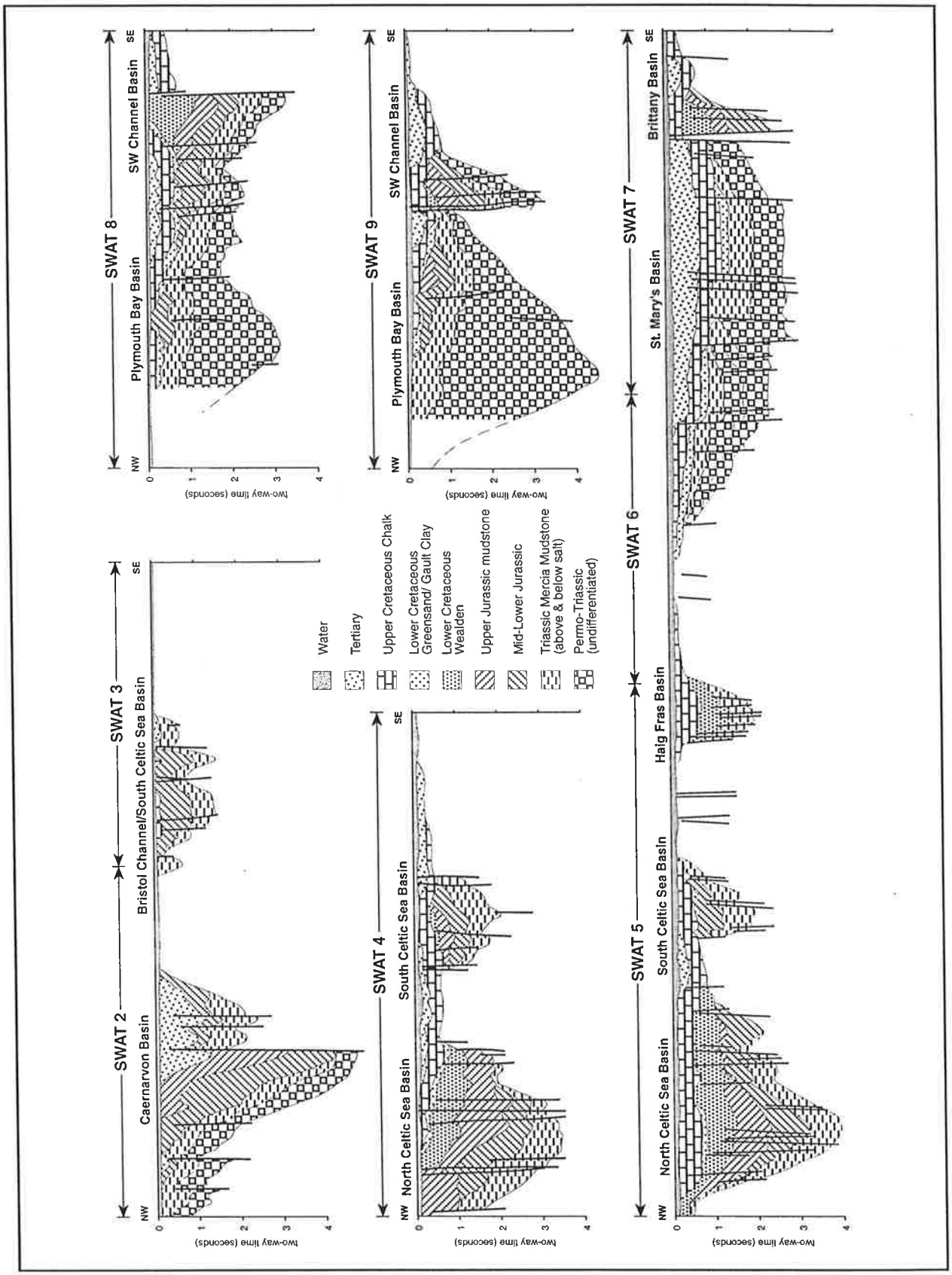

Fig. 2.2. Interpreted British Institutions Reflection Profiling Syndicate (BIRPS) South-West Approaches Traverse (SWAT) deep seismic reflection profiles from the Celtic Sea/South-Western Approaches (after Bois *et al.*, 1991; Hillis, 1988). Section localities are shown in Figure 2.3.

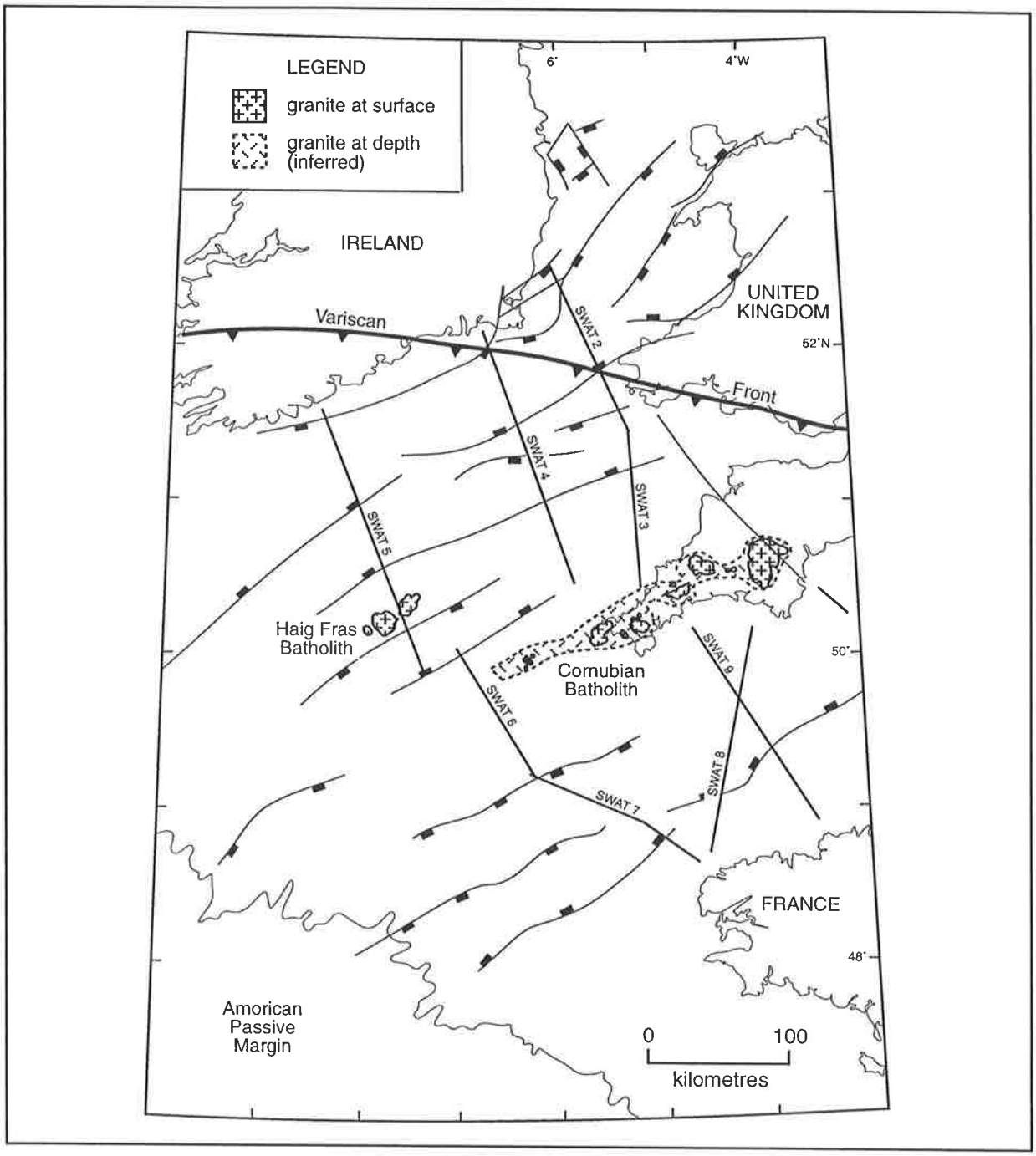

Fig. 2.3. Celtic Sea/South Western Approaches SWAT profile localities. The Variscan deformation front, Amorican passive margin, Haig Fras batholith, and Cornubian batholith are also shown (adapted from Evans, 1990, and Tappin *et al.*, 1994).

pre-existing Variscan and Caledonian structural trends (Petrie *et al.*, 1989).

2.2.1 Caledonian and Variscan structural trends

The Caledonian structural features of the Celtic Sea/South-Western Approaches are related to translational collision along the Iapetus suture zone during the Late Silurian-Early Devonian (Petrie *et al.*, 1989). These features comprise southeast-directed overthrust zones, and associated anticlines and synclines, with a dominant northeast-southwest trend.

Era	Period	Epoch	Stage	Major lithologies	Nomenclature
Cenozoic	Quaternary	Holocene		sandstones, shales, and limestones	Tertiary (undifferentiated)
		Pleistocene			
	Tertiary / Neogene	Pliocene	Piacenzian		
			Zanclian		
		Miocene	Messinian		
			Tortonian		
			Serravallian		
			Langhian		
			Burdigalian		
			Aquitanian		
	Tertiary / Palaeogene	Oligocene	Chattian		
			Rupelian		
		Eocene	Priabonian		
			Bartonian		
			Lutetian		
			Ypresian		
		Palaeocene	Thanetian		
			Danian	chalk	Danian Chalk
Mesozoic	Cretaceous	Senonian	Maastrichtian	chalk	Upper Cretaceous Chalk
			Campanian		
			Santonian		
			Coniacian		
		Gallic	Turonian		
			Cenomanian		
			Albian	sandstones, shales	Greensand/Gault Clay
			Aptian		
			Barremian	sandstones, shales	Wealden
		Neocomian	Hauterivian		
			Valanginian		
			Berriasian		
	Jurassic	Malm	Tithonian	shales, limestones	Upper Jurassic (undifferentiated)
			Kimmeridgian		
			Oxfordian		
		Dogger	Callovian	shales, limestones	Mid-Jurassic (undifferentiated)
			Bathonian		
			Bajocian		
			Aalenian		
		Lias	Toarcian	shales, limestones	Lias (undifferentiated)
			Pliensbachian		
			Sinemurian		
			Hettangian		
	Triassic	Tr_3	Rhaetian	limestone, marl	Penarth Group
			Norian	halite / mudstone	Mercia Mudstone Group
			Carnian		
		Tr_2	Ladinian	sandstone	Sherwood Sandstone Group
			Anisian		
		Scythian	Spathian		
			Nammalian		
			Griesbachian		
Pz.	Permian			sandstones, shales	undifferentiated

Fig. 2.4. Stratigraphic nomenclature for the Celtic Sea/South-Western Approaches (after Harland *et al.*, 1989; Shannon, 1995; Tappin *et al.*, 1994; Evans, 1990).

In much of the Celtic Sea/South-Western Approaches, Caledonian trends have been overprinted by the Devonian-Carboniferous Variscan orogeny. However, some of the features of the Caledonian orogeny are preserved in Wales and southeast Ireland, north of the Variscan Front (Fig. 2.3), which forms the northern limit of Variscan thin-skinned deformation (Petrie *et al.*, 1989).

The Variscan orogeny was the result of north- to northwest-directed compression, associated with accretion of late Palaeozoic rocks onto a northern craton (Petrie *et al.*, 1989). Variscan structures are dominantly east-west trending onshore southern Ireland and the Cornubian Peninsula, however in southwest Ireland the trend becomes more east-northeast to west-southwest, and may possibly complement the pre-existing Caledonian trends (Petrie *et al.*, 1989; Tappin *et al.*, 1994). Numerous onshore features such as the Carrick thrust in Cornwall can be correlated with basement events on offshore seismic, and dipping events that are interpreted as thrusts in the basement are widespread, except where granites are present (Hillis & Chapman, 1992). North- to northwest-oriented transfer zones and lateral ramps are associated with the Variscan thrusts, and movement on these played an important role in the subsequent development of many of the Mesozoic basins that followed (Petrie *et al.*, 1989).

2.2.2 Cornubian batholith

During the closing stages of the Variscan orogeny, in latest Carboniferous - early Permian times, and following the major thrusting episode, at least two major granite batholiths were intruded into the deformed Late Palaeozoic strata (Evans, 1990). These granites, the Cornubian batholith, which is exposed in a series of inliers from Dartmoor to the Isles of Scilly, and the offshore Haig Fras batholith (Fig. 2.3), have a trend which is consistent with the north-north-westerly closure of the Variscan Foredeep Basin (Evans, 1990). Chen *et al.* (1996) used U-Pb monazite dating to demonstrate that the granite plutons of the Cornubian batholith were emplaced diachronously from 293 ± 1.2 Ma to 274.5 ± 1.4 Ma. The granites were intruded more or less contemporaneously with the extrusion of the Permian Exeter Volcanic Series (Evans, 1990).

2.2.3 Mesozoic structural elements

The North Celtic Sea-Caernarvon-Cardigan Bay graben system obliquely transects the Variscan deformation front (Fig. 2.3), whilst the other Celtic Sea/South-Western Approaches basins are entirely superimposed on the Variscan fold-belt (Ziegler, 1987*b*). The North and South Celtic Sea basins, the composite Western Approaches Trough, and the Haig Fras Basin all follow the same trend as the strike of Variscan thrusts mapped in detail on the Cornubian Platform, and interpreted beneath the Western Approaches Trough from reflection seismic records by Hillis & Chapman (1992).

In the vicinity of SWAT 4 (Figs. 2.2, 2.3), the North Celtic Sea Basin lies in the hangingwall of a major SSE-dipping reflector which exhibits a ramp and flat geometry, and has a Variscan trend (Cheadle *et al.*, 1987; Petrie *et al.*, 1989). Further west, however, the North Celtic Sea Basin is a deep, symmetrical basin with no major basement fault control (Cheadle *et al.*, 1987). Further northeast, the Caernarvon and Cardigan Bay basins have formed north of the Variscan deformation front by the reactivation of northwest-dipping Caledonian faults (Tappin *et al.*, 1994). The Caernarvon Basin is a deep (8-10 km) basin cut by a major northward-dipping listric fault, which may be a reactivated Caledonian thrust (Cheadle *et al.*, 1987). The eastern end of the

Bristol Channel Basin is a pronounced hangingwall basin associated with a south-dipping Variscan detachment surface (Brooks *et al.*, 1988). The South Celtic Sea Basin, however, is not associated with any clearly imaged basement detachments. Cheadle *et al.* (1987) suggested that a ramp flat geometry on a deeper detachment surface may be the main structural control on the geometry of the South Celtic Sea Basin.

In the Western Approaches Trough, the Scilly fault system, a major Variscan thrust system, shows evidence of reactivation along the northern margin of the trough (Cheadle *et al.*, 1987). Hillis & Chapman (1992) documented numerous planar dipping deep seismic events in the South-Western Approaches, believed to represent Variscan thrusts, which have undergone various degrees of reactivation. Extensional reactivation of one such Variscan thrust has been interpreted by Hillis & Chapman (1992) as controlling the development of the asymmetrical Melville half-graben. The St. Mary's and Plymouth Bay basins however are more symmetrical basins, without clear basin-controlling faults (Evans, 1990; Hillis & Chapman, 1992). Hillis & Chapman (1992) noted the clear parallelism between the structural trend of the St. Mary's Basin and that of the underlying Variscan structure, and suggested that whether basinal faults in the St. Mary's Basin link directly with Variscan thrusts is a matter of subjective interpretation.

Cheadle *et al.* (1987) suggested that the thinning of the basement below the Plymouth Bay Basin indicated that it originated as a result of crustal extension, and hence may be a pull-apart basin bounded by N-S trending strike-slip faults that were not crossed by the BIRPS (British Institutions Reflection Profiling Syndicate) deep-seismic reflection profiles. Coward (1990) suggested that dip-slip movement over ramps on Variscan thrusts produced the anomalously thick Plymouth Bay Basin, whilst Harvey *et al.* (1994) suggested that the basin initially formed through extensional collapse of the Variscan nappe pile, before subsidence was localised at the intersection of northwest-southeast - trending strike-slip faults and the east-west - trending Variscan thrust system.

All of the Celtic Sea/South-Western Approaches basins are associated with crustal thinning, as Moho-depth reflections show that the crystalline crust is thinned dramatically beneath the basins (Cheadle *et al.*, 1987). It is likely that the crust was of at least average thickness (35 km) immediately after the Variscan and Caledonian orogenies, therefore the origin of these basins must be related to crustal thinning (Cheadle *et al.*, 1987).

2.3 Permo-Triassic Basin Formation

The culmination of the Variscan orogeny and the intrusion of the granites produced an area with considerable relief (Evans, 1990). Deep Permo-Triassic basins formed in the Celtic Sea/South-Western Approaches as the Variscan orogenic belt became a zone of continental spreading above a crust weakened by tectonic thickening and the addition of the granite plutons, analogous to the Basin and Range in the western USA (Coward, 1990).

2.3.1 Permo-Triassic post-orogenic collapse

The end of the Variscan orogeny resulted in post-orogenic collapse basins trending generally northeast-southwest, with the Cornubian Platform constituting a resistant massif, while Variscan structures on either side were reactivated, and material eroded from the Variscan mountains of the Cornubian Terrane accumulated to considerable thicknesses in the Permian troughs (Cheadle *et al.*, 1987; Tappin *et al.*, 1994). The Variscan thrust belt was rapidly eroded,

and Lake & Karner (1987) suggested that the fold belt had been virtually peneplaned by the late Permian. Thick sequences of undifferentiated Permian to Early Triassic non-marine conglomerates, sandstones, mudstones, as well as volcanics were deposited in the Kish Bank Basin (Fig. 2.5), St. Mary's and Plymouth Bay basins (Fig. 2.6), Melville Basin (Figs. 2.7 & 2.8), and South-West Channel Basin (Fig. 2.9).

Redbeds of Permian to Triassic age have also been identified in the Bristol Channel Basin (Tappin *et al.*, 1994), and the Fastnet and North Celtic Sea basins (Shannon, 1995), however few wells in these basins have penetrated deeper than the Upper Triassic (Figs. 2.10, 2.11, & 2.12). Wells in the South Celtic Sea Basin (Fig. 2.13) and Caernarvon Basin (Fig. 2.5) intersected Early Triassic sandstones sitting on Variscan basement, as does the only well in the Cardigan Bay Basin (well 103/2-1B) to have intersected basement (Fig. 2.14). Some of the wells in the Brittany Basin intersected Lower Jurassic strata on Variscan basement (Figs. 2.9, 2.15), however a number of wells also terminate in Upper Triassic strata. The thickness of Permian to Early Triassic strata in these basins is unclear, as well intersections are rare and these sediments are difficult to distinguish from the Middle to Late Triassic on seismic sections.

Numerous authors (e.g. Ziegler, 1987*b*; Van Hoorn, 1987; Tucker & Arter, 1987) have suggested that rifting of the Mesozoic basins of the Celtic Sea/South-Western Approaches began in the Early Triassic, and may have begun as early as the Permian (Chapman, 1989). However, a recent study by Musgrove *et al.* (1995) has suggested that the Sherwood Sandstone Group of Early Triassic Scythian age was deposited in palaeotopographic lows of the Variscan thrust belt in the Celtic Sea/South-Western Approaches, the positions of which were controlled by erosion around massifs and resistant thrust belt hangingwalls that formed the palaeotopography. The exact timing of transition from post-orogenic collapse due to the relaxation of compressional forces to active extension related to North Atlantic opening is difficult to establish, however Musgrove *et al.* (1995) suggested that active rifting in the Celtic Sea/South-Western Approaches commenced in the Mid- to Late Triassic.

2.3.2 Mid- to Late Triassic rifting

The onset of northwest-southeast continental lithospheric extension related to opening of the proto-North Atlantic during Triassic times led to further reactivation of the pre-existing Variscan and Caledonian faults throughout the Celtic Sea/South-Western Approaches, with the clastics of the Sherwood Sandstone Group grading upward with apparent conformity into the playa-lake evaporitic mudstones of the Mid- to Late Triassic Mercia Mudstone Group (Petrie *et al.*, 1989).

As can be seen in Figures 2.5 - 2.15, the evaporitic mudstones in the Caernarvon, Kish Bank, Melville, South Celtic Sea, and Cardigan Bay basins grade upwards into a massive halite unit. The thickness and distribution of this halite unit has been altered by later halokinesis, however Chapman (1989) suggested that in the northern Melville Basin the distribution of the halite unit is probably also the result of syntectonic deposition. Further evaporitic mudstones of the Mercia Mudstone Group were then deposited in these basins. In the Fastnet, North Celtic Sea, Brittany, South-West Channel, St. Mary's, and Plymouth Bay basins, however, the evaporitic mudstones of the Mercia Mudstone Group continued without change throughout Late Triassic times. The onset of the thermal subsidence phase, combined with a eustatic

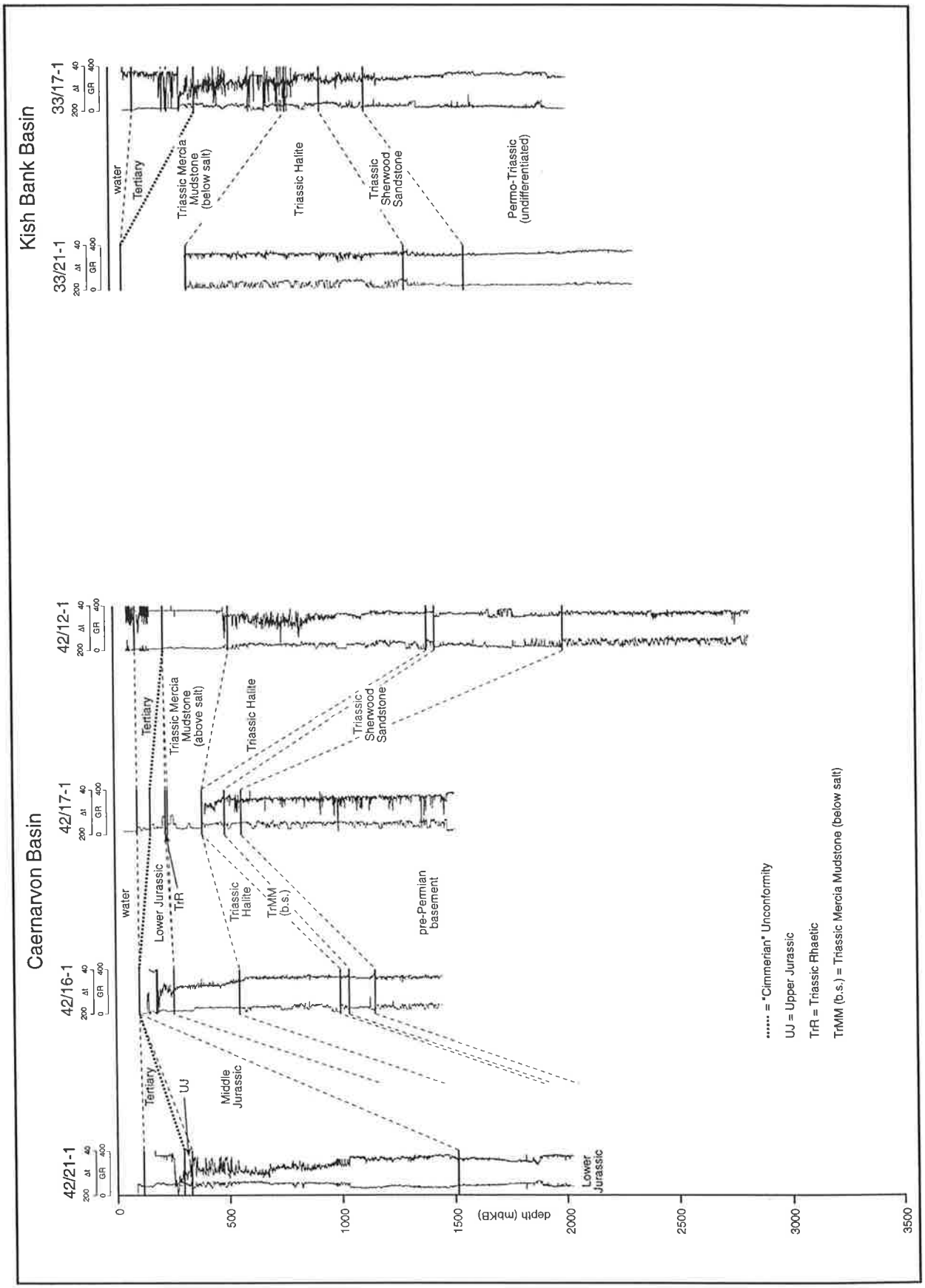

Fig. 2.5. Well correlation diagram for the Caernarvon and Kish Bank basins. Reference datum is Kelly Bushing (0 metres). Gamma ray (GR, API units) log is plotted on the left, sonic log (Δt, μs/ft) is plotted on the right. See Figure 1.1 for well localities.

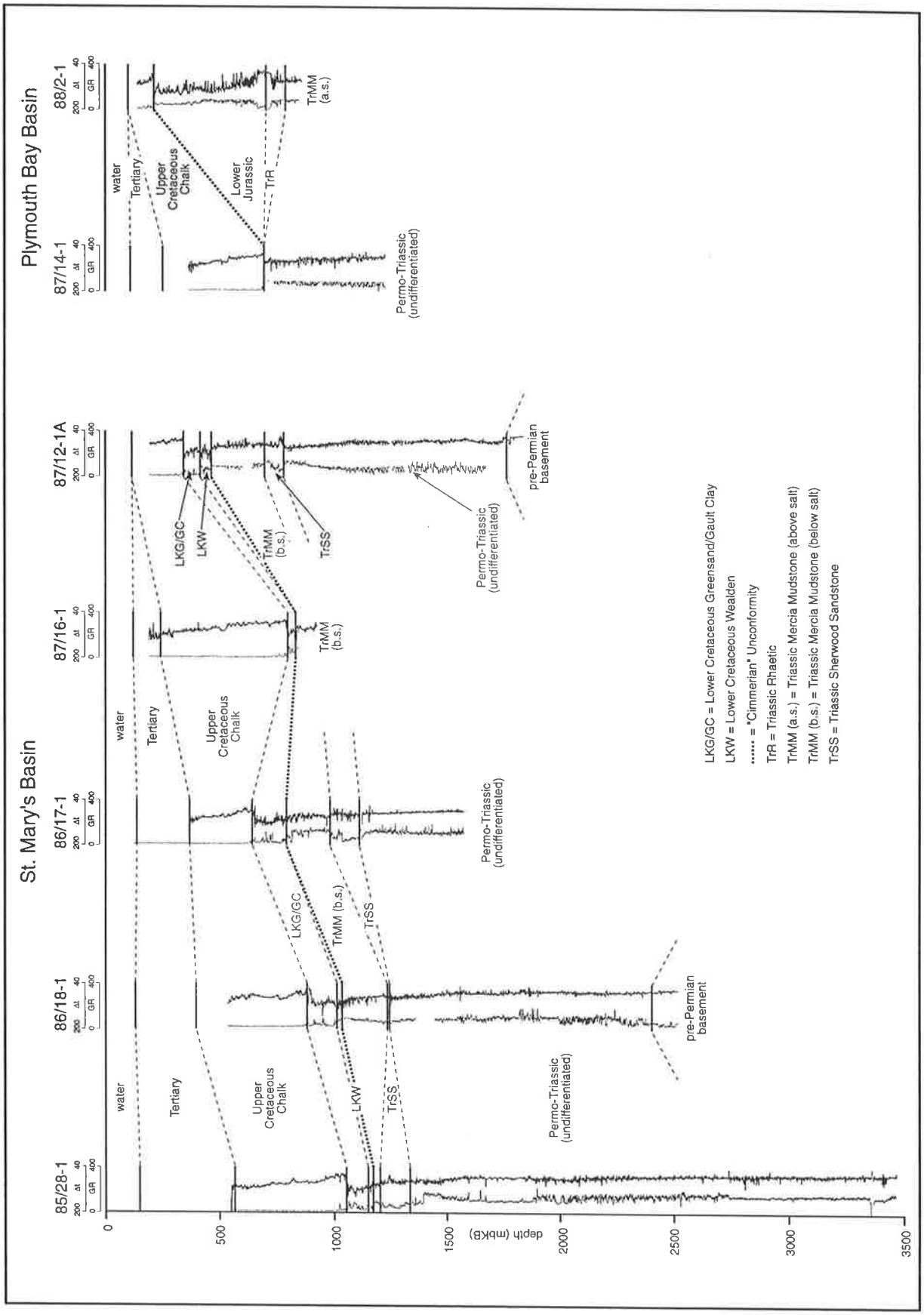

Fig. 2.6. Well correlation diagram for the St. Mary's and Plymouth Bay basins. Reference datum is Kelly Bushing (0 metres). Gamma ray (GR, API units) log is plotted on the left, sonic log (Δt, μs/ft) is plotted on the right. See Figure 1.1 for well localities.

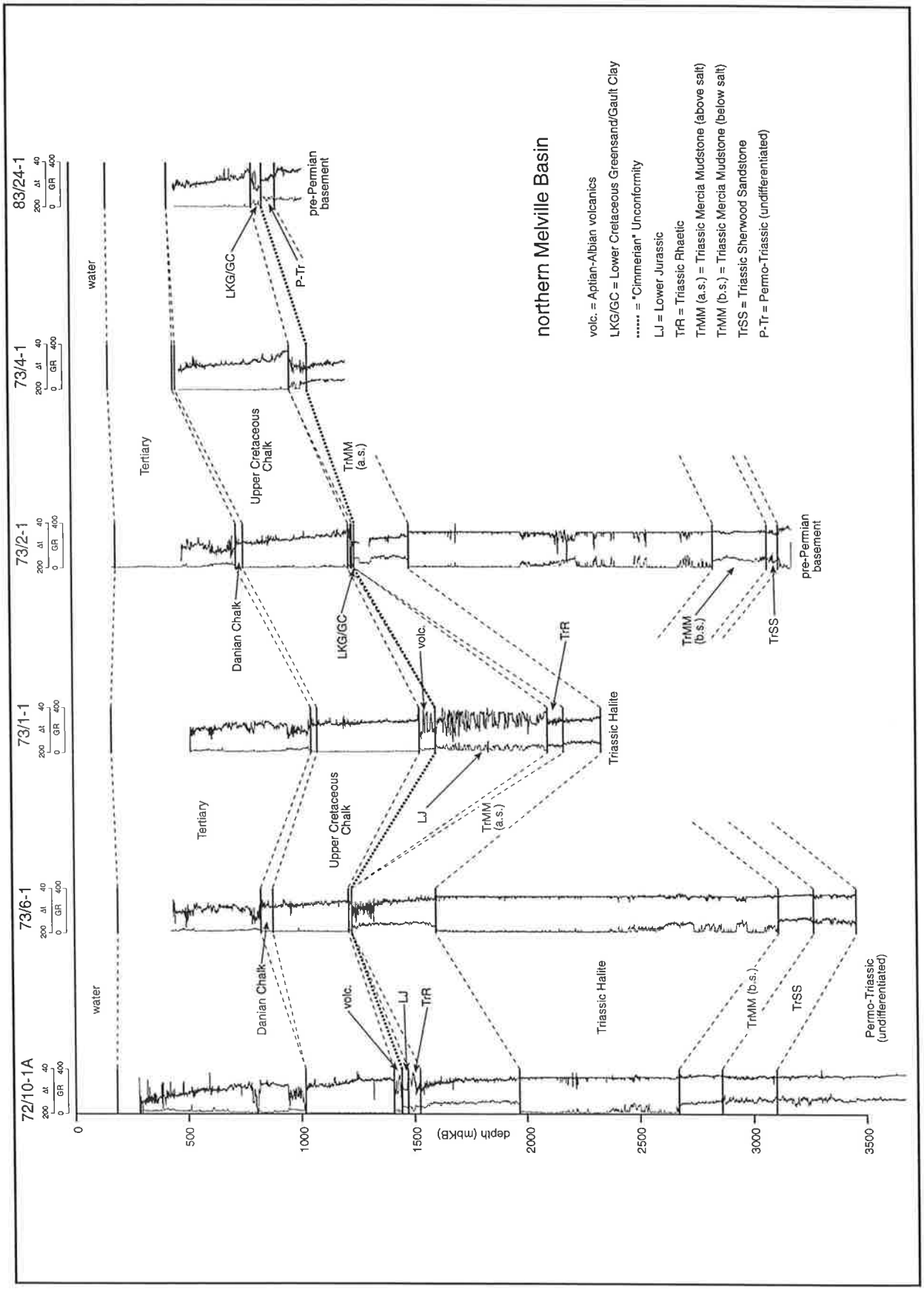

Fig. 2.7. Well correlation diagram for the northern Melville Basin. Reference datum is Kelly Bushing (0 metres). Gamma ray (GR, API units) log is plotted on the left, sonic log (Δt, μs/ft) is plotted on the right. See Figure 1.1 for well localities.

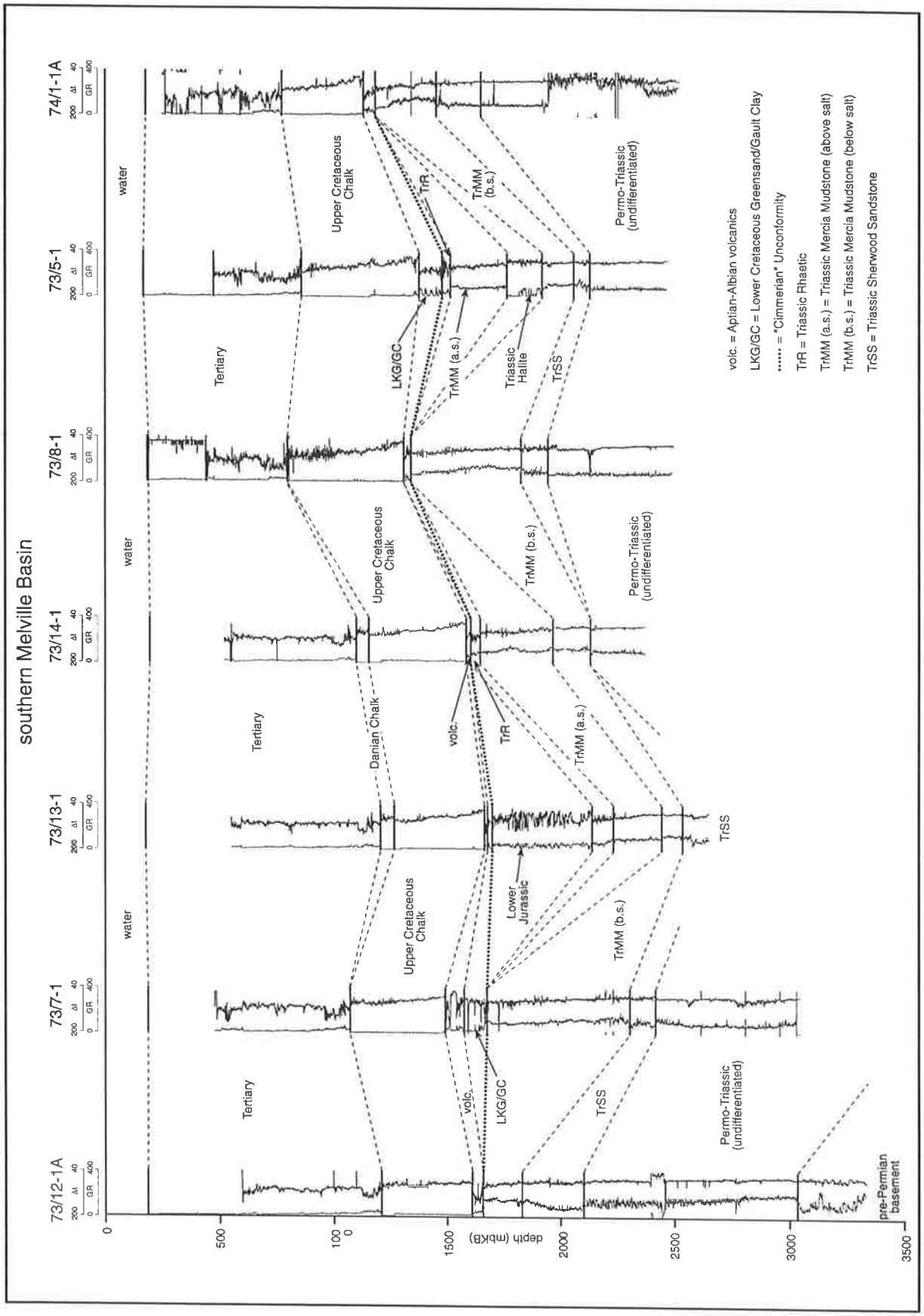

Fig. 2.8. Well correlation diagram for the southern Melville Basin. Reference datum is Kelly Bushing (0 metres). Gamma ray (GR, API units) log is plotted on the left, sonic log (Δt, μs/ft) is plotted on the right. See Figure 1.1 for well localities.

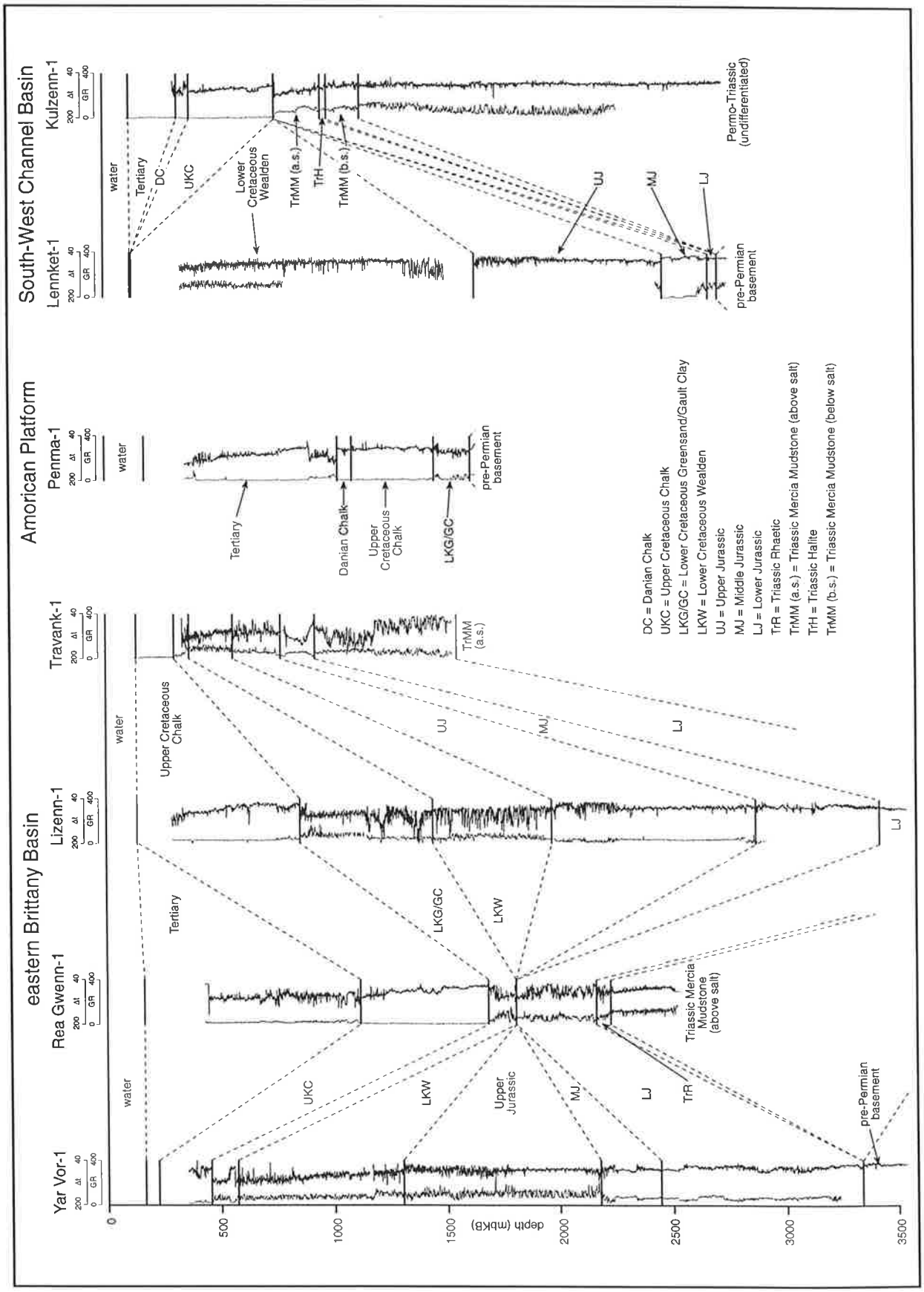

Fig. 2.9. Well correlation diagram for the eastern Brittany Basin, South-West Channel Basin, and the Amorican Platform. Reference datum is Kelly Bushing (0 metres). Gamma ray (GR, API units) log is plotted on the left, sonic log (Δt, $\mu s/ft$) is plotted on the right. See Figure 1.1 for well localities.

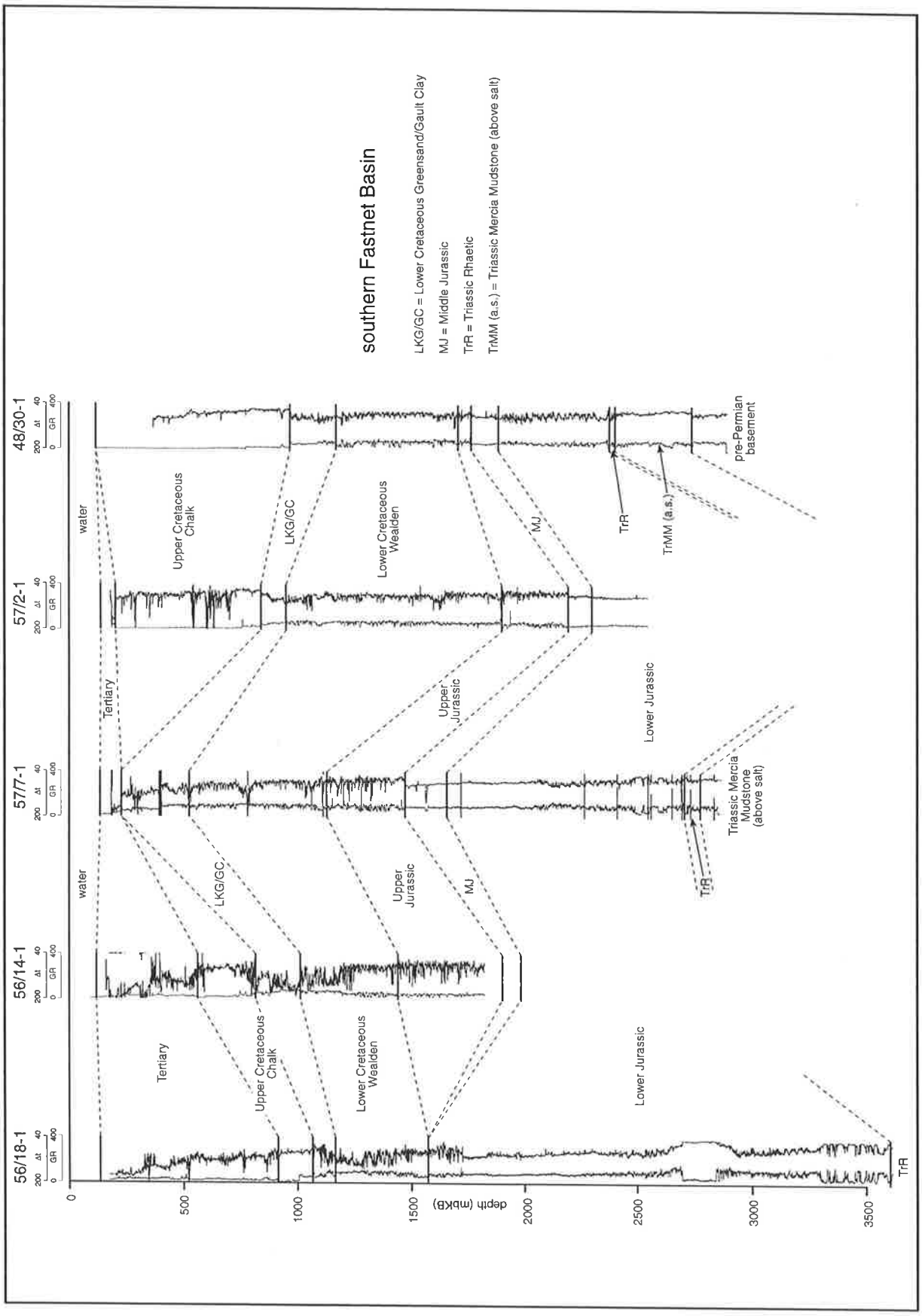

Fig. 2.10. Well correlation diagram for the southern Fastnet Basin. Reference datum is Kelly Bushing (0 metres). Gamma ray (GR, API units) log is plotted on the left, sonic log (Δt, μs/ft) is plotted on the right. See Figure 1.1 for well localities.

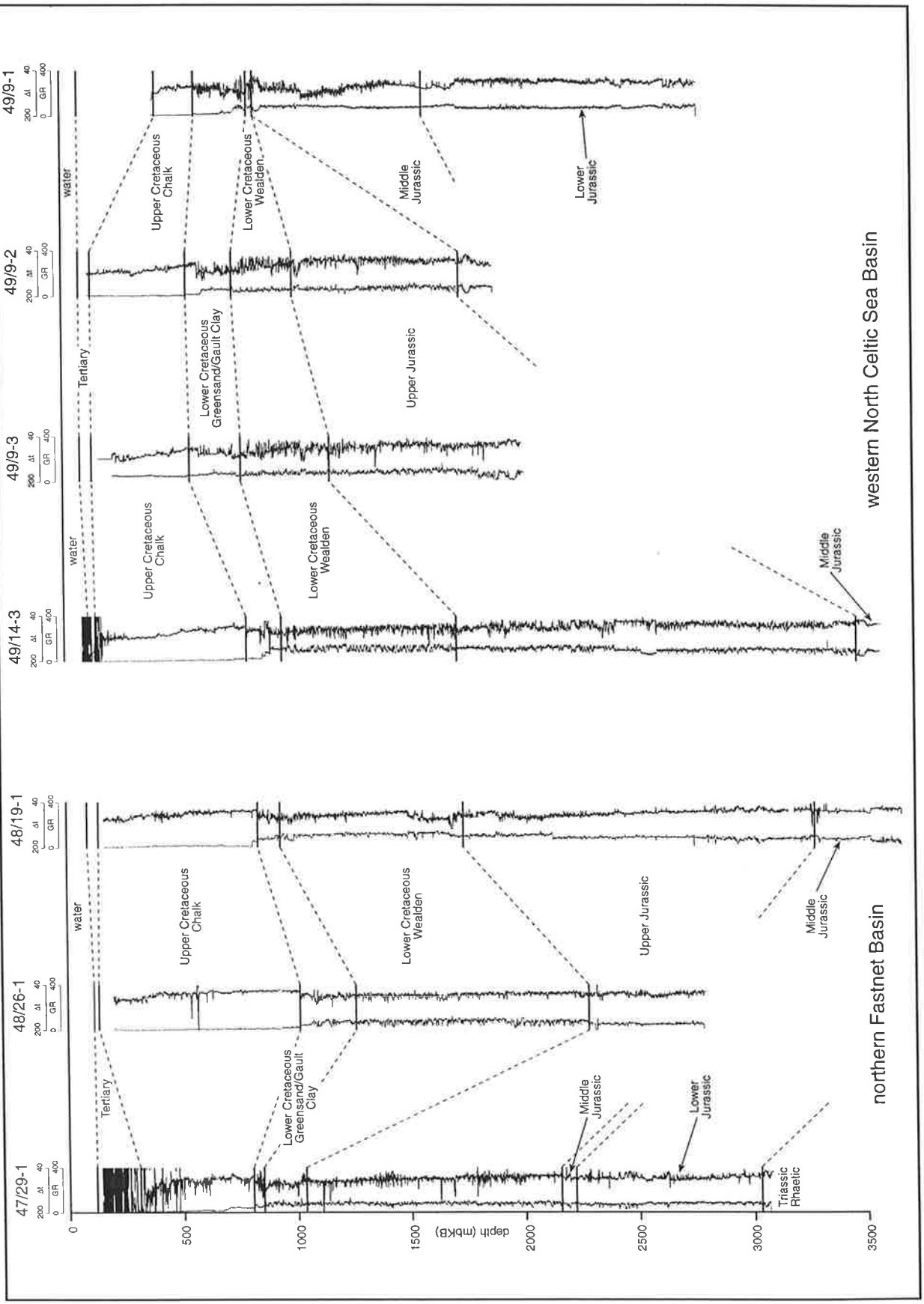

Fig. 2.11. Well correlation diagram for the northern Fastnet Basin and western North Celtic Sea Basin. Reference datum is Kelly Bushing (0 metres). Gamma ray (GR, API units) log is plotted on the left, sonic log (Δt, μs/ft) is plotted on the right. See Figure 1.1 for well localities.

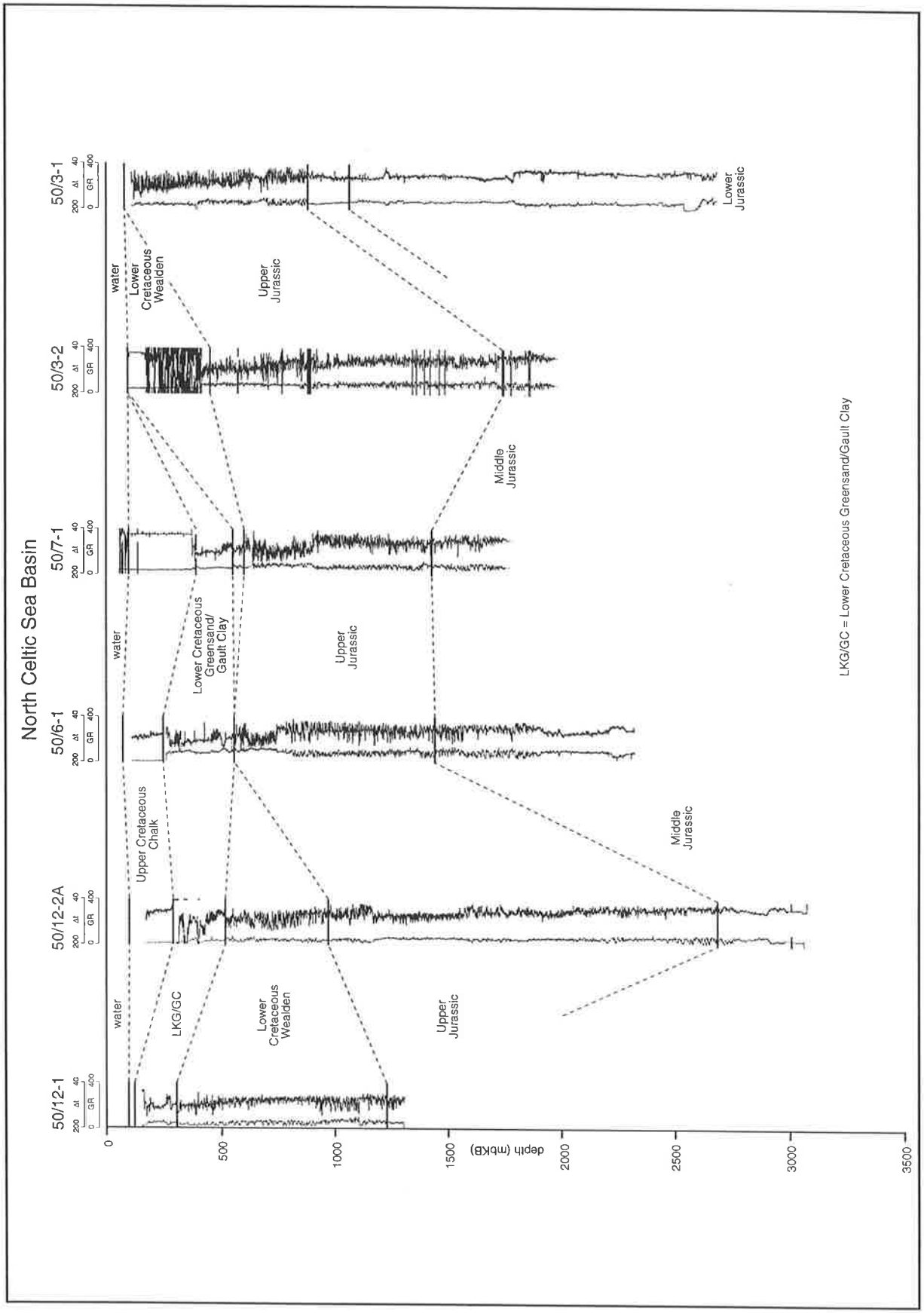

Fig. 2.12. Well correlation diagram for the North Celtic Sea Basin. Reference datum is Kelly Bushing (0 metres). Gamma ray (GR, API units) log is plotted on the left, sonic log (Δt, μs/ft) is plotted on the right. See Figure 1.1 for well localities.

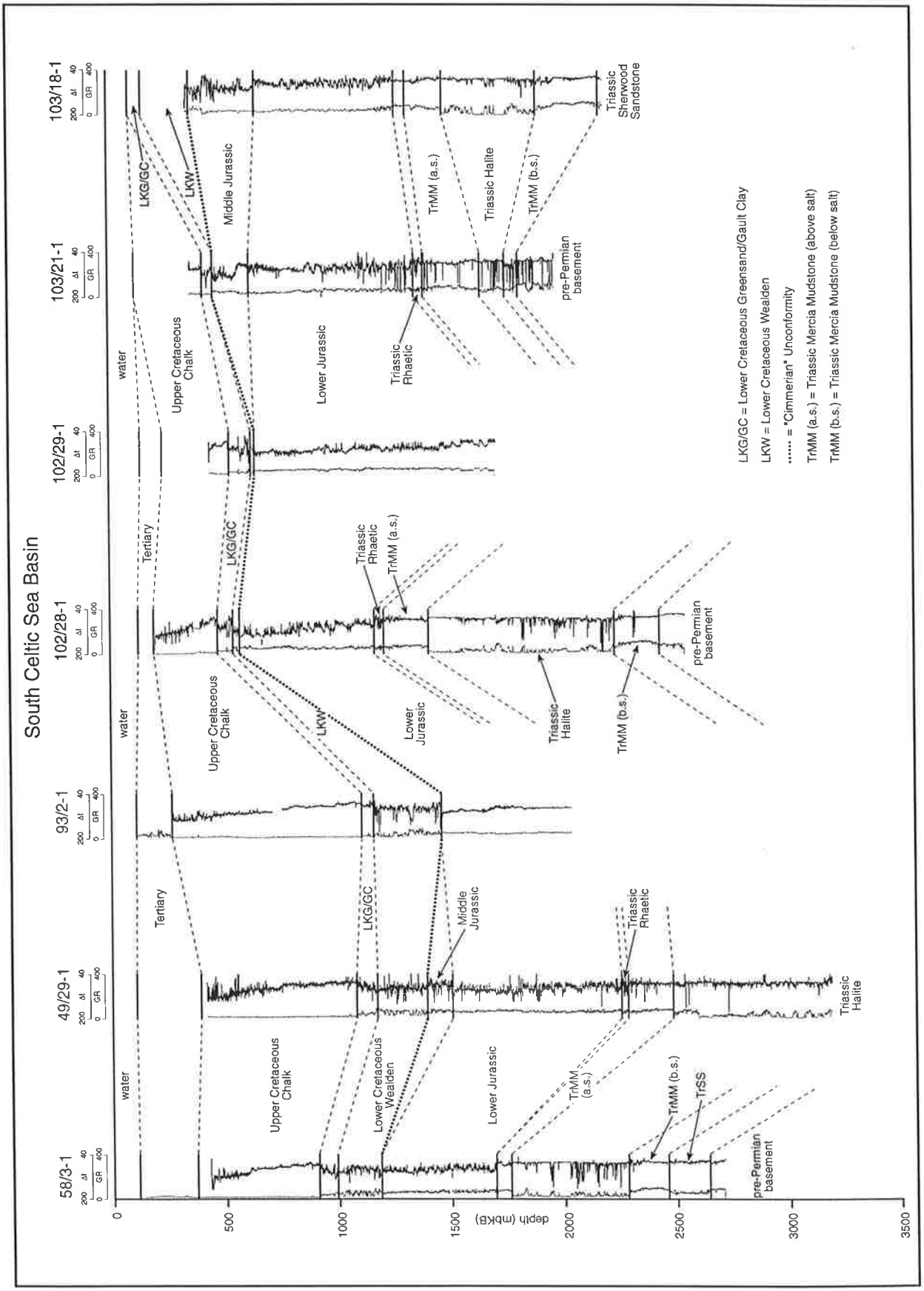

Fig. 2.13. Well correlation diagram for the South Celtic Sea Basin. Reference datum is Kelly Bushing (0 metres). Gamma ray (GR, API units) log is plotted on the left, sonic log (Δt, μs/ft) is plotted on the right. See Figure 1.1 for well localities.

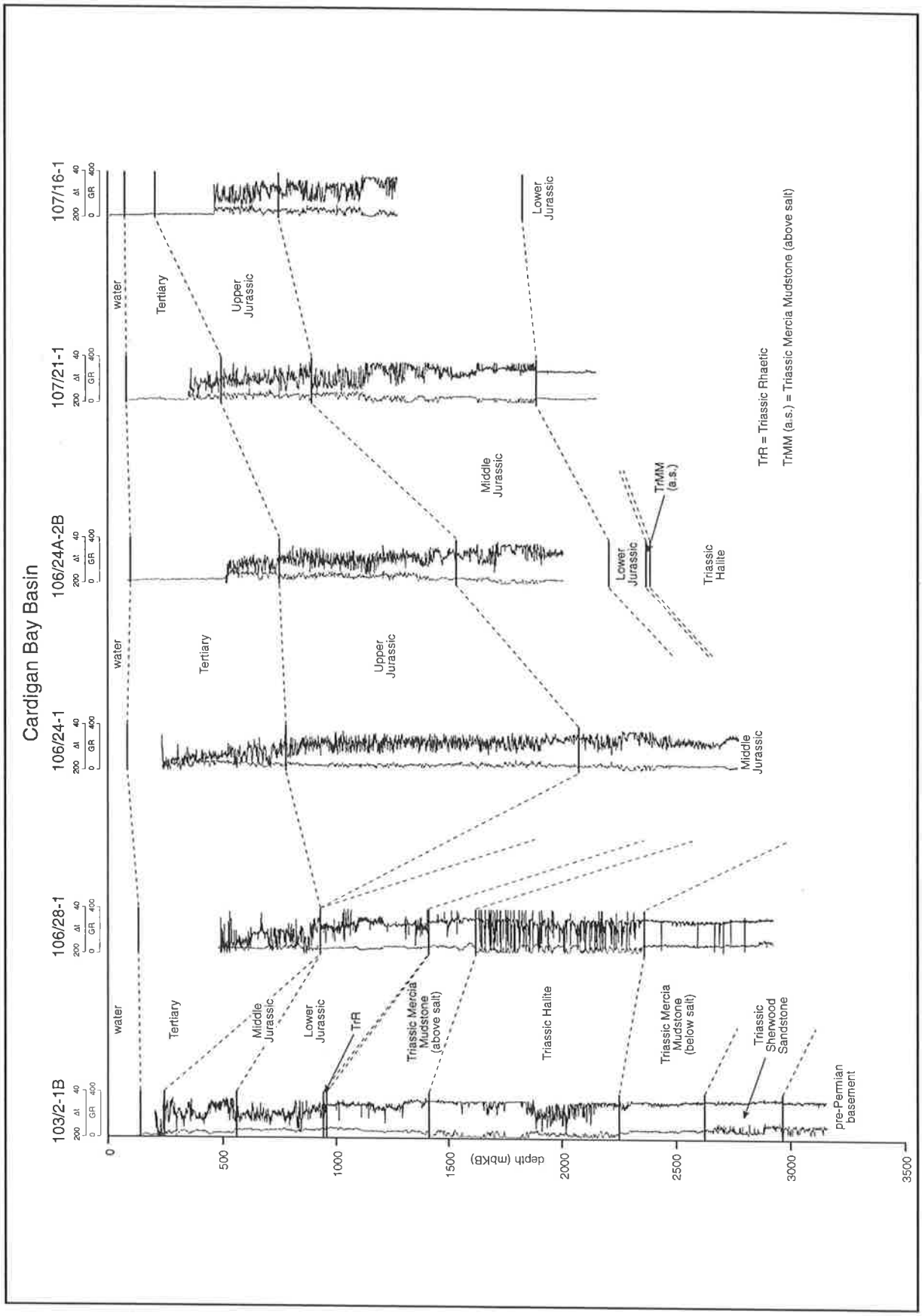

Fig. 2.14. Well correlation diagram for the Cardigan Bay Basin. Reference datum is Kelly Bushing (0 metres). Gamma ray (GR, API units) log is plotted on the left, sonic log (Δt, μs/ft) is plotted on the right. See Figure 1.1 for well localities.

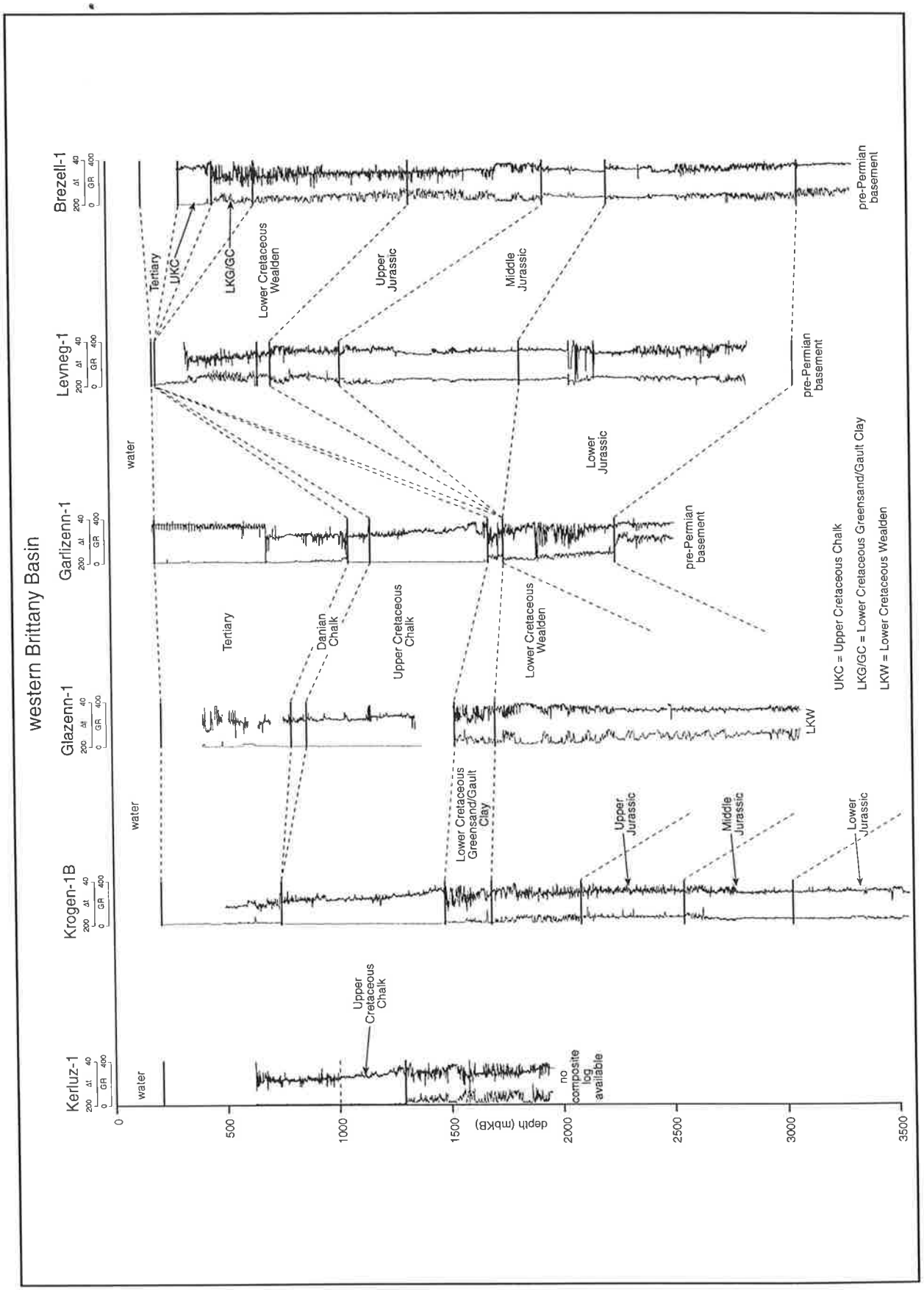

Fig. 2.15. Well correlation diagram for the western Brittany Basin. Reference datum is Kelly Bushing (0 metres). Gamma ray (GR, API units) log is plotted on the left, sonic log (Δt, µs/ft) is plotted on the right. See Figure 1.1 for well localities.

sea level rise, led to marine transgression over the peneplaned Late Triassic landscape (Evans, 1990), and the deposition of the restricted marine marls and limestones of the Rhaetian Penarth Group (Figs. 2.6 - 2.11, 2.13, 2.14).

Triassic sediments are thin or absent in the South-West Channel and Brittany basins (Figs. 2.9, 2.15) because the Triassic rifting event had little to no effect in these areas. However, rifting commenced in these basins at the beginning of the Jurassic, and persisted in the Brittany Basin at least until the Pliensbachian (Evans, 1990).

2.4 Early-Middle Jurassic Thermal Subsidence

Thermal-relaxation subsidence inherited from the Permo-Triassic lithospheric thinning in the Celtic Sea/South-Western Approaches lasted throughout the Jurassic until Bathonian to Callovian times, resulting in the deposition of thick calcareous mudstones and limestones in a progressively increased area of deposition (Evans, 1990; Tappin *et al.*, 1994). Deposition during this period is characterised by a series of regressive-transgressive cycles within gently subsiding basins. Water depths at maximum transgression were at most moderate (Petrie *et al.*, 1989). Thick sequences of Early-Middle Jurassic age are preserved in the Caernarvon Basin (Fig. 2.5), Brittany Basin (Figs. 2.9, 2.15), South-West Channel Basin (Fig. 2.9), Fastnet Basin (Figs. 2.10, 2.11), North Celtic Sea Basin (Figs. 2.11, 2.12), and Cardigan Bay Basin (Fig. 2.14). Localised erosional remnants of Early Jurassic sedimentary rocks are also preserved in the Plymouth Bay Basin (Fig. 2.6) and the Melville Basin (Figs. 2.7, 2.8), with preservation in the Melville Basin related to withdrawal of Triassic salt (Evans, 1990).

2.5 Late Jurassic-Early Cretaceous Rifting and the "Cimmerian" Unconformity

The onset of renewed lithospheric stresses related to the opening of the North Atlantic resulted in major episodes of rifting and uplift from late-Middle Jurassic to Early Cretaceous times across the Celtic Sea/South-Western Approaches (Evans, 1990). Early in Late Jurassic times, rifting intensified along the Grand Banks-Iberian margin, controlled by a northwest-southeast extension vector (Petrie *et al.*, 1989). The main areas of renewed rifting and subsidence in the Celtic Sea/South-Western Approaches were the axes of the North Celtic Sea, Cardigan Bay, Caernarvon, Brittany, and South-West Channel basins. The Fastnet, South Celtic Sea, and Bristol Channel basins were also actively subsiding, but the resulting depocentres were areally restricted and minor (Petrie *et al.*, 1989). A variety of environments were established in the Celtic Sea/South-Western Approaches basins, ranging from fluvio-lacustrine and lagoonal to marginal marine (Petrie *et al.*, 1989). As a result, Upper Jurassic sediments in these basins are dominated by mudstones, interbedded with thin limestones, siltstones, and sandstones (Figs. 2.5, 2.9 - 2.12, 2.14, 2.15).

In contrast, major regional uplift in Late Jurassic-Early Cretaceous times of the basins surrounding the Cornubian Platform resulted in erosion of up to 2 km of Permian to Jurassic sediments from the Melville, St. Mary's, and Plymouth Bay basins (Chapman, 1989), and to a lesser extent the South Celtic Sea Basin, resulting in the so-called Cimmerian unconformity (Van Hoorn, 1987; Tappin *et al.*, 1994; Evans, 1990). Evans (1990) suggested that the magnitude of local subsidence related to strike-slip

motion along basin bounding faults with some extensional component in the Brittany and South-West Channel basins was greater than that of the regional uplift, resulting in restricted yet rapid deposition, with up to 2.5 km of sediment accumulating in these basins.

Previous authors (e.g. Tucker & Arter, 1987; Ziegler, 1987*b*) have suggested that fault controlled subsidence continued throughout Late Jurassic-Early Cretaceous times in the Celtic Sea/South-Western Approaches. Petrie *et al.* (1989) however suggested that two discrete events occurred during Late Jurassic-Early Cretaceous times, with rifting related to northwest-southeast extension ceasing in the Celtic Sea region in the Tithonian, prior to intensified rifting along the Bay of Biscay-Amorican margin in the Berriasian. The onset of this east-northeast to northeast extension vector reactivated existing northeast-to-southwest and east-west trending faults in a translational sense in the Celtic Sea basins (Van Hoorn, 1987) and South-Western Approaches (Ziegler, 1987*b*), whilst the early Mesozoic northwest-southeast trending transfer faults were reactivated in an extensional sense (Petrie *et al.*, 1989). This event terminated in the Aptian, with crustal separation occurring along the Grand Banks-Iberian margin and along the Bay of Biscay-Amorican-Newfoundland margin (Petrie *et al.*, 1989), and the formation of oceanic crust in the early Aptian in the proto-North Atlantic (Evans, 1990; Tappin *et al.*, 1994).

Early Cretaceous rifting in the Celtic Sea/South-Western Approaches resulted in the deposition of the thick Wealden sequences in the North Celtic Sea, Brittany, South-West Channel, Haig Fras, and Fastnet basins (Figs. 2.9 - 2.12, 2.15), with thinner, areally limited deposition occurring in the South Celtic Sea and St. Mary's basins (Figs. 2.6, 2.13). The Wealden sequences are predominantly non-marine alluvial fans, interbedded sandstones, siltstones, and mudstones, with sporadic intervals of marine sediments, followed by the rapid re-establishment of fluvio-deltaic conditions.

2.6 Late Cretaceous/Tertiary Thermal Subsidence

After crustal separation between the Newfoundland margin and the Iberian-Amorican margin and the onset of seafloor spreading in the North Atlantic (Tappin *et al.*, 1994), active fault-controlled subsidence ended within the Celtic Sea/South-Western Approaches, with passive subsidence coupled with a high sea level characterising the remainder of the Mesozoic (Petrie *et al.*, 1989). Clastic deposition in a shallow to marginal-marine environment increased in areal extent across the region, with deposition of the Lower Cretaceous Greensand and Gault Clay in the St. Mary's, Melville, Brittany, Fastnet, North and South Celtic Sea basins (Figs. 2.6 - 2.13, 2.15), and on the Amorican passive margin (Fig. 2.9).

The Greensand/Gault Clay was followed by the accumulation of up to one kilometre of Upper Cretaceous Chalk across the entire Celtic Sea/South-Western Approaches, including the Cornubian Platform (Evans, 1990), the Amorican margin (Fig. 2.9), and the Pembroke Ridge (Tappin *et al.*, 1994). Thickness variations in the Chalk across the area show that the basinal areas subsided faster than the flanking basement highs. Post-Cretaceous erosion has removed all evidence of Cretaceous sedimentation from the Caernarvon Basin (Fig. 2.5) and the Cardigan Bay Basin (Fig. 2.14), however the lack of terrigenous clastic material in the Upper Cretaceous Chalk suggests it blanketed much of the region (Tappin *et al.*, 1994).

2.7 Tertiary Inversion

Most discussions of the Late Cretaceous-Tertiary development of the basins of the southern United Kingdom and surrounding areas have focused on the widely recognised inversion structures/axes such as the classic Purbeck monocline and Wealden anticline. In the Celtic Sea/South-Western Approaches area, inversion structures have been described in the Brittany and South-West Channel Basins (Ziegler, 1987*b*; Hayward & Graham, 1989), the South Celtic Sea-Bristol Channel Basin (Van Hoorn, 1987; Roberts, 1989), the North Celtic Sea-Cardigan Bay Basin (Tucker & Arter, 1987), the Fastnet Basin (Robinson *et al.*, 1981), and the adjacent continental slope (Masson & Parson, 1983). However, as will be demonstrated in Chapters 3 & 4, there is also clear evidence of regional Tertiary exhumation in areas removed from the recognised inversion axes.

2.7.1 Palaeocene exhumation

By the early Palaeogene, the Celtic Sea/South-Western Approaches lay between two plate boundaries: the extensional boundary in the mid-Atlantic, and the collisional boundary that ran through the Mediterranean between the Eurasian and African plates (Evans, 1990). The tectonic events in the area during the Tertiary were the result of transmitted stresses developed at these boundaries, although the events at the continent-continent boundary in the Mediterranean which produced the Alpine mountain chain were the most important (Evans, 1990).

The first significant Tertiary exhumation in the Celtic Sea/South-Western Approaches occurred between Maastrichtian and Middle Eocene times, with uplift and erosion particularly severe north of the Variscan front in the Cardigan Bay, Caernarvon, and Kish Bank basins. Tappin *et al.* (1994) and Tucker & Arter (1987) attributed these movements to the end-Cretaceous 'Laramide' event. South of the Variscan front, compression during lateral movements along north-west trending strike-slip faults resulted in post-Maastrichtian to pre-middle Eocene inversion of the Fastnet Basin (Robinson *et al.*, 1981). The first pulse of crustal shortening and inversion in the North Celtic Sea Basin was roughly synchronous with inversion of the Fastnet Basin (Tucker & Arter, 1987), with uplift and erosion most severe in the west (Tappin *et al.*, 1994), whilst the South Celtic Sea Basin also underwent structural inversion in the Palaeocene to middle Eocene (Van Hoorn, 1987; Evans, 1990).

In the south, the occurrence of chalks of Danian age in the Melville Basin (Figs. 2.7, 2.8), South-West Channel Basin (Fig. 2.9), and Brittany Basin (Fig. 2.15) constrains the first Tertiary exhumation event in the southern area of the Celtic Sea/South-Western Approaches as post-Danian. This event may be contemporaneous with the first Tertiary inversion of the North and South Celtic Sea basins and the Fastnet Basin, however the degree of exhumation of the northern basins has removed any evidence of Palaeocene deposition. In contrast with the northern basins, Palaeocene tectonic movements across the southern basins resulted in regional uplift that produced a widespread, uniform unconformity (Evans, 1990), without specific evidence of structural inversion (Tappin *et al.*, 1994).

2.7.2 Eocene-Oligocene subsidence

Following the End Cretaceous - Eocene uplift, regional thermal-relaxation subsidence and deposition of clastic sediments resumed throughout the Celtic Sea/South-Western Approaches. No true extensional faulting took place at this time, but sinistral movement on the marginal faults of the Cardigan Bay Basin and other northwest-southeast trending faults

such as the Sticklepath Fault (Fig. 2.1) resulted in local fault-bounded basins with thick Eocene-Oligocene sequences (Tappin *et al.*, 1994). Dobson & Whittington (1987) suggested that the uplift of the Cornubian and Welsh Massifs may have occurred at this time.

A thick sequence of Eocene - Oligocene shallow marine carbonates and shales is preserved in the Melville and St. Mary's basins. Elsewhere, in the North and South Celtic Sea, Fastnet, Brittany, South-West Channel, and Plymouth Bay basins, later inversion resulted in the removal of the Palaeogene section (Evans, 1990; Tappin *et al.*, 1994).

2.7.3 Oligo-Miocene exhumation

Sedimentation in the Celtic Sea/South-Western Approaches was interrupted in Oligo-Miocene times by a second pulse of crustal shortening and basin inversion. North of the Variscan front, evidence for inversion is restricted to reversal of the antithetic fault in the Caernarvon Basin and local upwarping of the basin centre (Tappin *et al.*, 1994). The North and South Celtic Sea basins experienced gentle upwarping of their basin centres and local reversal of their basin-margin faults, leading to a thicker preservation of the post-extensional sequence on the Pembroke Ridge than in the basins (Tappin *et al.*, 1994).

By contrast, the Brittany and South-West Channel basins underwent major structural inversion during Oligo-Miocene times (Ziegler, 1987*b*), resulting in the removal of the Tertiary and in places the Upper Cretaceous strata (Figs. 2.9, 2.15). The St. Mary's, Melville, and Plymouth Bay basins show only localised evidence for crustal shortening (Evans, 1990).

2.8 Internal and External Basin Geometries

Basin development in the Celtic Sea/South-Western Approaches shows a pronounced symmetry across the Cornubian Platform. The basins immediately north and south of the Cornubian Platform, the South Celtic Sea, Melville, St. Mary's, and Plymouth Bay basins, underwent relatively minor Late Cretaceous-Tertiary inversion, and the Jurassic-Lower Cretaceous sequence is relatively thin or absent in these basins. The basins further away from the Platform, the North Celtic Sea, Brittany, and Fastnet basins, underwent stronger Late Cretaceous-Tertiary inversion, and also contain a thicker Jurassic-Lower Cretaceous sequence (Fig. 2.2). A similar relationship is also observed in the Wessex Basin, with the Jurassic-Lower Cretaceous sequence thick in the inverted areas, and relatively thin in the uninverted areas (Simpson *et al's* 1989 Figs. 4-7). Regionally, it is apparent that maximum Late Cretaceous-Tertiary inversion occurred in the regions of maximum Jurassic to Early Cretaceous subsidence. The basins adjacent to the Cornubian Platform, the South Celtic Sea, Melville, St. Mary's, and Plymouth Bay basins, have thicker Permo-Triassic sequences than the North Celtic Sea, Brittany, and Fastnet basins (Figs. 2.5-2.15). It is apparent that there is some relationship between proximity to the Cornubian Platform and the resultant geological histories of the basins of the Celtic Sea/South-Western Approaches. The potential mechanisms responsible for the observed symmetry across the Cornubian Platform shall be addressed in Chapter 8.

Due to the symmetry across the Cornubian Platform it is useful to distinguish the basins adjacent to the Cornubian Platform from those further away.

The South Celtic Sea Basin on the northern margin of the Cornubian Platform, and the Melville, St. Mary's, and Plymouth Bay basins on the southern margin, are here termed the internal basins of the Celtic Sea/South-Western Approaches. The external basins are the North Celtic Sea and Fastnet basins to the north of the Cornubian Platform, and the Brittany and South-West Channel basins to the south.

The basins further away from the Cornubian Platform and north of the Variscan front, the Cardigan Bay, Caernarvon, and Kish Bank basins, have undergone such extensive Late Cretaceous-Tertiary inversion that the Jurassic-Cretaceous histories of these basins are unclear.

Chapter 3

Quantifying Exhumation using Compaction Methodology

3.1 Introduction

The porosity of sedimentary rocks decreases with burial due to mechanical and chemical compaction. Porosity loss due to compaction is largely irreversible with exhumation (removal of overburden). Hence if the normal, or undisturbed, compaction (porosity/ depth) trend is known, exhumation can be quantified from the amount of overcompaction with respect to the normal trend.

Skagen (1992) reviewed several methods for quantifying exhumation in sedimentary basins: opal-CT transition, illite crystallinity, apatite fission track analysis, vitrinite reflectance, shale compaction and drilling parameters (drilling exponent-based). Of these methods, shale compaction, drilling parameters and vitrinite reflectance have the best resolution, with a potential for accuracy of ±200 m (Skagen, 1992). The drilling parameter and compaction methods have an additional advantage, particularly offshore, of utilising data that are directly available from exploration wells, enabling a far greater coverage than the other methodologies, which rely on the availability of samples. In this project the compaction methodology was chosen to quantify exhumation in the Celtic Sea/South-Western Approaches.

Most studies have, like Skagen (1992), used the (over) compaction of shales to quantify exhumation (e.g. Jankowsky, 1962; Marie, 1975; Magara, 1976; Lang, 1978; Wells, 1990; Issler, 1992; Japsen, 1993). Other lithologies have not been widely analysed, presumably because their compaction trends were not believed to be so directly burial-depth controlled. Here lithologies other than shales are used to quantify exhumation.

The compaction methodology relies upon identifying the degree of compaction, or amount of porosity loss due to burial, of sedimentary rocks. Hence, before addressing the quantification of exhumation using the compaction methodology, the basic principles of porosity and compaction in sedimentary rocks are discussed.

3.2 Porosity in Sedimentary Rocks

The porosity of a sedimentary rock is the ratio of its total pore space to its total volume, conventionally expressed as a percentage. Hence:

$$\text{porosity}(\phi) = \frac{\text{volume of total pore space}}{\text{volume of rock}} \times 100 \qquad \text{.....(3.1)}$$

3.2.1 Primary and secondary porosity

Sedimentary rock porosity may be classified into two main varieties: primary porosity, which is present immediately after the rock has been deposited, and secondary or post-depositional porosity, which forms after sedimentation by a variety of diagenetic causes (Table 3.1). It is significant to the compaction-based determination of exhumation that the destruction of primary porosity is burial-depth controlled, as discussed in the following section, but the generation of secondary porosity is not strongly burial-depth controlled.

3.2.2 Intergranular and intragranular porosity

Intergranular porosity consists of the void spaces

	type	origin
primary porosity	(a) Intergranular (b) Intragranular	sedimentation
secondary porosity	(c) fracture	tectonic movement, compaction or dehydration
	(d) intercrystalline (e) fenestral	cementation
	(f) moldic (g) vuggy	solution

Table 3.1. Classification of porosity types (after Selley, 1988).

between the detrital grains which form the framework of a sedimentary rock. Intragranular porosity is the pore space within detrital grains. Intragranular porosity is most common in carbonate grains of skeletal origin, such as the cavities in fossils and microfossils.

3.2.3 Absolute and effective porosity

Absolute (or total) porosity includes both the interconnected and isolated pores within a rock. Effective porosity is only the interconnected part of absolute porosity.

3.3 Compaction of Sedimentary Rocks

Compaction of sedimentary rocks is a physical process which results from burial. However, porosity loss may also be caused by other burial-depth independent diagenetic processes. The main diagenetic processes are now discussed in terms of burial-depth dependence or independence.

3.3.1 Processes of porosity loss dependent on burial-depth

Compaction of sedimentary rocks occurs in three burial-depth dependent stages: mechanical rearrangement, mechanical deformation, and chemical deformation (Fig. 3.1). With initial burial, the weight of overburden upon a sedimentary rock is increased. The resultant increase in pressure leads to the expulsion of pore fluids, and the mechanical rearrangement of grains into a more tightly packed mass.

Once the grains are tightly packed and in contact with each other, compaction due to increasing burial and hence pressure must proceed through other avenues, and mechanical deformation becomes prevalent. Softer grains such as clay minerals are deformed around harder grains such as quartz, increasing the amount of grain-grain contact, and reducing the intergranular porosity. Harder grains are cracked and displacement occurs along the fractures so as to further reduce the porosity.

With further burial and pressure, grains begin to undergo chemical deformation. Contact points between grains dissolve due to pressure solution, with the dissolved material re-precipitating in the pore spaces, thereby further reducing porosity.

The relative importance of these mechanisms in the way sedimentary rocks evolve during burial varies enormously as a function of the nature of the grains making up the sedimentary rock. However these

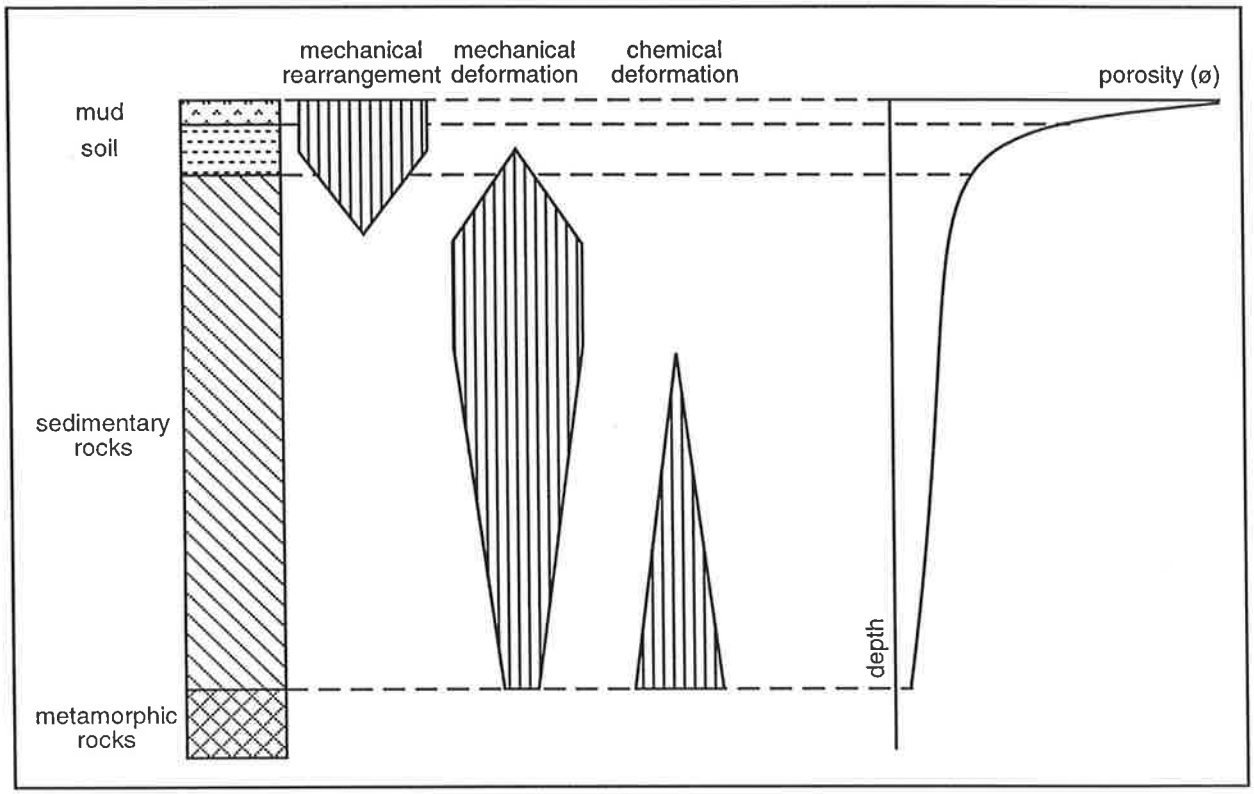

Fig. 3.1. The principle mechanisms causing compaction and porosity loss (after Schneider *et al.*, 1994).

processes are all burial-depth (pressure) controlled, and provided they are the primary mechanisms of porosity loss, the degree of (over) compaction can be used to quantify exhumation.

3.3.2 Processes of porosity loss independent of burial-depth

There are a large number of processes of porosity loss that are independent of burial-depth. Of these, cementation is the most important. Environmental changes within a sedimentary rock, such as the introduction of externally-derived waters of differing chemistry into pore fluids, may result in the precipitation of minerals in the pore spaces. The precipitated mineral not only fills pore voids, but may also cement grains together, preventing them from reorienting into a closer packed arrangement with increased burial. The introduction of cementation may therefore not only reduce porosity independently of depth, but may also prevent further porosity loss due to increased burial.

Although porosity loss can occur independently of burial-depth, provided burial-depth dependent processes are demonstrably the primary cause of porosity loss in a sedimentary rock, the degree of overcompaction of the rock may be used to quantify exhumation.

3.3.3 Examples of compaction trends

Figure 3.2 shows a number of examples from around the world of sandstones which exhibit a decrease in porosity with burial-depth. The relationship between porosity and burial-depth indicated by all of these sandstones clearly show that burial-depth is a primary control upon porosity in sandstones. Furthermore, the linear nature of the

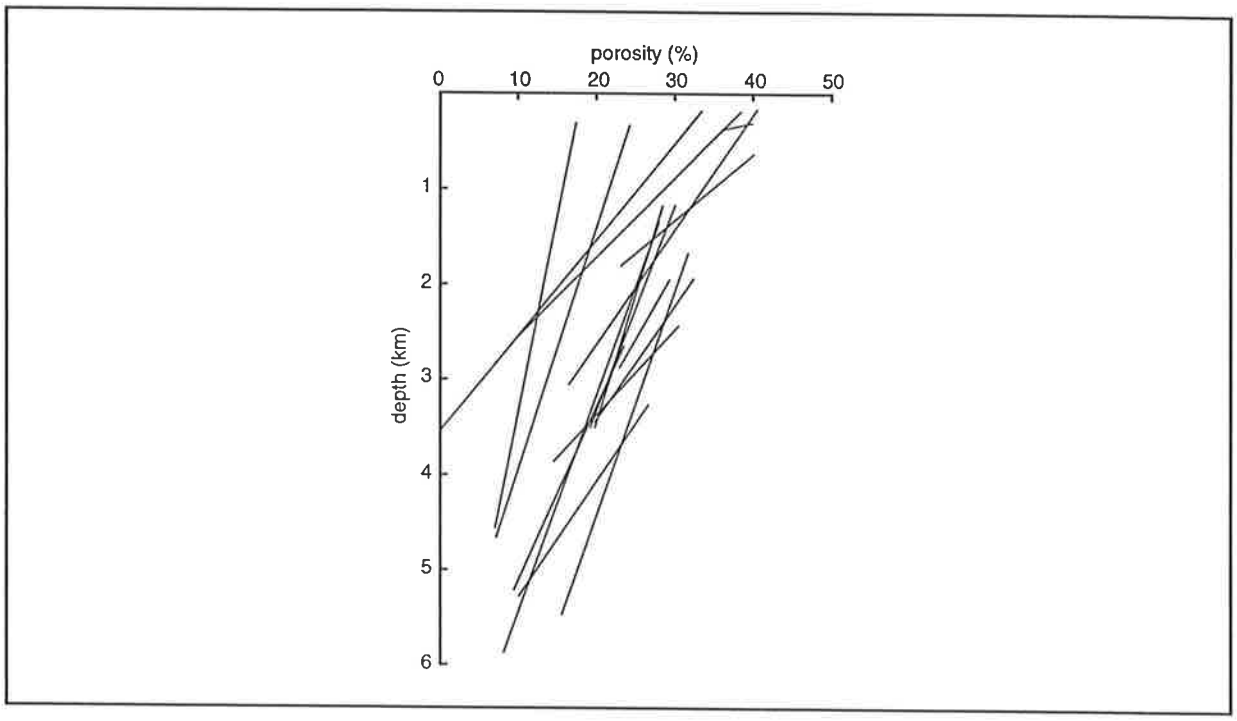

Fig. 3.2. Sandstone porosity gradients (after Selley, 1988).

relationship between porosity and depth, even at shallow burial-depths, suggests that near-surface processes such as mechanical rearrangement do not have a major influence on sandstone compaction. The different initial porosities and porosity/depth gradients are probably due to different initial compositions for the sandstones.

Figure 3.3 shows a number of porosity/burial-depth curves for mudstones and shales. The rapid porosity loss at shallow depth of burial shows that mechanical rearrangement is an important process in the early compaction of clays and muds, reducing porosity rapidly from 70-80% to 30-50% with a few hundred metres of burial. However, again it is clear that porosities in mudstones and shales are closely related to burial-depth.

For the majority of carbonates, chemical deformation and cementation commence at the very beginning of burial (Selley, 1988). As a result, the majority of carbonates do not show burial-depth dependent porosity trends (Selley, 1988). In a number of cases, however, such as the Cretaceous European Chalks and the Cenozoic Floridan limestones shown in Figure 3.4, carbonates may display clearly burial-depth related porosity trends.

Burial-depth is clearly a first-order control upon porosity in sandstones, mudstones, and shales, and hence these sedimentary rocks are suitable for quantifying exhumation using the compaction methodology (e.g. Magara, 1976; Lang, 1978; Bulat & Stoker, 1987; Hillis, 1991; Issler, 1992; Hillis *et al.*, 1994). Porosity loss in carbonates is generally burial-depth independent, with the exception of a few cases such as the European Cretaceous Chalks, where burial-depth is the primary control on porosity.

3.4 Geophysical Logs and Porosity Determination

3.4.1 Porosity logs

Rock porosity can be obtained from the sonic log, the neutron porosity log, or the bulk density log. The

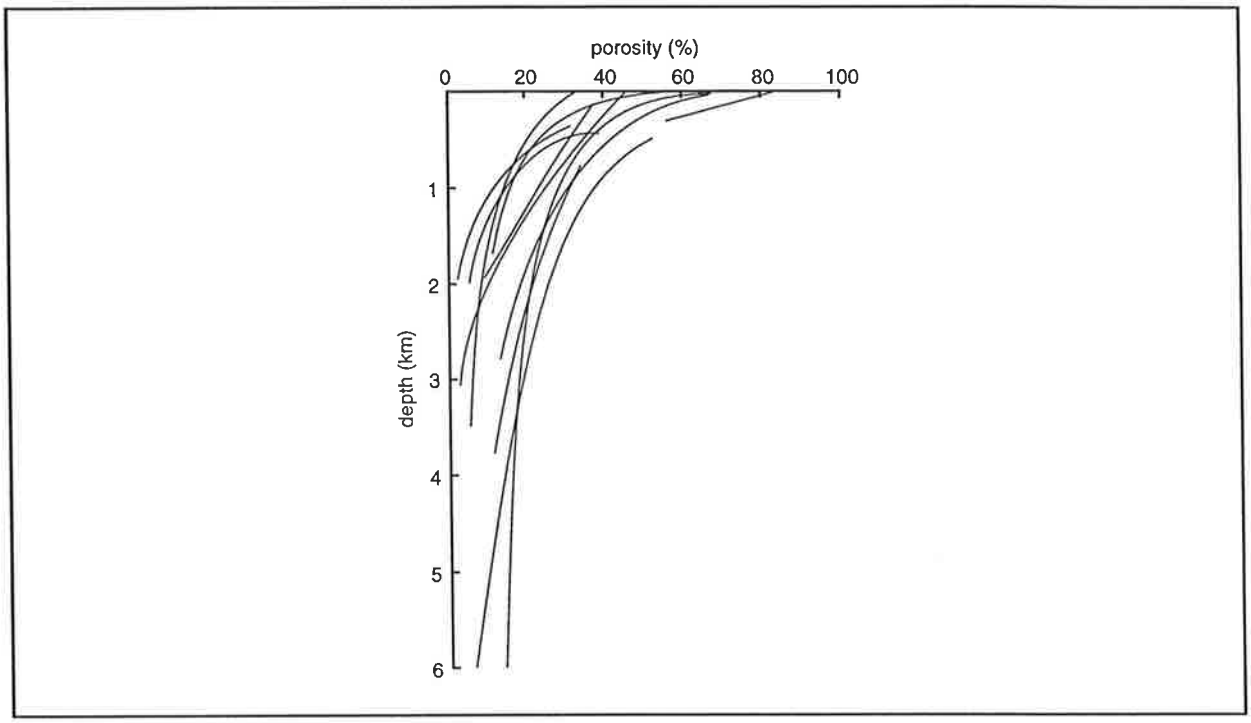

Fig. 3.3. Mudstone/shale porosity gradients (after Selley, 1988).

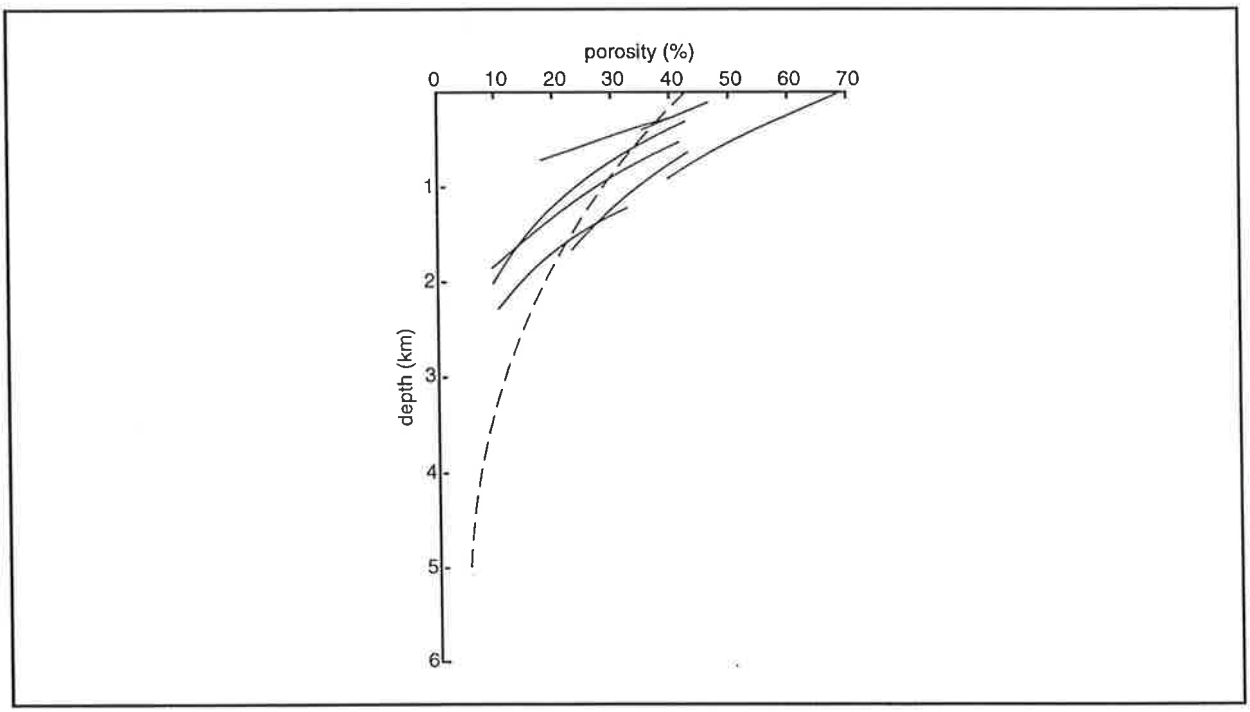

Fig. 3.4. Carbonate porosity gradients (after Selley, 1988). Solid lines = European Cretaceous Chalks, dashed line = Floridan Cenozoic limestones.

parameters measured by all of these tools are affected by the formation porosity, pore fluid composition, and matrix (Schlumberger, 1987). If the fluid and matrix effects are known or can be determined, the tool

response can be related to porosity. All of the modern porosity tools are borehole compensated, to greatly reduce any spurious effects caused by borehole size variations, as well as errors due to tilting of the tool.

The parameters measured by the porosity tools are summarised below. Further details on the porosity tools may be found for example in Schlumberger (1987) or Asquith & Gibson (1982).

Sonic log. The sonic tool measures the shortest time for a compressional sound wave to travel through the formation, which is known as the interval transit time (Δt). Δt is the reciprocal of velocity, and is generally given the units of microseconds per foot ($\mu s/ft$).

Neutron porosity log. The neutron porosity tool measures the hydrogen ion concentration in a formation. In shale-free formations where the porosity is filled with water or oil, the neutron porosity log measures liquid-filled porosity. Whenever pores are filled with gas rather than oil or water, neutron porosity will be lowered, because there is less concentration of hydrogen in gas compared to oil or water. The presence of bound water in the lattice of clay minerals results in spurious porosity measurements in shaly units. In sandstones and dolomites, the measured neutron porosity must be corrected to true porosity using published charts (Schlumberger, 1987). Only in pure limestones is the measured neutron porosity equal to true porosity.

Bulk density log. The bulk density tool measures the electron density in a formation. Electron density can be directly related to the bulk density (ρ_b) of a formation in g/cm^3. The bulk density log (ρ_b) is usually plotted along with a correction curve (Δ_ρ), and wherever the correction curve exceeds 0.20 g/cm^3, the value of the bulk density curve should be considered invalid (Asquith & Gibson, 1982). Formation bulk density is a function of matrix density, porosity, and density of the pore fluid (salt water, fresh mud, or hydrocarbons).

3.4.2 Selection of porosity log for compaction analysis

The sonic log has been selected as the geophysical log to be used in compaction analysis. As previously mentioned, the sonic tool measures the shortest time for a compressional wave to travel through the formation adjacent to the borehole wall. The first sonic pulse to arrive will normally circumvent any vugular or fracture (secondary) porosity developed in the formation (Merkel, 1981). Hence where secondary porosity is widely developed, the sonic log-derived porosity is too low (Schlumberger, 1987). The development of secondary porosity is largely depth-independent, hence the insensitivity of the sonic log to secondary porosity is an advantage in compaction studies.

The borehole compensation of the sonic tool involves averaging the interval transit times for two transmitter-receiver sets, thus cancelling errors from variation in borehole size. Although the nuclear logs (neutron porosity and bulk density) are empirically compensated for hole condition, these logs are more sensitive to borehole condition (Schlumberger, 1987).

The sonic log has the additional advantage of being the most commonly and extensively run geophysical log in exploration wells in the Celtic Sea/South-Western Approaches. The nuclear logs (neutron porosity and bulk density) are often only recorded in the deeper sections of a borehole of specific interest to exploration companies, therefore these logs are not as useful for regional analysis of the compaction of units of all ages.

The adjusted sonic log is a sonic log which has

been drift-corrected using check shot surveys (Schlumberger, 1987). Drift correction of the sonic log is necessary when translating surface seismic time into depth. Sonic velocities (measured at 20000 Hz) may be as much as 3% higher than seismic velocities (measured at roughly 50 Hz) because of velocity dispersion with frequency (Schlumberger, 1987). The effects of sonic drift are not a concern in the compaction methodology, provided mutually consistent data (i.e. all sonic log data) are compared between different wells.

3.4.3 Determining porosity from the sonic log

Wyllie *et al.* (1956) proposed the popular time average equation as a sonic-porosity transform:

$$\Delta t_{log} = \Delta t_{ma}(1-\phi) + \phi \cdot \Delta t_f \qquad .....(3.2)$$

where Δt_{log}, Δt_{ma}, and Δt_f are the sonic log, matrix, and interstitial fluid interval transit times respectively, and ϕ is the porosity. However, at porosities above approximately 30%, it is necessary to apply an empirical 'lack of compaction' correction factor to the time average equation, as it over-estimates porosity (Schlumberger, 1987). Furthermore, in the range 5-25% (Raymer *et al.*, 1980) the time average equation yields porosities which are too low.

Raiga-Clemenceau *et al.* (1988) introduced the following relation for more accurate porosity determination from sonic transit time data:

$$\phi_{sonic} = 1 - \left(\frac{\Delta t_{ma}}{\Delta t_{log}}\right)^{1/x} \qquad .....(3.3)$$

where ϕ_{sonic} is the sonic derived porosity, Δt_{ma} is the interval transit time of the matrix, Δt_{log} is the interval transit time of the formation, and the exponent x is specific to matrix lithology. Hillis (1991) converted sonic velocities from the Upper Cretaceous Chalk to porosities using the above relation for his exhumation study in the South-Western Approaches. However, as the majority of formations in the Celtic Sea/South-Western Approaches do not have the relatively simple monomineralic matrix of the Chalk, it is not possible to determine their absolute porosity from the sonic log alone (Schlumberger, 1987). Although porosity directly describes compaction state, sonic velocity (or its reciprocal, interval transit time) is used here, and in numerous other studies (e.g. Magara, 1976; Lang, 1978; Bulat & Stoker, 1987; Hillis *et al.*, 1994; Hillis, 1995*b*) as an indicator of compaction because it is strongly dependent on porosity.

3.5 Basic Principles of the Compaction Methodology

3.5.1 Introduction

Since depth-controlled compaction is largely irreversible, units that are shallower than their maximum burial-depth will be overcompacted with respect to their present burial-depth (e.g. Magara, 1976; Lang, 1978; Bulat & Stoker, 1987; Hillis, 1991; Issler, 1992; Hillis *et al.*, 1994). It is assumed that all units follow a normal compaction (i.e. porosity) trend with burial, and that compaction is not reversed by subsequent exhumation. With these assumptions, the amount of elevation of exhumed sedimentary rocks above their maximum burial-depth (termed apparent exhumation) is given by the displacement, along the depth axis, of the observed compaction trend from the normal, undisturbed trend (Fig. 3.5).

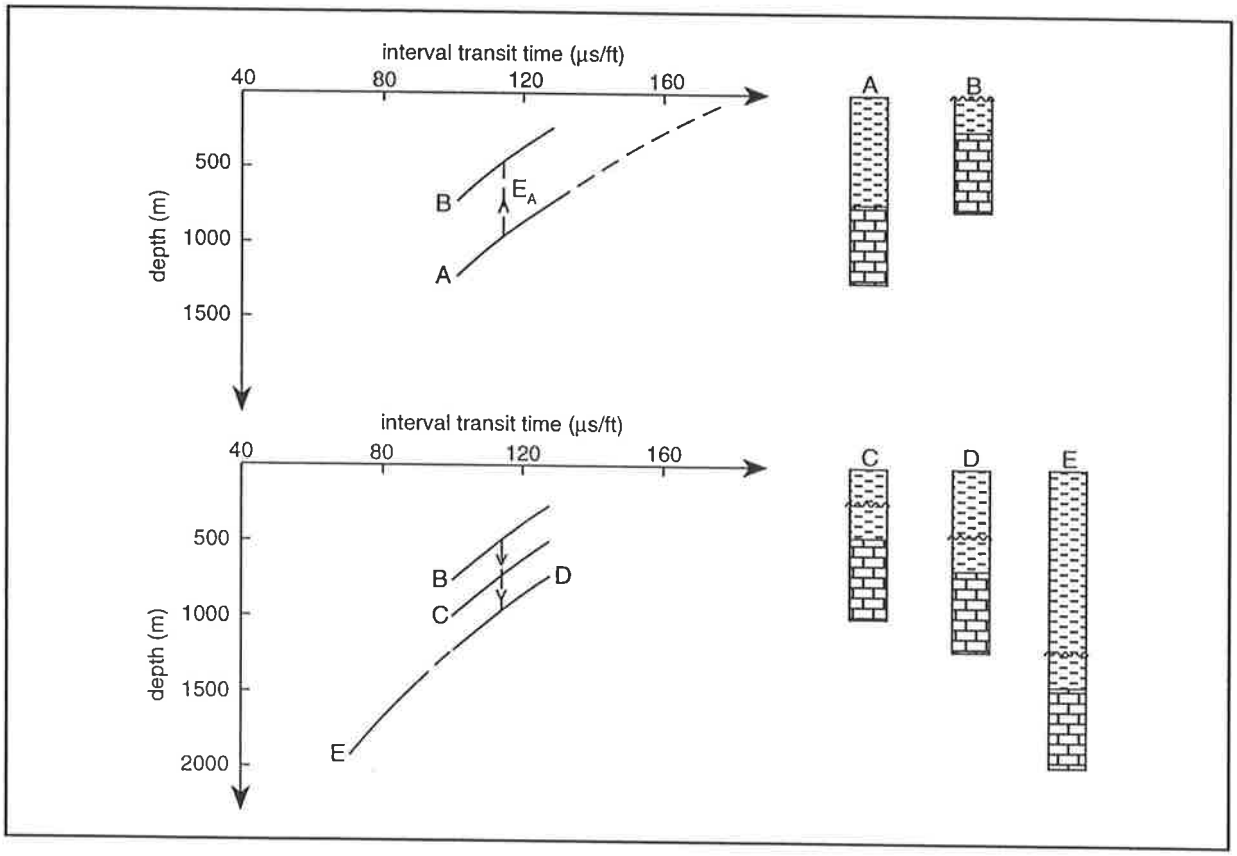

Fig. 3.5. Interval transit time evolution for a chalk unit (brick pattern) during burial (A), subsequent exhumation (B), and post-exhumational burial (C, D and E). The apparent exhumation (E_A) is the amount of exhumation not reversed by subsequent burial (i.e. height above maximum burial-depth).

3.5.2 Previous studies involving compaction-based quantification of exhumation

The velocities of shales have generally been analysed in the compaction-based quantification of exhumation (e.g. Jankowsky, 1962; Marie, 1975; Magara, 1976; Lang, 1978; Wells, 1990; Issler, 1992; Skagen, 1992; Japsen, 1993). Shales have generally been preferred to other lithologies because of the, usually implicit, assumption that shales show the most predictable and directly burial-depth controlled compaction (i.e. velocity/depth) trends. However, lithologies other than shales have been demonstrated to give reliable results. Bulat & Stoker (1987) quantified exhumation in the Southern North Sea using every stratigraphic unit above and including the Carboniferous, with the exception of the Upper Permian Zechstein evaporites. Hillis (1991) showed that compaction in the Chalk of the South-Western Approaches was strongly burial-depth controlled, and used velocities in the Chalk to quantify exhumation. Velocities in the Chalk and the Kimmeridge Clay of the Inner Moray Firth yield statistically similar exhumation magnitudes (Hillis *et al.*, 1994), as do velocities in the Chalk, the Bunter Shale and the Bunter Sandstone of the Southern North Sea (Hillis, 1995*b*).

3.5.3 The advantages of using multiple stratigraphic units in compaction analyses

The use of multiple stratigraphic units in the compaction-based analysis of maximum burial-depth

has several important advantages. Firstly, and of particular relevance to the Celtic Sea/South-Western Approaches, often no single stratigraphic unit is encountered in all the wells in an area of study. Hence in order to quantify apparent exhumation in as many wells as possible, it is necessary to analyse several stratigraphic units. Secondly, assuming exhumation post-dated the youngest unit analysed, and only one exhumation event occurred, all the stratigraphic units in the same well should yield the same magnitude of exhumation. Hence, by using the mean value from several stratigraphic units in the same well, the anomalous influence of any burial-depth-independent, sedimentological and/or diagenetic processes, that may effect the compaction state of a particular unit in the well, is lessened.

Another advantage of analysing multiple stratigraphic units is the potential for determining the age of exhumation. Hillis (1992*b*) showed that exhumation at Ashmore Reef in the Timor Sea post-dated overcompacted Miocene sedimentary rocks, and pre-dated normally compacted Pliocene sedimentary rocks. Figure 3.6 (a) shows a theoretical burial history plot for several wells in a basin in which there has been two periods of exhumation, both followed by further burial. Units A and B, which predate the first event, yield higher apparent exhumation estimates than Units C and D (Fig. 3.6(b)). Units C and D in turn yield higher apparent exhumation estimates than Unit E, which is normally compacted (Fig. 3.6(b)). Units A and B exhibit the same amount of apparent exhumation, as do Units C and D (Fig. 3.6(c)). Clearly there is more scatter in real data, however, this example illustrates the potential of the analysis of multiple stratigraphic units for determining the age of exhumation.

3.6 Quantifying Exhumation and Maximum Burial-Depth

3.6.1 Quantifying exhumation

Apparent exhumation (E_A) is the vertical displacement of the Δt/depth trend (for a particular unit in a particular well) from that of the normal compaction relation (Fig. 3.5). Apparent exhumation can be estimated graphically from the plots of mean Δt against depth to unit midpoint. However, in practice it is determined numerically using the equation:

$$E_A = \frac{1}{m}\left(\Delta t_u - \Delta t_o\right) - d_u \qquad \text{.....(3.4)}$$

where m is the gradient, and Δt_o the surface interval transit time, of the normal compaction relation (Table 3.3), Δt_u is the mean interval transit time, and d_u the midpoint depth, of the unit in the well under consideration (all data and results are listed in Appendix I).

3.6.2 Exhumation, apparent exhumation, and maximum burial-depth

The quantity determined from Δt data is referred to as *apparent* exhumation because it is exhumation not reversed by subsequent burial. It is not necessarily the same as the amount of exhumation that occurred at the time the rocks were being denuded. If renewed burial follows exhumation, the magnitude of apparent exhumation determined from Δt data is reduced by the amount of that subsequent burial (Fig. 3.5, well C). Once the unit again reaches its maximum burial-

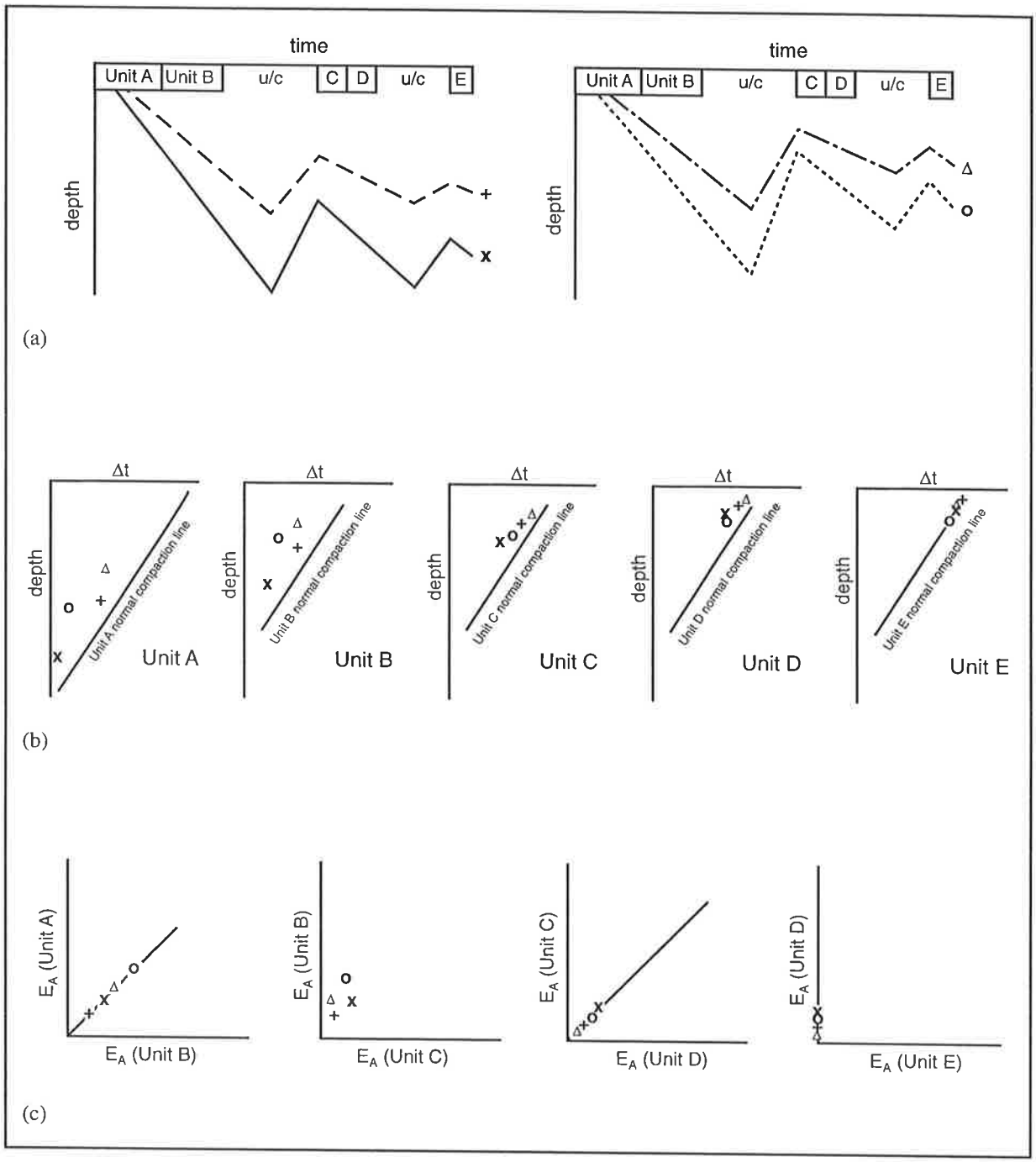

Fig. 3.6. (a) Theoretical burial history plot for four wells in a basin which has undergone two distinct exhumation events, both followed by further burial. All wells in the basin have similar burial histories, with slightly different magnitudes of exhumation and burial. (b) x, +, o, and Δ are the Δt's in the given unit for different wells in the basin. Units A and B exhibit greater apparent exhumation than Units C and D, which in turn exhibit greater apparent exhumation than Unit E, which is normally compacted. (c) Units A and B yield the same apparent exhumation values, as do Units C and D. Unit B exhibits greater apparent exhumation than Unit C, and Unit D exhibits greater apparent exhumation than Unit E, which is normally compacted and exhibits no exhumation.

depth (Fig. 3.5, well D), it is normally compacted, and no evidence of previous exhumation can be detected by this method. In general:

total exhumation at the time the rocks were being denuded (E_T) = apparent exhumation (E_A) + post-exhumational burial (B_E)

	E_T	=	E_A	+	B_E
Figure 3.5, well B (km):	0.5	=	0.5	+	0
Figure 3.5, well C (km):	0.5	=	0.25	+	0.25
Figure 3.5 well D (km):	0.5	=	0	+	0.5.

Maximum burial-depth (B_T) is given by the sum of present (B_P) burial-depth and apparent exhumation (E_A):

$$B_T = E_A + B_P$$

Figure 3.7 further illustrates these fundamental relationships with respect to wells A and C from Figure 3.5.

3.6.3 Uplift, erosion, and exhumation

Previous workers (e.g. Bulat & Stoker, 1987; Hillis, 1991) have used the term uplift in reference to the displacement of rocks with respect to the surface which is quantified using the compaction methodology. England & Molnar (1990) defined three different uses of the term uplift which depend upon the frame of reference:

- displacement of the earth's surface with respect to the geoid (surface uplift);
- displacement of rocks with respect to the geoid (uplift of rocks), and;
- displacement of rocks with respect to the surface (exhumation).

It is important to distinguish these different quantities because only surface uplift requires work against gravity, and hence a tectonic driving force. Uplift of rock or exhumation may be caused solely by changes in sedimentary or erosional base level (e.g. sea level changes). Following England & Molnar (1990), the term exhumation is now preferred for the description of the displacement of rocks with respect to the surface, as quantified by the compaction methodology.

The term erosion as used by Hillis *et al.* (1994) and others is also avoided, because this refers not only to the process of elevating rocks with respect to the surface, but also to the removal and transport of weathered material. Only removed rocks are eroded; however, the entire rock column is exhumed as a result of erosion.

3.7 Selection of Stratigraphic Units for Analysis

Stratigraphically-equivalent units that exhibit a vertically- and laterally-consistent porosity/depth relation are required for the determination of maximum burial-depth. The sonic velocities of the following stratigraphic units were used in the analysis of exhumation in the Celtic Sea/South-Western Approaches:

- Danian Chalk;
- Upper Cretaceous Chalk;
- Lower Cretaceous Greensand/Gault Clay;
- Lower Cretaceous Wealden;
- Upper Jurassic mudstone;
- Triassic Mercia Mudstone (above salt);
- Triassic Mercia Mudstone (below salt), and;
- Triassic Sherwood Sandstone.

Ideally, Tertiary units younger than the Danian

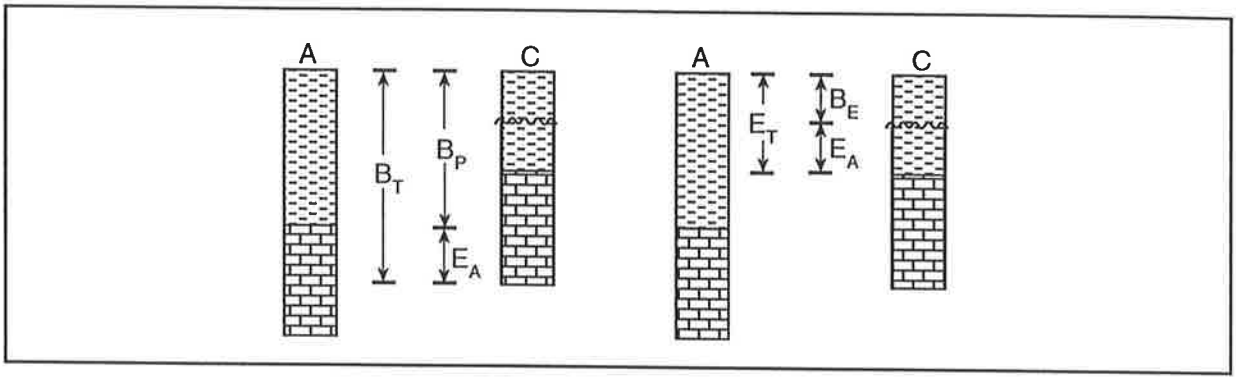

Fig. 3.7. Relationship between apparent exhumation (E_A), present burial-depth (B_P), maximum burial-depth (B_T), post-exhumational burial (B_E), and exhumation at the time of denudation (E_T), for the mid-point of the chalk unit illustrated in Figure 3.5. Wells A and C are the same as in Figure 3.5, i.e. well A has undergone normal, undisturbed burial (no exhumation), well C has been buried, exhumed, and partially re-buried.

Chalk would have been analysed in order to further constrain the age of uplift, however, post-Danian units are not widely encountered in exploration wells in the area, and even where encountered, log data are not always available.

Inspection of log data reveals that there is too much lateral facies variation within the Middle and Lower Jurassic to enable these units to be incorporated. The highly variable limestone/shale ratios in the Middle and Lower Jurassic has a first order effect on mean Δt which makes them unsuitable for compaction-based analysis of exhumation. Salt does not compact with depth, hence the salt interval within the Mercia Mudstone Group was excluded from the analysis, and the Mercia Mudstone Group was split into intervals above and below the salt.

The extremely variable thickness (0 - 1.5 km) of the low density salt must be taken into account in the analysis of compaction of the units below the salt (i.e. the Mercia Mudstone below salt and the Sherwood Sandstone). The compaction of units underlying the salt is less than that which it would be at the same depth if overlain by units of normal, higher density. In wells where salt is present, the thickness of the salt interval was weighted by the ratio of its average density to the average density of the units immediately above and below. This correction reduces the effective burial-depth of units overlain by low density salt.

The tops and bases of the units analysed were consistently picked from vertically-compressed (1:4000 depth-scale) plots of the sonic and gamma ray logs. Such compressed plots facilitate the picking of tops and bases, which, for internal consistency within this study, were often slightly modified from those on operators' composite logs (because different operators often have slightly different picks). The picked depths of tops and bases of the units analysed are listed in Appendix I.

The stratigraphic units analysed, and their definitions, are briefly summarised below.

Triassic Sherwood Sandstone. The top of the Sherwood Sandstone was picked at the top of the first sandstone below the Mercia Mudstone Group. The base of the Sherwood Sandstone was picked at the base of the last sandstone in the sequence (often the top of a conglomeratic unit). The unit is predominantly sandstone, with rare shale interbeds. The Sherwood Sandstone is of Scythian age in the

northern basins of the study area (e.g. Musgrove *et al.*, 1995). In the southern basins, the suggested age of the sandstones below the Mercia Mudstone Group varies between Late Permian to mid-Triassic (Evans, 1990).

Triassic Mercia Mudstone (below salt). The Mercia Mudstone (below salt) comprises the red/brown mudstones with abundant anhydrite beneath the Carnian salt. Its top was picked at the base of the salt, and its base picked at the top of the first underlying sandstone (i.e. top of the Sherwood Sandstone). This unit is probably Carnian - Ladinian in age, but may extend to Anisian - Scythian.

Triassic Mercia Mudstone (above salt). The top of the Mercia Mudstone (above salt) was picked, where the Rhaetic is present, at the base of the basal Rhaetic limestone, or by the change from grey Rhaetic shales to red/brown mudstones with abundant anhydrite. The base of the Mercia Mudstone (above salt) was picked at the top of the Carnian salt, or where the salt is not present, at the top of the Carnian as indicated on the operators' composite logs. This unit is Norian in age.

Upper Jurassic mudstone. The Upper Jurassic cannot be subdivided into consistent correlatable units because of its lateral lithological variability. Hence the Upper Jurassic was treated as a single unit, picked biostratigraphically (following the data on the composite logs), with its top at the top of the Tithonian, and base at the base of the Oxfordian. The Upper Jurassic comprises predominantly shales and mudstones, with interbedded sandstones and limestones. Although sub-units within the Upper Jurassic cannot be correlated regionally, because of lateral lithological variability, there is a gross consistency in the bulk lithological composition of the Upper Jurassic. In interpreting the apparent exhumation results from the Upper Jurassic, it must be remembered that they may be influenced not only by maximum burial-depth, but also by lateral lithological variability. However, it was considered necessary to include the Upper Jurassic because several wells on the inversion axes in the area do not encounter the other, more lithologically consistent units.

Lower Cretaceous Wealden. The Wealden comprises silty/shaly sandstones, with shale/ claystone interbeds, and minor coal and limestone intervals. The Wealden was picked biostratigraphically (following the data on the composite logs), with its base at the base of the Berriasian and its top at the top of the Barremian or in the Early Aptian.

Lower Cretaceous Greensand/Gault Clay. The Lower and Upper Greensand comprise Aptian - Albian aged sandstones with claystone interbeds. The Gault Clay lies stratigraphically between the Upper and Lower Greensand units, but is not a distinct, correlatable unit throughout the Celtic Sea/South-Western Approaches. Furthermore, the Upper and Lower Greensand are rarely differentiated on composite logs in the area. Hence the Upper and Lower Greensand, and intervening Gault Clay, have been treated as a single unit. Some wells intersect Aptian - Albian sandstones classified as Wealden on the composite logs. These Aptian - Albian sandstones have been classified as Greensand/Gault Clay herein to ensure consistency. Albian aged basalts and tuffs occur in a number of wells in the Melville Basin. These volcanics have been excluded from the study.

Upper Cretaceous Chalk. The Upper, Middle and Lower Chalk were treated as a single unit, which

ranges in age from Cenomanian to Maastrichtian. The base of the Chalk is marked by a distinctive (downwards) decrease in velocity and increase in natural gamma ray. If the Upper Cretaceous Chalk is overlain by Danian Chalk its top is picked biostratigraphically following the data on the operators' composite logs. If the Upper Cretaceous Chalk is overlain by the younger Tertiary units, its top is marked by a distinctive (upwards) decrease in velocity and increase in natural gamma ray. Some sections of the Chalk, where the sonic log data are unreliable (often at the top of the logging run) were omitted, and the resultant mid-point depth adjusted to allow for the omitted intervals.

Danian Chalk. Danian Chalk was taken as that part of the chalk identified biostratigraphically as being of Tertiary, rather than Cretaceous, age.

3.8 Interval Transit Time/Depth Plots and Normal Compaction Relations

Since apparent exhumation is given by the displacement, on the depth axis, of a given Δt/depth point from the normal Δt/depth relation (i.e. that unaffected by exhumation), *the crux of apparent exhumation determination lies in the selection of the normal or undisturbed Δt/depth relation.*

3.8.1 Linear versus exponential normal compaction relations

The form (linear, exponential etc.) of the normal compaction relation should be dictated by the porosity/depth curve because Δt decreases with burial-depth due to its dependence on porosity. Figure 3.2 shows than the relationship between porosity and depth in sandstones is linear, whilst Figures 3.3 and 3.4 show that mudstones and some limestones have an exponential porosity/depth relationship. Schneider *et al.* (1994) suggested the most rapid reduction of porosity with burial in mudstones (i.e. the most exponential part of the porosity/depth relation) occurs at the beginning of burial in the near surface (Fig. 3.1). The porosity/depth relation then becomes close to linear with further burial (Fig. 3.1). Apparent exhumation estimates derived for the Upper Cretaceous Chalk using both exponential and linear Δt/depth relations were crossplotted to determine whether a linear Δt/depth relation could be used to represent the normal compaction relation (Fig. 3.8). Statistically, the apparent exhumation estimates derived using the two different normal compaction relations are essentially the same (Fig. 3.8). As a result, the normal compaction relations used in this thesis were taken to be linear in form.

3.8.2 Normal compaction relations and reference wells

The mean sonic Δt of the stratigraphic units analysed was plotted against the depth of the midpoint of the unit (Figs. 3.9 & 3.10). In an area subject to exhumation, the wells with the highest Δt (lowest velocity) for their given burial-depth should be taken to be normally compacted, provided their relatively high Δt is not due to phenomena that may inhibit normal compaction (such as overpressure or hydrocarbon-filled porosity). For a linear decrease of Δt with depth, any two wells on Figures 3.9 and 3.10 that can be linked by a straight line that has no points falling to its right, less compacted side, define normal compaction. These are termed the reference wells.

The above selection criteria does not always define a unique pair of reference wells for the normal compaction relation (Figs. 3.9 & 3.10). An additional constraint on the selection of the reference wells for

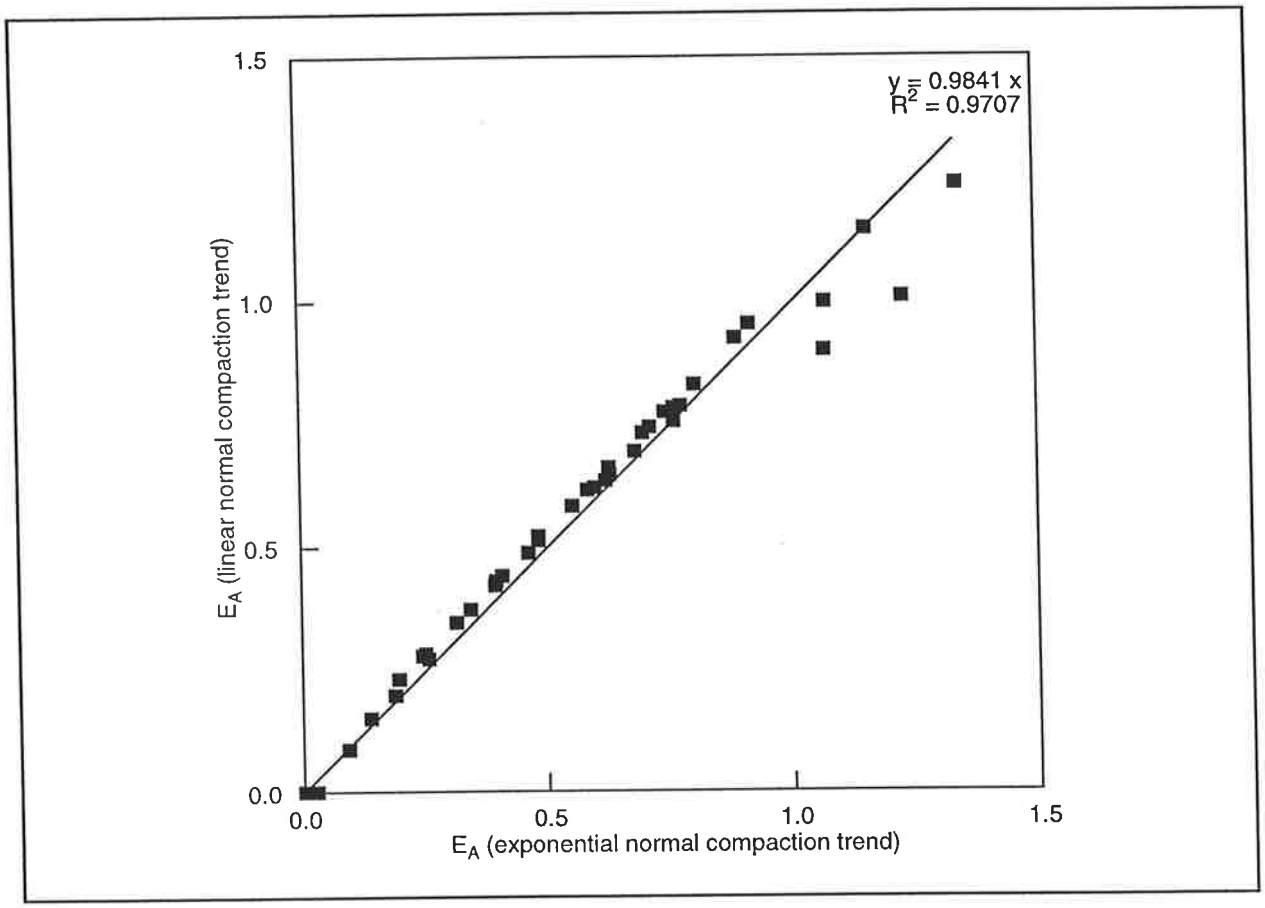

Fig. 3.8. Cross-plot of apparent exhumation values (in km) determined using both linear and exponential normal compaction relationships for the Upper Cretaceous Chalk. The best fit linear regression line with resultant equation and regression co-efficient (R^2) are also shown.

the normal compaction relation is required. Raiga-Clemenceau *et al.* (1988) demonstrated that when porosities are above 50%, (i.e. in unconsolidated sediments near the surface) the relationship between Δt and porosity changes from Equation 3.3 to a "compressibility" equation, as there is no continuity of the solid matrix frame for porosities above 50%. The normal compaction relation between Δt and depth would therefore also change for porosities above 50%. The additional constraint upon the selection of the reference wells is thus that the normal compaction relation should pass through a defined depth range for near surface porosities. Figures 3.2, 3.3, and 3.4 have been used to establish the near surface porosity-depth constraints for sandstones, mudstones, and limestones respectively. These near surface constraints upon the normal compaction relations are given in Table 3.2. For all the units analysed, except the Upper Jurassic, the above criteria clearly define the normal compaction relation/reference wells (Figs. 3.9 & 3.10).

None of the potential normal compaction relations for the Upper Jurassic pass through the near surface porosity-depth constraint for mudstones. The two closest relations have surface intercepts of approximately 130 and 230 µs/ft. There is no entirely satisfactory method of choosing between the two possible normal compaction relations. However, that with a surface intercept of 230 µs/ft yields apparent exhumation values which agree more closely with

Stratigraphic unit	Lithology	Porosity range	Interval transit time range	Depth range
Danian Chalk	chalk	50%	160 μs/ft	0 - 500 m
Upper Cretaceous Chalk	chalk	50%	160 μs/ft	0 - 500 m
Greensand/Gault Clay	50% sandstone 50% mudstone	50%	160 - 170 μs/ft	0 - 500 m
Wealden	50% sandstone 50% mudstone	50%	160 - 170 μs/ft	0 - 500 m
Upper Jurassic	mudstone	50%	160 μs/ft	0 - 500 m
Mercia Mudstone (above salt)	mudstone	50%	160 μs/ft	0 - 500 m
Mercia Mudstone (below salt)	mudstone	50%	160 μs/ft	0 - 500 m
Sherwood Sandstone	sandstone	35 - 50%	110 - 170 μs/ft	0 m

Table 3.2. Near surface constraints on normal compaction relations. Interval transit times for sandstones and chalks were calculated using Equation 3.3. Equation 3.3 is not appropriate for mudstones (see Section 6.5.1), hence mudstone interval transit times were calculated using Equation 3.2 with a correction factor. The Greensand/Gault Clay and Wealden are mixtures of sandstone and mudstone.

those from the Wealden (which is present in the same well as the Upper Jurassic more than any other unit analysed). Furthermore, the normal compaction relation with a surface intercept of 130 μs/ft results in very low apparent exhumation estimates for the wells in the strongly (stratigraphically) inverted Cardigan Bay Basin. Hence the normal compaction relation with a surface intercept of 230 μs/ft was selected. It is appreciated that the above justification for the selection of the normal compaction relation for the Upper Jurassic is potentially a circular argument. However, there is no entirely satisfactory method of choosing between the two possible normal compaction relations.

As previously stated, the crux of apparent exhumation determination from compaction (Δt) data lies in the selection of the normal compaction relation, and hence in the selection of two reference wells as defined above. The success (or otherwise) of the compaction methodology depends upon the accuracy of the normal compaction relation. A normal compaction relation defined by two wells at maximum burial-depth cannot exactly represent the undisturbed, pre-exhumational burial depth/Δt relationship in all wells. The normal compaction relation in different wells would exhibit some scatter around the defined normal compaction relation. The amount of this scatter is unclear because exhumation cannot be separated from other, broadly sedimentological/ diagenetic influences on the porosity/depth relationship. If there was an unlimited amount of porosity data from wells drilled in structurally low areas of maximum burial-depth, a scatter may be observed around the proposed normal compaction relation, and hence a more accurate estimate of the normal compaction relation could be made. The proposed normal compaction relation may even itself be shown to be overcompacted. Each of the formations analysed in the Celtic Sea/South-Western Approaches has more than two wells on or

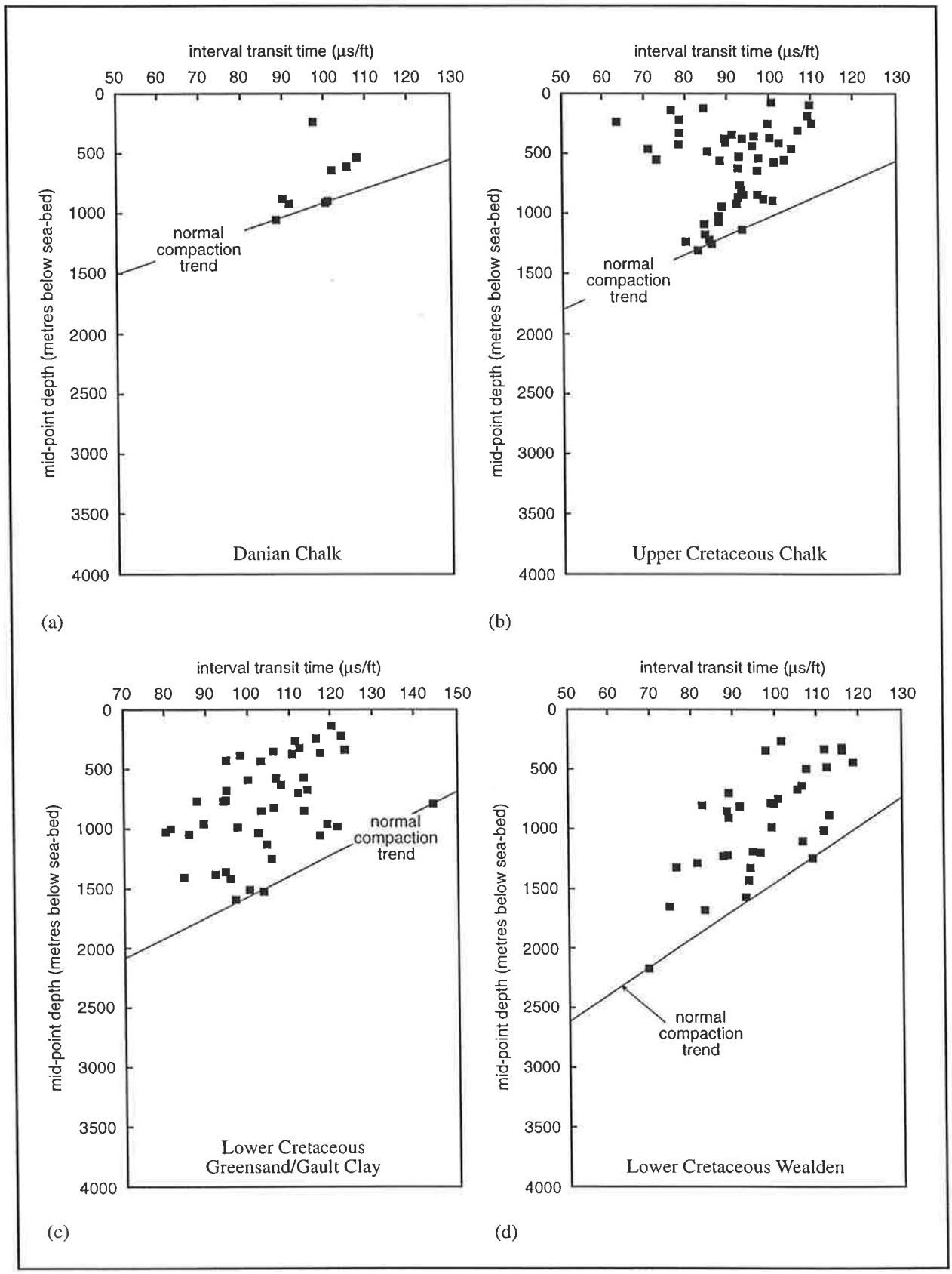

Fig. 3.9. Interval transit time/mid-point depth plots for units analysed in the Celtic Sea/South-Western Approaches (a) the Danian Chalk, (b) the Upper Cretaceous Chalk, (c) the Lower Cretaceous Greensand/Gault Clay, and (d) the Lower Cretaceous Wealden.

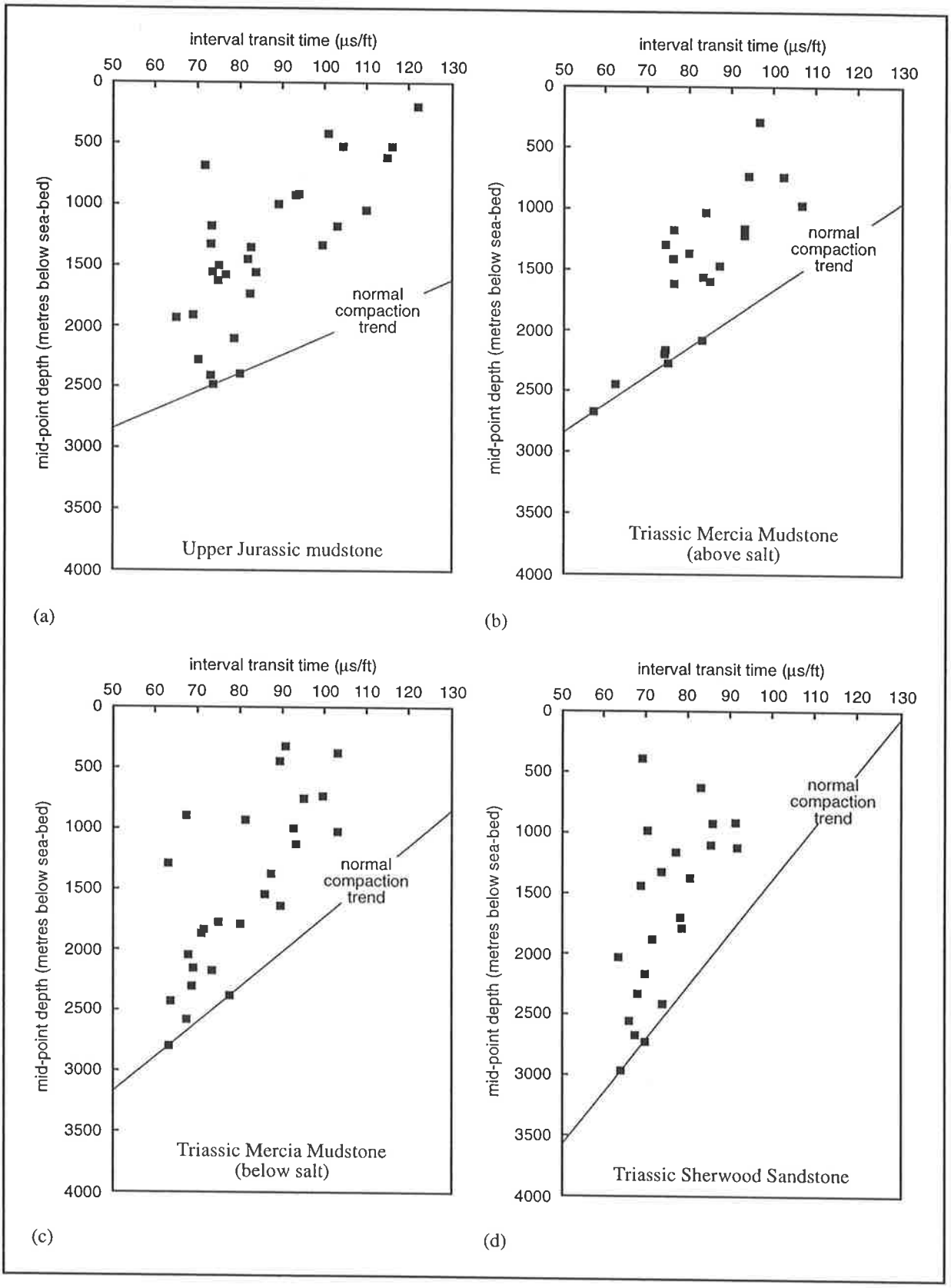

Fig. 3.10. Interval transit time/mid-point depth plots for units analysed in the Celtic Sea/South-Western Approaches (a) the Upper Jurassic mudstone, (b) the Triassic Mercia Mudstone (above salt), (c) the Triassic Mercia Mudstone (below salt), and (d) the Triassic Sherwood Sandstone.

near the normal compaction relation (Figs. 3.9 & 3.10). This increases the confidence that the normal compaction relations defined for each formation by the above method are the best possible approximations of the true normal compaction relations, and are not based on wells with anomalously low velocities.

It must be assumed that the reference wells defining the normal compaction relation are at maximum burial-depth, and have not themselves been exhumed. In the event that the reference wells have been exhumed from maximum burial-depth, all apparent exhumation values will be underestimated by the amount of exhumation undergone by the reference wells. Compaction-based analyses of exhumation should cover as wide a geographic area as possible (within the constraint that the lithology of the units analysed does not vary laterally) in order to ensure that the reference wells are at maximum burial-depth.

Table 3.3 summarises the reference wells and linear relations defining normal compaction for each of the units analysed.

Stratigraphic unit	Reference wells	Mean interval transit time (μs/ft)	Mid-point depth (mbsb)	Equation of normal compaction relationship
Danian Chalk	73/13-1	87.9	1059	$\Delta t = 178 - 0.085\ d$
	Garlizenn-1	100.4	913	
Upper Cretaceous Chalk	73/01-1	93.2	1137	$\Delta t = 167 - 0.065\ d$
	73/13-1	82.4	1303	
Greensand/Gault Clay	56/14-1	144.4	796	$\Delta t = 190 - 0.057\ d$
	Garlizenn-1	103.3	1521	
Wealden	56/18-1	108.7	1234	$\Delta t = 161 - 0.042\ d$
	Glazenn-1	69.0	2172	
Upper Jurassic	48/19-1	79.4	2393	$\Delta t = 233 - 0.064\ d$
	49/14-3	73.4	2487	
Mercia Mudstone (above salt)	49/29-1	74.8	2279	$\Delta t = 171 - 0.042\ d$
	73/01-1	83.0	2084	
Mercia Mudstone (below salt)	73/06-1	62.8	3000	$\Delta t = 160 - 0.035\ d$
	106/28-1	77.0	2505	
Sherwood Sandstone	73/02-1	69.5	2908	$\Delta t = 132 - 0.023\ d$
	73/06-1	64.0	3171	

Table 3.3. Data defining normal compaction relations (Δt = interval transit time, d = mid-point depth (in m), mbsb = metres below sea-bed).

Chapter 4

Tertiary Exhumation in the Celtic Sea/South-Western Approaches

4.1 Introduction

This chapter compares apparent exhumation results from the eight stratigraphic units analysed in the Celtic Sea/South-Western Approaches. The exhumation and maximum burial-depth of the Celtic Sea/South-Western Approaches are then described and compared with published studies, and the direct implications of these results for models of basin evolution are outlined. The exhumation and maximum burial-depth results presented herein are incorporated into the more detailed modelling in Chapters 6 - 8 of the subsidence/uplift history of the Celtic Sea/South-Western Approaches.

4.2 Comparison of Apparent Exhumation Results from the Eight Stratigraphic Units Analysed

If maximum burial-depth is the primary control on the compaction (as expressed by Δt) of the eight stratigraphic units analysed in the Celtic Sea/South-Western Approaches, and burial to, and exhumation from, maximum depth post-dated the deposition of the youngest unit analysed, then all units analysed in the same well should yield similar apparent exhumation values. Burial-depth-independent sedimentological and/or diagenetic processes would be expected to have a unique effect on the compaction trend of any given lithology, and their associated under- or over-compaction would not be expected to be mirrored in other lithologies/units. Hence if burial-depth-independent, sedimentological and/or diagenetic processes exert a primary control on compaction, the different units analysed in the same well would be expected to yield inconsistent apparent exhumation values. To assess whether all units analysed in the same well yield statistically similar apparent exhumation values, the statistical test outlined in the following section was applied.

4.2.1 Statistical testing of apparent exhumation results

Previous studies which compare apparent exhumation estimates from analysis of multiple units have used regression analyses to determine least-squares, best-fit linear relationships between the apparent exhumation values from the different units, and then carried out statistical tests such as the t-test on the associated co-efficients of correlation (e.g. Bulat & Stoker, 1987; Hillis, 1995*b*). Whilst such statistical tests are valid for establishing whether apparent exhumation estimates from different formations are related linearly, these tests do not establish whether a one-to-one relationship exists (i.e. that estimates from different formations in an individual well are statistically similar). To test whether a one-to-one relationship exists between estimates from different formations, the one-tailed statistical methodology of Draper & Smith (1981) for testing a one-to-one linear hypothesis against a fitted regression line is appropriate. Draper & Smith's (1981) methodology is outlined below.

Apparent exhumation results from the eight units analysed were plotted against each other in order to check their consistency (Figs. 4.1 - 4.4). The apparent exhumation estimates were then tested for a statistically significant deviation from the one-to-one lines shown in Figures 4.1-4.4. To test a one-to-one linear hypothesis against a fitted regression line:

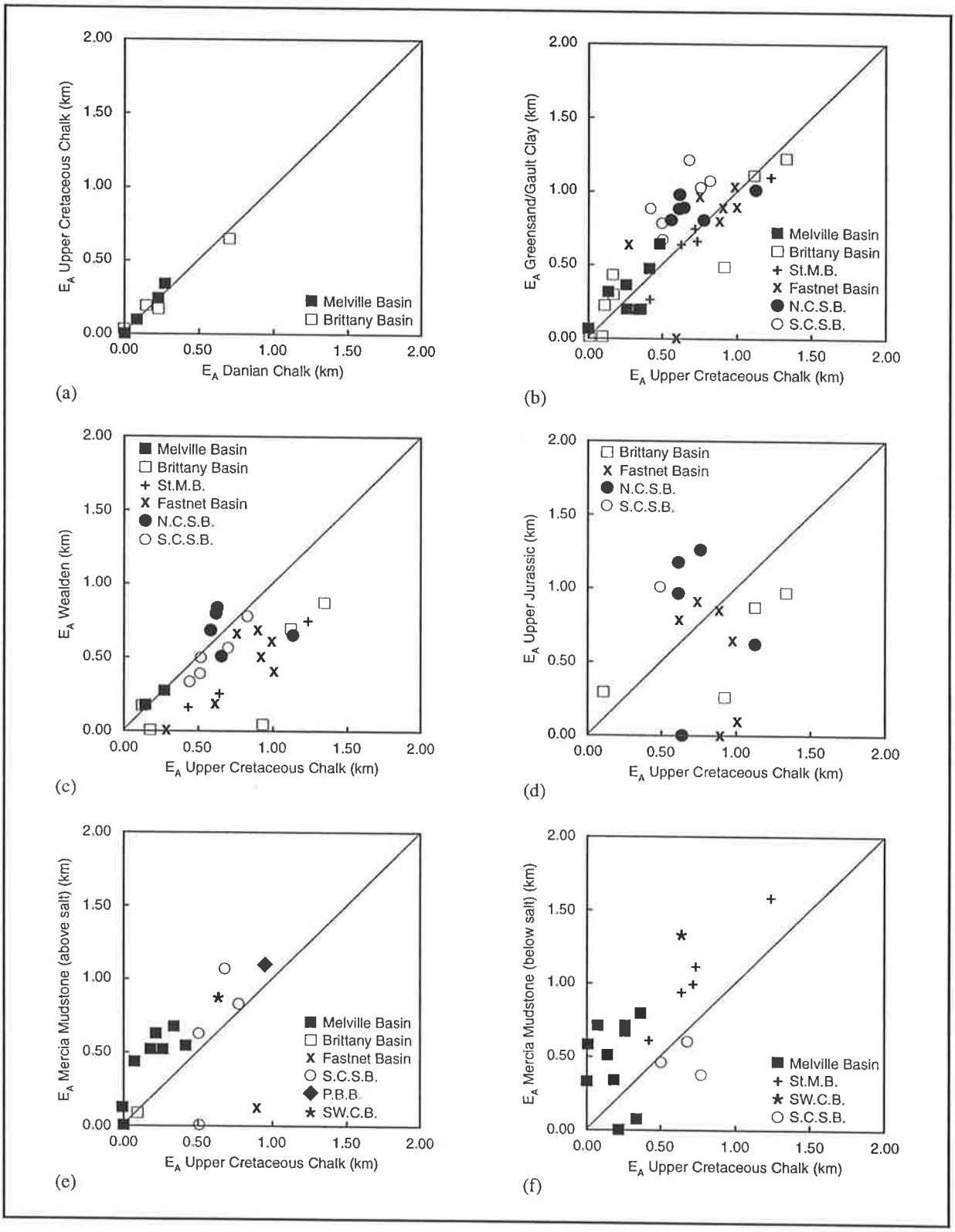

Fig. 4.1. Crossplots of apparent exhumation (E_A, in kilometres) derived from the eight stratigraphic units studied: (a) Upper Cretaceous Chalk vs Danian Chalk, (b) Greensand/Gault Clay vs Upper Cretaceous Chalk, (c) Wealden vs Upper Cretaceous Chalk, (d) Upper Jurassic vs Upper Cretaceous Chalk, (e) Mercia Mudstone (above salt) vs Upper Cretaceous Chalk, and (f) Mercia Mudstone (below salt) vs Upper Cretaceous Chalk. St.M.B. = St. Mary's Basin, N.C.S.B. = North Celtic Sea Basin, S.C.S.B. = South Celtic Sea Basin, P.B.B. = Plymouth Bay Basin, SW.C.B. = South-West Channel Basin.

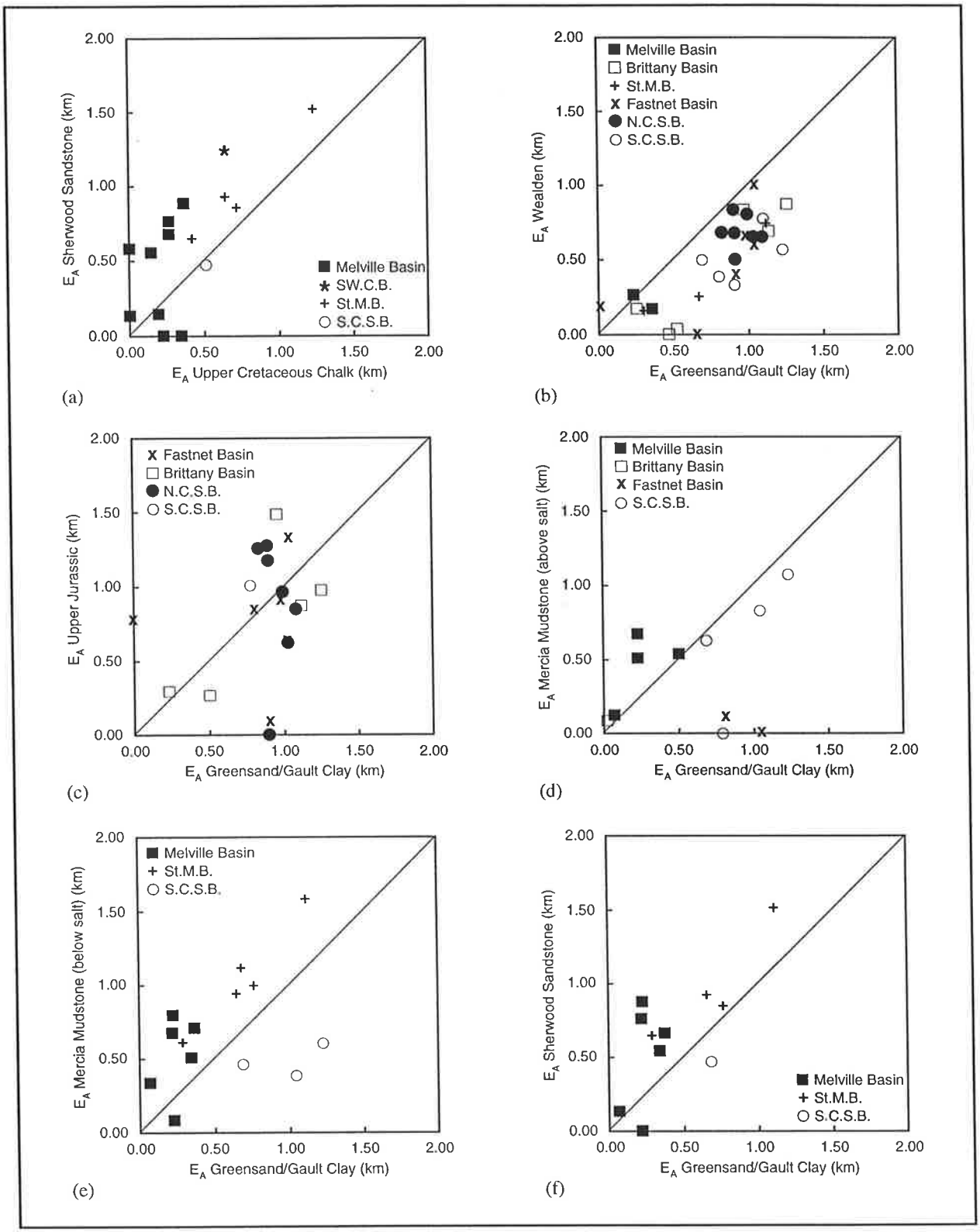

Fig. 4.2. Crossplots of apparent exhumation (E_A, in kilometres) derived from the eight stratigraphic units studied: (a) Sherwood Sandstone vs Upper Cretaceous Chalk, (b) Wealden vs Greensand/Gault Clay, (c) Upper Jurassic vs Greensand/Gault Clay, (d) Mercia Mudstone (above salt) vs Greensand/Gault Clay, (e) Mercia Mudstone (below salt) vs Greensand/Gault Clay, and (f) Sherwood Sandstone vs Greensand/Gault Clay. St.M.B. = St. Mary's Basin, N.C.S.B. = North Celtic Sea Basin, S.C.S.B. = South Celtic Sea Basin, SW.C.B. = South-West Channel Basin.

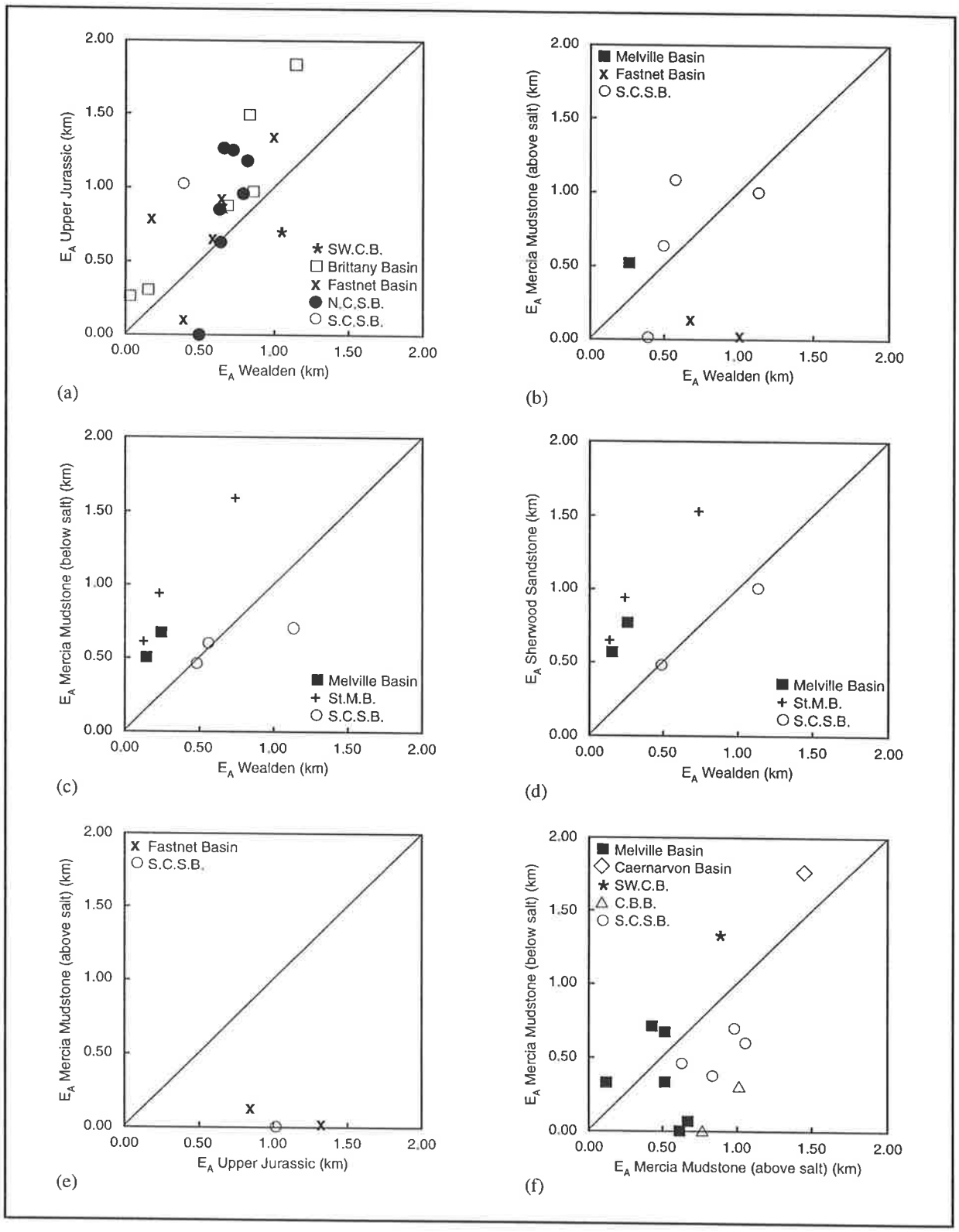

Fig. 4.3. Crossplots of apparent exhumation (E_A, in kilometres) derived from the eight stratigraphic units studied: (a) Upper Jurassic vs Wealden, (b) Mercia Mudstone (above salt) vs Wealden, (c) Mercia Mudstone (below salt) vs Wealden, (d) Sherwood Sandstone vs Wealden, (e) Mercia Mudstone (above salt) vs Upper Jurassic, and (f) Mercia Mudstone (above salt vs below salt). St.M.B. = St. Mary's Basin, N.C.S.B. = North Celtic Sea Basin, S.C.S.B. = South Celtic Sea Basin, SW.C.B. = South-West Channel Basin, C.B.B. = Cardigan Bay Basin.

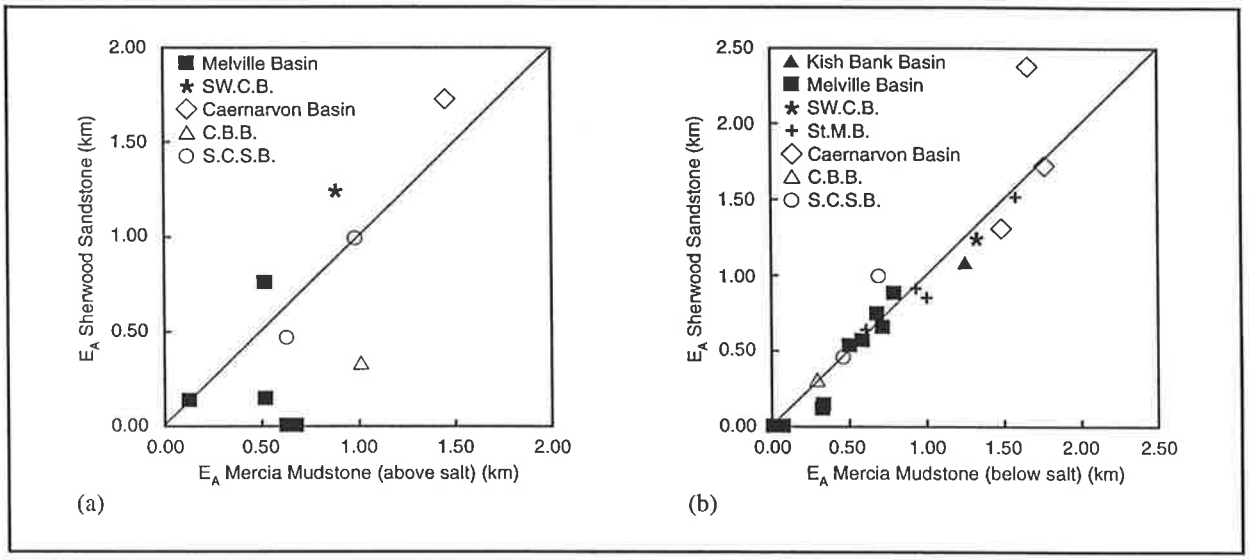

Fig. 4.4. Crossplots of apparent exhumation (E_A, in kilometres) derived from the eight stratigraphic units studied: (a) Sherwood Sandstone vs Mercia Mudstone (above salt) and (b) Sherwood Sandstone vs Mercia Mudstone (below salt). St.M.B. = St. Mary's Basin, S.C.S.B. = South Celtic Sea Basin, SW.C.B. = South-West Channel Basin, C.B.B. = Cardigan Bay Basin.)

- the regression of y on x was fitted (i.e. the E_A estimates from one formation were regressed against the other formation), and the residual sum of squares, SS_1, was calculated:

$$SS_1 = \sum_{i=1}^{n} \left(y_i - \hat{a} - \hat{b}x_i \right)^2 \qquad \text{.....(4.1)}$$

where y_i is the 'i'th E_A estimate from one formation, x_i is the 'i'th E_A estimate from the other formation, $\hat{a}$ and $\hat{b}$ are the coefficients of the regression line.

Under the null hypothesis that a one-to-one relationship exists between the E_A estimates from different formations:

- the sum of the squares of the differences between individual E_A data pairs, SS_2, was calculated:

$$SS_2 = \sum_{i=1}^{n} \left(y_i - x_i \right)^2 \qquad \text{.....(4.2)}$$

At all times $SS_2 \geq SS_1$.

- the test statistic, F, was calculated:

$$F = \frac{(SS_2 - SS_1)/2}{SS_1/(n-2)} \qquad \text{.....(4.3)}$$

which is distributed as $F(2,n\text{-}2)$, where n is the number of E_A data pairs.

The hypothesis that a one-to-one relationship exists between the E_A estimates from different formations was rejected if $F > F(2,n\text{-}2)$ at the chosen confidence level.

The above statistical procedure is then repeated, but x is regressed on y, to examine the consistency of

the result. This statistical test for a one-to-one relationship is very stringent, hence a confidence interval of 99.5% was chosen, to make some allowance for the variation inherent in the apparent exhumation estimates, which is discussed later. The results of the statistical test are given in Table 4.1, and are discussed in the following section.

4.2.2 Discussion of statistical results

The correlations between apparent exhumation results determined from the different units are discussed below. Where only a small number of E_A pairs are being compared, in particular where the number of pairs is less than 10, the statistical results should be viewed with caution.

As can be seen from Table 4.1 and also Figures 4.1 - 4.4, apparent exhumation results derived from the Upper Cretaceous Chalk tend to be consistent with the Lower Cretaceous Greensand/Gault Clay, and those from the Triassic units below the salt also tend to be consistent with each other. However, there is less consistency when apparent exhumation results are compared between Cretaceous and Triassic units, in particular between the Upper Cretaceous Chalk and the Triassic units below the salt. Exhumation values derived from the Upper Cretaceous Chalk have been found to be reliable in several studies around the UK continental shelf (e.g. Hillis, 1991; Hillis *et al.*, 1994; Hillis, 1995*b*). Exhumation results from the Upper Cretaceous Chalk are believed to be reliable due to the lack of lateral lithological variation within the Chalk, and the clear dependence of its compaction state on burial-depth, as witnessed by log trends within individual wells (Figs. 2.5-2.15). Unfortunately, the Upper Cretaceous Chalk has been eroded from the inversion axes where other stratigraphic units must be used to estimate the magnitude of exhumation.

The lack of consistency between apparent exhumation results from Cretaceous and Triassic units may, in part, reflect Jurassic, 'Cimmerian' exhumation. In fact, the compaction method is intrinsically insensitive to 'Cimmerian' periods of exhumation which predate Tertiary exhumation. In order for 'Cimmerian' exhumation to be witnessed by the units analysed, maximum burial-depth prior to 'Cimmerian' exhumation must have been in excess of that prior to Tertiary exhumation, i.e. Jurassic ('Cimmerian') exhumation must have exceeded the maximum burial-depth of the base Cretaceous. For example, up to 2.8 km of 'Cimmerian' exhumation (in well 48/26-1) would be unrecognised by this analysis.

If maximum burial-depth prior to 'Cimmerian' exhumation was in excess of that prior to Tertiary exhumation, pre-'Cimmerian' units in any given well should exhibit consistent apparent exhumation values which are greater than those derived from post-'Cimmerian' units. Comparisons of apparent exhumation from the Upper Cretaceous Chalk and the Triassic units (Figs. 4.1(e), 4.1(f) & 4.2(a)) may indicate that Triassic units may have been more deeply buried than Cretaceous units (presumably due to 'Cimmerian' exhumation). However, this is less clear from comparisons of apparent exhumation from the Greensand/Gault Clay and the Triassic units (Figs. 4.2(d), 4.2(e) & 4.2(f)). It appears that there is some indication of maximum burial-depth prior to 'Cimmerian' exhumation having exceeded maximum burial-depth prior to Tertiary exhumation in some of the wells analysed. The wells in which greater apparent exhumation is witnessed by the Triassic units than the Cretaceous units tend of be in the Melville and St. Mary's Basins which is where the 'Cimmerian' unconformity has its most marked development (Figs. 2.6-2.8). However, the excess of apparent exhumation determined from Triassic units above that determined from Cretaceous units, where it

y,x	Upper Cretaceous Chalk	Greensand/ Gault Clay	Wealden	Upper Jurassic	Mercia (above salt)	Mercia (below salt)	Sherwood Sandstone
Danian Chalk	F = 0.89, 0.39 n = 9 Y:Y	F = 1.03, 3.56 n = 5 Y:Y	- n = 1 -	- n = 0 -	F = 5.04, 9.44 n = 6 Y:Y	F = 0.63, 6.84 n = 5 Y:Y	F = 0.57, 5.44 n = 4 Y:Y
Upper Cretaceous Chalk	-	F = 3.12, 5.94 n = 40 Y:Y	F = 23.8, 11.0 n = 27 N:N	F = 4.28, 15.2 n = 16 Y:N	F = 1.72, 4.67 n = 16 Y:Y	F = 5.69, 13.3 n = 19 Y:N	F = 4.10, 13.1 n = 15 Y:N
Greensand/ Gault Clay		-	F = 50.0, 34.9 n = 31 N:N	F = 1.94, 15.7 n = 20 Y:N	F = 4.93, 2.64 n = 11 Y:Y	F = 3.22, 3.38 n = 14 Y:Y	F = 3.08, 8.21 n = 11 Y:Y
Wealden			-	F = 3.07, 27.4 n = 22 Y:N	F = 1.31, 4.87 n = 7 Y:Y	F = 3.76, 4.61 n = 8 Y:Y	F = 5.57, 4.98 n = 7 Y:Y
Upper Jurassic				-	F = 341, 24.0 n = 3 Y:Y	- n = 0 -	- n = 0 -
Mercia (above salt)					-	F = 1.75, 11.5 n = 14 Y:N	F = 0.91, 8.58 n = 10 Y:Y
Mercia (below salt)						-	F = 0.34, 3.05 n = 21 Y:Y

Table 4.1. Comparison between apparent exhumation results from the eight different stratigraphic units analysed. (F = calculated test statistic (Equation 4.3); n = number of wells containing the two units under consideration). Y:Y indicates that the F-test is passed for regression of both y-on-x and x-on-y (i.e. a one-to-one linear correlation exists between E_A pairs), Y:N indicates that the F-test is failed for either y-on-x or x-on-y regression, and N:N indicates that the F-test is failed for both y-on-x and x-on-y regression, at the 99.5% level.

occurs, is generally only 200-400 m and within the error limits of the methodology. Hence there is not a sufficiently clear indication of 'Cimmerian' exhumation for it to be quantified separately.

Salt movements may also result in different stratigraphic units exhibiting different apparent exhumation values. For example, consider the growth of a salt dome, where the units underlying the salt growth structure will tend to show lower apparent exhumation than those overlying the salt structure because of exhumation of units above the salt growth structure. Hence salt movements may be, in part, responsible for some of the poorer correlations in apparent exhumation values derived from different stratigraphic units, in particular when comparing the Triassic Mercia Mudstone (above salt) with the Triassic Mercia Mudstone (below salt) and Triassic Sherwood Sandstone.

Inspection of the apparent exhumation crossplots of the Wealden (Figs. 4.1 - 4.4) reveals that the Wealden yields consistently lower apparent exhumation results than the other units, with the exception of the Mercia Mudstone (above salt). This may be attributed to the fact that the Wealden is restricted to the inverted regions, and is considered nowhere to be at its maximum burial-depth. Hence, the reference wells defining the normal compaction relation for the Wealden may not reflect maximum burial-depth.

There is no significant one-to-one correlation between apparent exhumation results from the Upper Jurassic mudstone and the other units analysed,

except the Mercia Mudstone (above salt). Even in the case of the Mercia Mudstone (above salt), only three wells intersect both formations (Fig. 4.3(e)), and the statistical result is clearly unrealistic, due to the small number of data points. As discussed in the section on selection of the stratigraphic units for analysis (Section 3.7), when interpreting the apparent exhumation results from the Upper Jurassic mudstone, it must be remembered that this unit exhibits considerable lateral lithological variability (variable mudstone/limestone/sandstone ratios). In different wells, the Upper Jurassic may have followed different normal compaction relations due to its lateral lithological variability. Hence, apparent exhumation values, as determined in this study, may not be entirely due to exhumation from maximum burial-depth. However, it is considered necessary to include the Upper Jurassic mudstone in the analysis because several wells on the inversion axes do not encounter the other units from which more reliable results can be obtained.

If a particular stratigraphic unit in a given well does not, with burial, follow the normal compaction relationship defined for that unit, then apparent exhumation, as determined here, will not be solely due to exhumation from maximum burial-depth. There will be an error equivalent to the amount of divergence of the actual normal compaction relation from the predicted relation. As discussed above, lateral lithological variation may cause the actual normal compaction relation to vary from that predicted for the unit. Diagenetic effects, such as the localised creation of secondary porosity in a limestone or sandstone, may also cause the actual normal compaction relation, for a given unit in a given well, to vary from that predicted regionally for the unit. It is not possible to rigorously determine the magnitude of the error in apparent exhumation caused by the actual normal compaction relation of a given unit in a given well, varying from that regionally predicted for the unit. However, an estimate of the likely error based on the lateral consistency of the log character of the units analysed is as followed:

Danian Chalk: ± 200 m;
Upper Cretaceous Chalk: ± 200 m;
Lower Cretaceous Greensand/Gault Clay: ± 300 m;
Lower Cretaceous Wealden:* ± 300 m;
Upper Jurassic mudstone: ± 400 m;
Mercia Mudstone (above salt): ± 200 m;
Mercia Mudstone (below salt): ± 200 m; and
Sherwood Sandstone: ± 200 m.

*As discussed earlier in this section, the reference wells for the Wealden are probably not at maximum burial-depth, hence in addition to errors associated with the Wealden not following the defined normal compaction relation in individual wells, estimates are probably consistently approximately 250 m too low.

4.3 Apparent Exhumation in the Celtic Sea/South-Western Approaches

The apparent exhumation results determined from the velocities in each of the units analysed are listed in Appendix II. Contoured maps of the apparent exhumation results from each of the units analysed, with the exception of the Danian Chalk (which is only present in nine wells), are presented in Figures 4.5 - 4.11. The contours in these maps are extrapolated from known data points/wells (which are shown on each map), and are unreliable in regions of low data density.

The mean of the apparent exhumation values derived from such of the units analysed that are present in each well, except the Wealden and Upper Jurassic, has also been calculated (Appendix II) and contoured (Fig. 4.12). The Wealden has been omitted

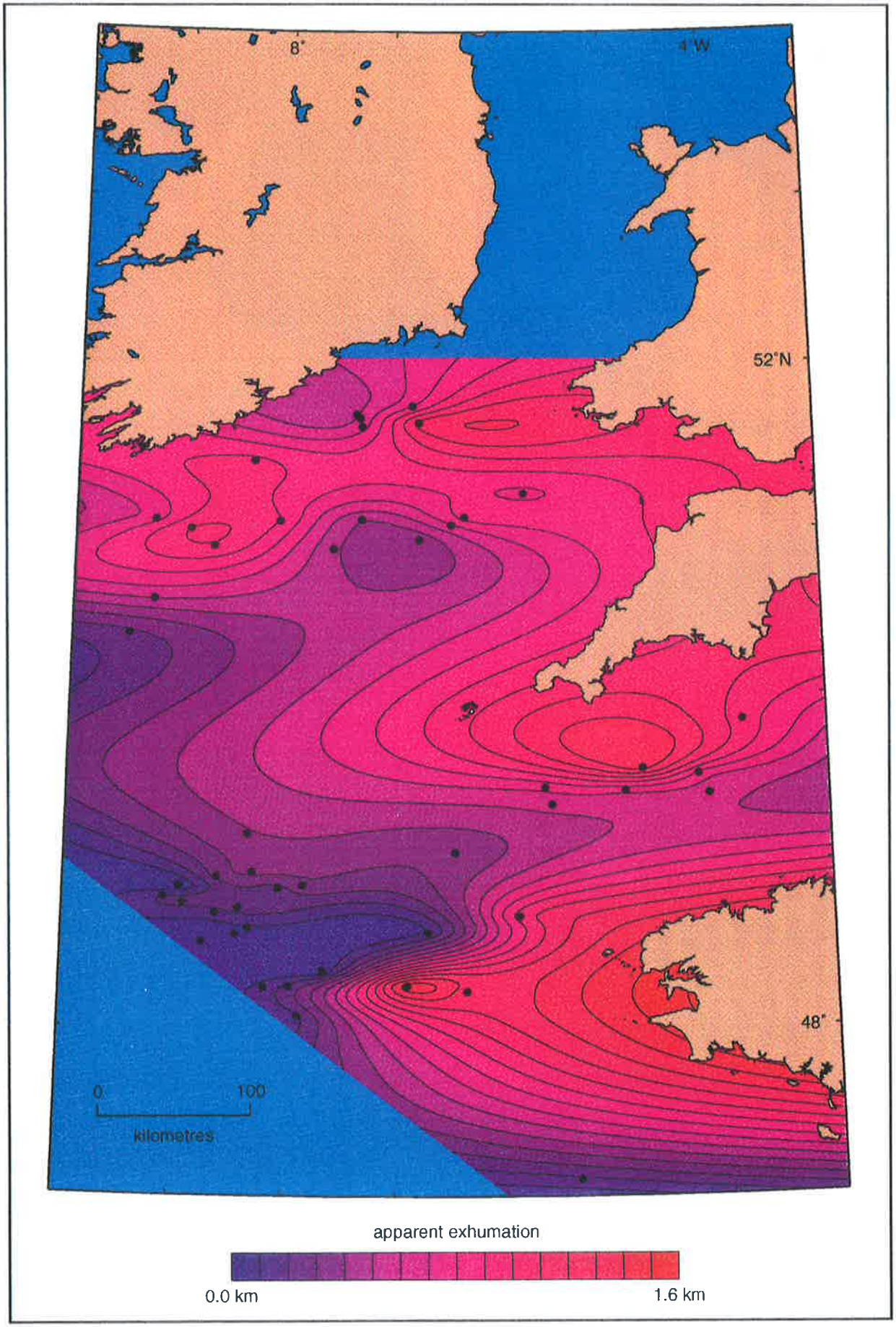

Fig. 4.5. Apparent exhumation map based on sonic velocities in the Upper Cretaceous Chalk.

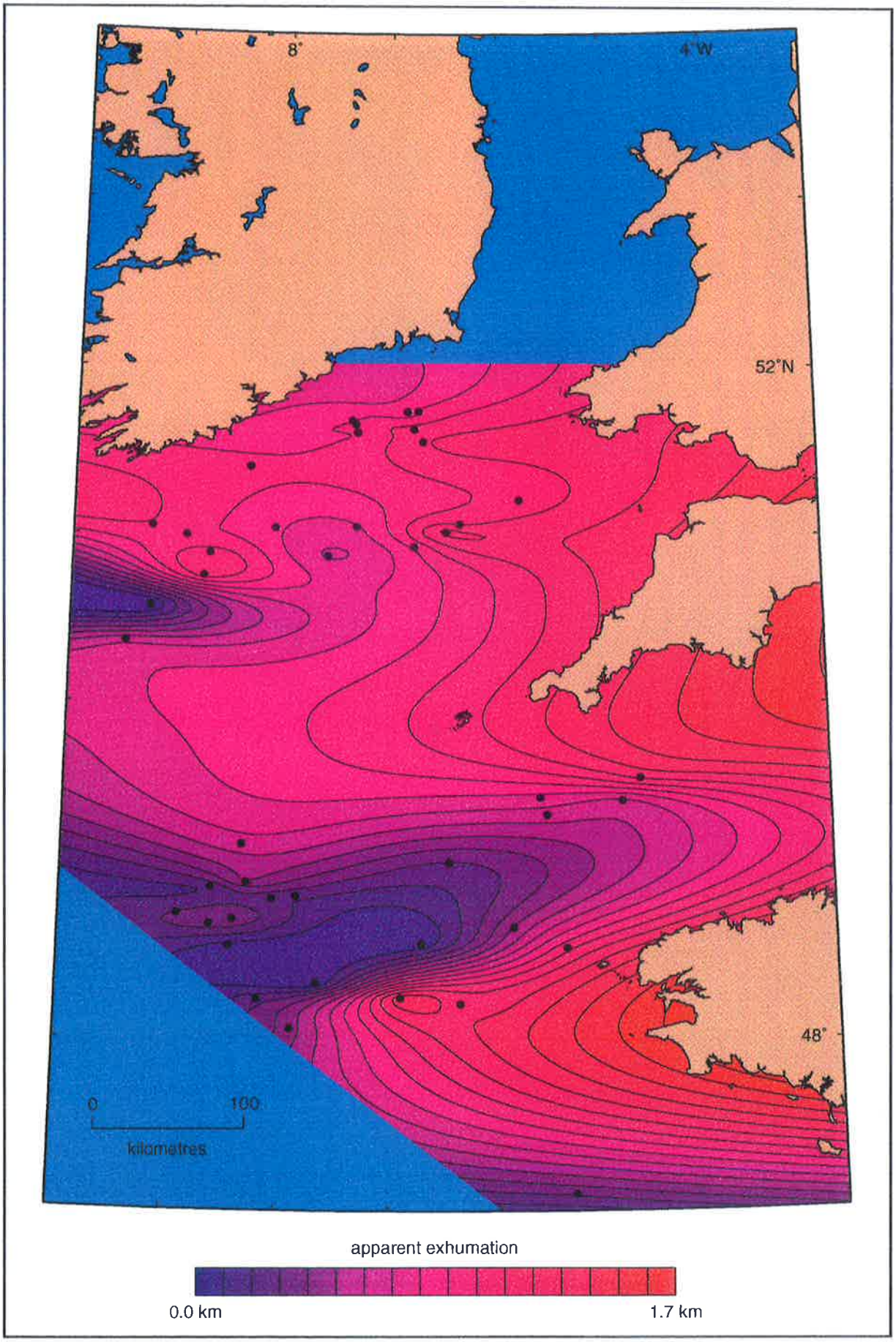

Fig. 4.6. Apparent exhumation map based on sonic velocities in the Lower Cretaceous Greensand/Gault Clay.

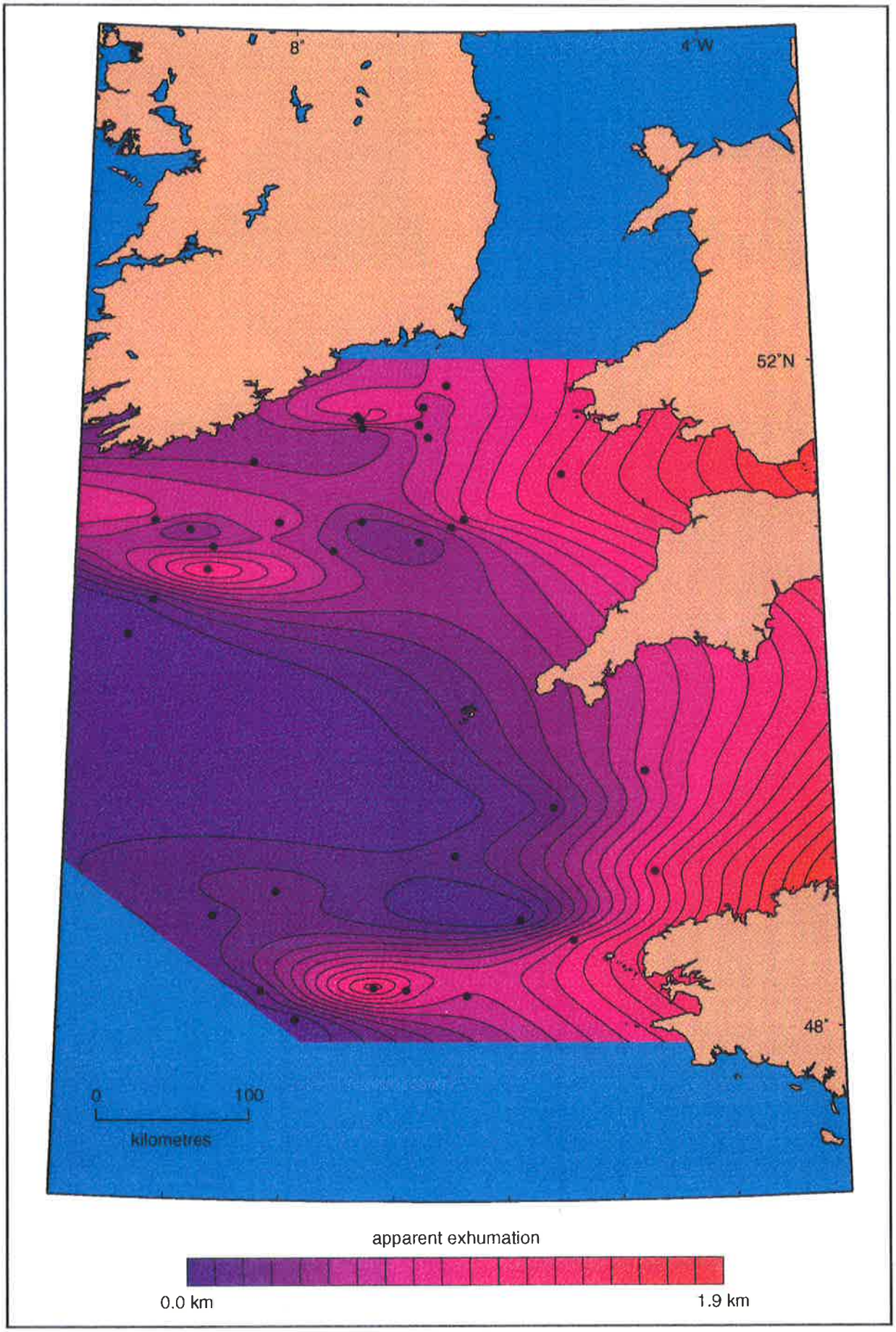

Fig. 4.7. Apparent exhumation map based on sonic velocities in the Lower Cretaceous Wealden.

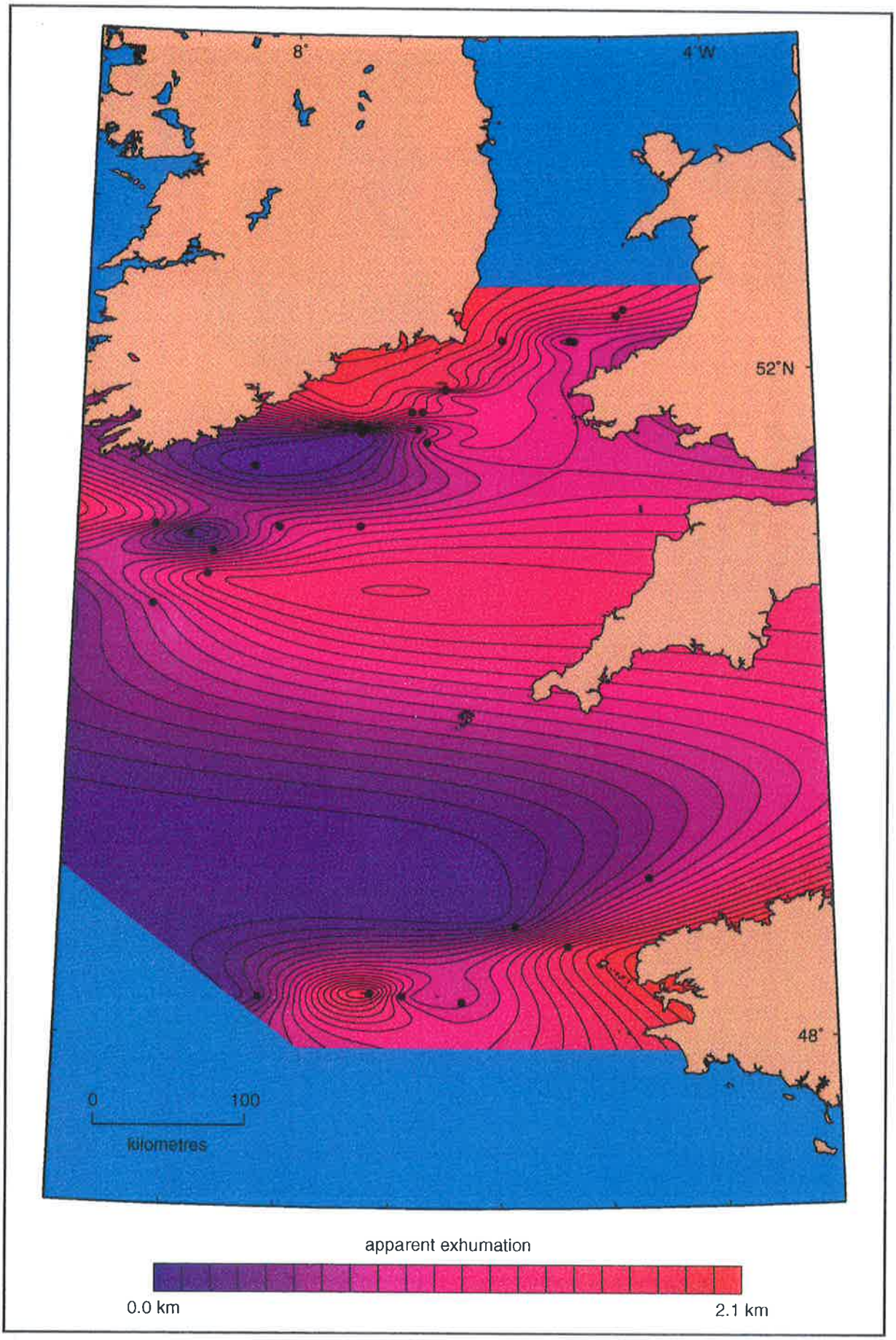

Fig. 4.8. Apparent exhumation map based on sonic velocities in the Upper Jurassic mudstone.

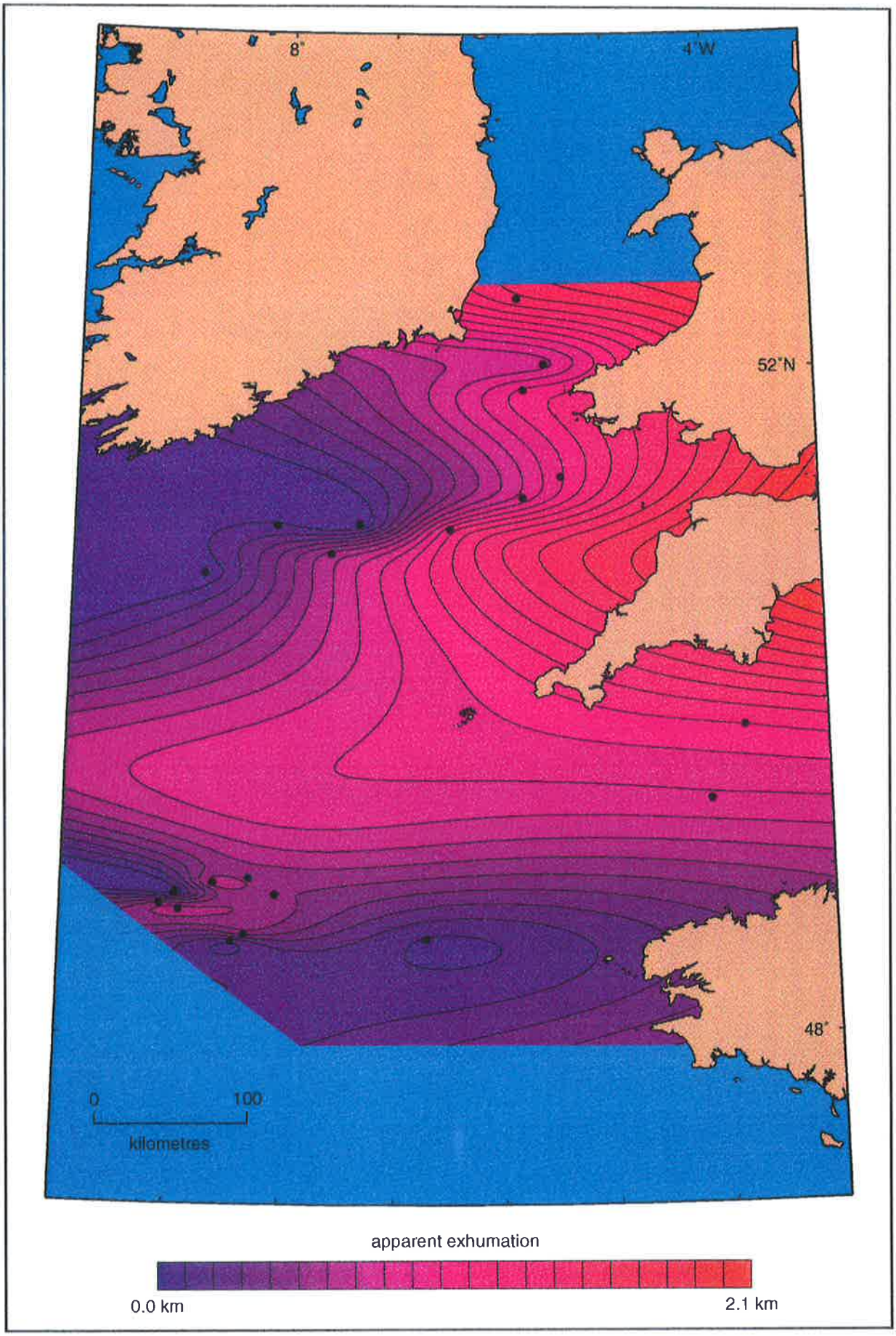

Fig. 4.9. Apparent exhumation map based on sonic velocities in the Triassic Mercia Mudstone (above salt).

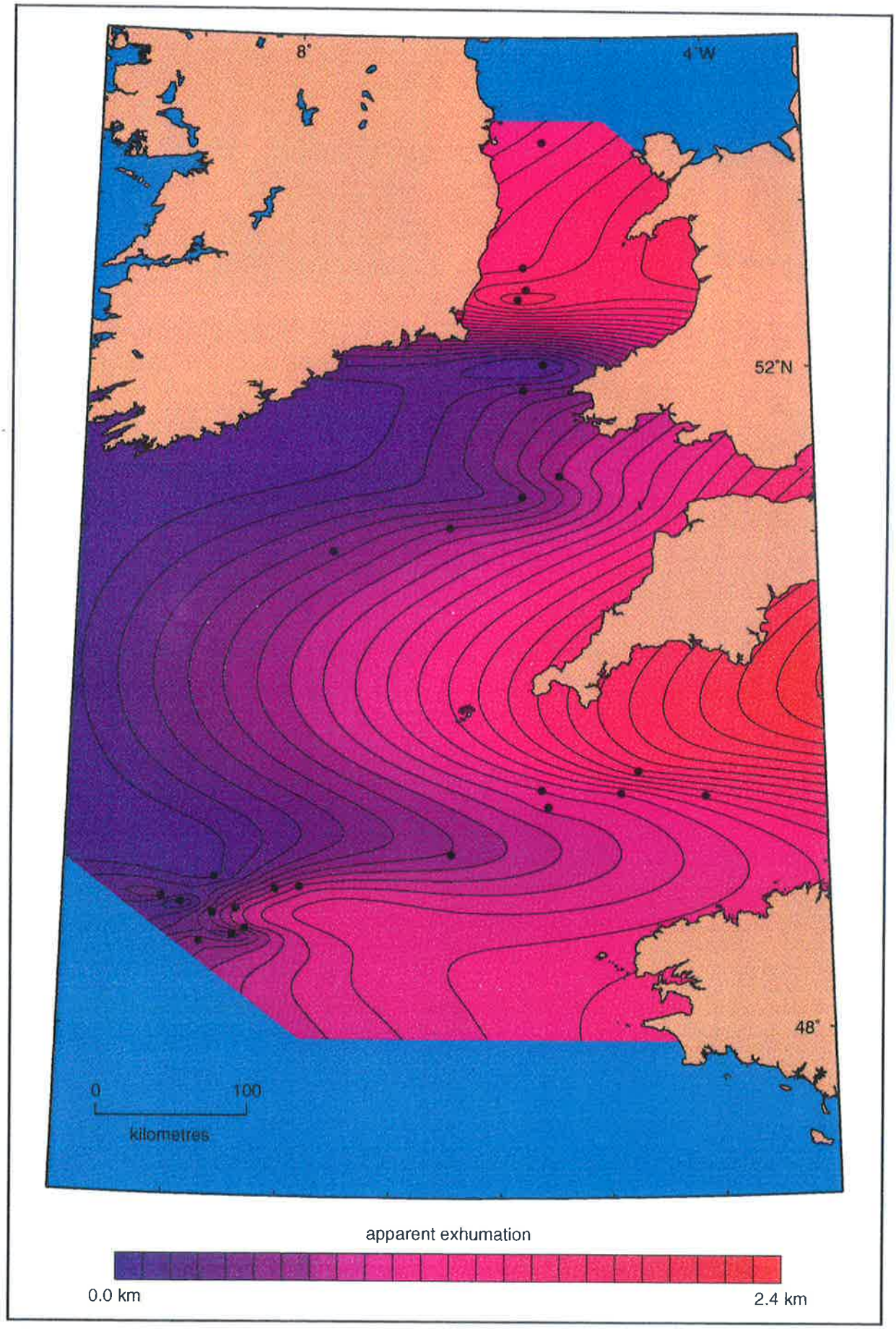

Fig. 4.10. Apparent exhumation map based on sonic velocities in the Triassic Mercia Mudstone (below salt).

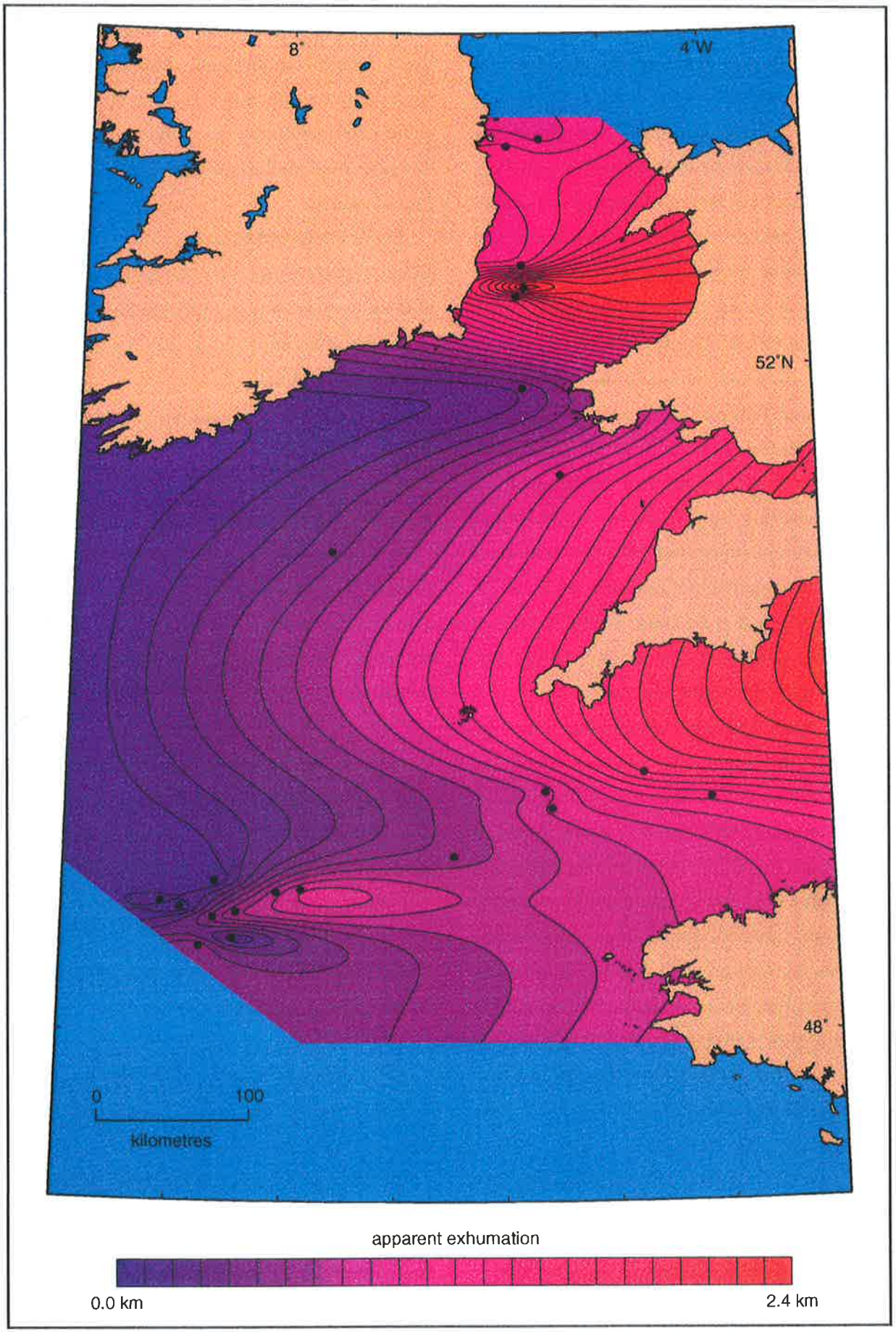

Fig. 4.11. Apparent exhumation map based on sonic velocities in theTriassic Sherwood Sandstone.

from this mean map because the reference wells may not be at maximum burial-depth, and hence the apparent exhumation values may be too low, as discussed in the previous section. The Upper Jurassic mudstone has also been omitted from this mean map, due to the poor correlation of apparent exhumation results from this unit with the other units analysed, as also discussed in the previous section.

The mean of the apparent exhumation values derived from such of all eight units analysed that are present in each well (including the Wealden and Upper Jurassic) has also been calculated (Appendix II) and contoured (Fig. 4.13). Although apparent exhumation values derived from velocities in the Lower Cretaceous Wealden and the Upper Jurassic mudstone are less reliable than those from other units, they are incorporated because nine wells on the inversion axes within the Celtic Sea/South-Western Approaches, including five in the Cardigan Bay Basin, do not encounter the other units.

The mean apparent exhumation maps are considered to give the most robust description of apparent exhumation because any lithology-specific sedimentological and/or diagenetic effects that might cause variation from the normal velocity/depth trend in individual units, and hence violate the assumption that all units follow the normal compaction trend with burial-depth, will tend to be reduced. It should be emphasised that such variations are considered to be of second order with respect to burial-depth because of the generally statistically significant similarity between apparent exhumation values from the different units.

The mean apparent exhumation maps, not including, and including the Wealden and the Upper Jurassic, are fairly similar (Figs. 4.12 & 4.13). The most significant difference between the two maps is that the apparent exhumation high in the Caernarvon Basin extends further eastwards into the Cardigan Bay Basin if the results from the Wealden and the Upper Jurassic are included. This high extends eastwards in the latter map because of the additional wells in the Cardigan Bay Basin that are included in the mean exhumation map which incorporates results from all the units.

It is clear from both Figures 4.12 and 4.13 that the major Tertiary-Quaternary depocentres of the southern Cardigan Bay and Melville Basins exhibit low apparent exhumation i.e. they are at or near maximum burial-depth.

The magnitude of apparent exhumation in strongly stratigraphically inverted areas can only be investigated with reference to the mean apparent exhumation map incorporating all units analysed (Fig. 4.13), because often only the Wealden and Upper Jurassic mudstone, of the units analysed, are intersected by wells in such areas. The strongly stratigraphically inverted areas exhibit high apparent exhumation:

- Cardigan Bay Basin up to 1.3 km at 107/16-1;
- North Celtic Sea Basin up to 1.7 km at 50/3-1;
- Brittany Basin up to 1.5 km at Levneg-1, and;
- Southwest Channel Basin up to 1.0 km at Kulzenn-1.

The mildly stratigraphically inverted areas exhibit lower apparent exhumation:

- Fastnet Basin up to 0.9 km at 57/7-1, and;
- South Celtic Sea Basin up to 1.0 km at 103/18-1.

The Caernarvon Basin, where Triassic crops out at or near sea-bed in the wells analysed, shows high apparent exhumation, with up to 2.0 km at 42/17-1. The Kish Bank Basin shows apparent exhumation of up to 1.5 km. The St. Mary's and Plymouth Bay Basins show apparent exhumation of up to 1.2 km.

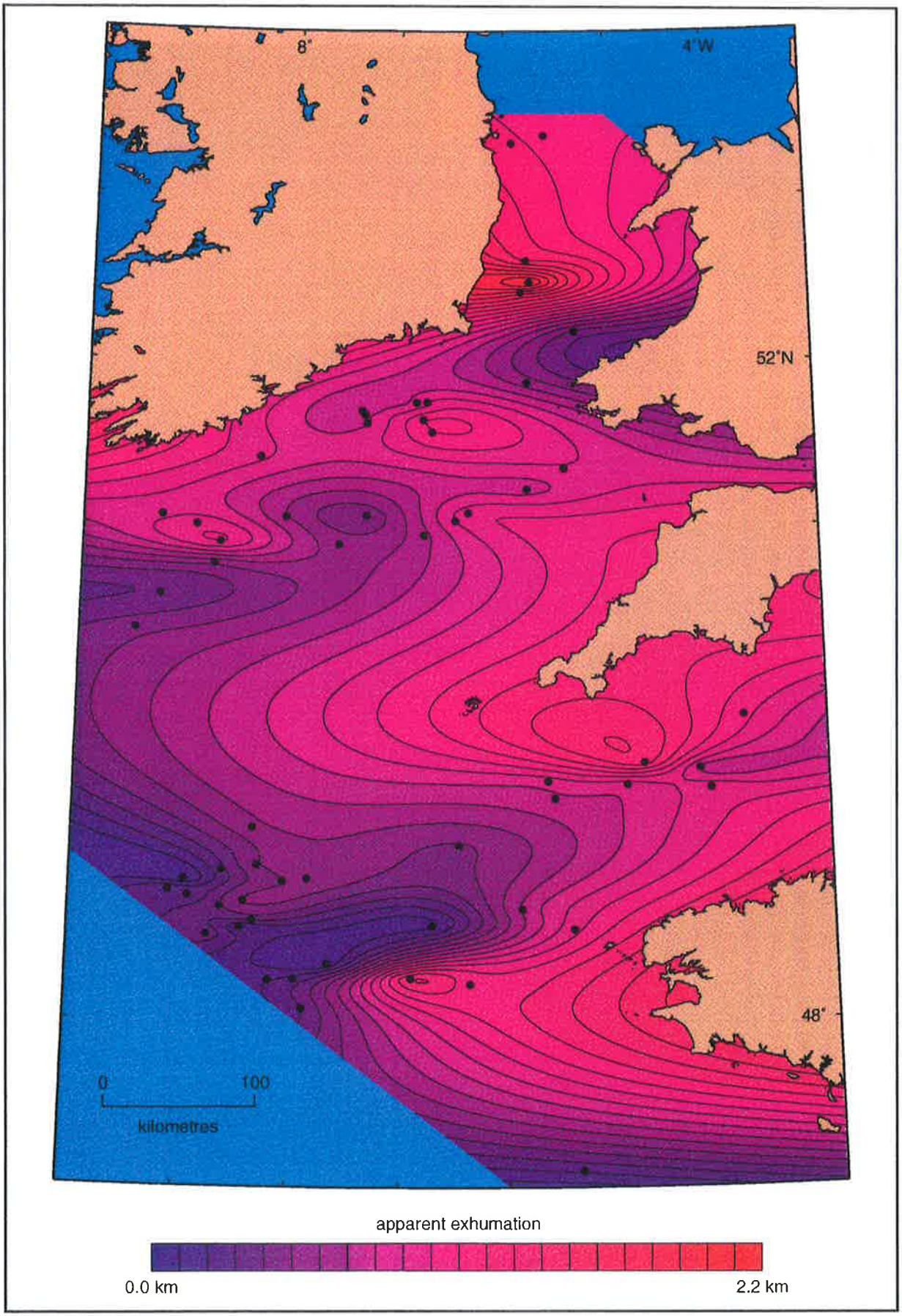

Fig. 4.12. Map of the mean apparent exhumation of all the wells analysed, excluding the Lower Cretaceous Wealden and Upper Jurassic Mudstone.

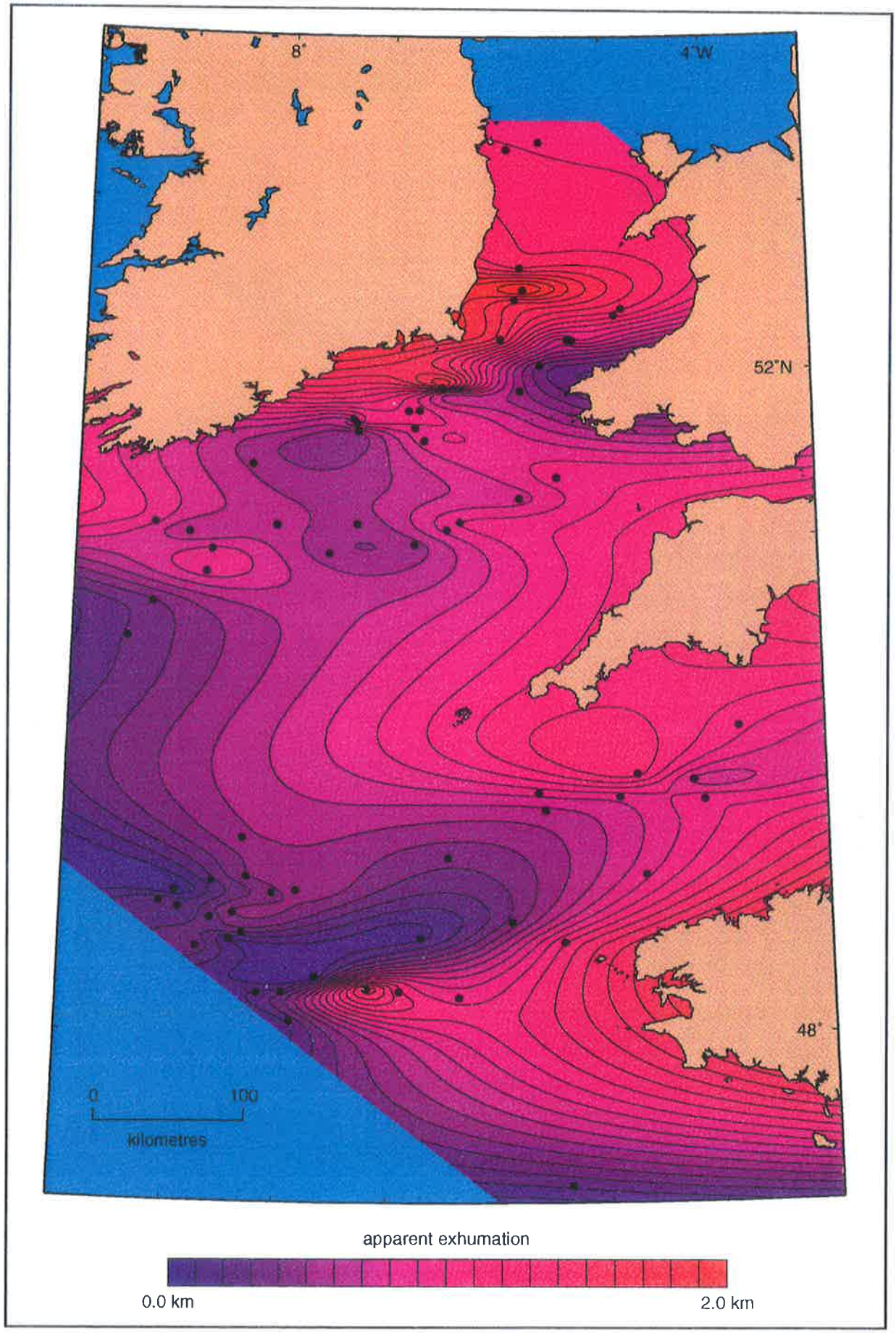

Fig. 4.13. Map of the mean apparent exhumation of all the units analysed.

One of the most significant features in Figures 4.5 - 4.13 is that apparent exhumation is not limited to recognised structural inversion axes shown on Figure 2.1. Apparent exhumation of up to 1 km has occurred on the margins of the Amorican and Cornubian Platforms and the Pembroke Ridge. Although the paucity of data over the platform areas themselves has resulted in poorly constrained contours over the platforms, exhumation clearly occurs on a regional scale, away from the localised apparent exhumation highs over the axes of structural inversion. The implications of this regional component of apparent exhumation will be discussed in Chapters 6 - 8.

4.4 Exhumation at the Time of Denudation in the Celtic Sea/South-Western Approaches

The quantity determined from the velocity data is referred to as apparent exhumation because it is exhumation not reversed by subsequent burial. It is not necessarily the same as the amount of exhumation that occurred when the rocks were being denuded. If renewed burial follows exhumation, the magnitude of apparent exhumation determined from velocity data is reduced by the amount of that subsequent burial. If there is no burial subsequent to exhumation, apparent exhumation equals the amount of exhumation that occurred when the rocks were being denuded. These concepts were discussed more fully in Section 3.6. In order to determine the magnitude of exhumation that occurred at the time the rocks were being denuded, it is thus necessary to know the timing of the exhumation and the magnitude of post-exhumational burial.

4.4.1 Timing of exhumation in the Celtic Sea/ South-Western Approaches

Apparent exhumation magnitudes from velocities in the Danian Chalk are comparable with those from the Upper Cretaceous Chalk (Table 4.1; Fig. 4.1), thus Tertiary exhumation post-dated the Danian. Ideally, Tertiary units younger than the Danian Chalk would have been analysed in order to further constrain the timing of uplift, however, post-Danian units are not widely encountered in exploration wells in the area, and even where encountered, log data are not always available. Hence the compaction methodology cannot be used to constrain the age of Tertiary exhumation beyond post-Danian.

The two most widely recognised Tertiary unconformities in the area are in the Palaeocene and the Oligo-Miocene (e.g. Tucker & Arter, 1987; Van Hoorn, 1987; Roberts, 1989; Tappin *et al.*, 1994; Murdoch *et al.*, 1995). Figure 4.14 illustrates exhumation at the time of denudation, assuming that the exhumation occurred during the hiatus associated with the Palaeocene unconformity. Figure 4.15 illustrates exhumation at the time of denudation, assuming that the exhumation occurred during the hiatus associated with the Oligo-Miocene unconformity. These results are tabulated in Appendix III. These results and maps were determined using the mean apparent exhumation data from all eight of the units analysed.

4.4.2 Magnitude of exhumation in the Celtic Sea/South-Western Approaches

Comparison of Figures 4.14 and 4.15 shows little difference in the magnitude of exhumation at the time of denudation in most of the Celtic Sea basins, regardless of whether all of the exhumation is assumed to have occurred during the Palaeocene, or during the Oligo-Miocene. This is because there is little or no Eocene-Oligocene section in most of the wells of the North Celtic Sea Basin, Fastnet Basin, South Celtic Sea Basin, Caernarvon Basin, or Kish

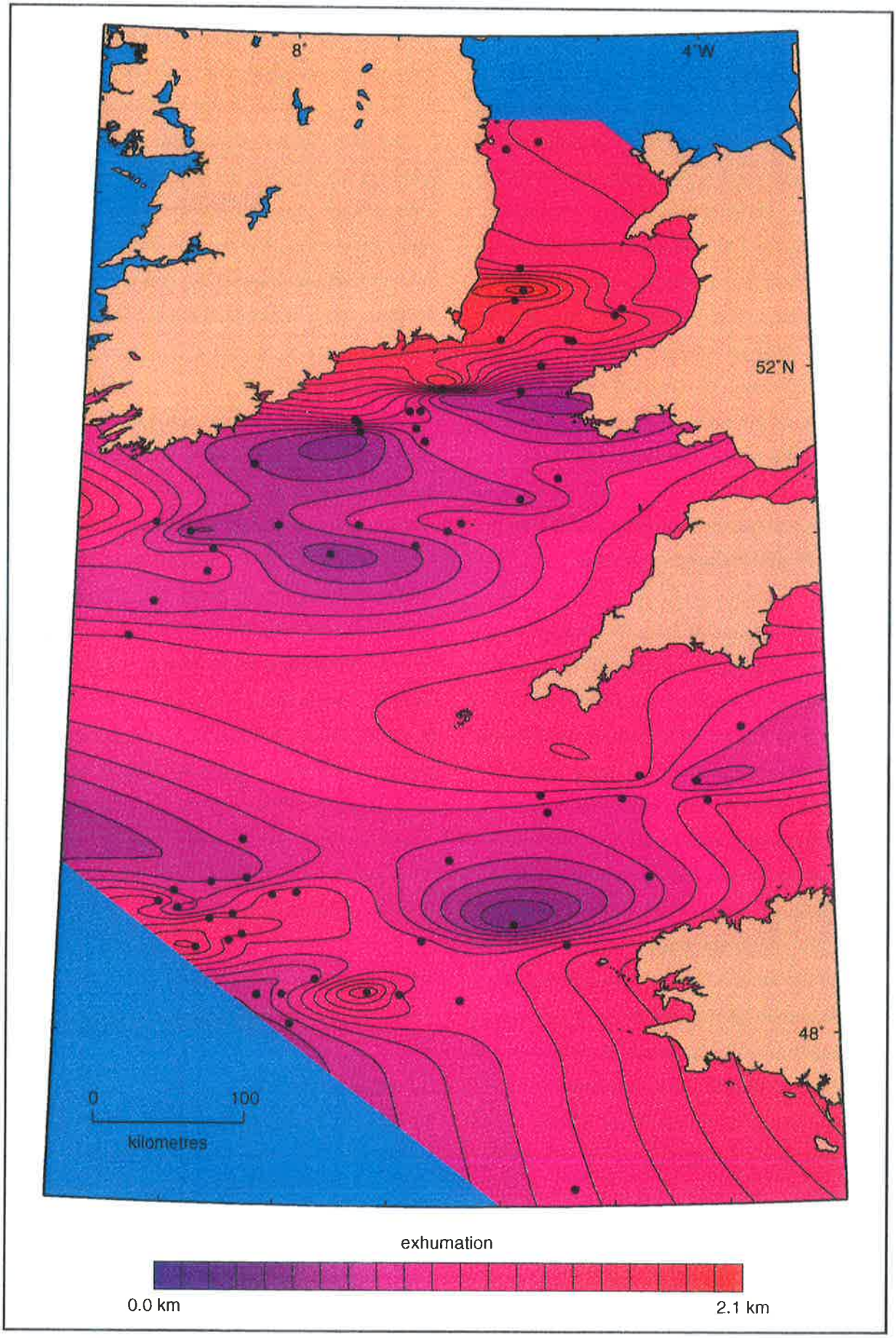

Fig. 4.14. Map of exhumation at the time of denudation, assuming Palaeocene denudation.

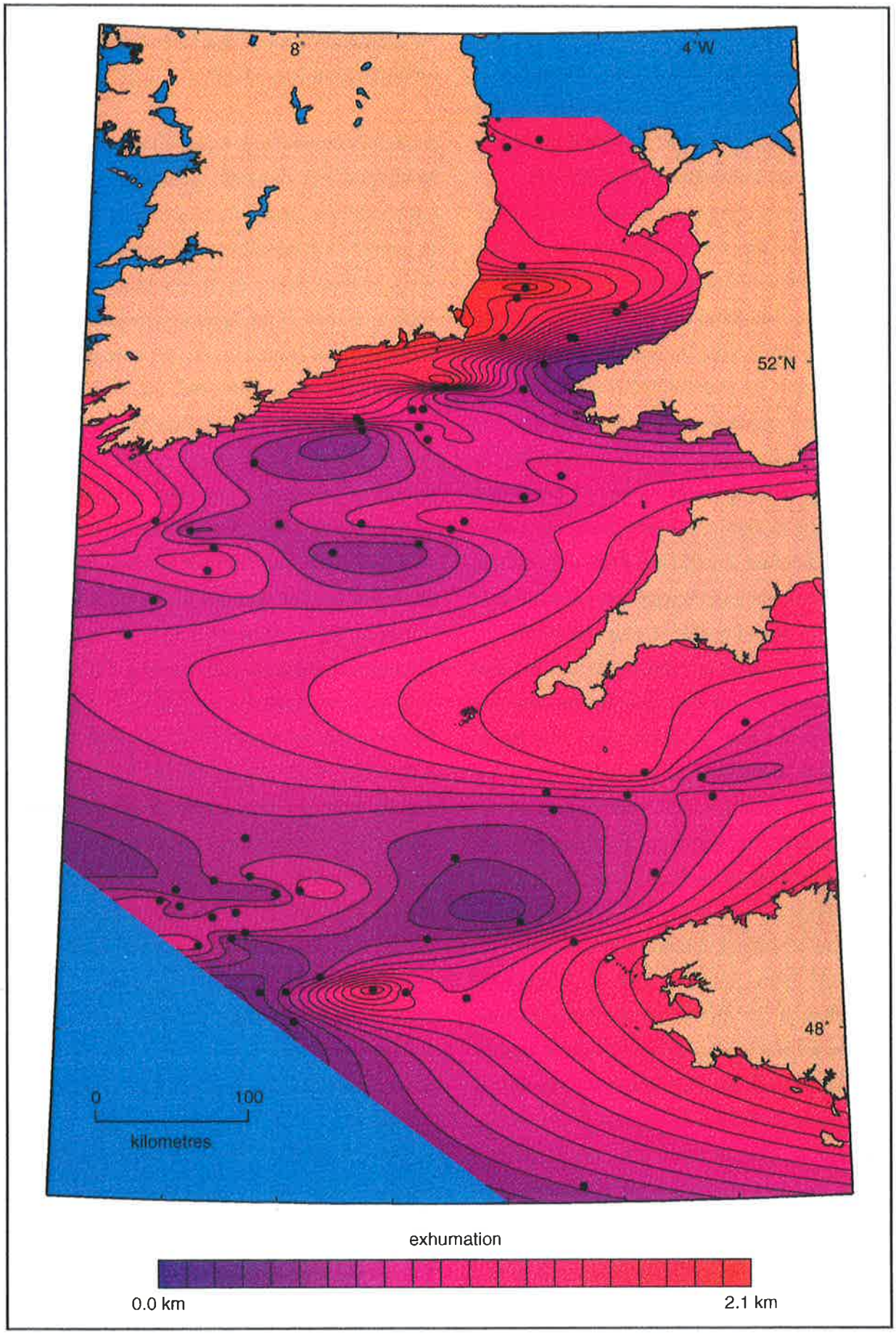

Fig. 4.15. Map of exhumation at the time of denudation, assuming Oligo-Miocene denudation.

Bank Basin. The amount of post-exhumation burial that must be added to apparent exhumation to determine exhumation at the time of denudation in these areas is thus the same, regardless of whether exhumation was Palaeocene or Oligo-Miocene.

The Tertiary depocentres of the Melville Basin and Cardigan Bay Basin, which contain a thick sequence of Eocene-Oligocene rocks (up to 0.7 km in the Cardigan Bay Basin and 0.6 km in the Melville Basin), provide the major differences between Figures 4.14 and 4.15. The Melville Basin and Cardigan Bay Basin exhibit exhumation of between 0.8 -1.2 km and 0.7 -1.7 km respectively if exhumation is assumed to have occurred during the Palaeocene. If exhumation is assumed to have occurred during the Oligo-Miocene, however, the Melville Basin and Cardigan Bay Basin exhibit significantly less exhumation of between 0.5 -0.8 km and 0.4 -1.4 km respectively.

Whether exhumation is assumed to have occurred in the Palaeocene or in the Oligo-Miocene, there is a regional component of between 0.5 - 1.2 km of exhumation, upon which exhumation related to the recognised stratigraphic inversion axes is superimposed. As previously suggested from the apparent exhumation results, Tertiary exhumation is clearly more widespread than are inversion structures in the Celtic Sea/South-Western Approaches.

It has been proposed that the Palaeocene unconformity in the Celtic Sea/South-Western Approaches was associated with a period of regional exhumation while the Oligo-Miocene unconformity was associated with a period of basin inversion (e.g. Tappin *et al.*, 1994; Murdoch *et al.*, 1995). However in this study, regional Palaeocene exhumation could not be distinguished from the superposed Oligo-Miocene structural inversion trends. The apparent exhumation estimates in this study reflect a combination of Palaeocene and Oligo-Miocene exhumation.

4.5 Maximum Burial-Depth in the Celtic Sea/ South-Western Approaches

Apparent exhumation is equal to the height of the rocks above their maximum burial-depth. Hence the maximum burial-depth of any horizon is the sum of its present burial-depth and the apparent exhumation at that location (Section 3.6.2). The maximum burial-depth of the base of the Upper Cretaceous Chalk has been calculated (Appendix III) and contoured (Fig. 4.16). This map is based only on the maximum burial-depths at the well localities analysed, and it was determined using the mean apparent exhumation data from all eight of the units analysed. For comparison, the present burial-depth of the base of the Upper Cretaceous Chalk has also been contoured for the well locations analysed (Fig. 4.17).

The onset of chalk deposition in the Upper Cretaceous corresponds approximately with the end of extensional, basin-forming rifting in the Celtic Sea/South-Western Approaches (Evans, 1990; Tappin *et al.*, 1994). From Figures 4.16 and 4.17, it is clear that the maximum burial-depth of the base of the Upper Cretaceous Chalk shows a more even, regional pattern of post-rift subsidence than its present burial-depth uncorrected for exhumation. When corrected for Tertiary exhumation, the post-rift sequence in the Celtic Sea/South-Western Approaches shows relatively little localisation over the thick syn-rift Jurassic-Lower Cretaceous sequence of the Brittany Basin, Southwest Channel Basin, and North Celtic Sea Basin.

The 'rift-drift' Avalon Unconformity of the conjugate, but largely uninverted Canadian margin is essentially flat-lying. There is no localisation of the post-rift sequence over the fault-controlled syn-rift basins of the Canadian margin (Keen *et al.*, 1987). Keen *et al.* (1987) proposed that during basin formation on the Canadian margin, the lower

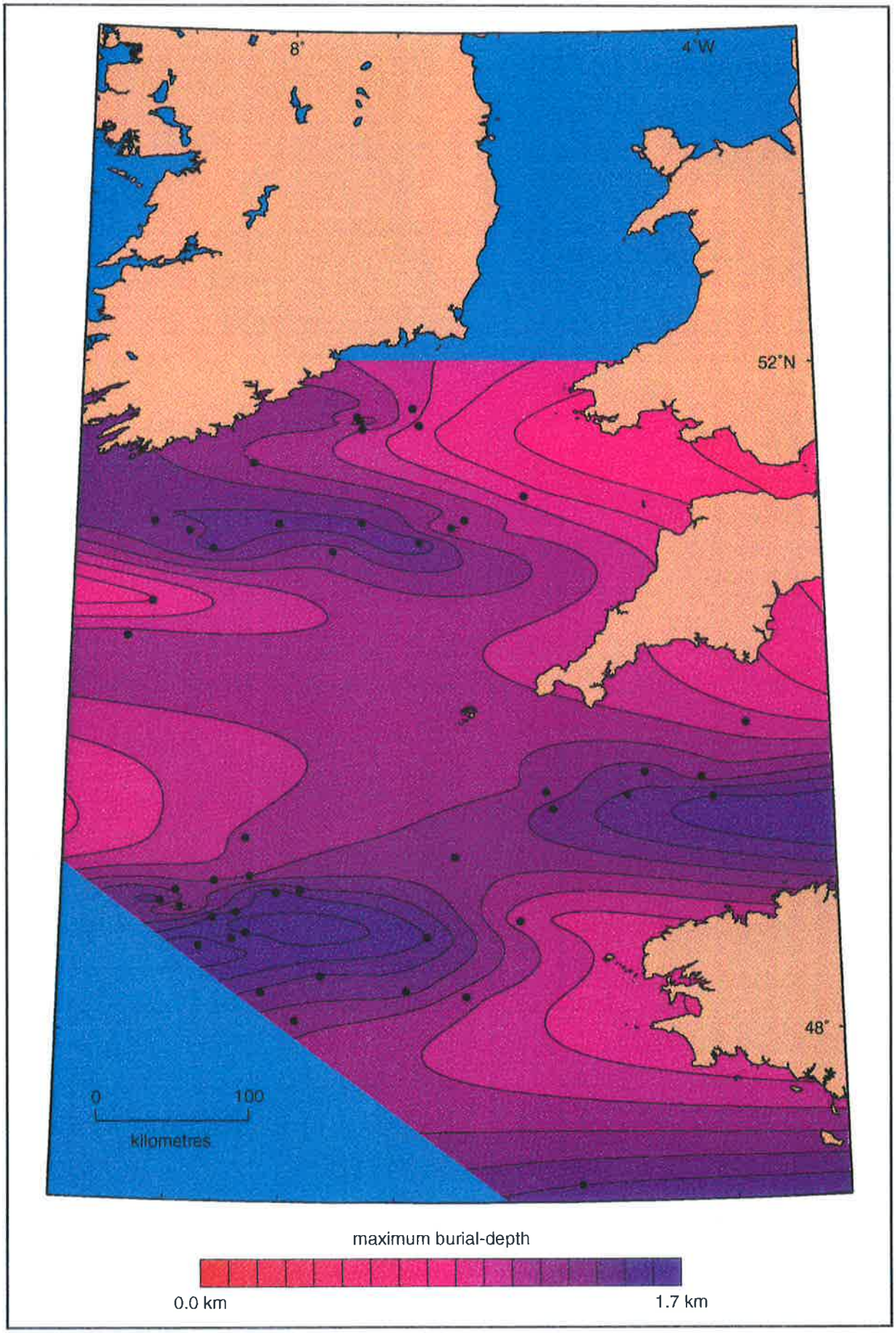

Fig. 4.16. Map of maximum burial-depth for the base of the Upper Cretaceous Chalk.

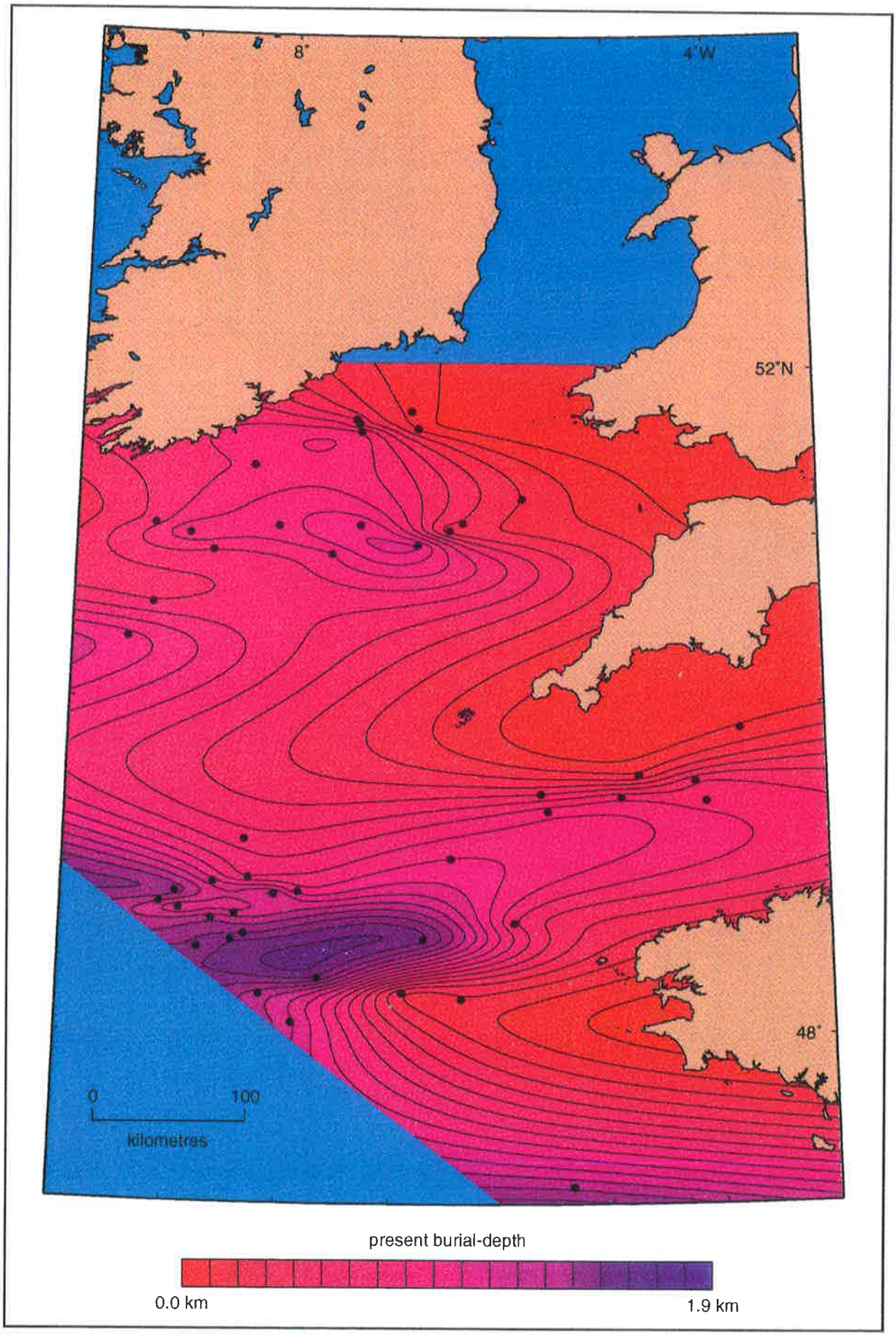

Fig. 4.17. Map of present burial-depth for the base of the Upper Cretaceous Chalk.

lithosphere, thermal re-equilibration of which controls post-rift subsidence, did not experience localised thinning on the scale of the syn-rift basins. This implies either that extension was decoupled between the upper and lower lithosphere, or that post-rift lithospheric flexural rigidities were sufficiently high that post-rift subsidence was regionally distributed. A similar argument is applicable to the corrected post-rift burial thicknesses of the Celtic Sea/South-Western Approaches.

4.6 Comparison of Results with Related Published Studies

A number of published studies on the Celtic Sea/South-Western Approaches have included estimates of the amount of Tertiary exhumation (Table 4.2). Most of the published estimates are fairly general, providing only approximate exhumation figures for an entire offshore basin. There are also some results for adjacent onshore locations. Comparisons between apparent exhumation as determined herein and these estimates can only be very general. However, most of the previously published estimates are broadly consistent with the estimates herein (Table 4.2).

The major discrepancy between this, and previously published results is with Van Hoorn's (1987) estimate of less than 350 m of Oligo-Miocene exhumation in the northeast part of the South Celtic Sea Basin. Velocities analysed herein suggest 0.8 -1.0 km apparent exhumation in wells 103/18-1 and 103/21-1. Unfortunately Van Hoorn (1987) provides no details of methodology for his estimate of less than 350 m beyond "on the basis of seismic evidence". However, Van Hoorn (1987) does recognise the earlier, Palaeocene unconformity, but does not quantify the amount of exhumation associated with this unconformity. One of the few previously published geographically-specific estimates, of 1.3 km of exhumation at well 33/22-1 in the Kish Bank Basin, based on vitrinite reflectance (Naylor *et al.*, 1993), is very similar to the estimate herein of 1.2 km for well 33/21-1 in the adjacent block.

Murdoch *et al.* (1995) used an Upper Cretaceous Chalk isopach and sonic velocity study, in addition to apatite fission track analyses and vitrinite reflectance measurements, to quantify apparent exhumation within the North Celtic Sea Basin. The velocity study of Murdoch *et al.* (1995) was based solely on North Celtic Sea Basin and Fastnet Basin wells, and suggested that apparent exhumation of the Upper Cretaceous Chalk in the North Celtic Sea Basin increases from approximately 0.2 km near the basin margins to approximately 1.1 km in the basin centre (Table 4.2). However, the results contained herein suggest that all of the wells of the North Celtic Sea Basin and Fastnet Basin are at least 0.3 km above maximum burial-depth. The study of Murdoch *et al.* (1995) thus underestimates apparent exhumation for the North Celtic Sea Basin by around 0.3 km. If an additional 0.3 km of apparent exhumation is added to the results of Murdoch *et al.* (1995), their apparent exhumation estimates for the North Celtic Sea Basin and Fastnet Basin are very close to the apparent exhumation estimates from the Upper Cretaceous Chalk contained herein.

4.7 Implications of Exhumation Results for Models of Basin Evolution

The identification and quantification of regional Tertiary exhumation has important implications for tectonic modelling of the evolution of the Celtic Sea/South-Western Approaches area. The key observations from this chapter that any models of

Author	Region (well)	Evidence for exhumation	Exhumation estimate	Suggested timing of exhumation	Apparent exhumation estimate (compaction methodology)
Roberts (1989)	Cornubian Peninsula	projected dips of base chalk, presence of flints	1 km	none	1.1 -1.3 km
	Celtic Sea	VR	1 - 2 km	Palaeogene/ Oligocene	0.5 - 1.7 km (NCSB) 0.5 - 1.0 km (SCSB)
	Cork, southern Ireland	spore coloration of Colbond Clay	up to 2 km	none	1.2 km
Van Hoorn (1987)	South Celtic Sea Basin (NE part)	seismic (no specifics of methodology given)	< 350m	Late Oligocene-Miocene	1.0 km (103/18-1) 0.8 km (103/21-1)
Tucker & Arter (1987)	North Celtic Sea Basin	formation pressures in Jurassic sandstones	up to 2.5 km	Palaeogene	up to 1.7 km
	Cardigan Bay Basin	methodology not stated	in excess of 1 km seems likely	Palaeogene	0.4 - 1.3 km
Keeley *et al.* (1993)	southeast Ireland	AFTA	1.3 - 2.5 km	Palaeocene	1.2 - 1.8 km
Naylor *et al.* (1993)	Kish Bank Basin (33/22-1)	VR	1.3 km	?Post-Jurassic	1.2 km (33/21-1)
Howell & Griffiths (1995)	North Celtic Sea Basin	VR	0.4 km (48/19-1)	Palaeocene	0.6 km (48/19-1)
Maddox *et al.* (1995)	Block 42/12 (Central Irish Sea Basin/ Caernarvon Basin)	unpublished VR, AFTA, and shale velocity data	1 - 2.5 km	Neogene	1.4 km (42/12-1)
Murdoch *et al.* (1995)	North Celtic Sea Basin	AFTA/ VR	1.3 km (50/3-1) 0.3 km (49/9-1) 0.1 km (48/19-1)	Palaeocene/ Oligo-Miocene	1.7 km (50/3-1) 0.7 km (49/9-1) 0.6 km (48/19-1)
		Chalk Group velocities & isopachs	up to 1.1 km in basin centre	Palaeocene/ Oligo-Miocene	up to 1.7 km
Murphy *et al.* (1995)	North Celtic Sea Basin	methodology not stated	~0.4 km (48/19-1)	Palaeocene/ Oligo-Miocene	0.6 km (48/19-1)

Table 4.2. Comparison of apparent exhumation estimates based on sonic velocities with other published estimates from other methodologies for the Celtic Sea/South-Western Approaches (VR = vitrinite reflectance, AFTA = apatite fission track analysis).

basin evolution must account for are:

- exhumation of the stratigraphically inverted areas of the Brittany and South-West Channel Basins, the South Celtic Sea-Bristol Channel Basin, the North Celtic Sea-Cardigan Bay Basin, and the Fastnet Basin, which occurred in association with upper lithospheric compression/thickening (i.e. basin inversion);
- regional exhumation of the uninverted St. Mary's and Melville Basins and the Amorican Platform, Cornubian Platform, and Pembroke Ridge margins, without associated upper lithospheric compression/thickening;
- burial prior to exhumation, during which the rocks became overcompacted, which is not preserved in the stratigraphic record.

In addition, the following observations must be explained:

- the regional nature of the Upper Cretaceous post-rift subsidence, with little basin localisation of the Upper Cretaceous Chalk;
- the occurrence of maximum stratigraphic/ structural basin inversion in the areas of maximum Jurassic-Early Cretaceous basin subsidence and syn-rift deposition;
- the symmetry of syn-rift subsidence and stratigraphic inversion around the Cornubian Platform: as discussed in Chapter 2 and as is apparent from the maps of total exhumation (Figs. 4.14 - 4.15), the basins adjacent to the Cornubian Platform underwent less syn-rift subsidence than those further to the north and south, and also underwent less stratigraphic inversion.

These observations will be addressed in the chapters on modelling the tectonic evolution of the Celtic Sea/South-Western Approaches (Chapters 6 - 8).

Chapter 5

Determining Apparent Exhumation from Chalk Outcrop Samples, Cleveland Basin/East Midlands Shelf

5.1 Introduction

Wells (1990) used porosity and seismic velocity measurements from samples of the upper Cenozoic mudstones of Wairarapa, North Island, New Zealand to quantify exhumation. Wells (1990) concluded that the porosity-depth relationship of exhumed mudstone in southeastern Wairarapa could be used to predict maximum burial-depth to within ± 100 m. The following study was undertaken to determine whether Chalk outcrop samples may be used to quantify apparent exhumation for the onshore United Kingdom, using similar principles to those of Wells (1990), and samples of the Upper Cretaceous Chalk from the Cleveland Basin/East Midlands Shelf (Fig. 5.1).

Although the main focus of this thesis is on the Celtic Sea/South-Western Approaches, the outcrop study described in this chapter was undertaken in the Cleveland Basin/East Midlands Shelf because of the lack of outcrop of suitable Mesozoic rocks onshore adjacent to the Celtic Sea/South-Western Approaches. The Upper Triassic and Liassic mudstones of the north Somerset coast were investigated, however these units tend to be strongly weathered at outcrop and are unsuitable for use in compaction-based analysis of exhumation.

A sequence exposed at the land surface that is suitable for estimating exhumation from porosity measurements should consist of one lithotype present over a large stratigraphic thickness, so that any porosity trends observed are independent of changes in lithology (Wells, 1990). In this respect, the Upper Cretaceous Chalk of the United Kingdom is an ideal lithology, because it consists of a thick, regionally extensive pure white limestone, composed of calcareous algal plates (coccoliths) deposited as copepod faecal pellets (Rawson & Wright, 1992). Provided care is taken to avoid the flint and marl bands within the Chalk, the sampler can be reasonably assured of sampling a consistent lithotype.

Hillis (1991) showed that compaction in the Chalk of the South-Western Approaches was strongly burial-depth controlled, and used velocities in the Chalk to quantify exhumation. Velocities in the Chalk and the Kimmeridge Clay of the Inner Moray Firth yield statistically similar exhumation magnitudes (Hillis *et al.*, 1994), as do velocities in the Chalk, the Bunter Shale and the Bunter Sandstone of the Southern North Sea (Hillis, 1995*b*). As shown in Chapter 4, the Upper Cretaceous Chalk yields statistically similar exhumation magnitudes to other lithologies in the Celtic Sea/ South-Western Approaches. The Upper Cretaceous Chalk has been chosen for this study because it consistently yields reliable results in compaction-based studies of exhumation.

5.2 Previous Studies of Apparent Exhumation of the Cleveland Basin/East Midlands Shelf

Marie (1975) estimated that the Cleveland Hills have been exhumed by a minimum of 1200-1800 m by comparing the maximum palaeo-depth derived from sonic velocities and the present depth of burial for the Triassic Bunter Shale. However, as noted by

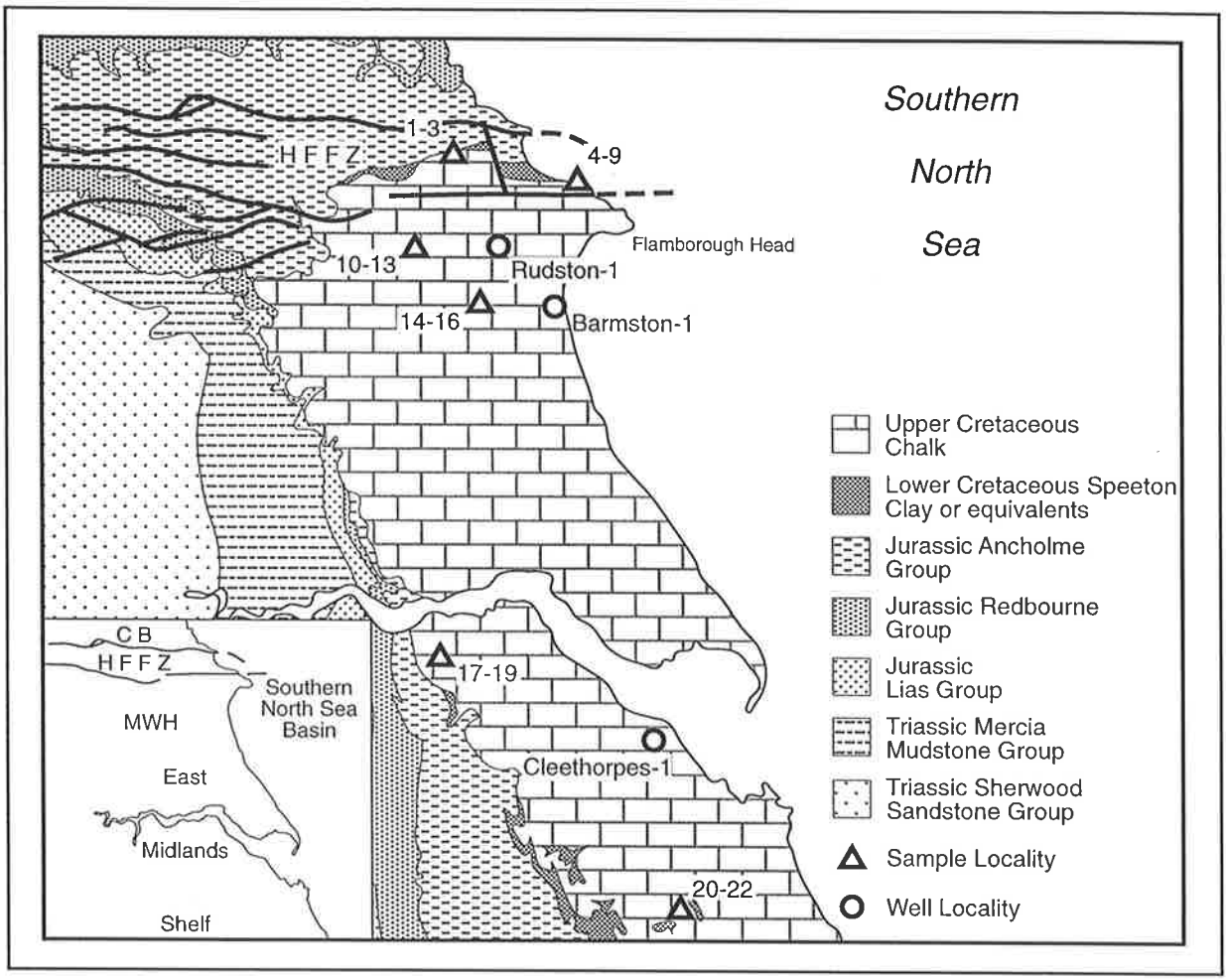

Fig. 5.1. Simplified onshore geological map of the Cleveland Basin/East Midlands Shelf showing locations of outcrop samples (triangles) and wells (circles). Unit nomenclature after BGS 1:250 000 scale Spurn and Tyne Tees solid geology sheets. (HFFZ = Howardian-Flamborough Fault Zone, CB = Cleveland Basin, MWH = Market Weighton High).

Hemingway & Riddler (1982), Marie's (1975) estimation of 1200-1800 m of exhumation, increasing westwards, is based only on offshore data, and thus cannot be considered reliable for the onshore Cleveland Hills. Kent (1980), based on evidence from sub-Upper Cretaceous Chalk thicknesses in areas adjacent to the Cleveland anticline, stated that the end-Cretaceous/early Tertiary inversion of the Cleveland anticline may be estimated to have removed between 500-800 m of section, and possibly around 1000-1300 m of section if the former Chalk cover showed variations analogous to those of the Sole Pit Trough. Hemingway & Riddler (1982) agreed that Upper Jurassic and Cretaceous cover rocks of estimated thickness 1.0-1.25 km have been eroded from the axis of inversion running approximately east-west along the Cleveland Basin's centre, but noted that such a thickness alone is inadequate to satisfy the known palaeo-temperatures of the Middle Jurassic along the axis. Based on the temperature of diagenesis determined from fluid inclusions in diagenetic sphalerite in the Middle Jurassic Dogger Formation, and Middle Jurassic coal vitrinite reflectance, Hemingway & Riddler (1982) concluded that 1.0-1.25 km of Tertiary sediment was also originally deposited in the region, then eroded, in

addition to the 1.0-1.25 km of Upper Jurassic and Cretaceous rocks that were removed.

Using sonic velocities in shales within the Permian Upper Marls and the Coal Measures intersected by wells in the Cleveland Basin/East Midlands Shelf, Whittaker *et al.* (1985) interpreted a maximum of 2.5 km of post-Cretaceous exhumation of the inverted Cleveland Basin, and an east-west increase in exhumation from less than 200 m to more than 1600 m across the East Midlands Shelf. Hillis (1993) analysed sonic velocities from the Upper and Middle Chalk, the Kimmeridge Clay, the Lias, and Bunter Sandstone in the Cleethorpes-1 and Welton-1 wells of the East Midlands Shelf, inferring apparent exhumation of 1.4-1.6 km and 1.6-1.7 km respectively, where Whittaker *et al.* (1985) inferred only 0.3 km and 0.6 km of exhumation respectively.

Green's (1989) apatite fission track analyses (AFTA) suggested a maximum of around 3.5 km of exhumation in the inversion axis of the Cleveland Basin, decreasing to 2.7-3 km in the Triassic 'fringe' of the Cleveland Basin. In addition, Green (1989) interpreted 1.3-1.7 km of late Cretaceous/Tertiary exhumation in the onshore East Midlands Shelf at Cleethorpes, and suggested that this value is exceeded over much of the East Midlands Shelf. Bray *et al.* (1992) combined vitrinite reflectance data from the East Midlands Shelf with AFTA results, and concluded there was a minimum of a little less than 1 km of exhumation over the area of Chalk outcrop near the coast, increasing westwards to more than 2 km towards the Pennines. The AFTA results of Green (1989) and AFTA and vitrinite reflectance results of Bray *et al.* (1992) yield higher exhumation estimates than the earlier compaction studies of Marie (1975) and Whittaker *et al.* (1985), but agree closely with the compaction-based exhumation estimates of Hillis (1993).

Holliday (1993) suggested that the use of a higher early Cenozoic mean surface temperature and a higher palaeogeothermal gradient in the exhumed section allows lower estimates of former cover to be made from Green's (1989) AFTA palaeotemperature determinations in the Cleveland Basin/East Midlands Shelf. Green's (1989) AFTA-based estimates of exhumation are consistently up to 1000 metres greater than suggested by stratigraphical data, or the mineralogical and shale compaction studies of Hemingway & Riddler (1982) and Whittaker *et al.* (1985) respectively (Holliday, 1993). However, both Green (1989) and Hillis (1993) suggested that the discrepancy between their results for the Cleveland Basin and East Midlands Shelf respectively and the earlier compaction studies of Marie (1975) and Whittaker *et al.* (1985) may be due to these studies using a reference compaction relationship from a region which is itself not at maximum burial-depth.

Clearly, recent estimates of the missing section in the Cleveland Basin/East Midlands Shelf that are based on AFTA (Green, 1989), AFTA combined with vitrinite reflectance (Bray *et al.*, 1992), or sonic velocities (Hillis, 1993), indicate higher amounts of exhumation in the Cleveland Basin/ East Midlands Shelf than stratigraphic reconstructions suggest. The above studies, as well as a number of more recent contributions, are discussed further in Section 5.5 with respect to the results of this study.

5.3 Post-Variscan Geological History of the Cleveland Basin/East Midlands Shelf

The Cleveland Basin and East Midlands Shelf comprise the onshore flank of the Mesozoic Southern North Sea Basin (Fig. 5.1). Following the cessation of Variscan shortening, the region began subsiding in Early Permian times. Lower Permian aeolian and

fluvial sands, lacustrine clays and halites were deposited into a Variscan postorogenic-collapse basin (Cameron *et al.*, 1992) which extended eastwards as far as northern Germany (Ziegler, 1990). At this time, the northern East Midlands Shelf formed an intrabasinal high (Cameron *et al.*, 1992). This basin configuration persisted through the Permian and most of the Triassic, with deposition of Upper Permian marine marls, sandstones, and evaporites giving way to the continental sandstones, evaporites, and mudstones of the Triassic Sherwood Sandstone and Mercia Mudstone Groups (Figs. 5.1, 5.2).

The Cleveland Basin and East Midlands Shelf began to develop through differential subsidence at the end of the Triassic (Rhaetian), with the Howardian-Flamborough Fault Zone (HFFZ, Fig. 5.1) forming the southern margin of the basin (Rawson & Wright, 1992). The Market Weighton High in the northern East Midlands Shelf formed an area of slow subsidence and shallow water deposition for much of the Jurassic (Fig. 5.1), while the Cleveland Basin to the north was subsiding rapidly (Rawson & Wright, 1992). Subsidence in the Cleveland Basin slowed in the Upper Jurassic, with the basin becoming a stable shelf with shallow water deposits, whilst the southern East Midlands Shelf continued to subside (Kent, 1980).

The northern part of the East Midlands Shelf was uplifted and eroded prior to an Albian marine transgression (Kent, 1980), resulting in a hiatus that increases progressively towards the Market Weighton High, where Lower Cretaceous Speeton Clay equivalents overlie the Lower Jurassic Lias (Figs. 5.1, 5.2). The shallow marine Upper Cretaceous Chalk which was subsequently deposited on the East Midlands Shelf shows little lateral variation in thickness or facies (Kent, 1980). The Cleveland Basin was inverted along a broadly east-west axis at the end of the Cretaceous/early Tertiary, resulting in the removal of the Upper Jurassic, Cretaceous, and Tertiary rocks of the basin (Hemingway & Riddler, 1982).

5.4 Methodology for Quantifying Apparent Exhumation

As shown in Chapter 3, apparent exhumation (E_A) is the vertical displacement of the Δt/depth trend (for a particular unit) from that of the normal compaction relation for that unit (Fig. 3.5). Apparent exhumation can be estimated graphically from plots of mean porosity against depth. However, in this study it was determined numerically using the equation:

$$E_A = \frac{1}{m}\left(\phi_u - \phi_o\right) - d_u \qquad \text{.....(5.1)}$$

where m is the reference porosity/depth gradient, ϕ_u and ϕ_o are the mean porosities of the well or sample under consideration and the surface porosity respectively, and d_u is the depth of the formation mid-point below sea-bed of the well under consideration, or the depth below the land surface of the sample under consideration. Although the porosity/depth relationship is exponential, over the depth range being considered, a linear relationship between porosity and burial-depth yields equivalent results (e.g. Hillis, 1991).

5.4.1 Selection of normal compaction relation

There have been a number of normal compaction relations proposed for the Upper Cretaceous Chalk (Fig. 5.3). Scholle (1977) suggested that porosity/burial-depth data from Deep Sea Drilling Program chalk samples, the Scotian Shelf, and the North Sea L/16-1 well probably provide typical compaction relations for offshore chalks. This normal porosity/depth curve was then converted by Scholle

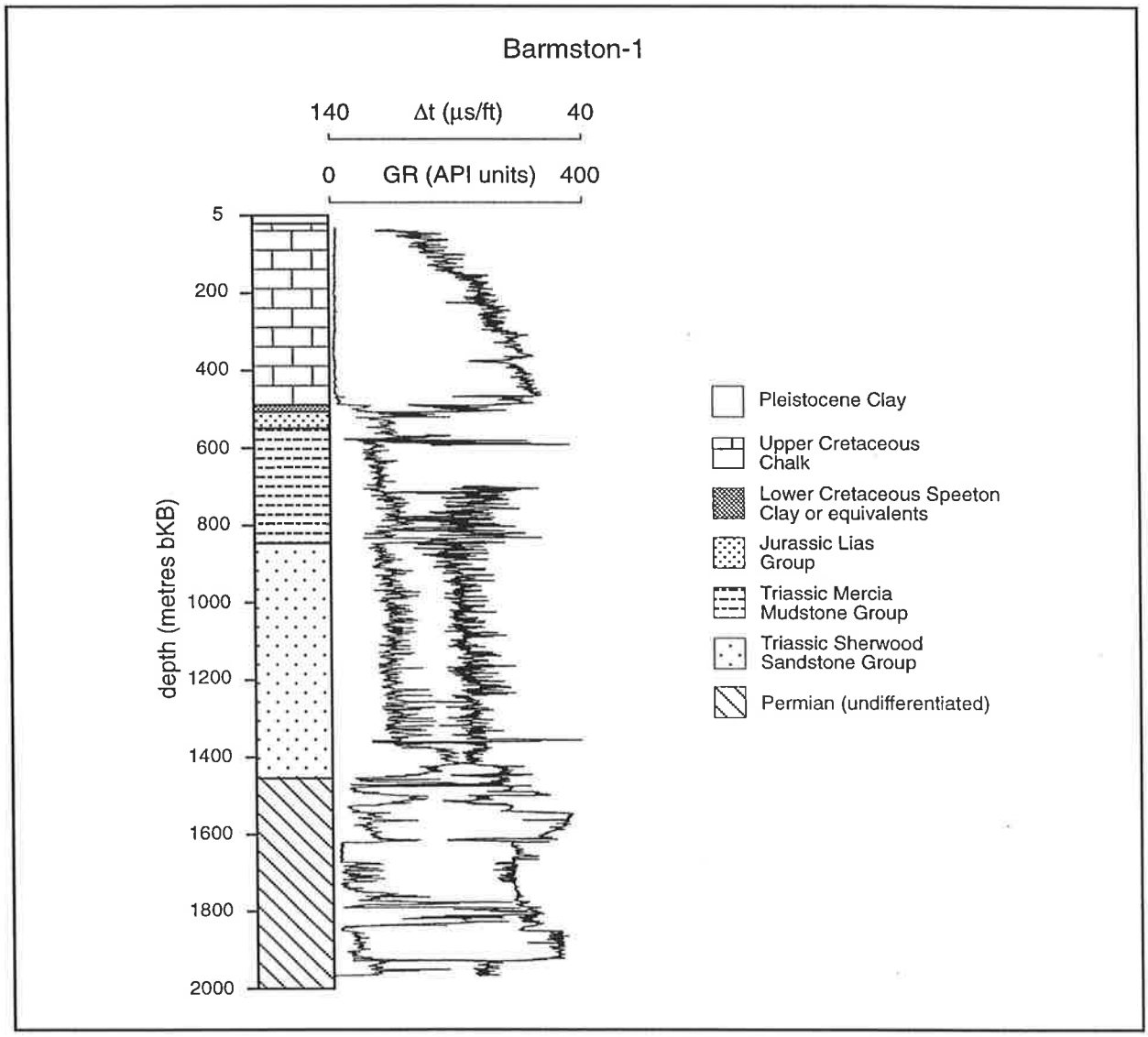

Fig. 5.2. Sonic transit time (Δt) and gamma ray (GR) log for Barmston-1, illustrating log characteristics for the Cleveland Basin/East Midlands Shelf.

(1977) to define sonic velocity versus depth relations for wet and dry chalk. The velocity/depth relations for wet and dry chalk of Scholle (1977) are shown in Fig. 5.3 in terms of Δt, the reciprocal of sonic velocity. Sclater & Christie (1980) combined near surface velocities from the Deep Sea Drilling Project chalks with the lowest limit of the porosity ranges in two wells in the Central Graben, to define a normal porosity/depth trend for the Upper Cretaceous Chalk. The porosity/depth trend of Sclater & Christie (1980) has been converted to Δt/depth using the velocity/porosity relations of Wyllie *et al.* (1956) and Raiga-Clemenceau *et al.* (1988) (Fig. 5.3).

Smith *et al.* (1994) noted that the porosity/depth relationship derived by Hillis (1993) for the Upper Cretaceous Chalk of the Southern North Sea differs significantly from the curves of Scholle (1977) and Sclater & Christie (1980), and suggested that Hillis (1993) consequently overestimated exhumation. However, Smith *et al.* (1994) used the relationship of Raiga-Clemenceau *et al.* (1988) to convert the normal porosity/depth trend of Sclater & Christie (1980) to a

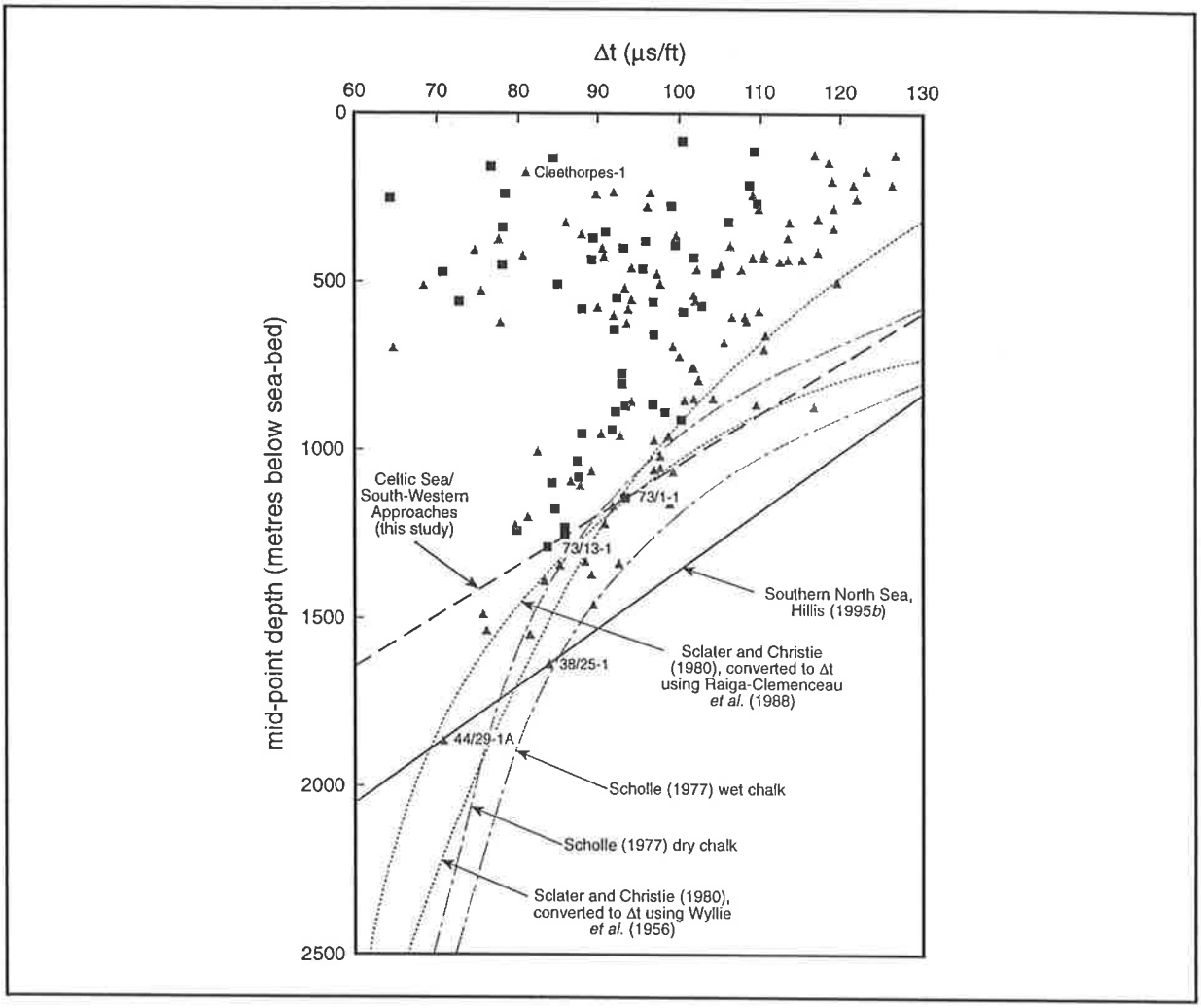

Fig. 5.3. Comparison of normal compaction relations for the Upper Cretaceous Chalk. Triangles are Southern North Sea wells from Hillis (1995*b*). Squares are Celtic Sea/South-Western Approaches wells from this study. The dot-dash curves are Scholle's (1977) velocity/depth relations for wet and dry chalk. The dotted curves are Sclater & Christie's (1980) porosity/depth relations converted to interval transit time using both Wyllie *et al*'s (1956) relation and Raiga-Clemenceau *et al*'s (1988) equation. The dashed line is the normal compaction relation for the Celtic Sea/South-Western Approaches derived in this study, whilst the solid line is the normal compaction relation for the Upper and Middle Chalk from Hillis' (1995*b*) Southern North Sea study.

velocity/depth trend as shown in Figure 5.3, whereas Sclater & Christie (1980) originally used the velocity/porosity relationship of Schlumberger (1974) to derive porosities from velocity. The author could not find a porosity/velocity relation in Schlumberger (1974). Such would be the appropriate relationship to convert Sclater & Christie's (1980) porosity/depth trend back to velocity/depth. In order to illustrate the significance of the porosity/velocity relation selected, Figure 5.3 shows the porosity/depth relation of Sclater & Christie (1980) converted to velocity/depth using the relations of both Raiga-Clemenceau *et al.* (1988) and Wyllie *et al.* (1956).

Hillis (1995*b*) slightly refined the normal

compaction trend for the Upper Cretaceous Chalk of the Southern North Sea using the selection criteria for reference wells outlined in Chapter 3 (Fig. 5.3). However, the normal compaction trend of Hillis (1995*b*) is still considerably less compacted than that of Scholle (1977) or Sclater & Christie (1980) (Fig. 5.3). However, as noted by Hillis (1994), the 'more compacted' normal relationships of Scholle (1977) or Sclater & Christie (1980) are based on very few wells (which may themselves be above maximum burial-depth), and do not disprove a relationship based on a significantly larger dataset.

Normal compaction relations from the Southern North Sea Basin are suitable for use in the Cleveland Basin/East Midlands Shelf because they comprise the onshore flank of the Southern North Sea Basin. Hillis' (1995*b*) normal compaction relation for the Upper and Middle Chalk, constrained by the normally compacted, or reference wells 38/25-1 and 44/29-1A, has been used in this study.

Skagen (1992) suggested that shale compaction-based estimates of exhumation have a potential accuracy of ± 200 m. As discussed in Chapter 4, the spread of the sonic logs of the reference wells around the normal compaction relation for the Upper Cretaceous Chalk in the Celtic Sea/South-Western Approaches allows an empirical estimate of the error in the normal compaction relation of ± 250 m. A potential error in the normal compaction relation of ±250 m is also suggested for this study of the Cleveland Basin/East Midlands Shelf.

5.4.2 Calculation of mean porosities from well data

Three Cleveland Basin/East Midlands Shelf wells intersecting geophysically logged Chalk units, Barmston-1, Cleethorpes-1, and Rudston-1, were analysed in this study (Fig. 5.1). The top and base of the Upper Cretaceous Chalk were picked from vertically-compressed (1:4000 depth-scale) plots of the sonic and gamma ray logs (e.g. Fig. 5.2). Geophysical logging commenced within the Chalk in each case and the top of the Chalk was picked at the first reliable sonic log data. The base of the Chalk is marked by a distinctive (downwards) increase in both the gamma ray and sonic logs (Fig. 5.2), and the base Chalk was picked at the top of this increase. The mean sonic interval transit time (Δt, the reciprocal of velocity) of the Chalk was determined from digital log data for the Chalk interval thus defined.

To enable comparison with sample porosities, it was necessary to convert interval transit time, as measured by the sonic log, to porosity. The mean interval transit times for the three Cleveland Basin/East Midlands Shelf wells, and the wells defining Hillis' (1995*b*) normal compaction relation, were converted to porosity using the equation of Raiga-Clemenceau *et al.* (1988):

$$\Delta t_{log} = \frac{\Delta t_{ma}}{(1-\phi)^{x}} \qquad \text{.....(5.2)}$$

where Δt_{log} is the sonic log interval transit time, Δt_{ma} is the matrix transit time, and the exponent x is specific to matrix lithology. In this case, for calcite, the appropriate matrix transit time is 47.6 μs/ft, and x is 1.76 (Raiga-Clemenceau *et al.*, 1988). The mid-point depths, mean interval transit times, and mean porosities of the Chalk intervals are given in Table 5.1.

5.4.3 Determination of porosity of Chalk samples

With the exception of the coastal cliff sections such as at Flamborough, much of the Chalk outcrop is limited to ten metre-scale exposures in the numerous small quarries throughout the Cleveland Basin/East

well	mid-point depth (metres)	mean interval transit time (µs/ft)	mean porosity (%)
38/25-1	1630	83.7	27.4
44/29-1A	1860	70.6	20.0
Barmston-1	260	78.4	24.7
Cleethorpes-1	180	81.6	26.0
Rudston-1	220	70.6	20.1

Table 5.1. Mid-point depths (metres below sea-bed/land surface), mean interval transit times (µs/ft), and mean porosities (%) for the wells analysed in this study. Mean porosities were calculated from mean interval transit times using Equation 5.2.

Midlands Shelf area. This limited vertical outcrop at inland exposures, combined with the generally flat-lying nature of the Chalk beds, limited sampling to restricted stratigraphic sections at individual locations. A minimum of three samples were taken from regularly-spaced intervals at the sampling sites shown on Figure 5.1 in order to determine Chalk porosity for the locality. The 100 m thick section of Chalk exposed in the Bempton Cliffs on the north side of Flamborough Head (samples 4-9 on Fig. 5.1) was sampled at a 15 m interval, to give an indication of the variation in porosity of the Chalk on a larger scale.

Care was taken at all times to ensure samples were fresh and well-consolidated, to avoid the possibility of weathered rock giving erroneous results. Where possible, samples were cut into two pieces to enable two density/porosity calculations for each sample, as a test of the variation inherent in the methodology described below.

A number of sample sites were also chosen for their proximity to onshore wells, to enable a comparison between exhumation estimates from samples and adjacent wells. However, it was found that wherever wells have been drilled where the Chalk outcrops, geophysical logging did not commence until beneath the base of the Chalk, hence no direct comparisons could be made.

Porosities of the 22 samples were determined using a modified version of the water imbibition method described by Emerson (1990). Each sample was soaked in deionised water for 72 hours to ensure saturation of the effective (interconnected) porosity of the rock. A Sartorius 2007 MP electronic balance was used to determine the mass of the water saturated sample when submerged in deionised water (m_{sub}), and to determine the mass of the water saturated sample (m_{sat}). The bulk volume V_B of the sample was calculated using Archimedes' buoyancy principle (Equation 5.3), where ρ_w is the density of deionised water (0.99821 g/cm^3).

$$V_B = \frac{m_{sat} - m_{sub}}{\rho_w} \qquad \text{.....(5.3)}$$

Each sample was then heated to 150°C for 24 hours to expel all water from the pore spaces of the rock, and the dry mass (m_{dry}) was determined. The dry bulk density ρ_B of the sample was calculated

using Equation 5.4.

$$\rho_B = \frac{m_{dry}}{V_B} \qquad .....(5.4)$$

Chalk porosity cannot be reliably determined from the volume of imbibed water because the water imbibition method assumes that occluded voids are negligible (Emerson, 1990). The low permeability of the Chalk prevents fluid access to much of the primary porosity of the rock, thus the apparent porosity calculated from the volume of imbibed water is significantly less than the true total porosity of the rock. Similarly, estimates of the grain density of the samples could not be calculated using this method. However, if the Chalk grain density (ρ_g) can be assumed to be 2.71 g/cm^3 (that of calcite), the porosity (ϕ) can be calculated using the relation:

$$\phi = \frac{\rho_g - \rho_B}{\rho_g} \qquad .....(5.5)$$

It should be noted that the low permeability of the Chalk does not affect measurement of bulk volume using Archimedes' principle, and assuming oven drying removes all water from primary porosity, the calculated dry density may be used to calculate porosity as above without causing erroneous results.

The modified water imbibition experimental procedure was repeated for each of the 22 samples to ensure that the bulk volumes calculated using Equation 5.3 were consistent. The results are given in Table 5.2. The measurement of the saturated mass proved to be the most likely source of error, as water began evaporating from the sample as soon as it was exposed to the atmosphere. However, the rate of water loss was sufficiently slow that a relatively accurate measurement of saturated mass could be made, as shown by the maximum percentage difference in calculated bulk volume of 1.1% (Table 5.2). Much of the difference between the sample masses between the first and second iteration can be attributed to loss of sample during handling, especially as a result of repeated saturation and desiccation, as the measurements for the second iteration are consistently lower. However this sample loss has no effect on the calculated bulk density.

As previously mentioned, where possible samples were halved to give an indication of the variation in bulk density and hence porosity within a sample. As can be seen in Table 5.3, there is a maximum difference of 2.3% between porosity measurements from two halves of the same original sample. This variation has an insignificant influence on estimates of apparent exhumation.

The porosities and grain densities of three of the samples were also measured using a commercial mercury injection technique (Emerson, 1990). The porosities calculated using the modified water imbibition method are at most 2% different to those calculated using the mercury injection technique, as shown in Table 5.4. The modified water imbibition method is thus considered a sufficiently accurate procedure for determining Chalk sample porosities.

5.5 Apparent Exhumation in the Cleveland Basin/East Midlands Shelf

The calculated porosity of each of the samples, and the mean porosity of the Chalk in each of the wells, was plotted against the mid-point depth (Fig. 5.4). With the exception of the samples from Flamborough Head (samples 4-9), all of the samples were at the surface, hence in these cases the depth d_u in Equation 5.1 is zero. Table 5.5 gives the apparent exhumation values for each of the samples calculated using Equation 5.1, as well as the average and standard deviation for each sample locality. The consistency

sample number	first measurement			repeat measurement			dry mass	average	% error
	m_{sub}	m_{sat}	v_B	m_{sub}	m_{sat}	v_B		v_b	in v_B
1	22.29	37.98	15.72	22.20	37.85	15.68	35.21	15.70	0.30
2	18.73	31.76	13.05	18.71	31.77	13.09	29.67	13.07	0.27
3A	40.07	67.53	27.51	39.98	67.45	27.52	63.93	27.52	0.04
3B	44.21	74.37	30.22				70.17	30.22	
4	22.06	37.08	15.05	22.04	37.08	15.06	34.92	15.06	0.09
5	15.38	25.32	9.95	15.36	25.31	9.96	24.44	9.96	0.07
6	16.43	27.56	11.15	16.40	27.56	11.18	25.97	11.16	0.26
7A	17.88	30.29	12.43	17.81	30.26	12.47	28.35	12.45	0.27
7B	35.23	59.11	23.92				55.97	23.92	
8A	17.26	29.60	12.36	17.23	29.59	12.38	27.34	12.37	0.21
8B	15.03	26.06	11.05				23.78	11.05	
9	12.73	21.12	8.40	12.69	21.17	8.50	20.22	8.45	1.12
10A	28.85	49.75	20.95	28.76	49.67	20.95	45.69	20.95	0.00
10B	41.66	71.69	30.09				66.09	30.09	
11A	17.52	30.74	13.25	17.40	30.62	13.25	27.74	13.25	0.02
11B	24.63	43.62	19.02				39.66	19.02	
12	13.34	23.29	9.97	13.26	23.20	9.96	21.13	9.96	0.05
13	20.16	34.87	14.74	20.14	34.85	14.74	31.93	14.74	0.01
14A	11.99	22.08	10.11	11.96	21.96	10.01	18.98	10.06	0.94
14B	25.39	46.38	21.03	25.39	46.32	20.97	40.28	21.00	0.30
15A	21.56	37.68	16.16	21.42	37.49	16.10	34.27	16.13	0.36
15B	34.10	59.92	25.86	34.14	59.94	25.85	55.15	25.86	0.06
16A	30.12	52.66	22.58	30.05	52.53	22.52	47.85	22.55	0.28
16B	34.18	59.55	25.42	34.20	59.52	25.37	54.45	25.40	0.22
17A	25.49	44.70	19.24	25.43	44.65	19.26	40.49	19.25	0.09
17B	24.07	42.08	18.04				38.34	18.04	
18	28.63	49.49	20.90	28.53	49.43	20.93	45.60	20.92	0.17
19A	28.20	48.61	20.45	28.15	48.60	20.48	44.69	20.47	0.16
19B	30.42	52.64	22.26				48.46	22.26	
20A	34.87	58.92	24.09	34.85	58.88	24.08	55.57	24.08	0.05
20B	51.40	87.06	35.73				82.11	35.73	
21	67.62	114.25	46.72	67.52	114.06	46.62	107.57	46.67	0.21
22A	33.07	57.90	24.88	32.99	57.74	24.79	52.27	24.84	0.35
22B	39.83	69.63	29.85				63.15	29.85	

Table 5.2. Measured sample masses and calculated sample bulk volumes. m_{sub} = mass of water saturated sample suspended in water (in grams); m_{sat} = mass of water saturated sample (in grams); V_B = bulk volume (cm^3) calculated by Equation 5.3. Where more than one piece of a sample was weighed, a second iteration was not performed.

of results from Flamborough Head (samples 4-9), where 100 m of section was sampled at the same location, suggests that even stratigraphically-limited Chalk outcrop samples may be used to reliably determine apparent exhumation based on overcompaction.

Figure 5.5(a) shows the contoured map of the mean apparent exhumation estimate for each sample and well locality. Apparent exhumation estimates from the Upper and Middle Chalk of 13 offshore wells analysed by Hillis (1995*b*) are also incorporated in the contour map of Figure 5.5(a). Figure 5.5(a)

sample	bulk density (g/cm^3)		porosity (%)		difference between
	A	B	A	B	calculated porosities
1	2.24		17.24		
2	2.27		16.22		
3	2.32	2.32	14.26	14.31	0.05
4	2.32		14.43		
5	2.46		9.41		
6	2.33		14.15		
7	2.28	2.34	15.96	13.65	2.31
8	2.21	2.15	18.44	20.57	2.14
9	2.39		11.70		
10	2.18	2.20	19.51	18.94	0.57
11	2.09	2.08	22.74	23.08	0.34
12	2.12		21.75		
13	2.17		20.04		
14	1.89	1.92	30.41	29.21	1.19
15	2.12	2.13	21.59	21.29	0.30
16	2.12	2.14	21.69	20.89	0.80
17	2.10	2.13	22.38	21.58	0.80
18	2.18		19.55		
19	2.18	2.18	19.41	19.68	0.26
20	2.31	2.30	14.85	15.19	0.34
21	2.30		14.95		
22	2.10	2.12	22.34	21.94	0.40

Table 5.3. Bulk densities and porosities calculated from Equations 5.4 & 5.5. A and B are two halves of an individual sample. The difference between the A and B calculated porosities from the same sample is given where applicable.

sample number	porosity (%) determined by water imbibition	porosity (%) determined by mercury injection	percentage error	grain density (g/cm^3)
14B	29.2	28.7	1.74	2.70
15B	21.3	21.1	0.95	2.71
16B	20.9	20.8	0.48	2.71

Table 5.4. Comparison between porosities determined using the modified water imbibition and commercial mercury injection techniques. The grain densities of the three samples were measured using the mercury injection technique.

shows an increase in apparent exhumation from east to west across the onshore East Midlands Shelf. In addition, the inversion of the Cleveland Basin is evident in the change from an east-west gradient to a northwards increase in apparent exhumation, with the maximum apparent exhumation occurring in the Cleveland Basin. The change in orientation of the apparent exhumation contours from north-south in the East Midlands Shelf to east-west at Flamborough Head is coincident with the Howardian-Flamborough Fault Zone (Fig. 5.1), which forms the southern margin of the Cleveland Basin. The apparent exhumation trends of Figure 5.5(a) mirror the onshore geology shown in Figure 5.1, with the greater apparent exhumation in the Cleveland inversion axis superimposed on a regional westward increase in apparent exhumation. The 2 km apparent exhumation contour closely coincides with the outcrop pattern of the base of the Upper Cretaceous Chalk.

Hillis' (1995*b*) study of exhumation in the

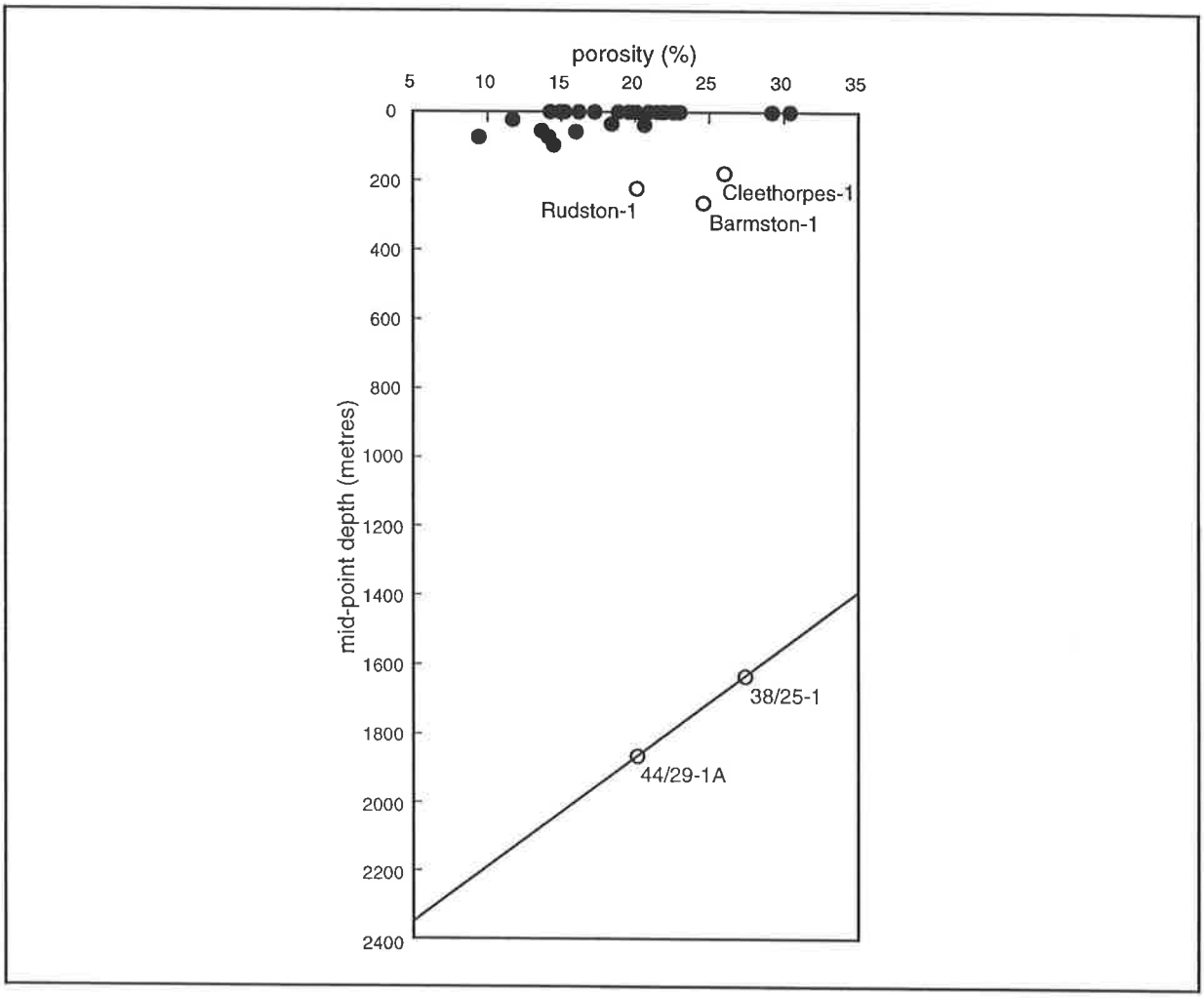

Fig. 5.4. Porosity versus mid-point depth plot for the Upper Cretaceous Chalk, where depth is in metres below surface for onshore wells, and metres below sea-bed for offshore wells. Open circles are wells, and closed circles are samples. Equation for normal compaction trend is ϕ=0.802-(3.24×10^{-1})d.

Southern North Sea based on velocities in the Upper Cretaceous Chalk was poorly constrained nearshore and onshore because of a lack of wells (Fig. 5.5b). However Hillis' (1995*b*) map of the mean of apparent exhumation estimates from velocities in the Upper and Middle Chalk, the Bunter Sandstone, and Bunter Shale (Fig. 5.5c) is better constrained (by more wells) than that based on velocities from the Chalk alone. The inclusion of the onshore estimates from this study results in a better constrained map of apparent exhumation based on compaction of the Upper Cretaceous Chalk (Fig. 5.5a) than that of Hillis (1995*b*). This improved map shows close agreement with Hillis' (1995*b*) mean apparent exhumation map based on velocities in the Upper and Middle Chalk, Bunter Sandstone, and Bunter Shale (Fig. 5.5c).

The Upper Cretaceous Chalk has been eroded from most of the Cleveland Basin, hence this study can only provide an apparent exhumation estimate for the southern margin of the basin. This estimate of 2 km exceeds the minimum exhumation estimate by Marie (1975) of 1200-1800 m for the Cleveland Basin. Whittaker *et al.* (1985) also suggest lower values of exhumation for the Cleveland Basin/East

sample no/ well	E_A (metres)	average E_A	standard deviation
1	1950	2000	40
2	1980		
3A	2040		
3B	2040		
4	1940	1970	100
5	2110		
6	1980		
7A	1940		
7B	2010		
8A	1870		
8B	1810		
9	2090		
10A	1880	1830	50
10B	1890		
11A	1780		
11B	1770		
12	1810		
13	1860		
14A	1540	1730	140
14B	1580		
15A	1810		
15B	1820		
16A	1810		
16B	1830		
17A	1790	1840	40
17B	1810		
18	1870		
19A	1880		
19B	1870		
20A	2020	1930	120
20B	2010		
21	2020		
22A	1790		
22B	1800		
Barmston-1	1460		
Cleethorpes-1	1490		
Rudston-1	1640		

Table 5.5. Apparent exhumation values calculated from Equation 5.1 for each sample/well, with mean and deviation for each sample locality. m=-3.24×10^{-1}, and ϕ_o=0.802.

Midlands Shelf than presented herein. The discrepancy between these compaction-based studies and the results of this study may be due to these earlier studies using a normal compaction relation from a region that is itself not at maximum burial-depth, as suggested by Green (1989) and Hillis (1993).

There has been much debate on both AFTA and compaction-based techniques of estimating exhumation and in particular on whether these methods over-estimate exhumation (e.g. Holliday, 1993; Green *et al.*, 1995; and the discussions/replies

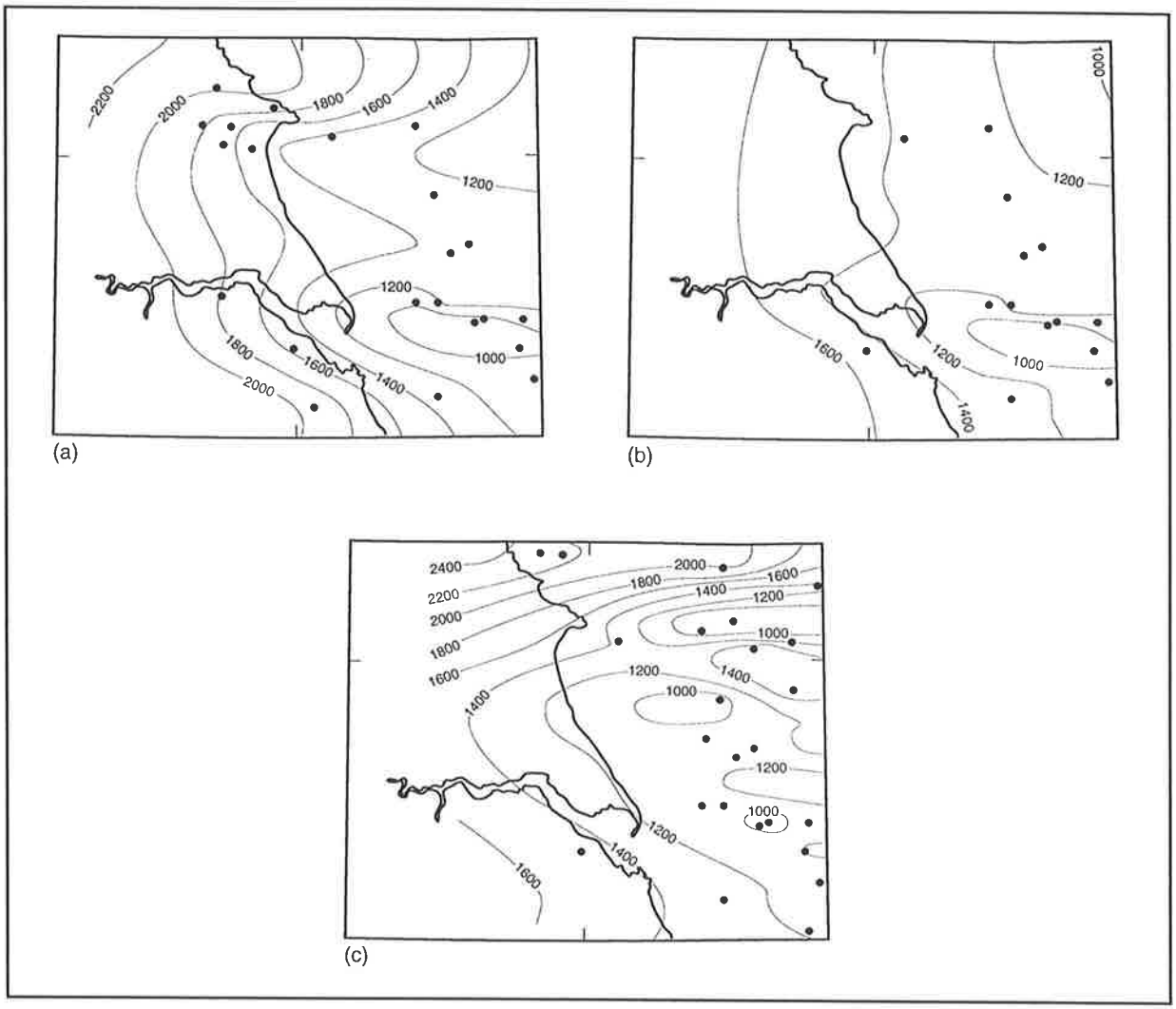

Fig. 5.5. Apparent exhumation maps for (a) the Upper Cretaceous Chalk, (b) the Upper and Middle Chalk of Hillis (1995*b*), and (c) the mean of estimates from the Upper and Middle Chalk, Bunter Sandstone, and Bunter Shale from Hillis (1995*b*).

of McCulloch, 1994/Holliday, 1994; Smith *et al.*, 1994/Hillis, 1994). This debate has been published in detail elsewhere, and only those issues directly related to the Cleveland Basin/East Midlands Shelf are addressed herein.

Holliday (1993) suggested that it was necessary to use higher early Cenozoic mean surface temperatures and higher palaeogeothermal gradients than those used by Green (1989) in modelling apatite fission track results. Assuming heat flow remained constant, Holliday (1993) thus predicted lower values of exhumation for the East Midlands Shelf than Green (1989). Chadwick *et al.* (1994) followed Holliday's (1993) approach in the Lake District Block, and estimated post-Cretaceous exhumation of the central Lake District was typically less than 1750 m, compared with estimates of around 3 km by Lewis *et al.* (1992). Bray *et al.* (1992) argued that a heat flow-based approach to thermal history reconstruction is subject to considerable uncertainty. Bray *et al.* (1992) used a combined AFTA and vitrinite reflectance methodology to estimate the palaeogeothermal gradients for a number of East Midland Shelf and Cleveland Basin wells, with the resultant palaeogeothermal gradients yielding lower apparent exhumation estimates than those of Green (1989), as

had been proposed by Holliday (1993).

However, Bray *et al.* (1992) suggested that to explain the observed cooling in the Cleveland Basin/East Midlands Shelf, approximately 1 km of exhumation is still required in the Cleethorpes-1 well, increasing westwards to more than 2 km towards the Pennines, with up to 2.6 km of Tertiary exhumation necessary in the southern Cleveland Basin. These results are comparable with the compaction-based estimates in this study, which are not subject to the same uncertainties due to thermal history reconstruction. The results herein thus provide independent support for the kilometre-scale exhumation of the Cleveland Basin/East Midlands Shelf suggested by the AFTA and vitrinite reflectance-based methods of Bray *et al.* (1992). The results herein suggest that exhumation was greater than that suggested by Holliday (1993).

Scotchman (1994) used organic biomarkers (triterpanes, steranes, and triaromatic steranes) to accurately determine maturity levels and hence burial history for the Kimmeridge Clay from the onshore UK. The hopane and sterane maturity values suggest that the Kimmeridge Clay had been exhumed by between 1.26 km and 1.53 km on the southern margin of the Cleveland Basin near the coast, increasing to between 2.0 km and 2.1 km inland, and between 1.05 km and 1.26 km of exhumation had occurred on the East Midlands Shelf. The results of Scotchman (1994) provide further support for the magnitude of apparent exhumation suggested for the Cleveland Basin/East Midlands Shelf by this study and by Bray *et al.* (1992).

As discussed in Section 5.2, several authors (e.g. Holliday, 1993; Smith *et al.*, 1994) have suggested that there are difficulties in reconciling the amount of apparent exhumation suggested by AFTA and compaction methods for the Cleveland Basin/East Midlands Shelf with the Mesozoic and Cenozoic stratigraphy preserved in the sedimentary basins around northern England. However, if Tertiary exhumation was regional as the above estimates based on petrophysical properties suggest, then the technique of reconstructing maximum probable sediment thickness from preserved thicknesses (e.g. Kent, 1980; Holliday, 1993) is flawed. Indeed, a previously unrecorded outlier of Tertiary sediments on the northeast corner of the East Midlands Shelf, about 50 km east of the Humberside coast, has recently been documented by Stewart & Bailey (1996). Stewart & Bailey (1996) suggested that the erosive truncation of sediments within the outlier shows that they are remnants of a more extensive Palaeogene cover on the East Midlands Shelf. This outlier provides some indication of the sedimentary sequences that compaction-based estimates of apparent exhumation suggest were eroded from the East Midlands Shelf. Kent (1980) and Holliday (1993) made no allowance for such eroded Tertiary sedimentary rocks in their stratigraphic reconstruction of the maximum burial-depth of northern England.

5.6 Conclusions

(1) The modified water imbibition method for determining density and porosity described in this chapter yields similar results to the more expensive mercury injection laboratory method, provided an assumption for the grain density can be made. For a consistent lithotype such as the Upper Cretaceous Chalk of eastern England, such an assumption is valid, provided care is taken to avoid flint bands within the Chalk when sampling.

(2) The consistency of results from Flamborough Head (samples 4-9), where 100 m of section was sampled at the same location, suggests that even stratigraphically-limited Chalk outcrop samples may

be used to reliably determine porosity and thus apparent exhumation.

(3) Sample and geophysical log-based Chalk porosities suggest that Late Cretaceous/Tertiary exhumation in the East Midlands Shelf increased from 1.2 km near the coast to more than 2 km inland to the west. The southern margin of the Cleveland Basin was exhumed by 2 km, with exhumation increasing towards the structural inversion axis in the basin centre. This pattern of apparent exhumation controls the regional outcrop distribution of the Upper Cretaceous Chalk in the Cleveland Basin/East Midlands Shelf.

(4) The apparent exhumation estimates for the Cleveland Basin/East Midlands Shelf presented herein, whilst being greater than earlier compaction-based estimates such as those of Marie (1975) and Whittaker *et al.* (1985), show very good agreement with the recent AFTA-based exhumation estimates of Bray *et al.* (1992), and the organic biomarker-based estimates of Scotchman (1994).

Chapter 6

Determining the Tectonic Subsidence/Uplift History of the Celtic Sea/ South-Western Approaches

6.1 Introduction

Geodynamic models of the tectonic subsidence/uplift of a sedimentary basin model the vertical response of the basement to driving or tectonic forces, in the absence of surface loads. These geodynamic models are essentially forward models, where an initial set of parameters or boundary conditions are established, and the models then run to predict tectonic subsidence and uplift through time. A number of such geodynamic models are discussed in Chapter 7. The parameters used in these models must, however, be constrained by reconstructing the so-called tectonic subsidence/uplift history of the basin from the present day basin stratigraphy. Thus, to model the geodynamic origin of the Celtic Sea/South-Western Approaches (as undertaken in Chapter 8), it is first necessary to reconstruct the tectonic subsidence/uplift history of the region. In this thesis, a two-dimensional approach to geodynamic modelling has been undertaken. The reasons for a two-dimensional model are addressed in Chapter 7. In this chapter, the principles of determining tectonic subsidence/uplift histories from preserved stratigraphy are discussed, and then applied to a regional cross-section constructed from SWAT deep seismic profiles (Chapter 2).

Before the tectonic subsidence/uplift history of the Celtic Sea/South-Western Approaches can be reconstructed, however, the SWAT seismic profiles must be converted from two-way time to depth. The following section addresses the selection and depth conversion of the SWAT profiles used in determining the tectonic subsidence/uplift history of the Celtic Sea/South-Western Approaches.

6.2 Selection and Depth Conversion of SWAT Seismic Profiles

Figure 2.3 shows the location of the SWAT deep seismic traverses. SWAT lines 5, 6, and 7 were selected to form a profile across the Celtic Sea/South-Western Approaches (Fig. 6.1). These lines were selected because they form the most continuous profile across the basins of the Celtic Sea/South-Western Approaches, with only a slight offset across the Cornubian Platform. An additional advantage of the selected lines is that they do not contain any significant Triassic salt, hence the complications of post-depositional salt movement do not need to be accounted for in the modelling process. It should be noted that the Oligo-Miocene unconformity shown in the St. Mary's Basin on Figure 6.1 is only an approximation based on Evans' (1990) surface geology map and reflections on SWAT 7 that are obscured by sea-bottom multiples.

The SWAT deep seismic lines of Chapter 2 needed to be converted from seismic two-way time to depth. A layer-cake approach to depth conversion was followed with a constant velocity assigned to each unit in the profile. The velocities assigned were derived from the sonic logs of all of the wells used in the study. The average Δt of each unit in each well was determined. The average Δt values from each well were then combined into a single average, which was weighted according to the thickness of the logged

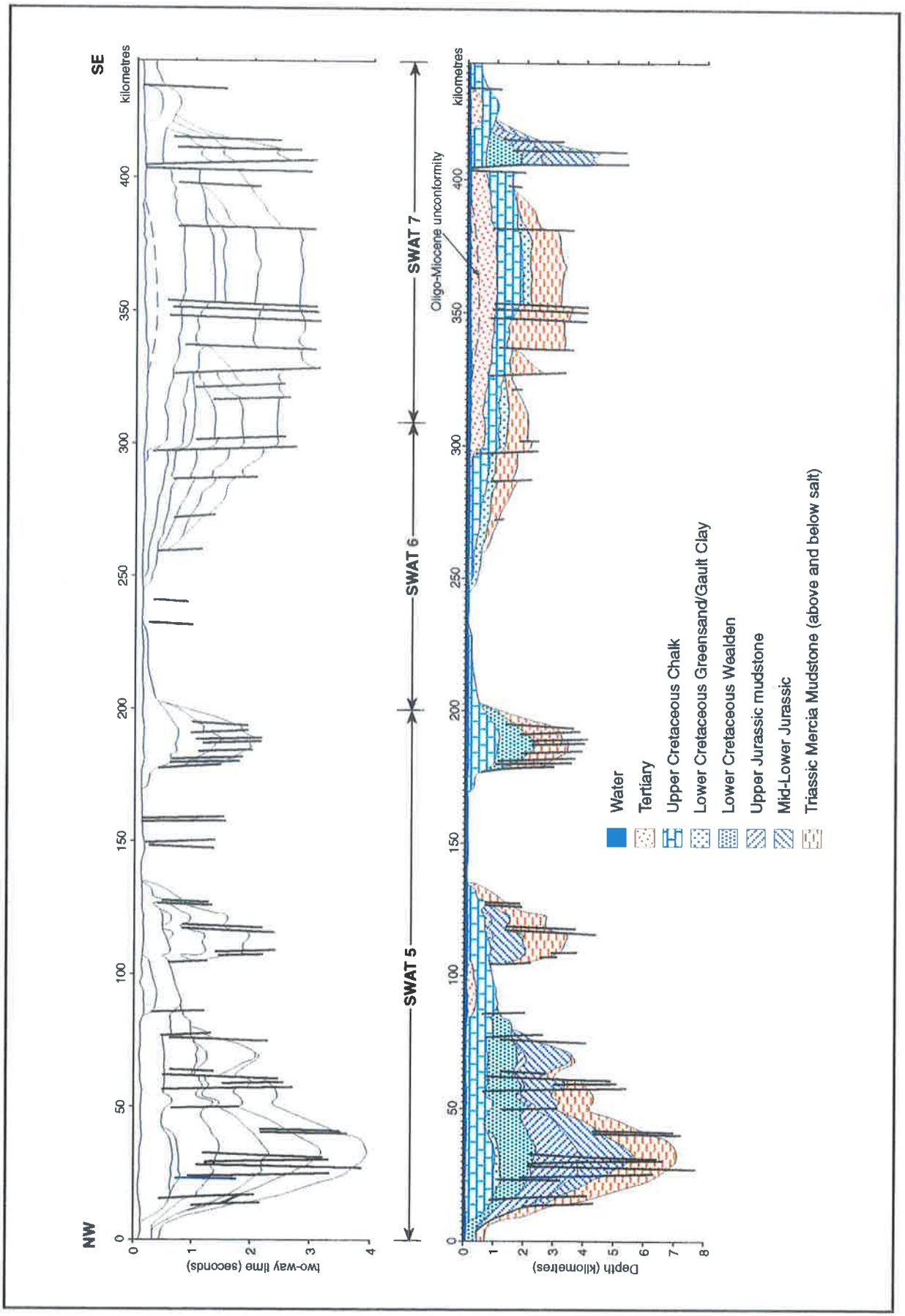

Fig. 6.1. Interpreted seismic (two-way time) profile and depth converted cross-section for modelling the subsidence/uplift history of the Celtic Sea/South-Western Approaches. See Figure 2.3 for location of sections.

interval in each well. The weighted average interval transit times were then converted to interval velocities (Table 6.1).

The Celtic Sea/South-Western Approaches profile was depth converted by multiplying the interval two-way time of each unit by the appropriate interval velocity. This operation was performed every 2.5 kilometres along the profile, at the points indicated along the top of the depth converted profile in Figure 6.1.

6.3 Basic Principles of Sediment Decompaction

As previously mentioned, geodynamic models of the subsidence/uplift of a sedimentary basin predict the response of the basin to tectonic forces in the absence of surface loads. When reconstructing the tectonic evolution of a basin it is thus necessary to remove the effects of the gravitational load of the basin fill. To calculate the gravitational load of the sedimentary sequence, the average density of the sequence through time must be calculated. However, as shown in Chapter 3, the porosity of a sedimentary layer decreases with burial as pore fluids are expelled, and the layer's density thus increases. The present-day density of a sedimentary layer is therefore not appropriate for determining the average density of the sedimentary sequence in the past. Similarly, sediment compaction and porosity loss implies that the present day thickness (volume) of a sedimentary layer is less than it was prior to burial by subsequent units. To determine the average density and thickness of a sedimentary sequence through time, the sequence must be progressively decompacted as each layer is backstripped from the top of the sequence.

The sediment backstripping and decompaction technique used in this thesis is adopted from that of Sclater & Christie (1980). A sedimentary unit is decompacted back to its original thickness by moving the unit back up its porosity/depth relation, to replace the porosity lost during compaction. Assuming that all lithologies follow an exponential porosity/depth relation (Section 6.5), Sclater & Christie (1980) derived the following equation for the decompacted thickness of a sedimentary layer after backstripping:

$$z_2' - z_1' = z_2 - z_1 - \frac{\phi_o}{c}\left(e^{-cz_1} - e^{-cz_2}\right) + \frac{\phi_o}{c}\left(e^{-cz_1'} - e^{-cz_2'}\right) \quad \text{.....(6.1)}$$

where z_1 and z_2 are the present depth of the top and bottom of the sedimentary layer being decompacted, z_1' and z_2' are the depth of the top and bottom of the sedimentary layer after backstripping and decompaction (Fig. 6.2), ϕ_o and c are constants from the porosity/depth relation (Equation 6.2; Section 6.5).

Beginning with the uppermost layer, one layer at a time is removed. Each time a layer is removed the underlying layers are decompacted, and a new depth to basement is calculated. The decompaction procedure is repeated until basement is restored to the surface.

Figure 6.3 illustrates the technique of backstripping and decompaction for the Penma-1 well on the Amorican Platform. Each time a layer is removed, the underlying units are decompacted, increasing in thickness. This thickness increase counteracts the removal of the top layer of sediment, hence the reduction in decompacted depth to basement is less than the thickness of the removed layer of sediment. For example, backstripping the 228 metre-thick Mio-Pliocene shale from the top of the sequence of Penma-1 results in a decrease in the basement depth of only 116 metres.

When approximately the middle of the stratigraphic sequence being backstripped is reached, the decompaction of the unit being backstripped

unit	generalised lithology	no. of wells	depth-conversion velocity (kms^{-1})
Tertiary	shaly limestone	22	2.55
Chalk	chalk	49	3.43
Greensand/Gault Clay	shaly sand	44	3.19
Wealden	shaly sand	35	3.45
Upper Jurassic	shale	29	3.74
Mid-Lower Jurassic	shaly limestone	40	3.74
Mercia Mudstone	shale	33	3.86

Table 6.1. Depth-conversion velocities for the Celtic Sea/South-Western Approaches.

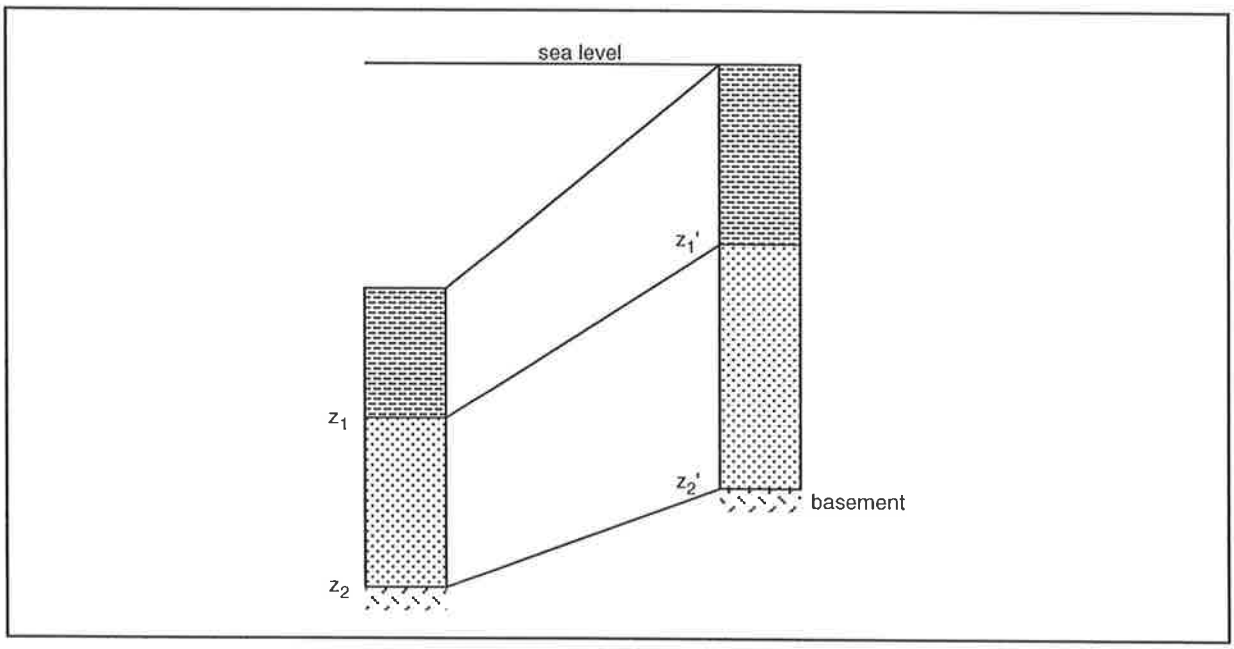

Fig. 6.2. Schematic diagram outlining the decompaction as a layer of sediment is removed (after Sclater & Christie, 1980).

becomes greater than the underlying sequence decompacts with its removal. As a result, the decompacted depths to basement change by more than the present-day thickness of the units being backstripped. Hence removal of the Upper Cretaceous Chalk from Penma-1, with a present thickness of 363 metres and decompacted thickness of 582 metres, results in a change in basement depth of 525 metres. Decompacting a sediment sequence thus predicts more rapid early subsidence and slower later subsidence than present well thicknesses (Fig. 6.3).

6.4 Decompaction of Exhumed Sequences

If a sedimentary sequence, such as that in the Celtic Sea/South-Western Approaches, has undergone exhumation, overcompaction of the pre-exhumation units and their non-compaction during later burial must be considered. Three types of exhumation and later subsidence patterns can be distinguished in terms

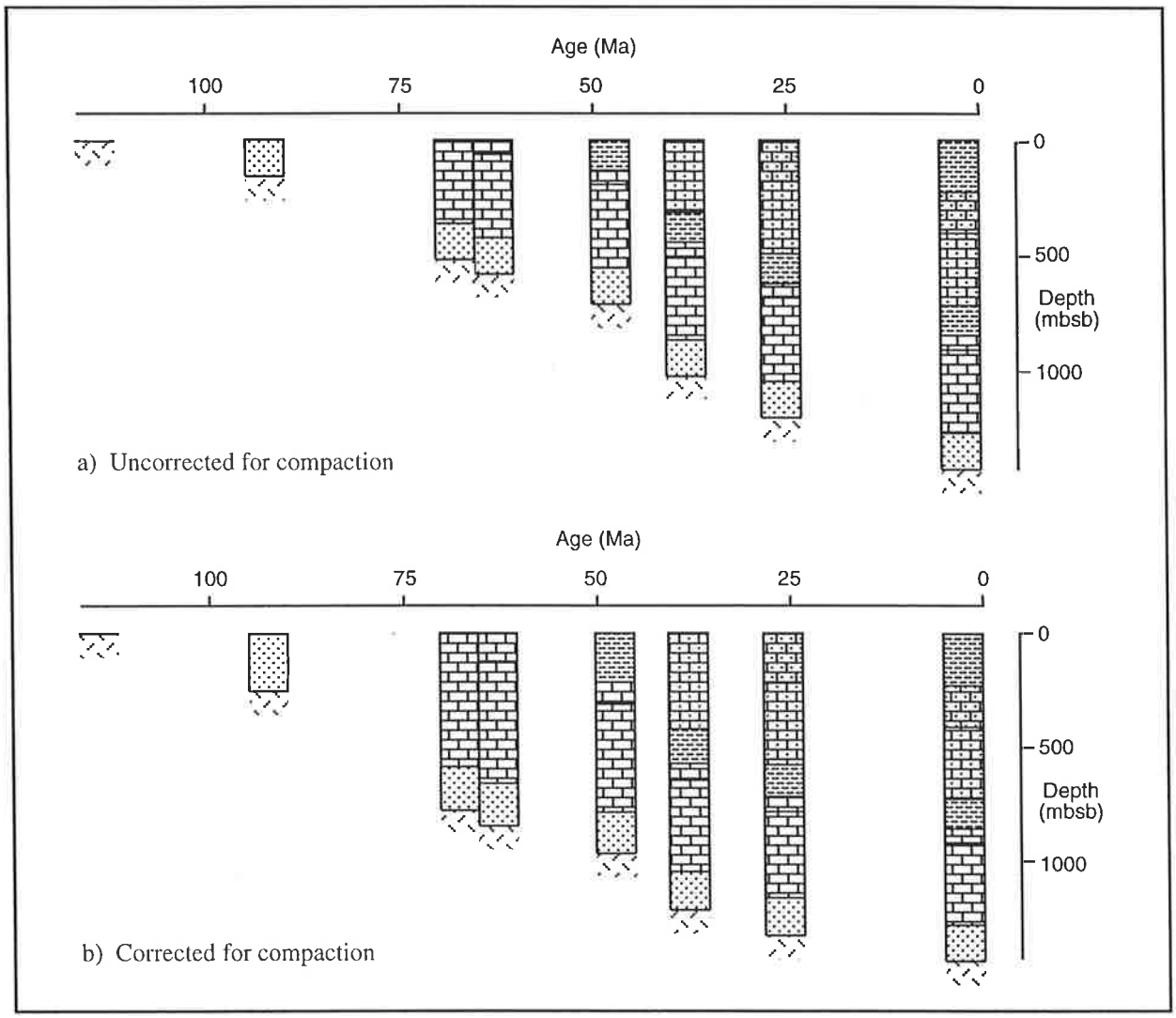

Fig. 6.3. (a) Sediment backstripping the Penma-1 well without correcting for compaction. (b) Sediment backstripping the Penma-1 well incorporating compaction.

of their treatment in sediment decompaction, and are discussed below.

6.4.1 Exhumation with no later subsidence

The simplest scenario which must be accounted for is where no subsidence has occurred subsequent to exhumation. In this case, the amount of apparent exhumation calculated in Chapter 4 is simply added to the present burial-depths and the sequence is then decompacted up the normal porosity/depth curve. Figure 6.4 shows decompacted depths to Palaeozoic basement in well 48/30-1 in the Fastnet Basin with (solid line) and without (dot-dash line) allowance for Tertiary exhumation. The dotted line shows the present-day backstripped depth to basement uncorrected for decompaction. The inclusion of sediments removed during Tertiary exhumation (dashed line) causes the underlying, preserved sedimentary sequence to decompact by a greater amount than when no allowance is made for Tertiary exhumation. The uncertainty in the timing and duration of Tertiary exhumation is also indicated in Figure 6.4.

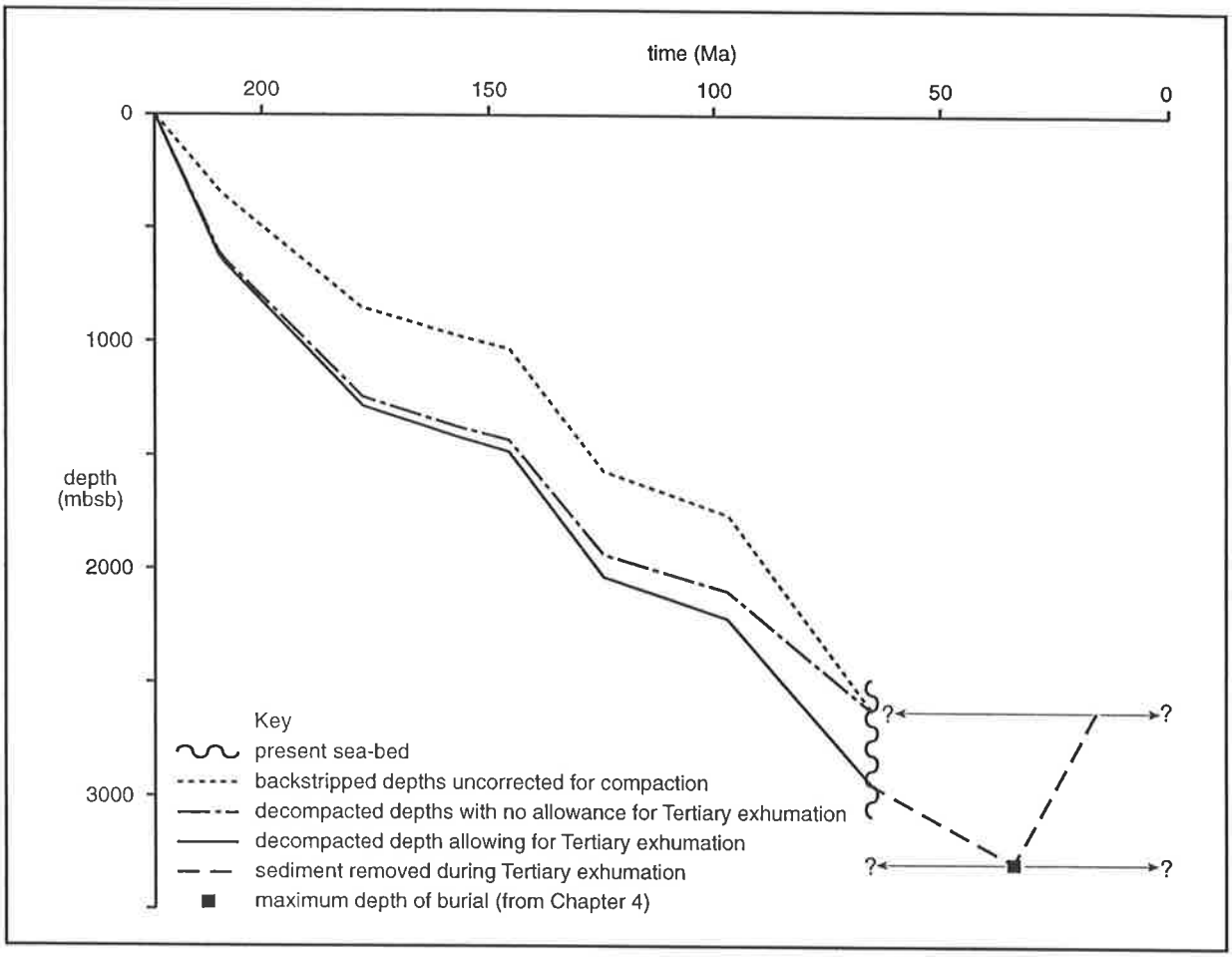

Fig. 6.4. Decompacted burial history with and without allowance for Tertiary exhumation, well 48/30-1. See text for discussion.

6.4.2 Exhumation of greater or equal magnitude to later subsidence

If exhumation is of greater magnitude than later subsidence, the pre-exhumation units will not have compacted during deposition of the post-exhumation sequence. The exhumation-related unconformity can thus be treated as the top of decompaction basement during decompaction of the post-exhumation sequence. The pre-exhumation sedimentary sequence is decompacted as a separate sequence, with the insertion of a topmost unit equal to the amount of exhumation at the time of denudation calculated in Chapter 4.

In areas of the Celtic Sea/South-Western Approaches where post-Danian sediments have been deposited, the pre-Palaeocene (assuming Palaeocene exhumation) or pre-Oligo-Miocene (assuming Oligo-Miocene exhumation) sedimentary sequence is decompacted separately as described above. Figure 6.5 shows the decompacted depth to the Cimmerian unconformity in well 72/10-1A in the Melville Basin. Assuming Palaeocene exhumation, the post-Palaeocene units are decompacted first, whilst those units below the Palaeocene unconformity remain at their present-day thicknesses. After the post-Palaeocene sequence has been backstripped the pre-Palaeocene units are decompacted following the

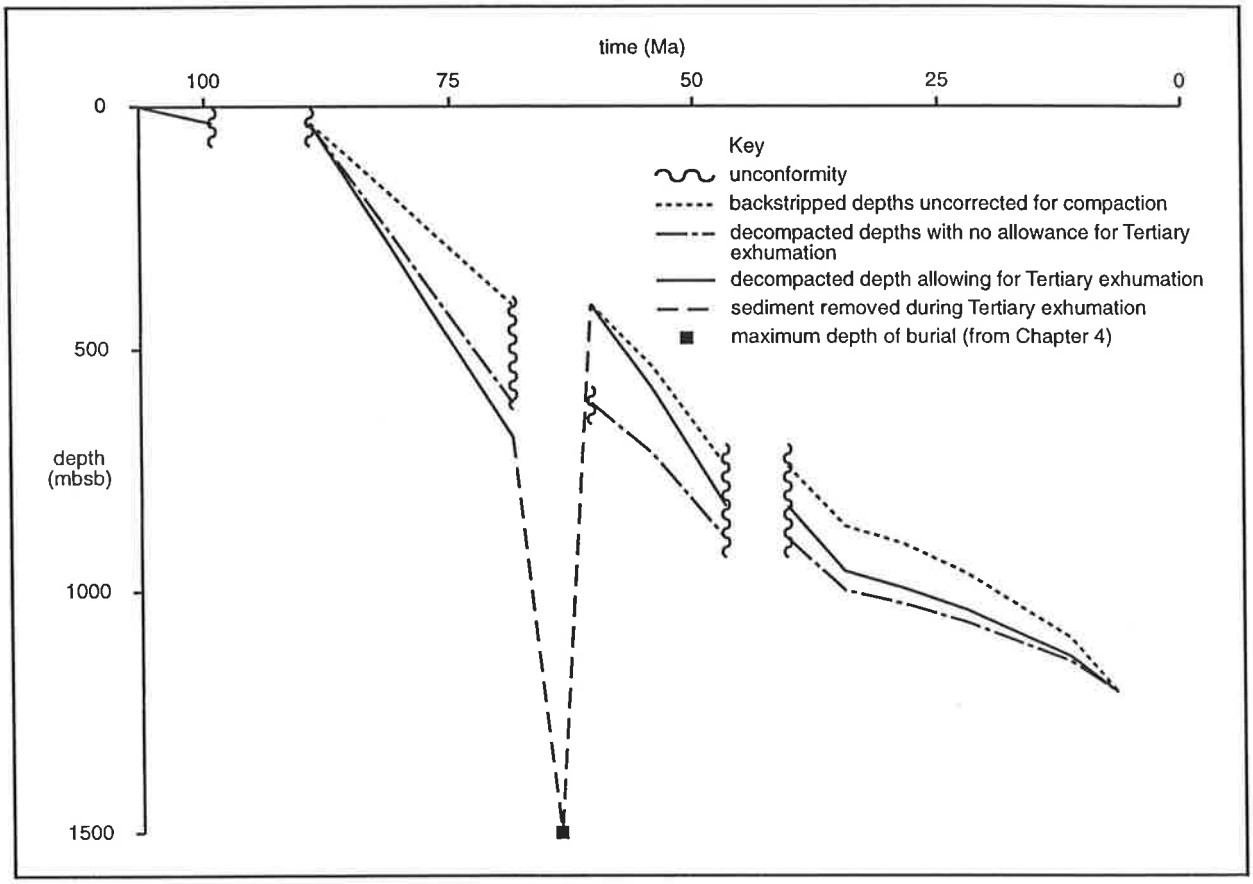

Fig. 6.5. Decompacted post-Cimmerian burial history with and without allowance for Tertiary exhumation, well 72/10-1A. See text for discussion.

addition of a unit equal to the amount of exhumation at the time of denudation calculated in Chapter 4. The lithology of the sedimentary unit added during backstripping to replace the sequence removed by exhumation is based where possible upon strata of a similar age that have been preserved elsewhere in the Celtic Sea/South-Western Approaches.

Exhumation associated with the Jurassic-Lower Cretaceous (Cimmerian) unconformity in the Celtic Sea/South-Western Approaches may be greater than later burial (Section 4.2.2). The Jurassic-Lower Cretaceous unconformity is hence treated as decompaction basement as described above in areas such as the South Celtic Sea Basin and St. Mary's Basin where the Cimmerian unconformity is strongly developed. The pre-Cimmerian sedimentary sequence is decompacted separately, after decompaction and backstripping of the post-Cimmerian sequence.

6.4.3 Exhumation of lesser magnitude than later subsidence

If exhumation is of lesser magnitude than later subsidence, then the pre-exhumation sequence will not initially compact during post-exhumation burial, but will start to compact further once it is buried beyond its previous maximum burial-depth. As stated in Section 3.6.2, the compaction methodology cannot quantify the exhumation of a sequence which is buried beyond its previous maximum burial-depth after exhumation has occurred. Consequently, all unconformities in the Celtic Sea/South-Western

Approaches other than the Cimmerian unconformity and the unconformity related to the Tertiary (Palaeocene or Oligo-Miocene) exhumation event are treated as non-depositional hiatuses, and are ignored in the decompaction and backstripping processes.

6.4.4 Exhumation and sediment densities

Although pre-and post-exhumation sequences can be decompacted separately, the density of the entire sequence must be considered when calculating the effect of sediment loading on subsidence (Section 6.7). Exhumation results in the removal of the uppermost, generally lower density, layers, increasing the average density of the remaining sedimentary sequence. Deposition of further low density sediment subsequent to exhumation then lowers the average density of the sequence. Similarly, as a sedimentary sequence is backstripped, the average density of the remaining sequence generally decreases due to the decompaction procedure. However in areas where exhumation has occurred, backstripping the post-exhumation sequence can result in an increase in the average density of the remaining sequence, as the pre-exhumation units are not decompacted. These density variations associated with exhumation are taken into account when calculating the tectonic subsidence and uplift of the Celtic Sea/South-Western Approaches (Sections 6.7 & 6.8).

6.5 Porosity/Depth Relations for Sediment Decompaction

As previously stated, a sedimentary unit is decompacted back to its original thickness by moving it back up its porosity/depth relation, to replace the porosity lost during compaction. Sclater & Christie (1980) suggested that most normally pressured sedimentary rocks have a lithology-specific exponential relationship between porosity (ϕ) and depth(z) of the form:

$$\phi = \phi_o e^{-cz} \qquad \text{.....(6.2)}$$

where ϕ_o is the surface porosity value, and c is the lithology-specific exponent. An exponential relation between porosity and depth is appropriate for mudstones, shales, and some limestones (Figs. 3.3 & 3.4), however a linear relationship is possibly more appropriate for sandstones (Fig. 3.2). Sclater & Christie (1980) argued however that the decrease in porosity with depth for sandstones is equally well accounted for by an exponential relation.

Backstripping and decompaction of the Celtic Sea/South-Western Approaches profile requires stratigraphic unit-specific porosity/depth relations rather than the lithology-specific porosity/depth relations of Sclater & Christie (1980), because stratigraphic units, not individual lithologies, are picked on seismic sections and need to be decompacted. It is thus necessary to establish porosity/depth relations for each of the units to be decompacted. Chapter 3 developed a number of stratigraphic unit-specific Δt/depth relations for the Celtic Sea/South-Western Approaches. The following section establishes a relationship between Δt and porosity for each of the units, allowing the Δt/depth plots of Chapter 3 to be converted to porosity/depth plots and thus to define porosity/depth relations for use in decompaction.

6.5.1 Interval transit-time/porosity relationships

Interval transit time (Δt) measured in chalks can be converted to porosity using Raiga-Clemenceau *et al*'s (1988) equation (Equation 5.2). Raiga-Clemenceau *et al.* (1988) also showed that their equation is valid for non-shaly limestones and sandstones, and their

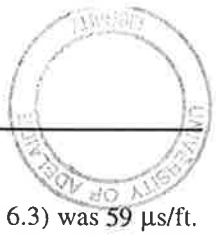

relation has hence been used in this thesis for converting Δt to porosity for non-shaly units such as the Upper Cretaceous Chalk (Table 6.2, Fig. 6.6). However, the majority of the formations to be backstripped from the Celtic Sea/South-Western Approaches profile are either shales, or are a mixture of shale and sandstone or limestone. It is hence necessary to define relationships between Δt and porosity for shales and shale/sand/limestone mixtures.

Numerous relationships between Δt and shale porosity have been published for different basins, using both Wyllie *et al*'s (1956) time average equation (Equation 3.2) (e.g. Magara, 1976; Brigaud *et al.*, 1992; Liu & Roaldset, 1994) and the equation of Raiga-Clemenceau *et al.* (1988) (e.g. Issler, 1992). Hansen (1996) compared measured porosities from sidewall cores and cuttings with sonic transit times for Tertiary and Cretaceous shales from the Norwegian Shelf, and fitted both Wyllie *et al*'s (1956) equation with a correction factor (after Schlumberger, 1989) and the equation of Raiga-Clemenceau *et al.* (1988) to the data. Wyllie *et al*'s (1956) time average equation with a correction factor is of the form:

$$\phi = \left(1/C_p\right)\left(\Delta t - \Delta t_{ma}\right)/\left(\Delta t_f - \Delta t_{ma}\right) \quad \text{.....(6.3)}$$

where ϕ is porosity, Δt is the interval transit time from the sonic log, Δt_{ma} is the matrix transit time, Δt_f is the transit time of the pore fluid, and C_p is the correction factor that should be applied to yield better estimates of porosity (Schlumberger, 1989).

Hansen (1996) showed that, whilst both equations were statistically almost equally significant, the shale matrix transit time (Δt_{ma}=76.5 μs/ft) calculated using the equation of Raiga-Clemenceau *et al.* (1988) was 20 μs/ft higher than the lowest shale transit time (56 μs/ft) from the Norwegian Shelf. In contrast, the shale matrix transit time calculated by Hansen (1996) using Wyllie *et al*'s (1956) time average equation with a compaction factor (Equation 6.3) was 59 μs/ft. Hansen (1996) thus concluded that Wyllie *et al*'s (1956) time average equation with a compaction factor (Equation 6.3) was more appropriate for converting Δt to porosity for shales on the Norwegian Shelf than the equation of Raiga-Clemenceau *et al.* (1988).

Although it would have been preferable to establish a specific Δt/porosity relationship for shales using core data from the Celtic Sea/South-Western Approaches, none were available. The shale Δt/porosity relation of Hansen (1996) has been selected because shales in the Celtic Sea/South-Western Approaches exhibit average interval transit times as low as 57.2 μs/ft (well 57/7-1, Mercia Mudstone, Appendix I). Hansen's (1996) relation has been used for calculating porosity from interval transit time for the Triassic Mercia Mudstone and the Upper Jurassic mudstones of the Celtic Sea/South-Western Approaches (Table 6.2, Fig. 6.6). Porosity was calculated for the Lower Cretaceous Greensand/Gault Clay and Lower Cretaceous Wealden from Δt assuming a mixture of 50% shale (Hansen, 1996) and 50% sandstone (Raiga-Clemenceau *et al.*, 1988; Table 6.2, Fig. 6.6). The Middle Jurassic, Lower Jurassic and Tertiary units were taken to be 50% shale (Hansen, 1996) and 50% limestone (Raiga-Clemenceau *et al.*, (1988); Table 6.2, Fig. 6.6).

6.5.2 Porosity/depth plots and relationships for decompaction

Porosity/depth plots for each of the interpreted units of the Celtic Sea/South-Western Approaches cross-section were generated by plotting the porosities calculated as described in the previous section against mid-point depth (Figs. 6.7 & 6.8). An exponential function was then fitted though the grouping of porosity-depth data points with the highest porosity

unit	interval transit time-porosity equation
Tertiary	$\phi = 0.5(1/1.57)([\Delta t_{log} - 59.0]/[189 - 59.0]) + 0.5\left(1 - (47.6/\Delta t_{log})^{1/1.76}\right)$
Chalk	$\phi = 1 - (47.6/\Delta t_{log})^{1/1.76}$
Greensand/Gault Clay	$\phi = 0.5(1/1.57)([\Delta t_{log} - 59.0]/[189 - 59.0]) + 0.5\left(1 - (55.5/\Delta t_{log})^{1/1.6}\right)$
Wealden	$\phi = 0.5(1/1.57)([\Delta t_{log} - 59.0]/[189 - 59.0]) + 0.5\left(1 - (55.5/\Delta t_{log})^{1/1.6}\right)$
Upper Jurassic	$\phi = (1/1.57)([\Delta t_{log} - 59.0]/[189 - 59.0])$
Mid-Lower Jurassic	$\phi = 0.5(1/1.57)([\Delta t_{log} - 59.0]/[189 - 59.0]) + 0.5\left(1 - (47.6/\Delta t_{log})^{1/1.76}\right)$
Mercia Mudstone	$\phi = (1/1.57)([\Delta t_{log} - 59.0]/[189 - 59.0])$

Table 6.2. Relationships between porosity and interval transit time for the units to be backstripped from the Celtic Sea/ South-Western Approaches cross-section (Fig. 6.1).

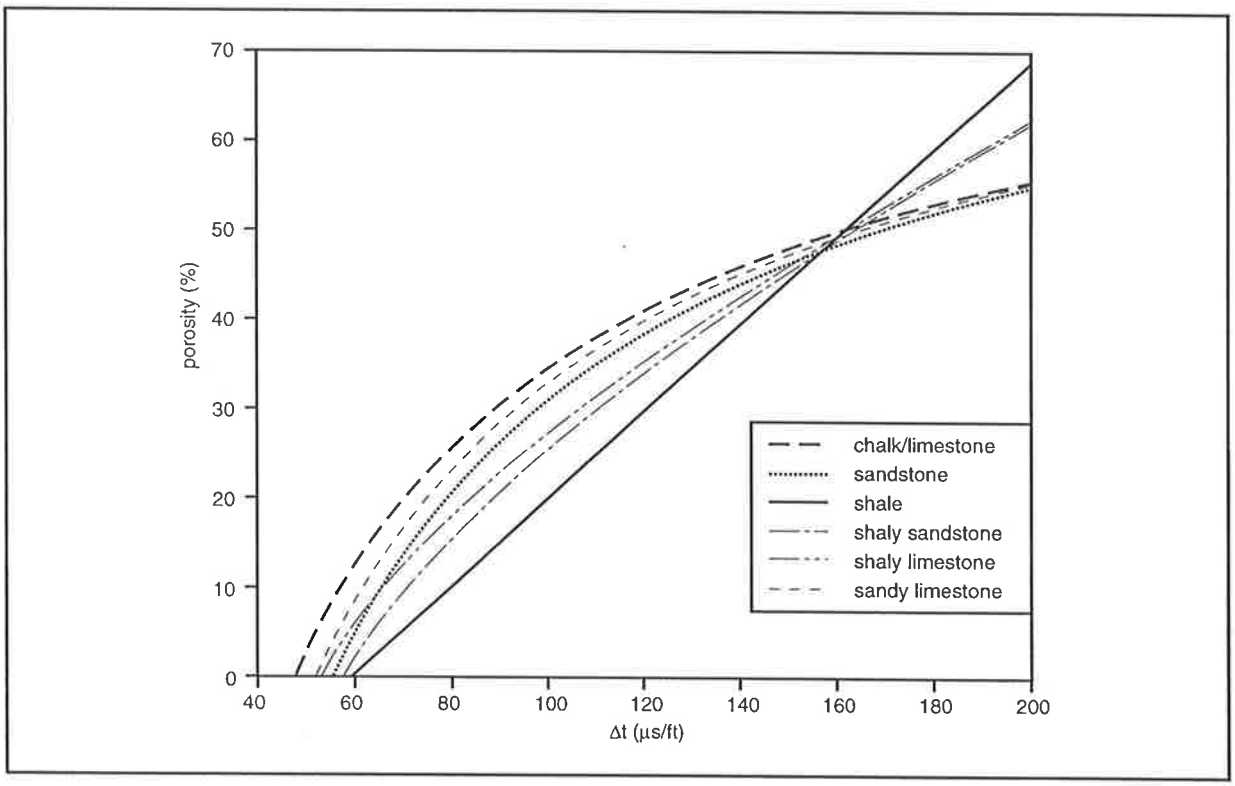

Fig. 6.6. Δt/porosity relationships. Chalk/limestone and sandstone Δt/porosity relationships are after Raiga-Clemenceau *et al.* (1988); shale Δt/porosity relationship is after Hansen (1996). Shaly limestone, shaly sandstone and sandy limestone relationships are 50/50 combinations of the shale, limestone, and sandstone relations.

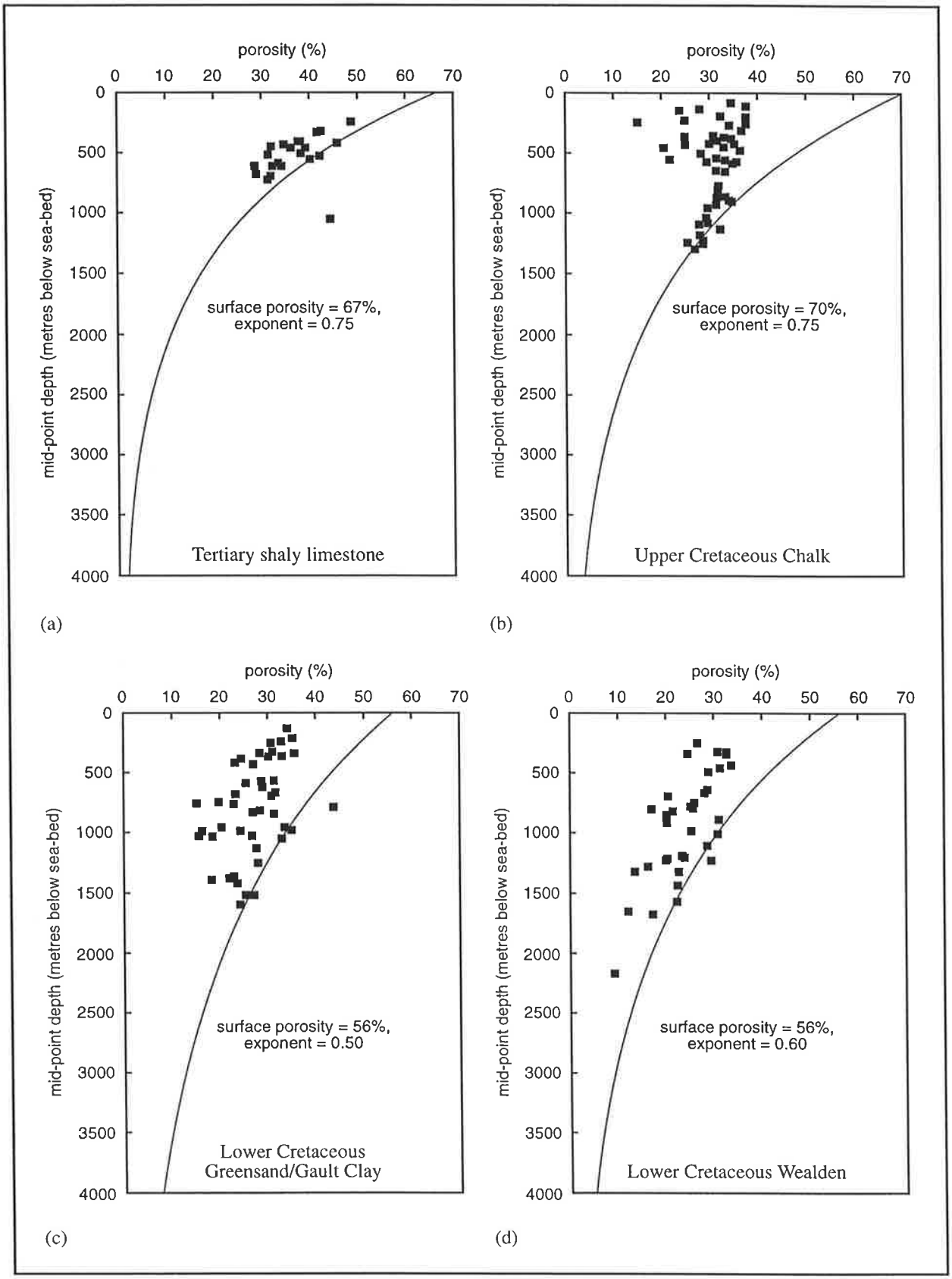

Fig. 6.7. Porosity/mid-point depth plots for units backstripped from the Celtic Sea/South-Western Approaches profile; (a) the Tertiary shaly limestones, (b) the Upper Cretaceous Chalk, (c) the Lower Cretaceous Greensand/Gault Clay, and (d) the Lower Cretaceous Wealden.

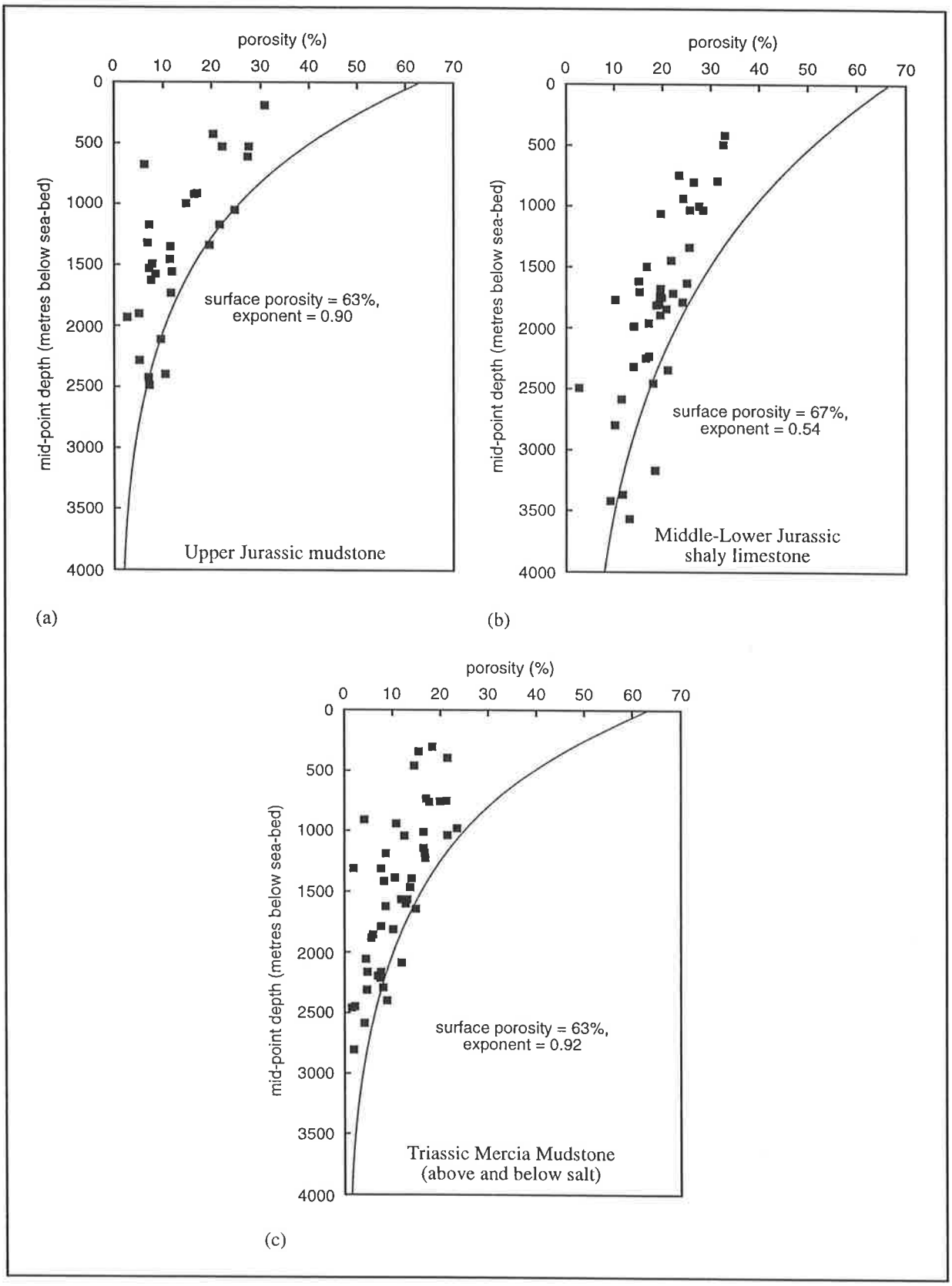

Fig. 6.8. Porosity/mid-point depth plots for units backstripped from the Celtic Sea/South-Western Approaches profile; (a) the Upper Jurassic mudstones, (b) the Middle-Lower Jurassic shaly limestones, and (c) the Triassic Mercia Mudstone (above and below salt).

for their burial depth (Figs. 6.7 & 6.8), with allowance being made for possibly erroneous points. The exponential porosity/depth relations were constrained by appropriate surface porosities, ϕ_o, which were taken from the literature. Scholle (1977) suggested 70% for the surface porosity of normally compacting chalk, and this was also used for limestone surface porosities. Sclater & Christie (1980) suggested 49% for sandstones, and 63% for shales. Shaly sandstone and shaly limestone surface porosities were taken as the average of the shale and sandstone/limestone values. The parameters ϕ_o and c of the exponential porosity/depth relations are given in Table 6.3.

6.6 Backstripping and Decompaction of the Celtic Sea/South-Western Approaches Profile

Having established appropriate porosity/depth relations for each of the units, Figure 6.1 can be backstripped and decompacted, to give an indication of the burial history of the Celtic Sea/South-Western Approaches. This burial history is the basis from which the tectonic subsidence/uplift history is obtained, once the gravitational load of the sedimentary fill, sea level changes, and palaeobathymetry are taken into account (Section 6.7). The stratigraphy of Figure 6.1 has been simplified, so that the burial history can be broken down into six distinct tectonic periods for modelling purposes:

- syn-rift 1 (235-209.5 Ma), the initial basin-forming rifting event, with basin fill comprising the Triassic Mercia Mudstone (above and below salt);
- post-rift 1 (209.5-157.1 Ma), the first thermal or sag phase, with deposition of the Lower-Middle Jurassic shales and limestones;
- syn-rift 2 (157.1-124.5 Ma), the second rifting event, resulting in deposition of the Upper Jurassic mudstones and Lower Cretaceous Wealden in the North Celtic Sea and Brittany basins, the Wealden in the Haig Fras Basin, and coeval with the Cimmerian unconformity in the South Celtic Sea and St. Mary's basins;
- post-rift 2 (124.5-60.5/35.4 Ma), the second thermal sag phase, with deposition of the Lower Cretaceous Greensand/Gault Clay, the Upper Cretaceous Chalk, and the pre-exhumation Tertiary sequences, including the thickness of the sedimentary sequence calculated in Chapter 4 to have been removed by Tertiary (Palaeocene or Oligo-Miocene) exhumation;
- Tertiary uplift (60.5/35.4 Ma), the present day preserved stratigraphy minus the post-exhumation (post-Palaeocene or post-Oligo-Miocene) sequence, and;
- post-uplift (60.5/35.4-0.0 Ma), the preserved stratigraphic succession.

The burial histories for the Celtic Sea/South-Western Approaches profile are portrayed for the end of each of the above periods on Figures 6.9 and 6.10.

It should be noted that there are no deep wells in the Haig Fras Basin and the stratigraphy of the basin on SWAT 5 is interpreted from seismic data only. Hence the stratigraphic age of the basin-fill is essentially unconstrained, as are the apparent exhumation estimates.

Although it is necessary to add a Cimmerian exhumation-related unit to enable more accurate decompaction of pre-Cimmerian units, the sediment removed by Cimmerian exhumation is not included on the post-rift 1 profile of Figures 6.9 and 6.10. Whilst the loading effects of sediment removed by Cimmerian exhumation must be accounted for, the uncertainty in the age of what was eroded prevents its inclusion into the burial history of Figures 6.9 and

unit	ϕ_o (%/100)	c (10^{-5} cm^{-1})
Tertiary	0.67	0.75
Upper Cretaceous Chalk	0.70	0.75
Lower Cretaceous Greensand/Gault Clay	0.56	0.50
Lower Cretaceous Wealden	0.56	0.60
Upper Jurassic mudstone	0.63	0.90
Mid-Lower Jurassic	0.67	0.54
Triassic Mercia Mudstone (above and below salt)	0.63	0.92

Table 6.3. Parameters of the exponential relation between porosity and depth for each of the units in the Celtic Sea/South-Western Approaches profile.

6.10. Figures 6.9 and 6.10 thus show the minimum thicknesses of sediment associated with the first rifting and thermal sag phases, constructed from the preserved stratigraphy only.

6.7 Calculation of Tectonic Subsidence

In order to isolate the driving force, or tectonic element, of basin subsidence it is necessary to remove the loading effect of sediment deposited in response to that driving force, and of any overlying water column or variation in the surface level of the water column. The aim is to calculate the depth to basement through time in the absence of surface loads, or assuming a constant water load. This quantity, tectonic subsidence, can be readily compared with predictions from geodynamic models of basin subsidence/uplift.

Under a load the lithosphere may attain isostatic equilibrium either by Airy (local) or flexural compensation. Airy isostasy implies that a surface load is supported locally by the thickness of buoyant lithosphere immediately beneath the load. Flexural isostasy implies that a surface load is supported by a region of lithosphere surrounding the load. The area of supporting lithosphere is dependent upon the flexural strength of the lithosphere, which is characterised by the thickness of the elastic lithosphere, which in turn is dependent on the thermal and compositional structure of the lithosphere.

Sclater & Christie (1980), as well as many other subsidence studies (e.g. LePichon & Sibuet, 1981; Bond & Kominz, 1984; Karner *et al.*, 1987; Hegarty *et al.*, 1988; White & McKenzie, 1988) have assumed Airy isostasy, and this assumption has been used in this study for calculating tectonic subsidence. The reasons for assuming Airy isostasy are addressed in Chapter 7.

Sclater & Christie (1980) showed that the water-loaded basement depth Y assuming Airy isostasy is given by:

$$Y = S\left(\frac{\rho_m - \rho_s}{\rho_m - \rho_w}\right) + W_d - \Delta_{SL}\left(\frac{\rho_m}{\rho_m - \rho_w}\right) \qquad \text{.....(6.4)}$$

where S is the decompacted sediment thickness, ρ_m, ρ_s and ρ_w are the densities of the mantle (3.33 g cm^{-3}), sediment, and water (1.03 g cm^{-3}) respectively, W_d is the palaeobathymetry, and Δ_{SL} is the eustatic sea-level change.

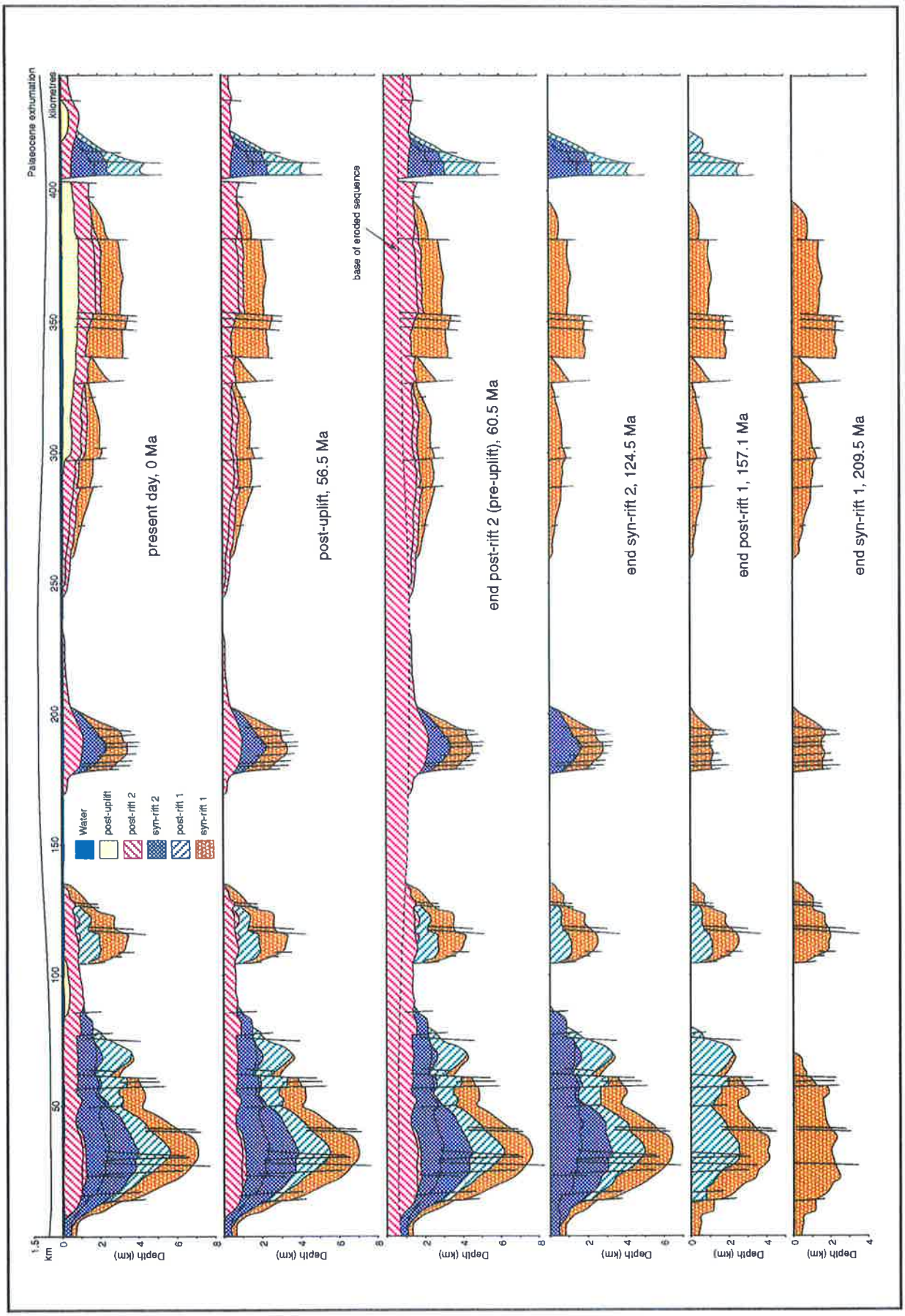

Fig. 6.9. Backstripped and decompacted Celtic Sea/South-Western Approaches profile, assuming Palaeocene exhumation. The amount of Palaeocene exhumation, from Figure 4.14, is indicated above the present day profile.

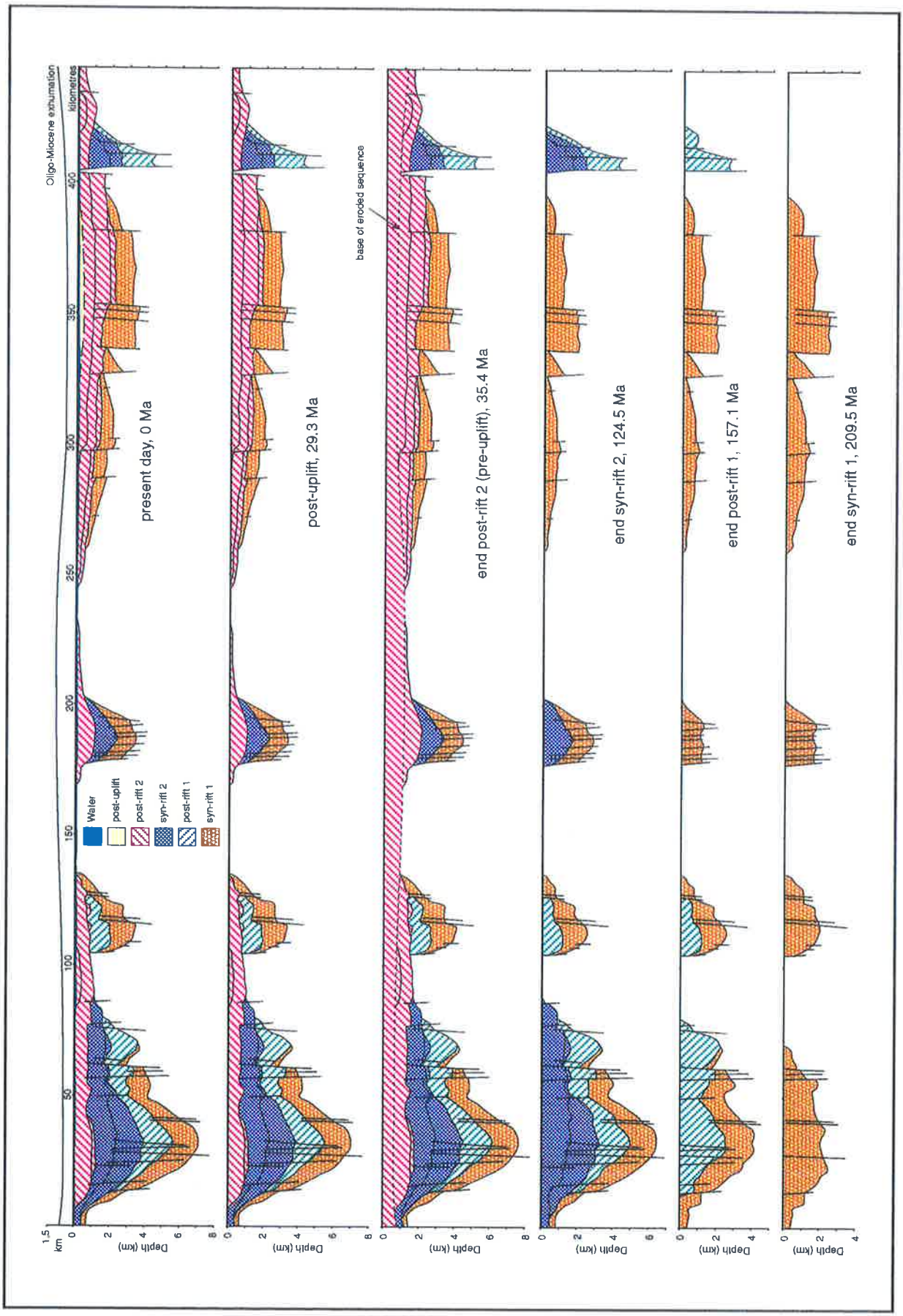

Fig. 6.10. Backstripped and decompacted Celtic Sea/South-Western Approaches profile, assuming Oligo-Miocene exhumation. The amount of Oligo-Miocene exhumation, from Figure 4.15, is indicated above the present day profile.

6.7.1 Sediment loading

Considering first the load of the sediment column only, the effect upon basement depth is accounted for by:

$$Y = S\left(\frac{\rho_m - \overline{\rho}_s}{\rho_m - \rho_w}\right) \qquad \text{.....(6.5)}$$

where $\overline{\rho}_s$ is the average density of the decompacted sediment column (Sclater & Christie, 1980).

To calculate the average density of the decompacted sediment column, the decompacted porosity of each layer must first be calculated. The porosity of a decompacted sedimentary layer, assuming an exponential porosity/depth relation (Equation 6.2), is given by:

$$\phi = \frac{\phi_o}{c}\left(\frac{e^{-cz_1'} - e^{-cz_2'}}{z_2' - z_1'}\right) \qquad \text{.....(6.6)}$$

where ϕ_o is the surface porosity value, c is the lithology-specific exponent, and z_1' and z_2' are the depth to the top and bottom of the sedimentary layer after backstripping and decompaction given by Equation 6.1 (Sclater & Christie, 1980). The average sedimentary column density is then given by:

$$\overline{\rho}_s = \sum_i \left(\frac{\overline{\phi}_i \rho_w + (1 - \overline{\phi}_i)\rho_{sgi}}{S}\right) z_i' \qquad \text{.....(6.7)}$$

where $\overline{\phi}_i$ is the mean porosity of the i'th layer, ρ_{sgi} is the sediment grain density of the i'th layer, S is the total decompacted sediment thickness, and z_i' is the decompacted thickness of the i'th layer (Sclater & Christie, 1980). The sediment grain densities used to calculate the average sedimentary column density are given in Table 6.4.

6.7.2 Palaeobathymetry

In addition to calculating the unloaded basement subsidence as above, the water depth during sediment deposition must be taken into account when calculating tectonic subsidence (Equation 6.4). For example, rapid basement subsidence may result in a dramatic increase in water depth. Whilst water fills the depression formed by basement subsidence almost instantaneously, sediment may take time to accumulate, because sedimentation is also dependent upon sediment supply. Hence, as shown in Equation 6.4, the palaeo-water depth (palaeobathymetry) during sediment deposition must be added to the unloaded basement subsidence calculated in Equation 6.5, to determine the water-loaded basement depth.

Hillis (1988) derived palaeobathymetric limits for the Mesozoic and Cenozoic sequence of the Western Approaches Trough from a number of biostratigraphic well reports, and these limits, combined with the stratigraphic and palaeogeographic descriptions of Evans (1990) and Tappin *et al.* (1994), have been used in this study (Fig. 6.11). All sub-aerial sediments have been arbitrarily assigned zero water depth. The error limits of palaeobathymetric resolution are indicated in the tectonic history curves of Figures 6.12 and 6.13.

6.7.3 Eustatic sea-level change

Global sea-level change can cause changes in palaeobathymetry that are independent of tectonic processes. Such sea-level changes result in changes in a gravitational (water) load upon basement independent of tectonic processes. Hence subsidence (or uplift) resulting from global eustatic sea-level change (Δ_{SL} in Equation 6.4) must be subtracted from the water-loaded basement subsidence when

unit	ρ_{sg} (g cm^{-3})
Tertiary (shaly limestone)	2.72
Upper Cretaceous Chalk	2.71
Lower Cretaceous Greensand/Gault Clay (shaly sandstone)	2.68
Lower Cretaceous Wealden (shaly sandstone)	2.68
Upper Jurassic mudstone	2.72
Mid-Lower Jurassic (shaly limestone)	2.72
Triassic Mercia Mudstone (above and below salt)	2.72

Table 6.4. Sediment grain densities (ρ_{sg}) used in calculating the average sedimentary column density. Grain densities for pure lithologies are from Schlumberger (1987), whilst for mixed lithologies grain densities are 50/50 combinations.

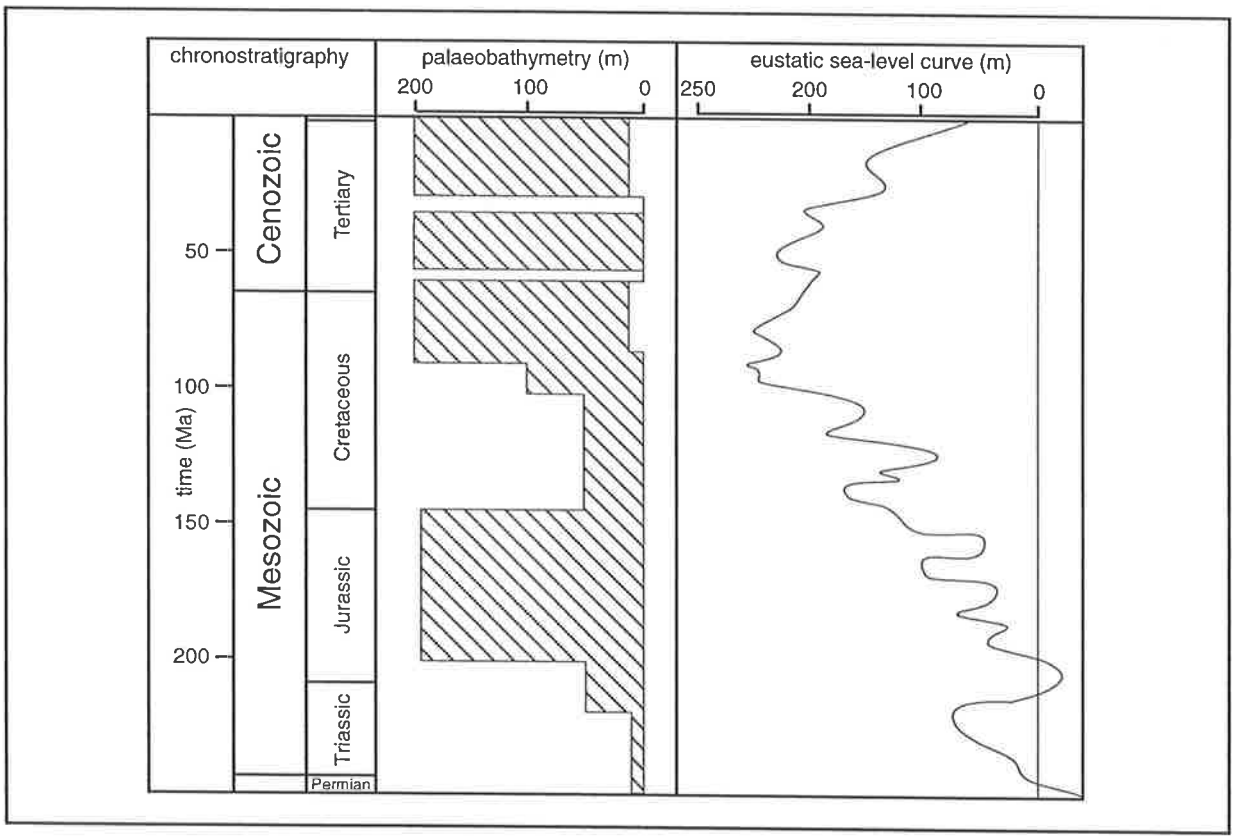

Fig. 6.11. Global eustatic sea-level curve and palaeobathymetry used in tectonic modelling. Eustatic sea-level curve is after Haq *et al.* (1988), and palaeobathymetric limits are compiled from Hillis (1988), Evans (1990), and Tappin *et al.* (1994).

modelling tectonic history.

There have been numerous global sea-level curves published by various authors, among the best known being the curves of Vail *et al.* (1977), and the updated curves of Haq *et al.* (1988). There are however major differences between many of the published global sea-level models, particularly in the timing and magnitude of the higher frequency sea-level events. In spite of the disagreement between the various published sea-level curves, there is broad agreement on the occurrence of long-term (first order) sea-level changes. The Late Cretaceous highstand, associated with the submergence of most land areas and chalk deposition in the Celtic Sea/South-Western Approaches, is one such first order sea-level change (Evans, 1990; Haq *et al.*, 1988).

As noted by Kendall & Lerche (1988), tectonic and eustatic effects have proven difficult to separate, hence the accurate determination of variations in eustatic sea-level is problematic. Kendall & Lerche (1988) suggested that only relative sea-level charts which combine tectonic and eustatic effects are possible. The short term variations in relative sea-level shown on second and higher order sea-level curves may at least partially be a result of tectonic activity, rather than a true reflection of global eustatic sea-level change. Consequently, second and higher order sea-level curves are not considered to be appropriate for use in modelling the tectonic history of the Celtic Sea/South-Western Approaches. Hence the long term (first order) global eustatic sea-level curve of Haq *et al.* (1988) has been deemed to give the most appropriate estimate of global eustatic sea-level changes, and is shown in Figure 6.11. For the calculation of the water-loaded basement depth in Equation 6.4 the eustatic sea-level curve was normalised to zero at the commencement of rifting in the Upper Triassic.

6.8 Calculation of Tectonic Uplift

As stated in Section 3.6.3, the compaction methodology quantifies the amount of section removed, or exhumation. Exhumation can occur as a result of either sea-level change (uplift of rocks), or as a result of tectonic processes (surface uplift) (England & Molnar, 1990). The amount of tectonic uplift (U) resulting in exhumation can be calculated as outlined by Garfunkel (1988) and Brown (1991) by:

$$U = E_T \times \left(\frac{\rho_m - \bar{\rho}_s}{\rho_m} \right) - \Delta_{SL} - \Delta H \quad \text{.....(6.8)}$$

where E_T is the amount of exhumation at the time of denudation (as calculated in Section 4.4), and ΔH is any change (pre-exhumational less post-exhumational) in surface elevation with respect to contemporary sea-level (Hillis, 1995*a*).

As shown in Equation 6.8, the amount of exhumation at the time of denudation does not equal the amount of tectonic uplift. As exhumation removes sedimentary section, the gravitational load upon the basement of a basin is diminished, and hence the basement rebounds to restore isostatic equilibrium, exaggerating the vertical displacement of the basement due to tectonic uplift. Thus for an average sediment density of 2.3 g cm^{-3}, and in the absence of changes in sea-level or of surface elevation pre- to post-exhumation, only 0.3 km of tectonic uplift is necessary to produce the approximately 1 km of regional exhumation witnessed during the Tertiary in the Celtic Sea/South-Western Approaches (Chapter 4).

Assuming no change in elevation with respect to sea-level before and after exhumation, a sea-level change of 0.3 km is necessary to account for regional Tertiary exhumation in the Celtic Sea/South-Western

Approaches in the absence of any tectonic processes. However, the first-order curve of Haq *et al.* (1988) in Figure 6.11 shows that the major eustatic sea-level falls during the Tertiary do not significantly exceed 0.1 km. Tertiary exhumation in the Celtic Sea/South-Western Approaches cannot thus solely be accounted for by sea-level change.

Equation 6.8 has not been used in calculating the tectonic uplift of the Celtic Sea/South-Western Approaches for two reasons. Firstly, the tectonic models to be used in Chapter 8 assume water-loaded basement, whereas Equation 6.8 assumes air-loading. Secondly, and more importantly, Equation 6.8 does not take into account the change in the average sediment column density that occurs as (generally less dense) units are eroded from the sedimentary sequence. Instead, the change in water-loaded basement depth (ΔY) was calculated from the equation:

$$\Delta Y = \left(S \times \left(\frac{\rho_m - \overline{\rho}_s}{\rho_m - \rho_w} \right) - S' \times \left(\frac{\rho_m - \overline{\rho'}_s}{\rho_m - \rho_w} \right) \right) - \Delta_{SL} - \Delta H \quad \text{.....(6.9)}$$

where S and S' are the total decompacted sediment thickness pre- and post-exhumation respectively, and $\overline{\rho}_s$, $\overline{\rho'}_s$ are the average sediment density pre- and post-exhumation respectively. For the case where there is no change in the average sediment density, this equation is equal to a water-loaded version of Equation 6.8.

6.9 Tectonic Subsidence/Uplift History of the Celtic Sea/South-Western Approaches

Figures 6.12 and 6.13 show the tectonic history of the Celtic Sea/South-Western Approaches calculated from the burial histories of Section 6.6, and assuming Palaeocene and Oligo-Miocene exhumation respectively. The maximum (solid line) and minimum (dashed line) palaeobathymetric limits from Section 6.7 are indicated on each profile.

As noted in Chapter 2, the first rifting event did not commence in the Brittany Basin until the Jurassic. However, as the Lower Jurassic syn-rift and post-rift sediments of the Brittany Basin are of the same facies, the syn-rift and post-rift components cannot be separated. The two components have been lumped together as post-rift 1 in Figures 6.9 and 6.10.

The post-rift 1 period is only constrained by the North Celtic Sea and Brittany basins for the Chapter 8 modelling, as Cimmerian exhumation in the South Celtic Sea, Haig Fras, and St. Mary's basins has removed almost all record of the post-rift 1 period in these areas. The first basin-forming rifting event is thus poorly constrained over much of the area. However, from the end of the second syn-rift period to the present day there is sufficient constraint that the tectonic modelling of Chapter 8 must closely match the tectonic histories constructed in Figures 6.12 and 6.13.

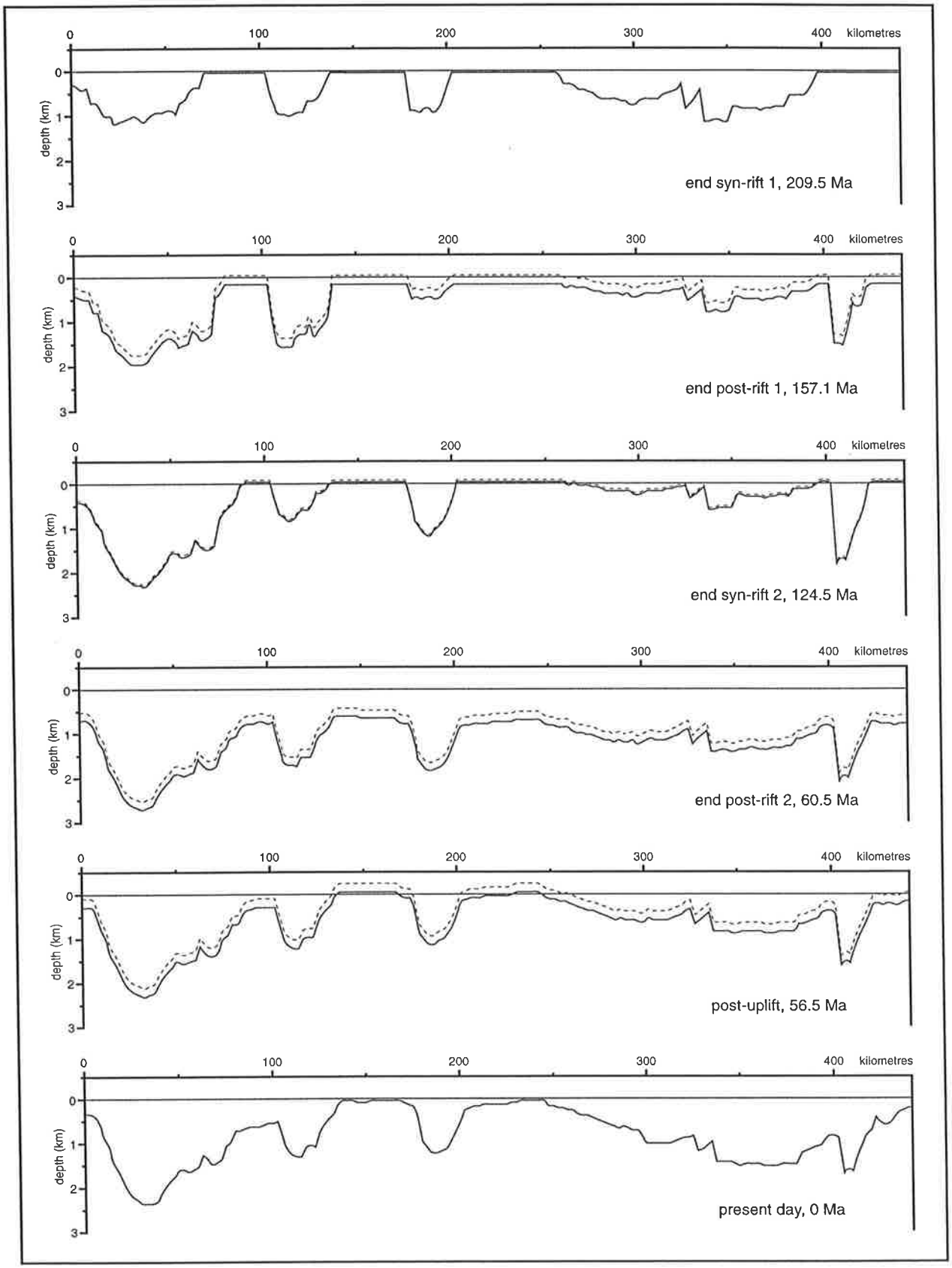

Fig. 6.12. Calculated tectonic subsidence for the Celtic Sea/South-Western Approaches cross-section, assuming Palaeocene exhumation. Dashed and solid lines are minimum and maximum palaeobathymetry limits respectively.

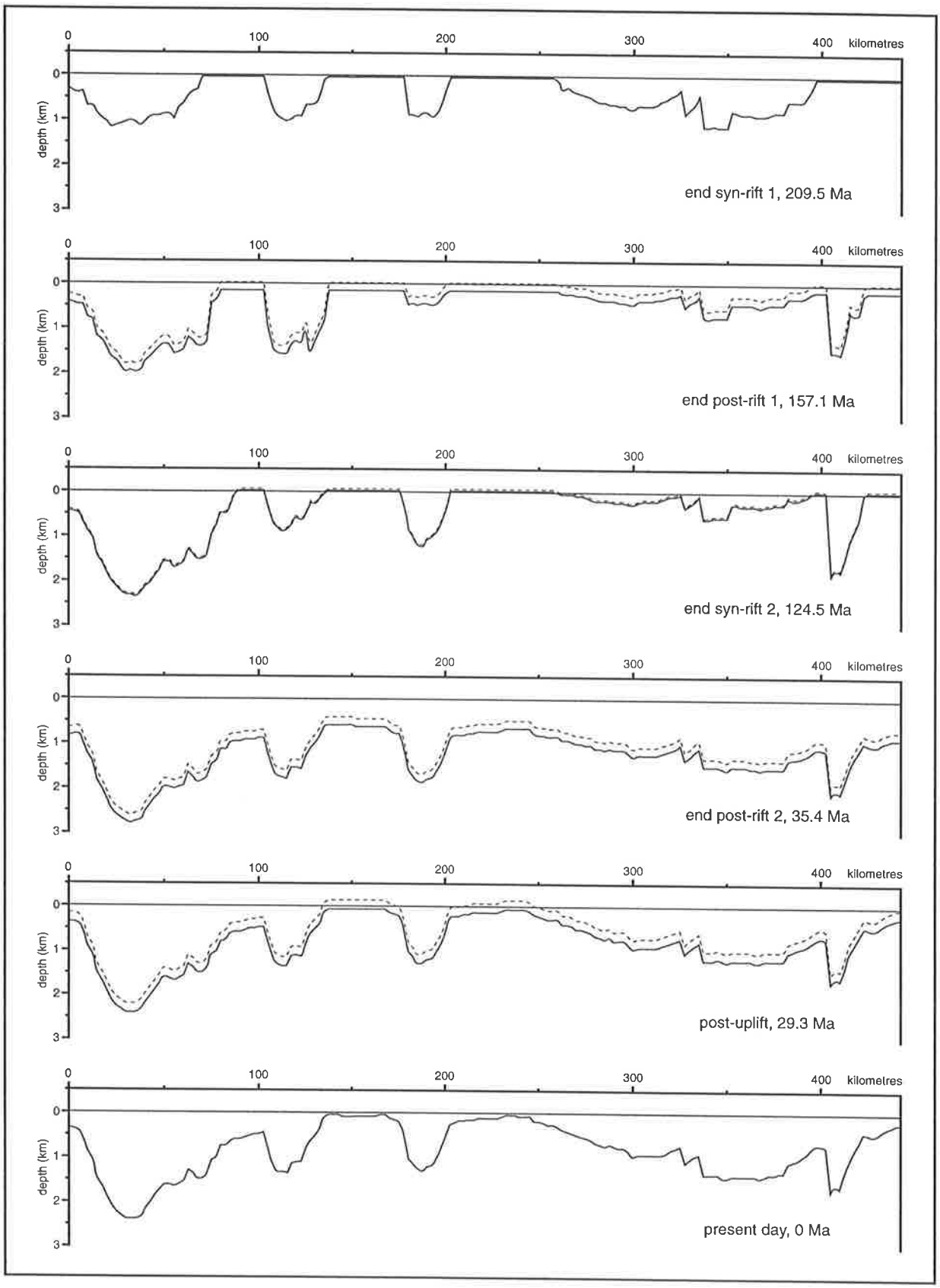

Fig. 6.13. Calculated tectonic subsidence for the Celtic Sea/South-Western Approaches cross-section, assuming Oligo-Miocene exhumation. Dashed and solid lines are minimum and maximum palaeobathymetry limits respectively.

Chapter 7
Tectonic Models of Basin Evolution

7.1 Introduction

Tertiary exhumation in the Celtic Sea/South-Western Approaches is regional in extent, and not limited to areas of structural inversion (Chapter 4). The Cretaceous-Tertiary post-rift sequences of the Celtic Sea/South-Western Approaches are also regional in extent, and are only slightly localised over the Jurassic-Lower Cretaceous syn-rift depocentres (Chapter 4). Hence, a two-layer, heterogeneous model of lithospheric deformation, in which extension/compression in the upper lithosphere is decoupled from, and distributed differently to, deformation in the lower lithosphere, may account for the observed patterns of subsidence/uplift (e.g. White & McKenzie, 1988; Hillis, 1992*a*, 1995*a*).

Numerous basins around the Northwest European Atlantic margin, such as the Wessex Basin (Karner *et al.*, 1987), the Rockall Trough (Hauser *et al.*, 1995), and the northern Viking Graben (Badley *et al.*, 1987; Lippard & Liu, 1992), have been successfully modelled by considering heterogeneous or depth-dependent lithospheric extension. This chapter discusses the formulation of a two-layer, pure shear, heterogeneous model of lithospheric deformation, which is applied to the Celtic Sea/South-Western Approaches in Chapter 8, and compares the advantages and disadvantages of this method with other published models of basin evolution. First, however, this chapter discusses the selection of the two-dimensional or cross-sectional modelling approach used in this thesis.

7.2 Modelling the Subsidence/Uplift History of Sedimentary Basins in One, Two, and Three Dimensions

The subsidence/uplift history of a sedimentary basin may be modelled in:

- one-dimension using well and pseudo-well locations;
- two-dimensions using cross-sections, or;
- three-dimensions using sediment isopach maps.

One-dimensional modelling has been widely undertaken (e.g. Steckler & Watts, 1978; Sclater & Christie, 1980; Royden & Keen, 1980; Wood, 1981; Karner *et al.*, 1987; White & Latin, 1993). However one-dimensional modelling may be unreliable, especially where based on stratigraphy intersected by wells, because wells tend to be inherently located on anomalous (often structurally high) positions (Giltner, 1987; White, 1990), and commonly do not penetrate the full sedimentary section (Giltner, 1987). Two-dimensional modelling has also been undertaken (e.g. Beaumont *et al.*, 1982; Hellinger *et al.*, 1989; Keen *et al.*, 1987; Kusznir & Egan, 1989; Lippard & Liu, 1992; Kusznir *et al.*, 1995; Roberts *et al.*, 1995) and the successful modelling of representative cross-sections through a basin provides more confidence in the suitability of a geodynamic model than can one-dimensional modelling. Three-dimensional modelling is obviously the most comprehensive approach and has been undertaken by authors such as Keen &

Dehler (1993). In this thesis the modelling approach is two-dimensional. This avoids the potential "lack of representativeness" of one-dimensional modelling. Three-dimensional modelling is not considered necessary because the basins of the Celtic Sea/South-Western Approaches show reasonable along-strike consistency. Furthermore, isopach maps for the region are not available.

7.3 Pure Shear Models of Lithospheric Deformation

Sleep (1971) showed that the subsidence history of Atlantic continental margins after continental breakup closely resembled the subsidence history of oceanic crust as it spreads away from a mid-oceanic ridge. This led Sleep (1971) to suggest that the post-breakup subsidence of these margins was probably due to thermal contraction of the lithosphere. McKenzie (1978) showed that uniform stretching of the lithosphere can account for the normal faulting and crustal thinning observed in rifted regions, and also showed that the thermal response to stretching is subsidence which decays exponentially with time, as described by Sleep (1971). McKenzie's (1978) stretching model is described below.

7.3.1 McKenzie's (1978) pure shear model

Figure 7.1 illustrates the stretching model of McKenzie (1978). At time t = 0 a unit length of continental lithosphere is extended instantaneously by pure shear to a length β, causing upwelling of hot asthenosphere. The resultant thermal perturbation gradually decays, producing subsidence. The model ignores crustal heat production, resulting in the simple linear temperature profile of Figure 7.1. The model also assumes that the temperature at a depth corresponding to the initial thickness of the lithosphere is fixed.

Assuming the lithosphere is locally isostatically compensated during and after extension, there is an initial subsidence S_i given by (corrected from McKenzie, 1978):

$$S_i = \frac{a\left[(\rho_m - \rho_c)\frac{t_c}{a}\left(1-\alpha T_m \frac{t_c}{2a}\right) - \frac{\alpha T_m \rho_m}{2}\right]\left(1-1/\beta\right)}{\rho_m(1-\alpha T_m)-\rho_w} \qquad \text{.....(7.1)}$$

where a is the thickness of the lithosphere and t_c the thickness of the continental crust, ρ_m, ρ_c, and ρ_w are the density of the mantle, crust, and water respectively. α is the thermal expansion co-efficient of both the crust and mantle, and T_m is the temperature of the asthenosphere. Dewey (1982) showed that the sign of S_i (*i.e.* whether the initial isostatic response to rifting is subsidence or uplift) depends upon the ratio t_c/a, and is independent of β.

After extension, the temperature profile is given by:

$$\begin{aligned} T &= T_m && 0 \le z \le a\left(1-1/\beta\right), \\ &= T_m\beta\left(1-z/a\right) && a\left(1-1/\beta\right) \le z \le a \end{aligned} \qquad \text{.....(7.2)}$$

where z is measured upwards from the base of the lithosphere before extension. McKenzie (1978) determined the subsidence due to the decay of the thermal anomaly by solving the one-dimensional heat flow equation (i.e. assuming no lateral heat conduction):

$$\frac{\partial T}{\partial t} = \kappa \frac{\partial^2 T}{\partial z^2} \qquad \text{.....(7.3)}$$

where κ is the thermal diffusivity, with boundary conditions:

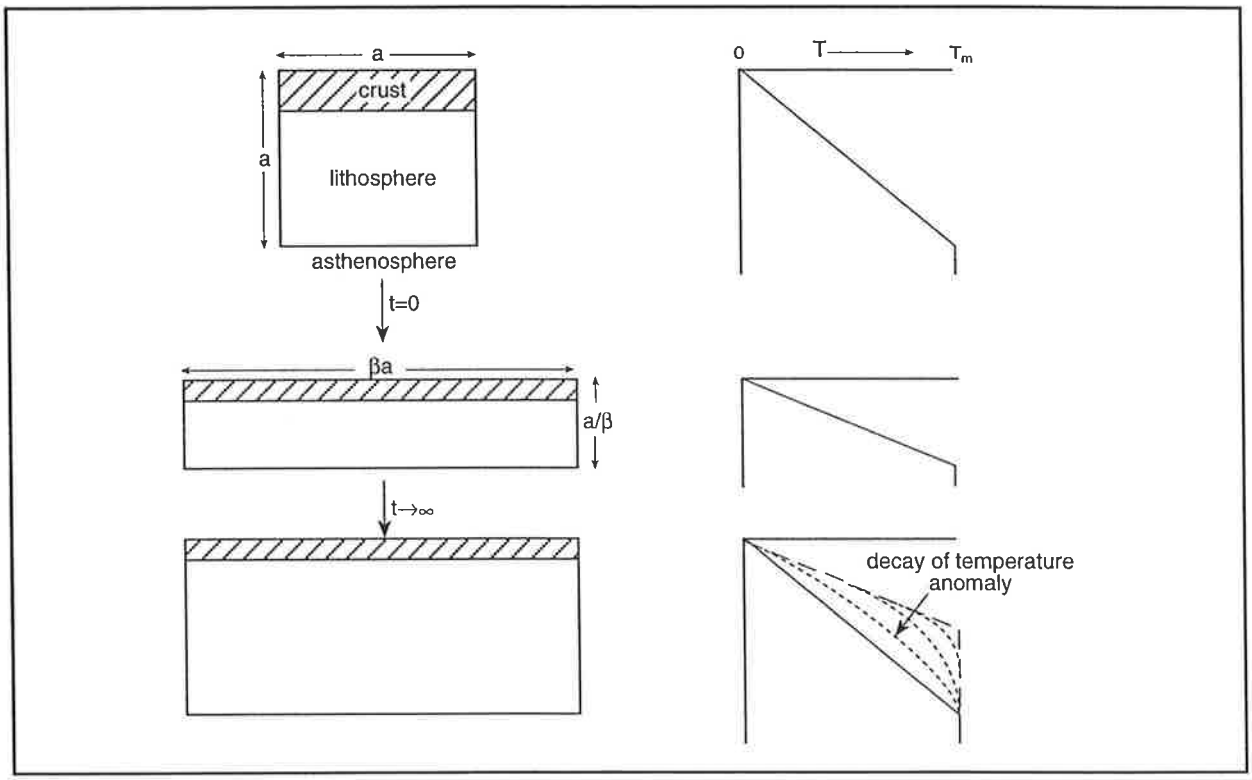

Fig. 7.1. At time t=0 a section of thermally equilibrated lithosphere is extended by β. Isostatic compensation causes upwelling of hot asthenosphere. Cooling of this hot asthenosphere results in subsidence as the temperature anomaly decays with time (after McKenzie, 1978).

$$\begin{aligned} T &= 0 \qquad z = a, \\ &= T_m \qquad z = 0 \end{aligned} \qquad \text{.....(7.4)}$$

The solution for T at time t is:

$$\frac{T}{T_m} = 1 - \frac{z}{a} + \frac{2}{\pi}\sum_{n=1}^{\infty}\frac{(-1)^{n+1}}{n}\left[\frac{\beta}{n\pi}\sin\frac{n\pi}{\beta}\right]\exp\left(\frac{-n^2 t}{\tau}\right)\sin\frac{n\pi z}{a} \qquad \text{.....(7.5)}$$

where:

$$\tau = \frac{a^2}{\pi^2 \kappa} \qquad \text{.....(7.6)}$$

Solving the one-dimensional heat equation in this way, with the boundary condition that the temperature at a depth corresponding to the initial thickness of the lithosphere is fixed ($T = T_m$ at $z = 0$), results in the lithosphere rapidly regaining its original thickness, and a thermal anomaly within the lithosphere which decays with time (Fig. 7.1). This observation is important for modelling multiple rifting events (Section 7.3.3).

The elevation $e(t)$, above the final depth to which the upper surface of the lithosphere sinks is:

$$e(t) = \frac{a\rho_m \alpha T_m}{\rho_m - \rho_w}\left\{\frac{4}{\pi^2}\sum_{m=0}^{\infty}\frac{1}{(2m+1)^2}\times \left[\frac{\beta}{(2m+1)\pi}\sin\frac{(2m+1)\pi}{\beta}\right]\exp\left(-(2m+1)^2\frac{t}{\tau}\right)\right\} \qquad \text{.....(7.7)}$$

Hence, the subsidence since extension, S_t, is:

$$S_t = e(0) - e(t) \qquad \text{.....(7.8)}$$

and the total subsidence is the sum of S_i and S_t.

It is now generally accepted that the lithospheric stretching model of McKenzie (1978) can explain, at least in outline, the main features of some but not all continental sedimentary basins and passive margins (White & McKenzie, 1988). Since it was first proposed, numerous refinements have enabled the model to explain several observations that cannot be explained by the model in its simplest form as described by McKenzie (1978). The following sections cover a number of important alterations to the original McKenzie (1978) model that are pertinent to the approach used in this thesis.

7.3.2 Two-layer pure shear heterogeneous extension

A number of sedimentary basins and continental shelves exhibit less crustal extension and initial subsidence and more thermal subsidence than predicted by the McKenzie (1978) model (Royden & Keen, 1980; Sclater *et al.*, 1980; Hellinger & Sclater, 1983). To account for this, both Sclater *et al.* (1980) and Royden & Keen (1980) have suggested that the input of heat to the subcrustal region during continental rifting may be greater than that predicted by McKenzie (1978). This led to models which allowed crustal thinning to be significantly less than subcrustal thinning, with extension in the crust decoupled from that in the subcrustal lithosphere. Such heterogeneous stretching can increase the heat input during extension by raising the lithosphere-asthenosphere boundary more than in the McKenzie (1978) model. To avoid a space problem, areas of excess subcrustal thinning must be compensated for by areas of excess crustal thinning (Hellinger & Sclater, 1983).

Assuming similar heat loss and isostatic conditions to McKenzie (1978), Hellinger & Sclater (1983) presented a simple reformulation of the treatment of the instantaneous two-layer extension models of Sclater *et al.* (1980) and Royden & Keen (1980). Hellinger & Sclater (1983) introduced the parameter β_L, the ratio of the initial thickness of the lithosphere to the thickness after extension, which is related to the crustal extension, β_c, and the subcrustal extension, β_{sc}, by the equation:

$$\frac{a}{\beta_L} = \frac{t_c}{\beta_c} + \frac{a - t_c}{\beta_{sc}} \qquad \text{.....(7.9)}$$

Equation 7.9 can be simplified by introducing the parameters $\gamma_L = 1 - 1/\beta_L$, $\gamma_c = 1 - 1/\beta_c$, and $\gamma_{sc} = 1 - 1/\beta_{sc}$:

$$a\gamma_L = t_c\gamma_c + (a - t_c)\gamma_{sc} \qquad \text{.....(7.10)}$$

Hellinger & Sclater (1983) showed that the initial subsidence is given by:

$$S_i = \frac{1}{\rho_m(1 - \alpha T_m) - \rho_w} \times \left\{ \left[(\rho_m - \rho_c) t_c \left(1 - \frac{\alpha T_m t_c}{2a} \right) - \frac{\alpha \rho_m T_m t_c}{2} \right] \gamma_c - \left[\frac{\alpha \rho_m T_m (a - t_c)}{2} \right] \gamma_L \right\} \qquad \text{.....(7.11)}$$

When $\gamma_c = \gamma_L$, Equation 7.11 reduces to Equation 7.1, the uniform extension model of McKenzie (1978).

Immediately after the extensional event the temperature distribution in the lithosphere is given by:

$$\begin{aligned} T &= T_m && 0 \le z \le a\gamma_L, \\ &= T_m\left[1+\beta_{sc}\left(\gamma_L - z/a\right)\right] && a\gamma_L \le z \le a - t_c/\beta_c, \\ &= T_m\beta_c\left(1 - z/a\right) && a - t_c/\beta_c \le z \le a \end{aligned} \quad \text{.....(7.12)}$$

Again, solving the one-dimensional heat equation (Equation 7.3) with boundary conditions (7.4), the solution for T at time t is:

$$\frac{T}{T_m} = 1 - \frac{z}{a} + \sum_{n=1}^{\infty} C_n \exp\left(\frac{-n^2 t}{\tau}\right)\sin\frac{n\pi z}{a} \quad \text{.....(7.13)}$$

where:

$$C_n = \frac{2(-1)^{n+1}}{\pi^2 n^2}\left[\left(\beta_c - \beta_{sc}\right)\sin\left(\frac{n\pi t_c}{a\beta_c}\right) + \left(\beta_{sc}\right)\sin\left(\frac{n\pi}{\beta_L}\right)\right] \quad \text{.....(7.14)}$$

The elevation $e(t)$ above the final depth to which the upper surface of the lithosphere sinks is obtained by:

$$e(t) \approx \frac{2a\rho_m\alpha T_m}{\left(\rho_m - \rho_w\right)\pi} \times \left\{\sum_{k=0}^{\infty} \frac{C_{2k+1}}{(2k+1)} \exp\left(-(2k+1)^2 \frac{t}{\tau}\right)\right\} \quad \text{.....(7.15)}$$

and the water loaded thermal subsidence is again given by Equation 7.8.

From the work of Hellinger & Sclater (1983) and White & McKenzie (1988), the following observations involving two-layer heterogeneous lithospheric extension can be made:

- subcrustal extension can exceed crustal extension in certain areas, provided it is balanced by areas of a compensating excess of crustal extension;
- where $\beta_c > \beta_{sc}$, more syn-rift and less post-rift subsidence occurs than predicted by the McKenzie (1978) model;
- the converse is true for areas where $\beta_{sc} > \beta_C$, and;
- in regions where $\beta_{sc} > \beta_c$, extension may result in initial uplift and erosion, followed by post-rift subsidence and stratigraphic onlap.

7.3.3 Incorporating multiple rifting events into two-layer, heterogeneous extension

Thermal anomalies inherited from prior rifting events can have dramatic effects on subsequent rifting events, in particular on the amount of post-rift subsidence (Giltner, 1987; Odling, 1992; Lippard & Liu, 1992). The time between consecutive rifting/uplift events in the Celtic Sea/South-Western Approaches is insufficient for complete decay of the thermal perturbation from previous events, hence thermal perturbations within the lithosphere must be incorporated into subsequent events. The equations of McKenzie (1978) and Hellinger & Sclater (1983) presented above assume an initially thermally unperturbed lithosphere, hence these equations must be adjusted to allow for prior events, in order to analyse the tectonic evolution of the Celtic Sea/South-Western Approaches.

Developed from the models from McKenzie (1978) and Jarvis & McKenzie (1980), Odling (1992) presented a method to calculate the effects of any extension on any initial temperature profile. This method has been used in this thesis to analyse the tectonic history of the Celtic Sea/South-Western Approaches, and it is described in the following section.

7.4 Odling's (1992) Method for Modelling Multiple Lithospheric Deformation Events

Odling's (1992) method divides the lithosphere into any number of layers (N) of equal thickness, each of which is assigned an extension factor. With this method, any form of non-uniform extension event can be modelled. More importantly, however, in terms of this thesis, extension of the lithosphere with a non-equilibrium temperature profile can be analysed by adjusting the extension factors for each layer to those necessary to obtain the final temperature profile from the equilibrium state (Section 7.4.1). As in the McKenzie (1978) model, the equilibrium temperature distribution of the lithosphere is assumed to increase linearly with depth.

On rifting, each layer within the lithosphere is extended by a factor β_n. This extension is associated with a change in elevation which is a balance between uplift due to thermal expansion and subsidence due to the replacement of light crust by denser mantle material (Odling, 1992). Isostatic equilibrium is assumed to be maintained. The contribution of each layer is calculated and the results summed. The change in elevation S_i is given by:

$$S_i = \frac{-a}{N\left[\rho_m(1-\alpha T_m)-\rho_w\right]} \times \left\{ \sum_{n=M}^{N} \rho_c \left(1-\frac{\alpha}{2}(T_{n+1}+T_n)\right)\left(1-\frac{1}{\beta_n}\right) + \sum_{n=1}^{M-1} \rho_m \left(1-\frac{\alpha}{2}(T_{n+1}+T_n)\right)\left(1-\frac{1}{\beta_n}\right) - \rho_m(1-\alpha T_m)\left(N-\sum_{n=1}^{N}\frac{1}{\beta_n}\right)\right\} \quad \text{.....(7.16)}$$

Once again, the decay of the temperature anomaly produced by the instantaneous extension event is modelled by solving the one-dimensional heat flow equation (Equation 7.3). In the multilayer method, that solution is:

$$T(z,t) = T_m\left(1-\frac{z}{a}\right) + T_m \sum_{k=1}^{\infty} b_k \exp\left(-k^2\pi^2 t \frac{\kappa}{a^2}\right)\sin\frac{k\pi z}{a} \quad \text{.....(7.17)}$$

where b_k are the Fourier coefficients of the temperature distribution immediately after instantaneous extension. Odling (1992) showed that the Fourier coefficients for the multilayer method are:

$$b_k = \frac{2}{k\pi}\sum_{n=1}^{N}\left[\frac{(\beta_n-\beta_{n-1})}{k\pi}\sin k\pi\left(1-\frac{1}{N}\sum_{m=n}^{N}\frac{1}{\beta_m}\right)\right] \quad \text{.....(7.18)}$$

Alternatively, Equation 7.18 can be expressed as:

$$b_k = \frac{2(-1)^{k+1}}{k^2\pi^2} \times \left\{ \sum_{n=1}^{N-1}\left[(\beta_{n+1}-\beta_n)\sin\left(\frac{k\pi}{N}\sum_{m=n+1}^{N}\frac{1}{\beta_m}\right)\right] + \beta_1 \sin\left(\frac{k\pi}{N}\sum_{m=1}^{N}\frac{1}{\beta_m}\right)\right\} \quad \text{.....(7.19)}$$

which, if β_{Sc} and β_c are substituted in the appropriate layers, reduces to the form of the equation for C_n (Equation 7.14) from Hellinger & Sclater's (1983) two-layer heterogeneous model.

The elevation above the final level to which the surface of the crust sinks is:

$$e(t) = \frac{-a\alpha T_m}{\pi\left[\rho_m(1-\alpha T_m) - \rho_w + Bt_c/a\right]} \times \sum_{k=1}^{\infty}\left[\frac{b_k}{k}\exp\left(-\frac{k^2\pi^2\kappa t}{a^2}\right)\left\{(\rho_m+\rho_c)\left[1-\cos k\pi\left(1-\frac{t_c}{a}\right)\right]+\rho_m-(-1)^n\rho_c\right\}\right] \quad .....(7.20)$$

where

$$B = \rho_w\left[1+\frac{\alpha T_m}{(1-\alpha T_m)}\right]\left(1-\frac{\rho_c}{\rho_m}\right)+(\rho_c-\rho_m) \quad .....(7.21)$$

Again, the water loaded thermal subsidence at time t, (S_t), is given by Equation 7.8.

7.4.1 Superimposing two lithospheric deformation events using Odling's (1992) method

The above equations for subsidence after instantaneous extension assume an initial equilibrium temperature profile. However, if extension follows a previous rifting event before the temperature perturbation from that event has completely decayed, the initial temperature distribution may differ significantly from the equilibrium state. Odling (1992) showed that every temperature profile can be described as an extension superimposed on the equilibrium temperature distribution. The magnitude of this extension will in general vary with depth, a situation which the multilayer method is able to accommodate (Fig. 7.2). To calculate the effect of a non-equilibrium temperature profile on thermal subsidence, a second set of β extension factors which are required to produce the final temperature profile from the equilibrium profile are calculated (Fig. 7.2). These modified β factors do not represent actual thinning of the lithosphere but the values required by the method to calculate cooling and resulting thermal subsidence for an initial thermal profile than is not in its equilibrium state (Odling, 1992).

The temperature perturbation of the lithosphere remaining from the initial rifting event can be calculated using Equation 7.17. The temperature values for the top and base of each of the N layers of the method can thus be calculated. These temperature values are input into Equation 7.16 to calculate the effect of the thermal perturbation on the change in elevation due to instantaneous extension. The resulting temperature profile immediately after the extension event can then be calculated using the β factors of the second event (Fig. 7.2). The depths to the temperature values for the top and base of each of the N layers are recalculated, and these depths are compared with the equilibrium temperature profile to calculate the modified β factors required by the method (Fig. 7.2).

7.5 Discussion of the Assumptions and Constraints used in Odling's (1992) Method in this Thesis

Table 7.1 lists the parameters used in analysing the tectonic evolution of the Celtic Sea/South-Western Approaches. The assumption of an initial crustal thickness of 35 km is based upon Cheadle *et al.* (1987), who suggested that the crust of the Celtic Sea/South-Western Approaches region was of at least average thickness (35 km) immediately after the Variscan Orogeny.

The models for lithospheric deformation discussed in the previous sections were all originally formulated to analyse the response of the lithosphere to extension. A major component of this thesis has been the recognition and quantification of Tertiary uplift in

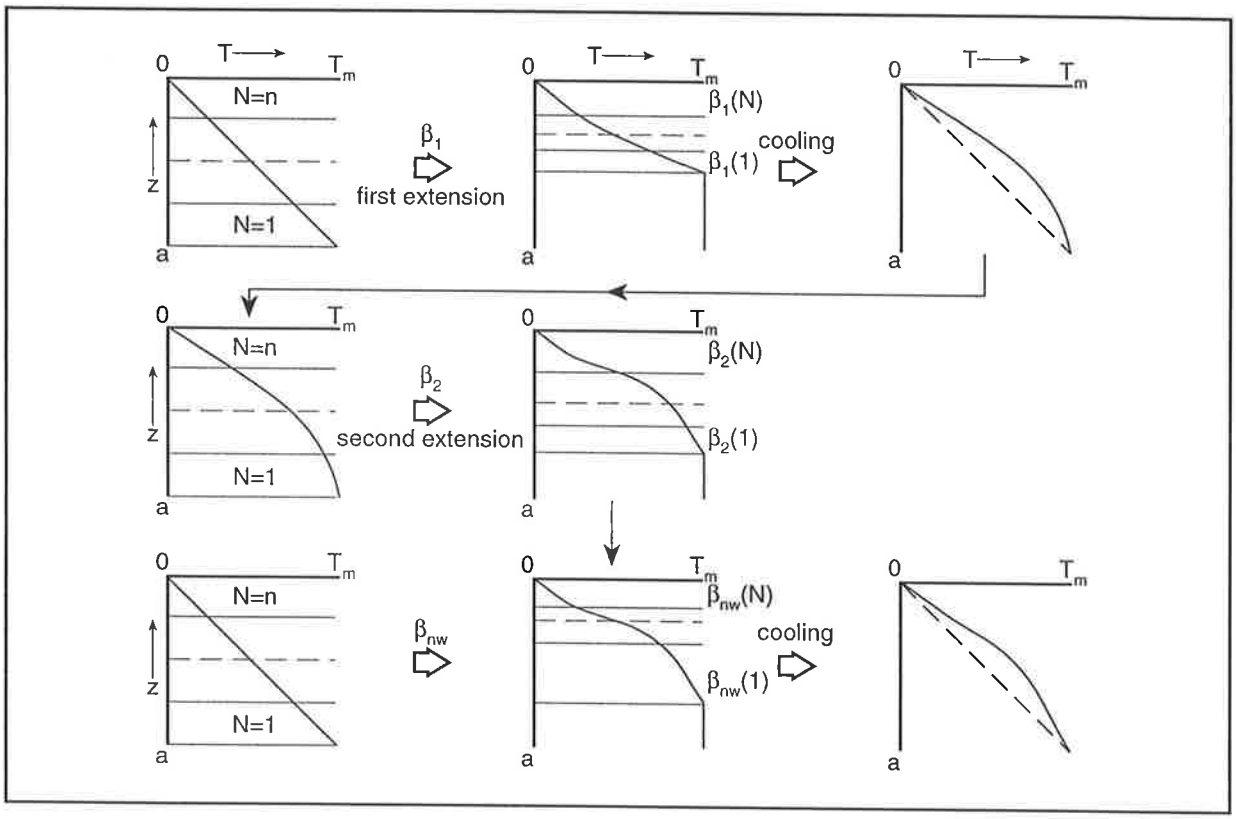

Fig. 7.2. Superposition of two rifting events. The initial rifting event β_1 causes a thermal anomaly which decays with time. A second rifting event β_2 causes further perturbation of the temperature profile. To calculate the subsidence due to the new temperature profile, a series of extension factors β_{nw}, that are required to produce the thermal profile of the second event from the equilibrium profile, are calculated. These beta factors do not represent actual thinning of the lithosphere, but are the values required by the method to calculate the changes in the temperature profile with time and hence to calculate thermal subsidence for the second event (after Odling, 1992).

parameter	definition	values
a	thickness of lithosphere	125 km
t_c	thickness of continental crust	35 km
ρ_m	density of mantle material at 0°C	3330 kg m^{-3}
ρ_c	density of crustal material at 0°C	2800 kg m^{-3}
ρ_w	water density	1030 kg m^{-3}
α	thermal expansion coefficient	3.28×10^{-5} °C^{-1}
T_m	temperature at base of lithosphere	1333 °C
κ	thermal diffusivity	25.21 m^2 yr^{-1}
N	no. of layers	125

Table 7.1. Physical and thermal parameters and assumed values (after Hellinger & Sclater, 1983, and Odling, 1992).

the Celtic Sea/South-Western Approaches. Hence, in the tectonic modelling of the Celtic Sea/South-Western Approaches, a compressional event resulting in Tertiary uplift must be analysed in addition to the earlier, basin-forming extensional events. This event can be analysed using the same equations of lithospheric deformation, however the input β factors are related to lithospheric thickening rather than thinning, and thus $0<\beta<1$ for compressional events.

The tectonic subsidence/uplift history of the Celtic Sea/South-Western Approaches determined in Chapter 6 assumed water-loaded basement for both subsidence and uplift (Section 6.8). The method used in this chapter is also normalised to water-loaded basement. If uplift results in elevation of basement above sea level, then Equation 6.9 must be used to calculate the amount of 'water-loaded' exhumation, and hence the change in crustal thickness. However, uplift which does not elevate basement above sea level is analysed as a change in water-loaded basement depth, and no change in crustal thickness due to exhumation occurs.

The final sections of this chapter discuss further possible modifications to models of lithospheric deformation. These further modifications have not been utilised in this study, and the reasons for not incorporating them are outlined.

7.5.1 Airy isostasy versus flexural isostasy

All of the models of extensional basin formation presented in this chapter, as well as the backstripping/decompaction procedure used in Chapter 6, have assumed local or Airy isostatic compensation. Several authors (e.g. Kusznir *et al.*, 1987; Roberts *et al.*, 1995; Kusznir *et al.*, 1995) have demonstrated that incorporating flexural isostasy into geodynamic models can have important implications for the distribution and relative thickness of syn- and post-rift sequences in extensional basins. However, White & McKenzie (1988) suggest that the flexural model of extensional basin formation is not in good agreement with observations from some passive margins and sedimentary basins. Hegarty *et al.* (1988) demonstrated that where $\beta < 1.6$, subsidence histories are similar for either an Airy or flexural isostatic response to loading. Sibuet *et al.* (1990) suggest that under these conditions, particularly during rifting when the lithosphere is mechanically very weak, Airy isostasy is appropriate.

White & McKenzie (1988) noted that several studies of passive continental margins and extensional basins have shown that the elastic thickness (T_e) of the lithosphere remains less than 5 km during the post-rift phase. White & McKenzie (1988) also showed that increasing flexural rigidity during post-rift cooling, as suggested by Watts *et al.* (1982), is not necessarily required to explain stratigraphic onlap at basin margins. White & Latin (1993) noted that the flexural cantilever model of Kusznir *et al.* (1991) itself places no independent physical constraints on the value of T_e. Elastic thickness is treated by Kusznir *et al.* (1991) and others as a variable whose effect on the final model is assessed qualitatively. White & Latin (1993) suggest that undue emphasis on an arbitrarily chosen T_e deflects attention from more important sources of error, such as uncertainty in the values of parameters such as the thicknesses and densities of the crust and lithospheric mantle, and the temperature of the asthenosphere. For the above reasons, the analysis of the subsidence/uplift history of the Celtic Sea/South-Western Approaches assumes Airy isostasy.

7.5.2 Pure shear versus simple shear

Wernicke (1985) proposed a simple shear tectonic model for the extension of the Basin and Range

Province. The model involves a large detachment surface which cuts through the crust and relays crustal extension into the mantle lithosphere (Fig. 7.3), resulting in extension of the crust and mantle lithosphere which is non-uniform in any vertical column of lithosphere. Karner *et al.* (1987) suggested the Wessex Basin formed by simple shear, with a reactivated Variscan thrust relaying extension into the ductile region of the lower crust/subcrustal lithosphere. An important consequence of such a model is that any uplift and/or subsidence related to the thermal re-equilibration of the lithosphere is offset from the rift basin (Fig. 7.3). Although reactivation of pre-existing Variscan thrusts has been proposed as a mechanism for the formation of many of the Celtic Sea/South-Western Approaches basins (Chapter 2), there is no observed offset between the syn-rift and post-rift basins in the area. Indeed, the post-rift sequence is almost uniform over the entire region, with some localisation over basin centres (Chapter 4). A Wernicke-type model is therefore deemed inappropriate for the Celtic Sea/South-Western Approaches.

Wernicke's (1985) model has been further developed by incorporating mixed pure and simple shear models, and thereby eliminating the requirement for offset of the post-rift sequence (e.g. Kusznir & Egan, 1989; Kusznir *et al.*, 1991; Roberts *et al.*, 1995; Kusznir *et al.*, 1995). These models address in detail the geometry and subsidence/uplift histories of faults and fault blocks within basins. However, White (1990) argued that in terms of heat flow and subsidence, such more complex lithospheric deformation models are indistinguishable from pure shear stretching models. The pure shear model previously described is thus considered sufficient to address the regional-scale subsidence and uplift patterns observed in the Celtic Sea/South-Western Approaches.

7.5.3 Instantaneous extension versus time-dependent extension

Finite extension rates can have important effects when calculating extension factors in extensional basins (Jarvis & McKenzie, 1980; Cochran, 1983). Heat lost during a finite duration rifting event increases the amount of syn-rift subsidence at the expense of the post-rift when compared to the subsidence predicted by an instantaneous stretching model. For rifting events which last less than 20 million years, the simpler instantaneous rifting model gives reasonably accurate results (Jarvis & McKenzie, 1980). The rifting events analysed in the Celtic Sea/South-Western Approaches are between 25 million years (Late Triassic) and 35 million years (Late Jurassic) in duration. The timing and duration of the Tertiary uplift event is poorly constrained (Chapter 2), but it is likely to be between 10 million years duration (assuming Palaeocene exhumation) and 20 million years duration (assuming Oligo-Miocene exhumation).

The Odling (1992) method described in Section 7.4 is capable of analysing time-dependent extension. However, the method becomes mathematically unwieldy when modelling the multiple deformation events of the Celtic Sea/South-Western Approaches. Whilst time-dependent extension represents a geologically more feasible model, the additional complications introduced into the modelling process do not alter the results of the analysis sufficiently to warrant inclusion. Instantaneous extension has thus been assumed in the analysis used in this thesis.

7.5.4 Depth of decoupling between upper and lower lithospheric deformation

Hellinger & Sclater (1983) placed the boundary between upper and lower lithospheric deformation at

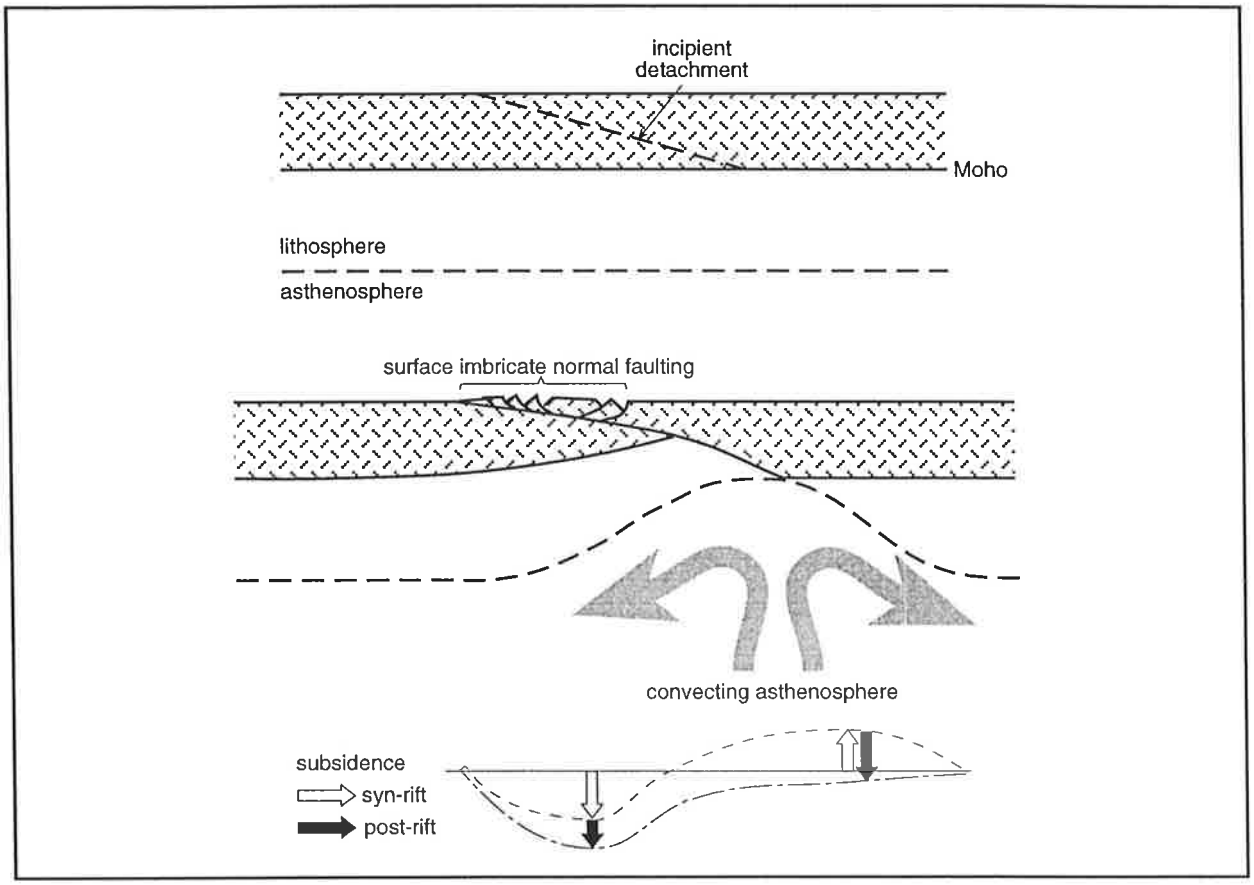

Fig. 7.3. Wernicke's (1985) simple shear model, in which a crustal detachment relays extension into, or even through, the mantle lithosphere. The model results in thermal uplift during extension of the crust of a region away from the rift basin, and deposition of a post-rift sequence that is offset from the syn-rift basin.

the base of the crust in their two layer heterogeneous model, and thus utilised crustal (β_c) and subcrustal (β_{sc}) stretching factors. The Odling (1992) method used in this thesis incorporates N layers, each potentially with different stretching factors. In this thesis, the same β factor is allocated to the layers which correspond to the crust, and the same subcrustal β factor to the layers which correspond to the mantle lithosphere. The method was also tested with a decoupling or detachment depth within the crust, so that the lower crust had the same β factor as the mantle lithosphere. However, the base of the crust was found to be the most appropriate depth for decoupling the upper and lower lithospheric deformation, producing the smallest errors in the analysis.

Chapter 8

Modelling the Tectonic Evolution of the Celtic Sea/ South-Western Approaches

8.1 Introduction

In this chapter the pure shear, heterogeneous model of lithospheric deformation developed in Chapter 7 is applied to the two-dimensional tectonic history of the Celtic Sea/South-Western Approaches determined in Chapter 6. The results are then compared with other published tectonic modelling studies from around the Northwest European Atlantic margin, and from the conjugate Canadian Atlantic margin.

8.2 Results of the Two-layer Heterogeneous Model of Lithospheric Deformation

The heterogeneous lithospheric deformation model appears a sensible choice to apply to the Celtic Sea/South-Western Approaches because:

- uplift occurred in the internal basins during Late Jurassic-Early Cretaceous rifting of the external basins;
- Late Cretaceous-Tertiary post-rift sedimentation was not localised over the Late Jurassic-Early Cretaceous syn-rift depocentres, and;
- Tertiary uplift was regional in extent, and not limited to structurally inverted areas.

At a first pass it would seem that these key aspects of the tectonic evolution of the Celtic Sea/South-Western Approaches might be accounted for by:

- $\beta_{sc} > \beta_c$ in the internal basins during Late Jurassic-Early Cretaceous rifting;
- β_{sc} (extension/thinning) more distributed than β_c during the Late Cretaceous-Tertiary post-rift phase, and;
- β_{sc} (compression/thickening) more distributed than β_c during Tertiary uplift.

8.2.1 An initial analysis of the tectonic evolution of the Celtic Sea/South-Western Approaches: balanced β factors

Initially, the two-layer, heterogeneous pure shear method developed in Chapter 7 was tested on the Celtic Sea/South-Western Approaches assuming crustal and subcrustal β factors were balanced across the region, to prevent the space problems discussed in Section 7.3.2. Figure 8.1 shows the β profiles initially used in analysing the tectonic evolution of the Celtic Sea/South-Western Approaches. Crustal β factors were calculated such that the initial subsidence/uplift of each event within the basins which undergo crustal deformation matched that observed on the Celtic Sea/South-Western Approaches profile. As the regional patterns of subsidence and uplift of the Celtic Sea/South-Western Approaches, and not local variations of subsidence within sub-basins and individual half-grabens, are the main point of interest in this thesis, a simple sinusoidal shape was chosen for the crustal β factor within each basin. The mantle lithospheric β factor was initially assumed to be uniform over the entire region, with the sum of β_{sc} equal to the sum of β_c across the area.

The resultant subsidence/uplift history is shown with the reconstructed tectonic history in Figure 8.2,

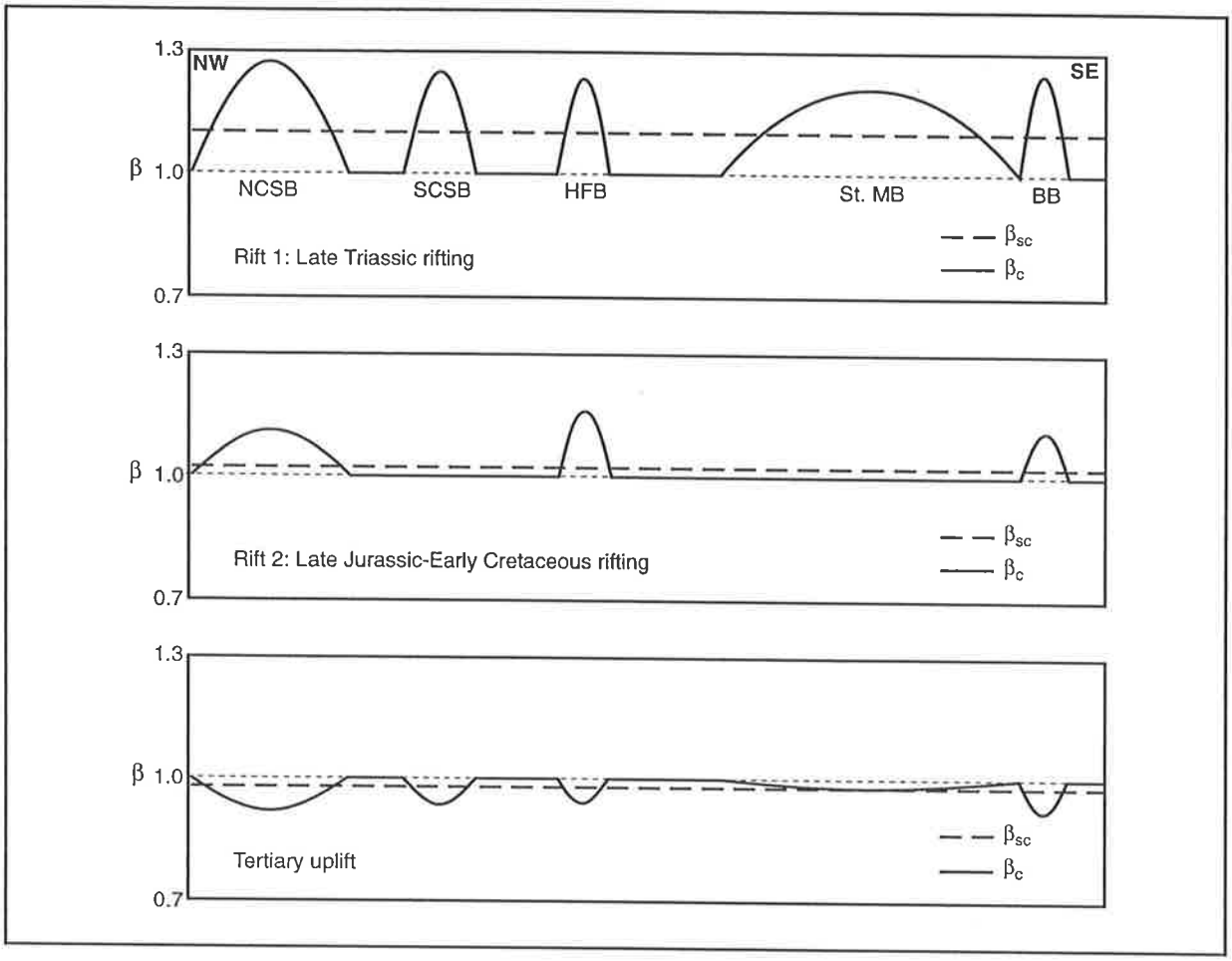

Fig. 8.1. Crustal (β_c) and subcrustal (β_{sc}) beta factors initially used to analyse the tectonic history of the Celtic Sea/South-Western Approaches. β factors balance across the section, to prevent space problems occurring. The line of the section is shown in Figure 2.3. NCSB = North Celtic Sea Basin, SCSB = South Celtic Sea Basin, HFB = Haig Fras Basin, St.MB = St. Mary's Basin, BB = Brittany Basin.

which shows that the β factors used in this initial model yield poor results. The following key points are apparent (bold letters refer to locations on Figure 8.2).

(i) Too much post-rift 1 subsidence may be predicted for the St. Mary's Basin (**A**). However, there is no stratigraphic control available on the post-rift 1 in this basin because the sequence was eroded in Late Jurassic-Early Cretaceous times, hence the β factors for the Late Triassic rifting event (rift 1) cannot be adjusted.

(ii) Significant syn-rift 2 ('Cimmerian') uplift occurred in the South Celtic Sea Basin, St. Mary's Basin, and surrounding platforms. The initial analysis attempted to model this by uniform sub-crustal stretching (β_{sc}) across the region with no associated crustal stretching in the basins exhibiting 'Cimmerian' uplift (Fig. 8.1). However, the rift 2 β_{sc} factor used does not predict sufficient uplift of these areas (**B**).

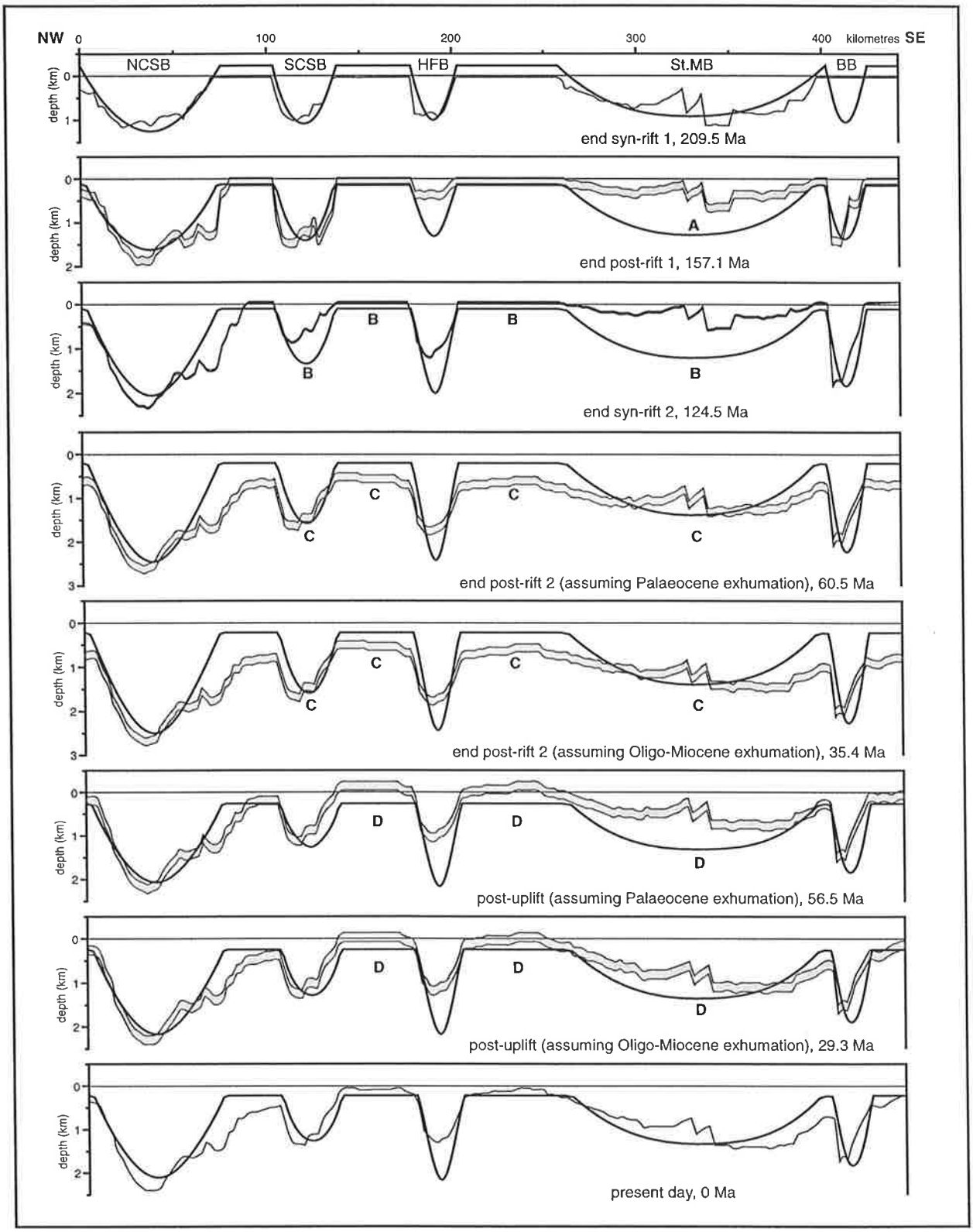

Fig. 8.2. Comparison between reconstructed tectonic histories from Chapter 6 (light solid line with shaded error bar for maximum and minimum palaeobathymetry) and modelled tectonic histories (heavy solid line) assuming β profiles of Figure 8.1. Reconstructions and models for both Palaeocene and Oligo-Miocene exhumation are presented. NCSB = North Celtic Sea Basin, SCSB = South Celtic Sea Basin, HFB = Haig Fras Basin, St.MB = St. Mary's Basin, BB = Brittany Basin. See text for discussion of points **A**, **B**, **C**, & **D**.

(iii) Given that the initial analysis does not generate sufficient syn-rift 2 uplift in the South Celtic Sea Basin, St. Mary's Basin, or surrounding platforms (**B**), the reasonable fit of the predictions for these areas at the end of the post-rift 2 period implies that the modelled amount of post-rift 2 subsidence is also insufficient in these areas (**C**). Again, this implies that the rift 2 β_{sc} factor for these areas is not large enough in this initial approach. Neither enough initial uplift (**B**), nor subsequent subsidence (**C**) is predicted.

(iv) There is significant Tertiary uplift observed in the Celtic Sea/South-Western Approaches away from the recognised structural inversion axes of the North Celtic Sea Basin, Brittany Basin, and South Celtic Sea Basin. The initial analysis attempted to model this uplift by uniform sub-crustal shortening (β_{sc}) across the region, with no associated crustal shortening (β_c) for the platform areas, and minimal crustal shortening for the essentially structurally uninverted St. Mary's Basin (Fig. 8.1). However, the β_{sc} factor used in the initial approach does not generate sufficient Tertiary uplift of the platforms or the St. Mary's Basin (**D**).

(v) The initial analysis does fit the observed tectonic history of the North Celtic Sea and Brittany basins for all three events (Fig. 8.2). The tectonic history of these external basins of the Celtic Sea/South-Western Approaches is thus best modelled as a two-layer, heterogeneous deformation in which crustal deformation is significantly greater than subcrustal deformation (Fig. 8.1).

The essential problem with the initial analysis of the tectonic evolution of the Celtic Sea/South-Western Approaches presented above is that a model with balanced β factors cannot produce sufficient syn-rift 2 uplift, post-rift 2 subsidence, or Tertiary uplift, to accurately model the observed tectonic histories in the relatively undeformed St. Mary's Basin, South Celtic Sea Basin, or surrounding platforms. The β factors necessary to predict the observed subsidence and/or uplift of each of the basin centres and the platform areas are addressed below. However, the poor stratigraphic control on the Haig Fras Basin makes the modelling results for this basin questionable, hence it has been omitted from the preceding and subsequent discussion.

8.2.2 A revised analysis of the tectonic evolution of the Celtic Sea/South-Western Approaches: required β factors

Figure 8.3 shows the revised β profiles that are required to generate sufficient subsidence/ uplift in the St. Mary's Basin, South Celtic Sea Basin, and surrounding platforms. There is no difference between the crustal β factors used in this revised approach and those used in Section 8.2.1. However, there is a dramatic difference between the revised subcrustal β factors and those used in the initial analysis. In the revised approach, the β_{sc} factors in the internal basins and the platform area are much larger for the second rifting event, to account for the amount of uplift associated with Cimmerian exhumation. In addition, the β_{sc} factors in these areas associated with the Tertiary uplift event are significantly smaller (for $0<\beta_{sc}<1$, the smaller the β_{sc}, the greater the subcrustal thickening). In contrast with these regions, the β_{sc} factors for the external basins remain the same as the initial approach for all of the deformation events, because the predictions of the initial analysis provided a reasonable fit to the observed subsidence/uplift history of these basins.

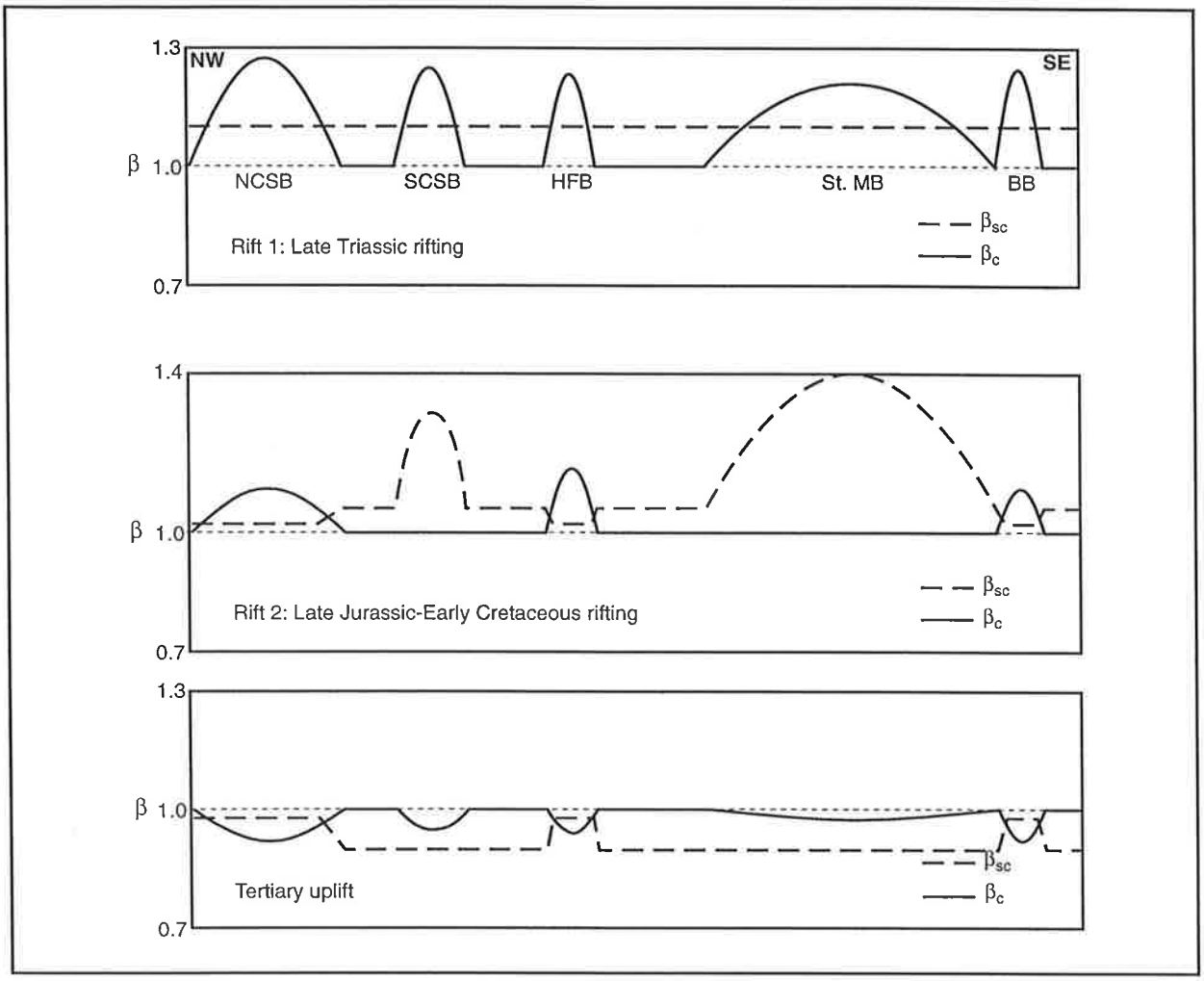

Fig. 8.3. Crustal (β_c) and subcrustal (β_{sc}) beta factors used in the revised analysis of the tectonic history of the Celtic Sea/ South-Western Approaches. The line of the section is shown in Figure 2.3. NCSB = North Celtic Sea Basin, SCSB = South Celtic Sea Basin, HFB = Haig Fras Basin, St.MB = St. Mary's Basin, BB = Brittany Basin.

Figure 8.4 shows the revised subsidence/uplift history of the Celtic Sea/South-Western Approaches obtained using the β profiles in Figure 8.3. The fit of the revised tectonic history is much better than that of Figure 8.2, especially in the South Celtic Sea Basin and the surrounding platform areas. In the St. Mary's Basin, the lack of Jurassic stratigraphic control places no constraints upon the thickness of post-rift 1 subsidence (Section 6.9), and hence the modelled post-rift 1 subsidence may be excessive, as discussed in Section 8.2.1 (point **A**, Fig. 8.4). As a result, a large syn-rift 2 β_{sc} factor is necessary to reverse the amount of modelled post-rift 1 subsidence, which in turn generates a large amount of post-rift 2 subsidence. A large amount of subcrustal shortening in the Tertiary uplift phase is also required to generate sufficient Tertiary uplift to match that observed. However, as the initial response to subcrustal shortening without associated crustal shortening is subsidence, the magnitude of the Tertiary uplift β_{sc} factor is constrained by the maximum observed subsidence of the basin (point **B**, Fig. 8.4). The modelled tectonic history for the St. Mary's Basin is still a poor fit if Tertiary uplift is assumed to have

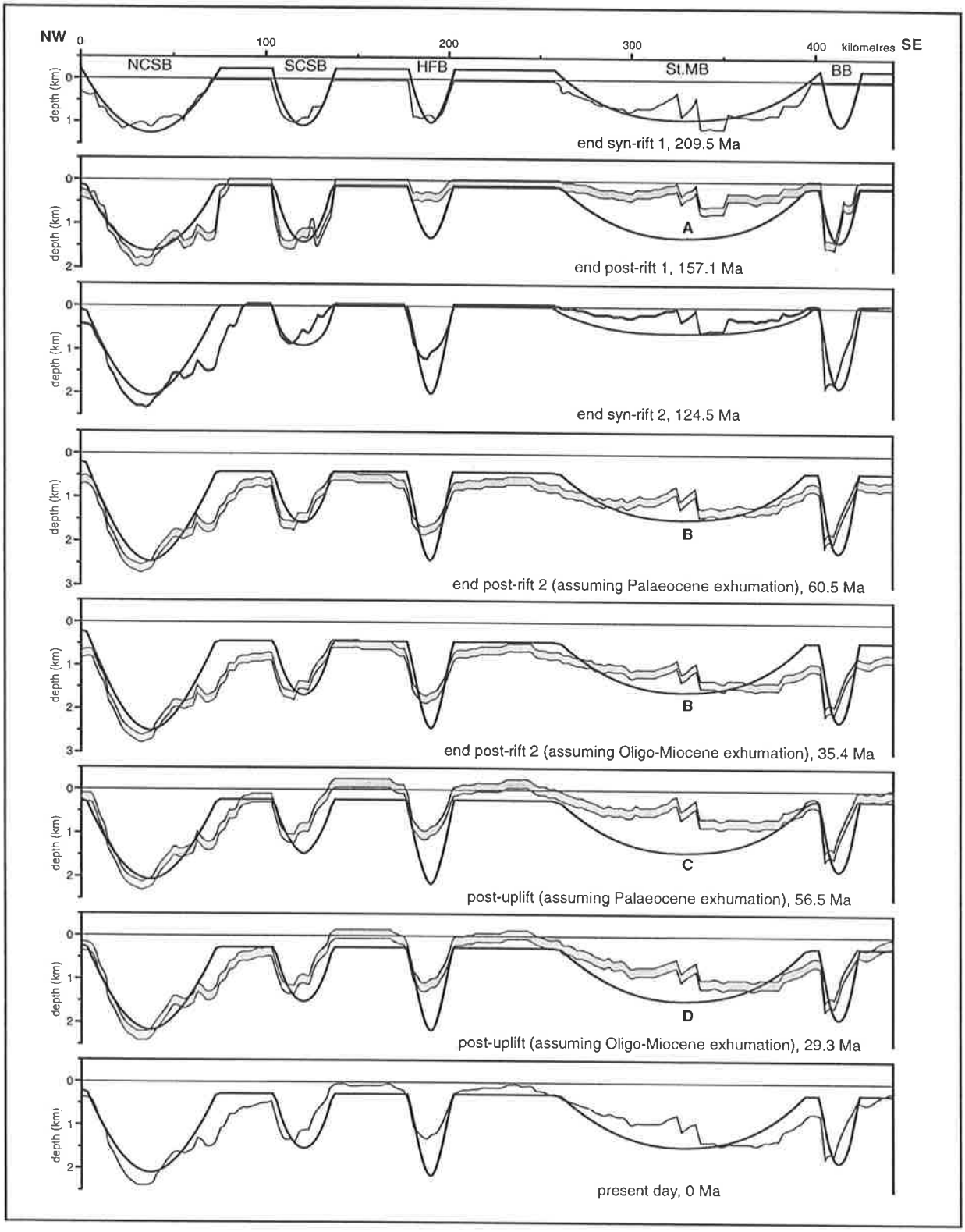

Fig. 8.4. Comparison between reconstructed tectonic histories from Chapter 6 (light solid line with shaded error bar for maximum and minimum palaeobathymetry) and modelled tectonic histories (heavy solid line) assuming β profiles of Figure 8.3. Reconstructions and models for both Palaeocene and Oligo-Miocene exhumation are presented. NCSB = North Celtic Sea Basin, SCSB = South Celtic Sea Basin, HFB = Haig Fras Basin, St.MB = St. Mary's Basin, BB = Brittany Basin. See text for discussion of points **A**, **B**, **C**, & **D**.

occurred during the Palaeocene (point **C**, Fig. 8.4), whilst a better fit is obtained if the uplift occurred during the Oligo-Miocene (point **D**, Fig. 8.4).

The results of the revised analysis suggest that significant excess subcrustal stretching/ compression occurred under the internal basins and the Cornubian Platform for both the second rifting event and the Tertiary compressional event. In comparison, beneath the external basins where crustal deformation was much higher, subcrustal deformation was minimal (Fig. 8.3). Regionally, the magnitude of the β_{sc} factors required to predict the observed subsidence and uplift histories from the second rifting event onwards is much greater than that of the associated β_c factors. Thus the analysis above suggests that for much of the tectonic history of the Celtic Sea/South-Western Approaches, subcrustal deformation was significantly greater than associated crustal deformation, and the tectonic evolution of the area cannot be explained by balanced crustal/subcrustal β factors. This concept is further discussed in the following section.

8.3 Discussion of the Results of the Two-layer Heterogeneous Modelling of Lithospheric Deformation

The crustal and subcrustal β factors required to fit the observed subsidence/uplift history in the internal basins result in major space problems, because the total subcrustal extension/ compression across the region greatly exceeds the amount of crustal extension/compression. Similar regions of potential strain incompatibility have been noted around the Northwest European Atlantic margin. Lippard & Liu (1992) suggested a non-uniform stretching model with $\beta_{sc}>\beta_c$ for the rift margins of the Viking Graben in the northern North Sea, especially for the northern Horda Platform, whilst the graben centre better fitted a uniform stretching model. In addition, Lippard & Liu (1992) suggested that β factors for Triassic rifting are fairly uniform across their northern North Sea section, implying a broad zone of fairly even extension, which contrasted with later mid-Jurassic events in which β_c is strongly localised within the Viking Graben. The excess β_{sc} under the Horda Platform of the mid-Jurassic event of Lippard & Liu (1992) is not balanced anywhere within their northern North Sea section.

White & Latin (1993) suggested from subsidence analyses from the North Sea 'triple-junction' that a time-dependent differential stretching model, in which the lithospheric mantle is initially stretched by a greater amount than the crust, may provide an explanation for localised relative uplift or 'doming' in the area prior to and during the early stages of the Jurassic-Cretaceous rift phase. Alternatively, these authors suggested the same data could be explained by invoking a small transient thermal anomaly in the asthenosphere.

Keen & Dehler (1993) investigated the subsidence history of the Goban Spur Atlantic margin to the west of the Celtic Sea/South-Western Approaches (Fig. 8.5), and documented subcrustal β factors that are significantly greater than crustal β factors (Fig. 8.6). In the same study, a similar situation was documented for the Grand Banks of the conjugate Canadian Atlantic margin. However, the half graben basins of the Grand Banks (the Jeanne d'Arc and Whale basins) were subjected to crustal stretching with almost no associated subcrustal stretching (Fig. 8.6), a situation very similar to the external basins of the Celtic Sea/South-Western Approaches (Fig. 8.3). In contrast, the Orphan Basin of the Grand Banks has significantly greater subcrustal than crustal stretching, as seen in the internal basins of the Celtic Sea/South-Western Approaches. Overall, the conjugate North Atlantic margins of the Goban Spur, Galicia Bank,

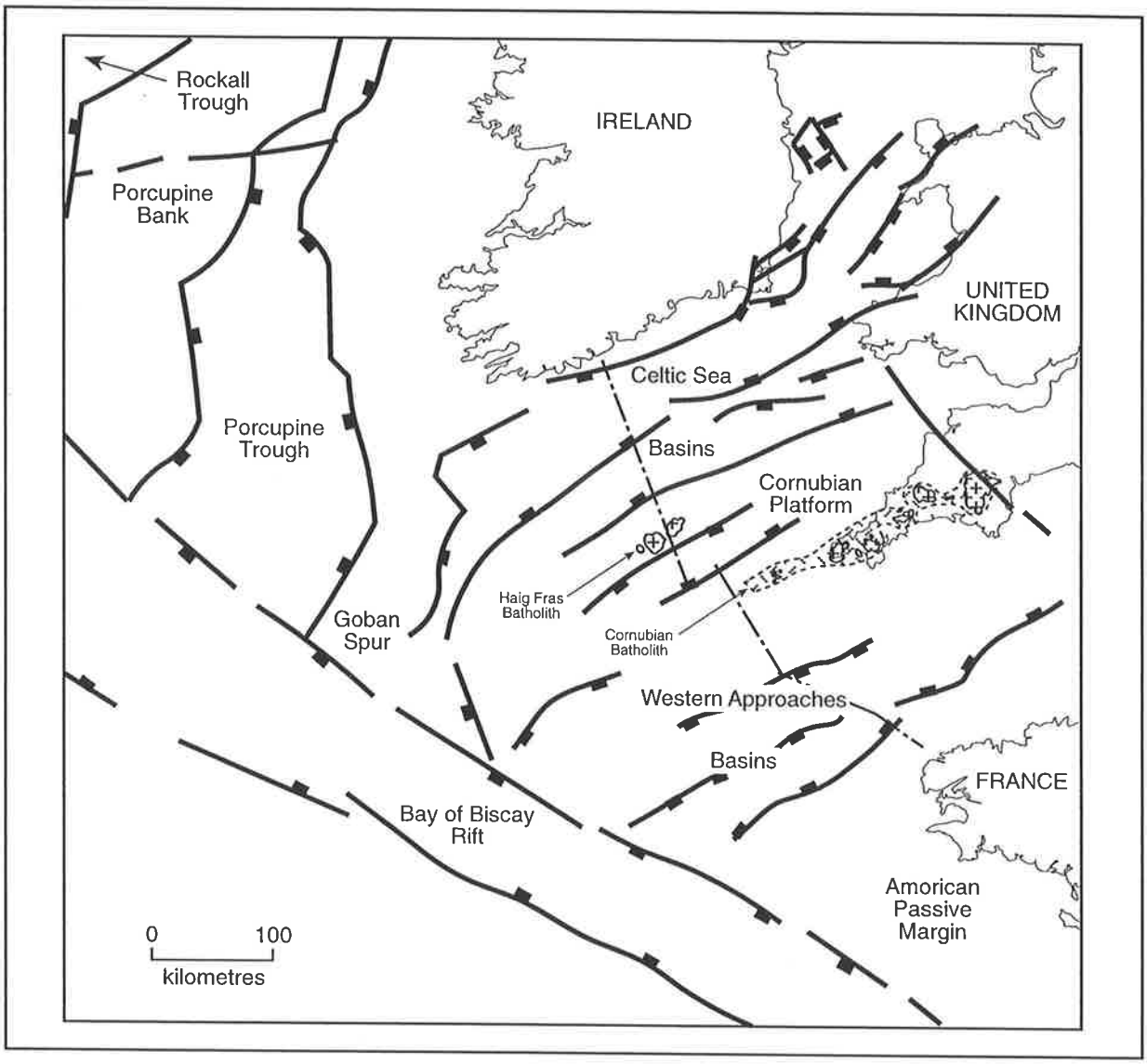

Fig. 8.5. Mid-Late Jurassic tectonic framework of the Celtic Sea/South-Western Approaches and surrounding areas, adapted from Ziegler (1990), showing the location of the Goban Spur and Rockall Trough. The location of the Celtic Sea/South-Western Approaches profile is also shown (dot-dash line). See text for discussion.

and the eastern Canadian margin show significantly greater subcrustal stretching than crustal stretching (Keen & Dehler, 1993). Keen & Dehler (1993) concluded that the reasons for the apparent non-conservation of volume are uncertain, but may indicate that processes other than stretching are important in the lower lithosphere.

The above studies, along with others such as that of Royden & Keen (1980) on the continental margin of eastern Canada, have documented regions similar to the Celtic Sea/South-Western Approaches in which a strain incompatibility between the crust and mantle lithosphere appears necessary to explain the subsidence histories of the regions. The following sections discuss possible explanations for the apparent strain incompatibility across the Celtic Sea/South-

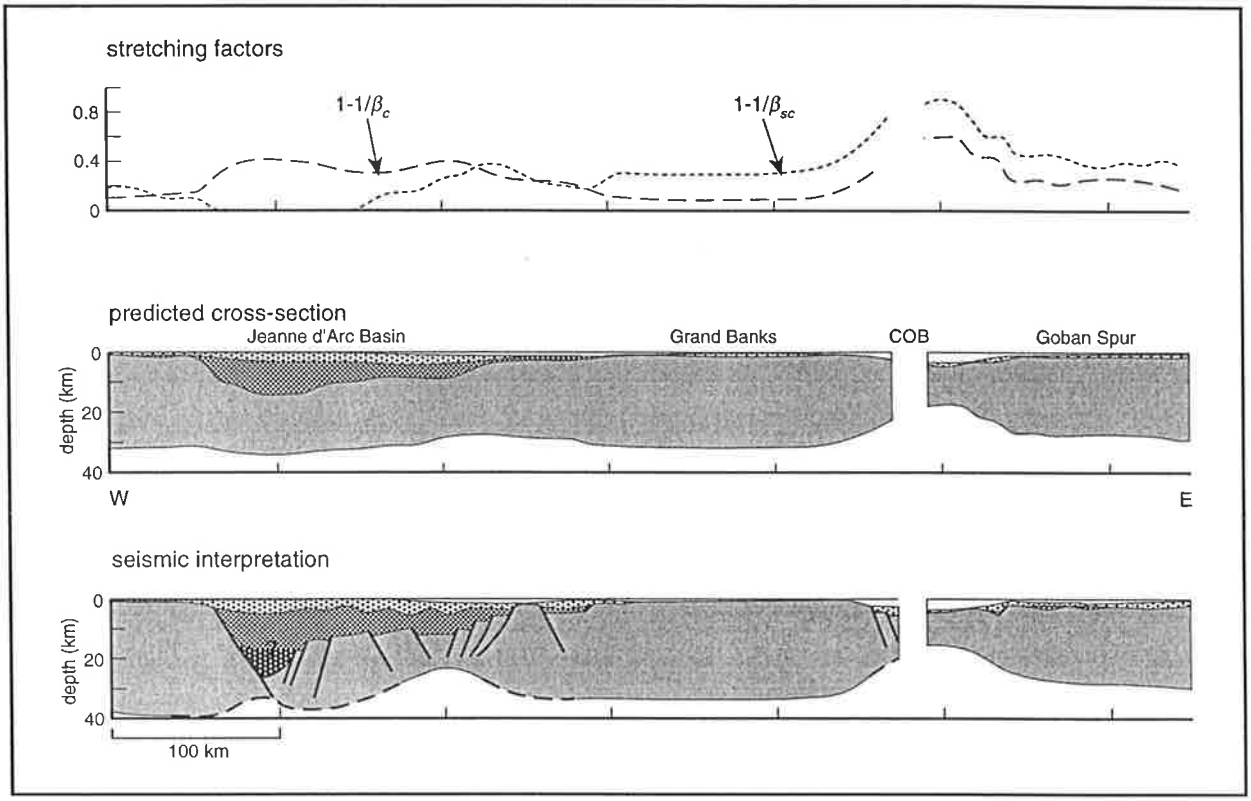

Fig. 8.6. Keen & Dehler's (1993) comparison of the predicted cross-section using crustal stretching parameters and an interpreted seismic cross-section of the Grand Banks, off eastern Canada, and the Goban Spur, west of the Celtic Sea/South-Western Approaches (Fig. 8.5). The Moho is shown dashed where it is uncertain on the seismic sections. Post-rift (light shading) and syn-rift (dark shading) sediments are indicated. Crustal stretching (β_c) is greatest over the Jeanne d'Arc Basin, where subcrustal stretching (β_{sc}) is minimal. For the rest of the section, β_{sc} is greater than β_c.

Western Approaches.

8.3.1 Subcrustal deformation distributed from adjacent areas

Karner *et al.* (1987) suggested that strain compatibility between the upper crust and lower crust/subcrustal lithosphere of the Wessex Basin (immediately east of the Celtic Sea/South-Western Approaches) is attained external to the basin. They found that the cumulative upper crustal extension over a number of rifting events from the Late Palaeozoic through the Mesozoic was significantly greater than lower crustal/subcrustal lithospheric extension (β_{uc} = 1.11, β_{lc} = 1.05), with ductile stretching of the lower crust/subcrustal lithosphere postulated to occur over an area approximately twice the size of the brittle extension within the Wessex Basin in order to explain the strain incompatibility. Karner *et al.* (1987) suggested that extension in the upper crust is relayed into the lower crust/subcrustal lithosphere along the basal Variscan thrust, resulting in thermal uplift of around 60 m of the northern Amorican Massif over the past 200 My. To the north-west of the Celtic Sea/South-Western Approaches, Hauser *et al.* (1995) suggested that differential Permo-Triassic through Jurassic stretching of the Rockall Trough (Fig. 8.5) resulted in stretching factors of β = 8 to 10 for the

upper crust, and β = 2 to 3 for the lower crust and mantle lithosphere. Hauser *et al.* (1995) suggested that the region of lower crustal and mantle lithospheric stretching extends under Ireland.

Whilst it appears that subcrustal extension in areas of the North Atlantic margin around the Celtic Sea/South-Western Approaches throughout the Late Palaeozoic-Mesozoic is much more regionally distributed than crustal extension, there are two major problems with appealing to subcrustal extension distributed from adjacent areas to account for the excess β_{sc} during Late Jurassic-Early Cretaceous rifting in the Celtic Sea/South-Western Approaches. Firstly, the external basins of the Celtic Sea/South-Western Approaches, the North Celtic Sea and Brittany basins, are best modelled by almost no subcrustal extension during this rifting phase (Fig. 8.3). A mechanism that concentrates subcrustal extension under the internal basins and the Cornubian Platform would therefore be necessary to account for the observed tectonic history. Subcrustal thickening resulting in thermal uplift of the internal basins and the Cornubian Platform during the Tertiary is similarly difficult to account for by requiring subcrustal deformation from regions outside the Celtic Sea/South-Western Approaches to impinge upon the area.

8.3.2 Thermal anomalies

White & Latin (1993) suggested that a transient thermal anomaly in the asthenosphere in the northern North Sea prior to and during rifting may be responsible for the apparent excess of subcrustal extension necessary to explain the initial subsidence history of the North Sea 'triple-junction'. In the Celtic Sea/South-Western Approaches, a thermal anomaly would be necessary during both Late Jurassic-Early Cretaceous rifting, and also during Tertiary compression, and would need to be localised under the internal basins and Cornubian Platform. The Variscan granites of the Cornubian Batholith are a region of well documented high heat flow (106-129 mWm^{-2}; Rollin, 1995). The Cornubian Platform is therefore a region with a long-lived perturbation of the geotherm. Odling (1992) and Lippard & Liu (1992) have demonstrated how a remanent perturbation of the geotherm from a previous rifting episode can affect later rifting events, and the same effects have been shown by the modelling in this thesis. It is likely that a long-lived thermal anomaly due to high heat production granites in the crust would have similar effects, and could accentuate subsidence and uplift due to subcrustal deformation.

Although the method of Odling (1992) has been used in this thesis to analyse the effects of transient thermal anomalies inherited from previous events, it cannot be used to analysis the effects of a geotherm perturbed by high crustal heat production in the modelling of the Celtic Sea/South-Western Approaches. Firstly, the Odling (1992) method used the one-dimensional heat flow equation (i.e. no lateral heat conduction), thus the effects of the high heat production of the Cornubian Batholith on the adjacent internal basins cannot be quantified by the method. Secondly, the Odling (1992) method assumes a linear equilibrium temperature profile, hence the method can only incorporate transient thermal anomalies, and not anomalies sustained by high heat production in the crust.

The thermal regime of the Cornubian Platform and surrounding basins may cause the subcrustal β factors derived for this area in Section 8.2.2 to be excessive. To determine whether this accounts completely for the excess β_{sc} in the Celtic Sea/South-Western Approaches suggested by this thesis requires modelling of the effects of high crustal heat production on subsidence and uplift histories which is

beyond the scope of this thesis. Such modelling may provide an explanation for the difference in tectonic histories between the internal and external basins of the Celtic Sea/South-Western Approaches. The perturbation of the geotherm due to the high heat production granites of the Cornubian Batholith may result in thermal weakening of the lithosphere, which may be a possible mechanism for localising β_{sc} under the internal basins and Cornubian Platform.

8.4 Comparison of Modelling Results with Other Studies in the Celtic Sea/South-Western Approaches

Dyment (1991) used a single event, uniform extension model to analyse the subsidence of the Celtic Sea basins, and compared the resultant β factors with crustal thinning estimates based on the thickness of the crystalline crust prior to and after extension. Table 8.1 summarises the results of Dyment's (1991) two approaches, and also gives the total crustal thinning factor, β_{cl}, obtained by multiplying the β_c factors for successive events derived in Section 8.2.2.

Dyment (1991) concluded that the process of basin formation of the Celtic Sea basins was different to that assumed by uniform extension. Table 8.1 shows that the multiple event, two-layer heterogeneous deformation model used in this thesis yields total crustal thinning β factors for the Celtic Sea basins which are closer to Dyment's (1991) crustal thinning factors determined from the thickness of the crystalline crust prior to and after stretching than Dyment's (1991) crustal thinning factors derived from subsidence modelling. The two-layer heterogeneous deformation model used in this thesis yields a better fit to the crustal thinning estimates determined from seismic sections by Dyment (1991) than a McKenzie (1978) uniform extension model for the Celtic Sea basins.

O'Reilly *et al.* (1991) suggested, on the basis of seismic refraction data in the North Celtic Sea Basin, that extension is greater in the lower lithosphere than in the upper crust, with a lower lithosphere β factor of about 2, compared with 1.2 to 1.3 in the upper crust. Whilst a comparable crustal β factor is suggested by the results in this chapter for the North Celtic Sea Basin, the modelling of Section 8.2.2 suggests the extension of the subcrustal lithosphere of the North Celtic Sea Basin is approximately 1.1 (Table 8.1). This large difference in lower lithospheric bulk extension factors is largely due to O'Reilly *et al's* (1991) upper/lower lithosphere boundary being associated with a crustal detachment at a depth of 12 km. If their upper/lower lithosphere detachment was modelled at the base of the crust, the lower lithospheric bulk stretching factor would reduce to 1.4. This is still significantly larger than the bulk subcrustal β factor determined for the North Celtic Sea Basin in this thesis.

O'Reilly *et al.* (1991) suggested that regional extension of the lower crust and mantle lithosphere of the Celtic Sea area occurs below a horizontal detachment in the lithosphere. They suggested the position of the detachment within the crust is controlled by the rheological properties of the crust, and thus indirectly by its thermal structure and composition. For consistency, in this thesis strain partitioning throughout the Celtic Sea/South-Western Approaches was assumed to occur at the base of the crust. As suggested by O'Reilly *et al.* (1991), regions will experience subsidence or uplift during extension depending on the depth to the detachment within the lithosphere. It is possible that different detachment depths may explain at least in part the different tectonic histories of the internal and external basins of the Celtic Sea/South-Western Approaches. However, as discussed above, an intracrustal detachment for the North Celtic Sea Basin requires an even greater

basin	SWAT profile	Dyment (1991) subs. modelling	Dyment (1991) crustal thinning	this study β_{ct}
North Celtic Sea	2	3.0	2.2	
	4	2.1	1.6	
	5	2.4	1.7	1.3
South Celtic Sea	3	1.2	1.1	
	4	1.5	1.2	
	5	1.5	1.3	1.2

Table 8.1. Comparison between β factors derived by Dyment (1991) for the North and South Celtic Sea basins, and the total crustal β factor, $\beta_{ct} = \beta_{c1}\beta_{c2}\beta_{c3}$, derived from Section 8.2.2.

difference between upper and lower lithospheric β factors. Thus the inclusion of a mid-crustal detachment for the North Celtic Sea Basin would result in even greater strain balancing problems than in the modelling of Section 8.2.2.

Sibuet *et al.* (1990) used deep seismic profiles and gravity models to show that the Moho is approximately at a constant depth below the Celtic Sea basins and surrounding areas, and that the layered lower crust does not vary significantly in thickness throughout the whole area. These authors suggested that the formation of the Celtic Sea basins could be explained by McKenzie's (1978) uniform extension model with a bulk stretching factor of β = 2.38, provided the initial thickness and depth of the lower crust are restored after the completion of the rifting phase. Specifically, up to 40% of the volume of the stretched lower crust has to be added after rifting, to account for the apparent lack of thinning of the lower crust (Sibuet *et al.*, 1990). One possible mechanism by which the lower crust may be thickened after rifting is by igneous underplating. Any mechanism which is proposed to explain the discrepancies in the Mesozoic rifting history of the Celtic Sea/South-Western Approaches must also account for the regional Tertiary uplift and exhumation away from recognised structural inversion axes which is documented in this thesis. The following section discusses the possibility of igneous underplating occurring in the Celtic Sea/South-Western Approaches, and whether underplating may be the cause of regional Tertiary exhumation.

8.5 Igneous Underplating as a Cause of Tertiary Exhumation

Brodie & White (1995) demonstrated that regional uplift and exhumation of the northwest European continental shelf during the Early Tertiary may be explained by igneous underplating of the crust. Specifically, these authors suggested that the absence of post-rift thermal subsidence-related sedimentary rocks in the extensional basins of the Irish Sea and to the north and west of Scotland was due to the generation of between 2 - 5 km of melt at the beginning of the Tertiary, much of which was probably trapped in the lower crust. Brodie & White (1995) suggested that the strongly reflective nature of the lower crust on deep seismic profiles collected around the British Isles could be explained by

gabbroic intrusions which underplate the lower crust. The onshore Tertiary igneous province of northwest Britain and Ireland, as well as extensive basaltic volcanism witnessed by refraction velocities and seaward dipping reflectors offshore northwest of Britain, provide further evidence to support the possibility of extensive magmatic activity occurring during the Early Tertiary (Brodie & White, 1995).

The kilometre-scale regional Tertiary exhumation of the Celtic Sea/South-Western Approaches suggested in Chapter 4 would require igneous underplating of approximately 2.25 km of basalt or gabbro with a density of 2.8 g cm^{-3}. Sibuet *et al.* (1990), amongst others, have shown from deep seismic profiles in the Celtic Sea/South-Western Approaches that the lower 12 km of the crust is strongly reflective, which could be explained by gabbroic intrusions which underplate the lower crust. However, the relative lack of Tertiary extrusive volcanism, with the exception of Lundy in the Bristol Channel, compared with that of the British Tertiary igneous province northwest of the United Kingdom, is a clear argument against extensive magmatic activity occurring in the Celtic Sea/South-Western Approaches. Indeed, White & McKenzie (1989) suggested that the continental margin southwest of Britain is a classic non-volcanic margin.

More importantly, however, igneous underplating cannot account for the subsidence that precedes uplift in structurally uninverted areas such as the St. Mary's, Melville, and Plymouth Bay basins, or the Cornubian Platform. The compaction methodology results of Chapter 4 show that the pre-inversion sedimentary fill of the Celtic Sea/South-Western Approaches must be buried to maximum burial-depth prior to exhumation (e.g. Fig. 6.5). Two-layer heterogeneous lithospheric compression can account for a burial pulse prior to exhumation, but igneous underplating cannot. For these reasons, igneous underplating is therefore not considered a significant source of uplift in the Celtic Sea/South-Western Approaches.

Chapter 9
Summary and Conclusions

9.1 Introduction

The primary aims of this thesis were to determine the extent and magnitude of both basin inversion and regional Tertiary exhumation in the Celtic Sea/South-Western Approaches, and to formulate and test a geodynamic model that can account for both the distribution of Tertiary exhumation, and the extension and subsidence history prior to Tertiary exhumation. This thesis also aimed to document the implications of Tertiary exhumation for the reconstruction of the tectonic history of the region. In particular, this required quantification of Tertiary inversion and regional exhumation by the compaction methodology, in order that its geodynamic origin could be modelled. This project also had the aim of testing the suitability of using outcrop samples as an extension to the borehole-based compaction methodology used to quantify exhumation.

This chapter summarises the results of the thesis and presents a number of recommendations for further research to build on the results presented herein.

9.2 Tertiary Exhumation, Celtic Sea/South-Western Approaches

Sonic velocities from the Danian Chalk, Upper Cretaceous Chalk, Lower Cretaceous Greensand/ Gault Clay, Lower Cretaceous Wealden, Upper Jurassic mudstones, Triassic Mercia Mudstone (above and below salt), and Triassic Sherwood Sandstone were used to quantify Tertiary apparent exhumation (i.e. height above maximum burial-depth) in the Celtic Sea/South-Western Approaches. Most of the relatively limited previously published apparent exhumation estimates for the Celtic Sea/South-Western Approaches are broadly consistent with the estimates presented in this thesis.

The strongly stratigraphically inverted areas of the Brittany, South-West Channel, North Celtic Sea, Kish Bank, and Cardigan Bay basins exhibit apparent exhumation of up to 2 km. The exhumation of these basins occurred in association with upper lithospheric compression/ thickening (i.e. basin inversion). The Fastnet and South Celtic Sea basins, which underwent milder Tertiary stratigraphic inversion, exhibit lower apparent exhumation of around 1 km. The major Tertiary-Quaternary depocentres of the southern Cardigan Bay and Melville Basins exhibit low apparent exhumation and are at or near maximum burial-depth.

The compaction analysis presented in this thesis also showed that Tertiary apparent exhumation is not limited to the recognised structural inversion axes of the Celtic Sea/South-Western Approaches. The uninverted St. Mary's and Plymouth Bay basins show apparent exhumation of up to 1.2 km, without associated upper lithospheric compression/thickening. The paucity of data over the Amorican and Cornubian Platforms, and the Pembroke Ridge prevented determination of apparent exhumation estimates for these areas, however the margins of the platform areas also exhibit apparent exhumation of up to 1 km. Tertiary exhumation of the Celtic Sea/South-Western Approaches clearly occurred on a regional scale, beyond the localised apparent exhumation highs associated with axes of structural inversion.

Apparent exhumation results from the Cretaceous units analysed in this thesis show a lack of

consistency with the Triassic units analysed. This lack of consistency between apparent exhumation results may, in part, reflect Jurassic-Early Cretaceous, 'Cimmerian exhumation. There is some indication of maximum burial-depth prior to 'Cimmerian' exhumation having exceeded maximum burial-depth prior to Tertiary exhumation. The wells in which greater apparent exhumation is witnessed by the Triassic units than the Cretaceous units tend of be in the Melville and St. Mary's Basins, which is where the 'Cimmerian' unconformity has its most marked development. However, the excess of apparent exhumation determined from Triassic units above that determined from Cretaceous units, where it occurs, is generally only 200-400 m and within the error limits of the methodology. Hence there is not a sufficiently clear indication of 'Cimmerian' exhumation for it to be quantified separately.

The lateral lithological variability of Tertiary units, combined with the paucity of sonic log data available for these units, prevented constraint of the age of Tertiary exhumation beyond post-Danian using the compaction methodology. However, it has been proposed that the Palaeocene unconformity in Celtic Sea/South-Western Approaches was associated with a period of regional exhumation, while the Oligo-Miocene unconformity was associated with a period of basin inversion (e.g. Tappin *et al.*, 1994; Murdoch *et al.*, 1995). The apparent exhumation estimates in this thesis probably reflect a combination of Palaeocene and Oligo-Miocene exhumation, as the regional Palaeocene exhumation could not be distinguished from the superimposed Oligo-Miocene structural inversion trends.

There is little difference in the burial/uplift history of most of the Celtic Sea/South-Western Approaches, regardless of whether exhumation is assumed to have occurred during the Palaeocene or the Oligo-Miocene. However, in the Tertiary depocentres of the Melville and Cardigan Bay basins, which contain thick sequences of Eocene-Oligocene rocks, differences between burial/uplift histories assuming Palaeocene or Oligo-Miocene exhumation become significant. Regardless of whether exhumation is assumed to be of Palaeocene or Oligo-Miocene age, there is a regional component of between 0.5 - 1.2 km of exhumation, upon which exhumation of recognised stratigraphic inversion axes was superimposed.

When corrected for Tertiary exhumation, the post-rift sequence in the Celtic Sea/South-Western Approaches shows relatively little localisation over the thick syn-rift Jurassic-Lower Cretaceous sequence of Brittany Basin, Southwest Channel Basin, and North Celtic Sea Basin. The 'rift-drift' Avalon Unconformity of the conjugate, but largely uninverted Canadian margin similarly exhibits no localisation of the post-rift sequence over the fault-controlled syn-rift basins (Keen *et al.*, 1987). Keen *et al.* (1987) proposed that during basin formation on the Canadian margin, the lower lithosphere, thermal re-equilibration of which controls post-rift subsidence, did not experience localised thinning on the scale of the syn-rift basins. This implies either that extension was decoupled between the upper and lower lithosphere, or that post-rift lithospheric flexural rigidities were sufficiently high that post-rift subsidence was regionally distributed. A similar argument is applicable to the corrected post-rift burial thicknesses of the Celtic Sea/South-Western Approaches.

Within the Celtic Sea/South-Western Approaches there is a marked symmetry of Jurassic-Tertiary basin formation and inversion around the Cornubian Platform. The basins adjacent to the Cornubian Platform, the South Celtic Sea, St. Mary's, Plymouth Bay, and Melville basins, underwent less Jurassic-Early Cretaceous syn-rift subsidence than those further to the north and south, and also underwent less

Tertiary inversion. Conversely, the areas of maximum Jurassic-Early Cretaceous basin subsidence and syn-rift deposition, the North Celtic Sea, Fastnet, Brittany, and South-West Channel basins, underwent the greatest Tertiary stratigraphic/structural basin inversion. The basins further away from the Cornubian Platform, the Cardigan Bay, Caernarvon, and Kish Bank basins, have undergone such extensive Tertiary inversion that the Jurassic-Cretaceous histories of these basins are unclear. It appears likely that upper lithospheric extension/compression throughout the Jurassic-Tertiary was localised in the North Celtic Sea, Fastnet, Brittany, and South-West Channel basins, herein termed the external basins given their location with respect to the Cornubian Platform, whilst lower lithospheric deformation was distributed more widely throughout the Celtic Sea/ South-Western Approaches.

9.3 Tectonic Modelling, Celtic Sea/South-Western Approaches

A two-layer, heterogeneous model of lithospheric deformation, in which extension/ compression in the upper lithosphere is decoupled from, and distributed differently to, deformation in the lower lithosphere, may account for the observed patterns of subsidence/ uplift (e.g. White & McKenzie, 1988; Hillis, 1992*a*). A multiple event, instantaneous stretching/shortening two-layer model, based upon the work of Odling (1992), with decoupling between upper and lower lithospheric deformation at the base of the crust, was tested on a profile through the Celtic Sea/South-Western Approaches. During the initial basin-forming Late Triassic extension, the analysis presented in this thesis shows that crustal and subcrustal stretching factors can be balanced regionally, with crustal extension localised in the basins, and subcrustal extension distributed uniformly across the area. During Late Jurassic-Early Cretaceous rifting and Tertiary inversion, the external basins which underwent maximum subsidence and subsequent Tertiary inversion are best modelled by minor subcrustal deformation, and significantly greater crustal deformation. In contrast, the internal basins and Cornubian Platform require significant subcrustal stretching/compression factors with little or no associated crustal deformation to account for the Late Jurassic-Tertiary subsidence/uplift histories. The crustal and subcrustal β factors of the two areas do not balance each other regionally, and the magnitude of the subcrustal β factors required to model the subsidence and uplift of the internal basins and Cornubian Platform is much greater than the crustal β factors associated with the external basins.

Similar regions of potential strain incompatibility have been investigated around the North Atlantic margin. Most notable is the study of Keen & Dehler (1993), which documented subcrustal β factors that are significantly greater than crustal β factors for the Goban Spur Atlantic margin to the west of the Celtic Sea/South-Western Approaches, and for the Grand Banks on the conjugate Atlantic margin. In a situation very similar to the external basins of the Celtic Sea/South-Western Approaches, Keen & Dehler (1993) found that the half graben basins on the Grand Banks, the Jeanne d'Arc and Whale basins, formed from crustal stretching with almost no associated subcrustal stretching. In contrast, the Orphan Basin of the Grand Banks was found by these authors to have undergone significantly greater subcrustal stretching than crustal stretching.

Numerous authors have proposed various mechanisms to account for strain incompatibility in basin formation, such as transient asthenospheric thermal anomalies (e.g. White & Latin, 1993), or deformation distributed from adjacent areas (e.g. Hauser *et al.*, 1995). These mechanisms can be

neither proven nor disproven for the Celtic Sea/South-Western Approaches. However, limits can be placed upon the appropriateness of these mechanisms. If the excess strain in the lower lithosphere of the Celtic Sea/South-Western Approaches is balanced externally to the region, then a plausible mechanism must be found, not only for localising subcrustal deformation under the Cornubian Platform and the internal basins, but also for bypassing the external basins of the region. If a thermal anomaly is proposed as the likely source of apparent strain incompatibility, then such an anomaly must be active during both Late Jurassic-Early Cretaceous rifting, and also Tertiary compression, and hence must be long-lived rather than transient. The perturbation of the geotherm due to the high heat production granites of the Cornubian Batholith may have a role in this process as is discussed further in Section 9.5.

9.4 Compaction Analysis, Cleveland Basin/East Midlands Shelf

The validity of using compaction analysis of Upper Cretaceous Chalk outcrop samples to quantify apparent exhumation for the onshore Cleveland Basin/East Midlands Shelf, a region where other independent methods have demonstrated significant Tertiary exhumation, was tested in this thesis. The motivation for this work is that the borehole-based methods applied to the Celtic Sea/South-Western Approaches are restricted to borehole localities, and reflect a desire for more detailed sampling of exhumation magnitudes. The consistency of results from Flamborough Head, where 100 m of section was sampled at the same location, suggests that even stratigraphically-limited Chalk outcrop samples may be used to reliably determine porosity and thus apparent exhumation.

A modification of the water imbibition method for determining density and porosity was presented in this thesis. This modified method yields similar results to the more expensive mercury injection laboratory method, provided an assumption for the grain density can be made. For a consistent lithotype such as the Upper Cretaceous Chalk of eastern England, such an assumption is valid, provided care is taken to avoid flint bands within the Chalk when sampling.

Sample and geophysical log-based Chalk porosities suggest that Late Cretaceous/Tertiary exhumation in the East Midlands Shelf increased from 1.2 km near the coast to more than 2 km inland to the west. The southern margin of the Cleveland Basin was exhumed by 2 km, with exhumation increasing towards the structural inversion axis in the basin centre. This pattern of apparent exhumation controls the regional outcrop distribution of the Upper Cretaceous Chalk in the Cleveland Basin/East Midlands Shelf.

The apparent exhumation estimates for the Cleveland Basin/East Midlands Shelf presented in this thesis, whilst being greater than earlier compaction-based estimates such as those of Marie (1975) and Whittaker *et al.* (1985), showed very good agreement with the recent AFTA-based exhumation estimates of Bray *et al.* (1992), and the organic biomarker-based estimates of Scotchman (1994). Compaction analysis of Upper Cretaceous Chalk outcrop samples was thus shown to yield reliable estimates of Tertiary apparent exhumation in the Cleveland Basin/ East Midlands Shelf.

9.5 Unresolved Issues and Recommendations for Future Research

This thesis has shown that the tectonic history of the Celtic Sea/South-Western Approaches requires a disparity in strain between the upper and lower

lithosphere. Similar regions of strain disparity have been documented around the North Atlantic margin, but to date, no definitive, testable mechanisms have been suggested. The long-lived thermal anomaly due to high heat production granites in the crust of the Cornubian Platform may provide some clues as to the origin of the strain incompatibility between the upper and lower lithosphere in the Celtic Sea/South-Western Approaches region, however this possibility requires extensive further research. In particular, the following unresolved issues require study:

- does the thermal anomaly associated with the high heat production granites exaggerate strain-related subcrustal β factors beneath the Cornubian Platform (i.e. are strain-related β_{sc} factors in fact smaller than apparent, with resultant subsidence and uplift magnified by the thermal state of the lithosphere);
- what are the effects of heat production in the crust of the Cornubian Platform on the geotherm beneath the surrounding basins;
- can the thermal blanketing effect of the low conductivity sediments in the internal basins account for subcrustal β factors which are larger than under the platform area, and;
- can the thermal anomaly cause localisation of subcrustal deformation by affecting the strength profile of the lithosphere, hence localising deformation impinging upon the Celtic Sea/South-Western Approaches from other areas?

To address these concerns, comprehensive modelling of the thermal structure of the lithosphere of the Celtic Sea/South-Western Approaches rather than the kinematic modelling undertaken in this thesis must be undertaken. The distribution of the thermal anomaly in three dimensions around the Cornubian Batholith, and the effects through time of the different thicknesses of low conductivity basin and platform sediments acting as a thermal blanket, must be investigated. Further, the effects of a non-linear equilibrium geotherm on subsidence and uplift models must be investigated, both for the area of high crustal heat production, and for comparison, in regions of more normal heat production. Finally, once the magnitude of the perturbed geotherm of the Cornubian Platform and surrounding basins has been documented, the effects of that perturbation on the theoretical strength profile of the lithosphere must be investigated, to determine whether a thermal mechanism for localising subcrustal deformation may be invoked.

Appendix I

Top, bottom, and mid-point depths (metres below sea-bed), and mean interval transit times (Δt) for the units analysed in the Celtic Sea/ South-Western Approaches

Basin	Well Name	Unit	Top (mbsb)	Bottom (mbsb)	Mid-point depth (mbsb)	Average Δt (μs/ft)
Kish Bank	33/17-1	Mercia (b.s.)	278.3	510.0	394.2	102.6
		Sherwood	829.1	1027.2	928.1	85.9
Kish Bank	33/21-1	Sherwood†	1251.5	1516.5	1328.5	73.7
Caernarvon	42/12-1	Mercia (b.s.)	1291.1	1329.2	1310.1	62.8
		Sherwood	1329.2	1565.5	1447.3	68.9
Caernarvon	42/16-1	Mercia (a.s.)	153.0	444.7	298.8	96.5
		Mercia (b.s.)	894.3	929.4	911.8	67.2
		Sherwood	929.3	1039.1	984.2	70.3
Caernarvon	42/17-1	Mercia (b.s.)	300.4	384.6	342.5	90.3
		Sherwood	384.6	416.7	400.7	69.1
Caernarvon	42/21-1	Upper Jurassic	180.1	213.7	196.9	121.7
Fastnet	47/29-1	U K Chalk*	360.0	657.5	509.4	84.8
		Greensand/Gault	658.4	702.9	680.6	94.8
		Wealden	702.9	888.8	795.8	99.4
		Upper Jurassic	888.8	2011.1	1449.9	81.2
Fastnet	48/19-1	U K Chalk	50.3	719.3	384.8	84.3
		Greensand/Gault	720.9	817.2	769.0	94.0
		Wealden	817.2	1623.1	1220.1	88.5
		Upper Jurassic	1623.1	3162.3	2392.7	79.4
Fastnet	48/26-1	U K Chalk*	66.0	877.0	470.8	70.7
		Greensand/Gault	877.0	1124.0	1000.5	81.2
		Wealden	1124.0	2147.5	1649.3	74.3
		Upper Jurassic	2147.5	2665.0	2406.3	72.3
Fastnet	48/30-1	U K Chalk	255.5	851.3	553.4	72.7
		Greensand/Gault	858.9	1053.1	956.0	89.1
		Wealden	1053.1	1591.4	1325.2	76.1
		Upper Jurassic	1591.4	1649.9	1620.6	74.4
		Mercia (a.s.)	2286.3	2623.6	2454.9	62.4
North Celtic Sea	49/9-1	U K Chalk	336.5	507.8	422.2	101.8
		Greensand/Gault	509.3	739.4	624.4	107.6
		Wealden	739.4	766.9	753.2	100.3
North Celtic Sea	49/9-2	U K Chalk	50.3	466.3	258.3	109.2
		Greensand/Gault	469.4	667.8	568.6	106.3
		Wealden	667.8	957.1	812.4	91.2
		Upper Jurassic	957.1	1687.7	1322.4	72.5
North Celtic Sea	49/9-3	U K Chalk	161.6	477.9	319.8	106.1
		Greensand/Gault	477.9	701.3	589.6	99.8
		Wealden	701.3	1115.0	908.2	88.7
		Upper Jurassic	1115.0	1953.8	1747.1	73.1

Basin	Well Name	Unit	Top (mbsb)	Bottom (mbsb)	Mid-point depth (mbsb)	Average Δt (μs/ft)
North Celtic Sea	49/14-3	U K Chalk	70.4	691.0	380.7	99.5
		Greensand/Gault	691.0	842.8	766.9	94.2
		Wealden	842.8	1612.7	1227.7	87.6
		Upper Jurassic	1612.7	3360.4	2486.6	73.4
South Celtic Sea	49/29-1	U K Chalk	310.9	973.3	642.1	92.1
		Greensand/Gault	1005.8	1078.7	1042.3	85.4
		Wealden	1078.7	1289.3	1184.0	94.6
		Upper Jurassic	1289.3	1400.9	1345.1	81.9
		Mercia (a.s.)	2177.2	2381.4	2279.3	74.8
North Celtic Sea	50/3-1	Upper Jurassic	32.6	800.1	416.4	100.1
North Celtic Sea	50/3-2	Wealden	330.7	355.1	342.9	116.0
		Upper Jurassic	355.1	1644.7	999.9	88.4
North Celtic Sea	50/6-1	U K Chalk	41.2	173.8	107.5	109.0
		Greensand/Gault	194.5	480.7	337.6	123.1
		Upper Jurassic	480.7	1367.3	924.0	92.6
North Celtic Sea	50/7-1	Greensand/Gault	292.0	450.5	371.3	117.1
		Wealden	450.5	491.0	470.8	112.4
		Upper Jurassic	491.0	1327.4	909.2	93.3
North Celtic Sea	50/12-1	Greensand/Gault	69.5	208.2	138.8	120.1
		Wealden	208.2	1131.7	670.0	105.2
		Upper Jurassic	1131.7	1220.1	1175.9	102.7
North Celtic Sea	50/12-2A	U K Chalk	75.0	188.0	131.5	84.2
		Greensand/Gault	310.0	415.0	362.5	110.4
		Wealden	415.0	870.0	642.5	106.3
		Upper Jurassic	870.0	2585.0	1727.5	81.9
Fastnet	56/14-1	U K Chalk	477.4	604.8	541.1	92.0
		Greensand/Gault	697.6	894.6	796.1	144.4
		Wealden	894.6	1323.9	1109.2	106.3
		Upper Jurassic	1323.9	1784.8	1554.3	83.1
Fastnet	56/18-1	U K Chalk	779.7	929.6	854.7	93.3
		Greensand/Gault	938.5	1029.9	984.2	97.0
		Wealden	1029.9	1438.1	1234.0	108.7
Fastnet	57/2-1	U K Chalk*	63.5	701.5	369.7	78.3
		Greensand/Gault	701.5	811.5	756.5	87.6
		Wealden	811.5	1758.5	1285.0	81.2
		Upper Jurassic	1758.5	2056.1	1909.8	68.5
Fastnet	57/7-1	Greensand/Gault	92.7	389.8	241.3	116.6
		Wealden	389.8	994.6	692.2	89.0
		Upper Jurassic	994.6	1337.8	1166.2	72.9
		Mercia (a.s.)	2643.9	2718.5	2681.2	57.2
South Celtic Sea	58/3-1	U K Chalk	330.0	798.3	564.1	96.8
		Greensand/Gault	798.3	880.6	839.4	102.9
		Wealden	880.6	1075.6	978.1	98.7
		Mercia (a.s.)	1587.7	1649.6	1618.6	76.1
		Mercia (b.s.)†	2169.9	2358.9	2167.5	68.8
		Sherwood†	2358.9	2505.2	2335.2	67.8
Melville	72/10-1A	U K Chalk	837.3	1224.1	1030.7	87.2
		Mercia (a.s.)	1341.4	1783.3	1562.4	82.9
		Mercia (b.s.)†	2488.3	2665.4	2445.8	63.3
		Sherwood†	2694.7	2920.3	2676.5	67.2

Basin	Well Name	Unit	Top (mbsb)	Bottom (mbsb)	Mid-point depth (mbsb)	Average Δt (μs/ft)
Melville	73/1-1	Danian Chalk	883.6	910.8	897.2	100.6
		U K Chalk	910.8	1362.4	1136.6	93.2
		Mercia (a.s.)	2001.3	2167.4	2084.4	83.0
Melville	73/2-1	Danian Chalk	534.9	566.0	550.5	107.8
		U K Chalk	566.1	1031.8	798.9	92.7
		Greensand/Gault	1047.6	1057.7	1052.6	117.2
		Mercia (a.s.)	1057.7	1298.2	1177.9	92.8
		Mercia (b.s.)†	2644.5	2885.0	2586.8	67.4
		Sherwood†	2885.0	2930.4	2729.7	69.5
Melville	73/4-1	U K Chalk*	313.9	801.9	566.6	102.7
		Greensand/Gault	802.4	882.4	842.4	113.4
		Mercia (a.s.)	882.4	1073.9	978.1	106.6
Melville	73/5-1	U K Chalk	691.6	1207.4	949.5	87.9
		Greensand/Gault	1207.9	1309.4	1258.7	105.3
		Wealden	1309.4	1347.5	1328.5	93.6
		Mercia (a.s.)	1347.6	1596.8	1472.2	86.8
		Mercia (b.s.)†	1751.4	1889.5	1780.1	74.6
		Sherwood†	1889.5	1959.9	1884.3	71.6
Melville	73/6-1	Danian Chalk	634.6	686.4	660.5	101.9
		U K Chalk	686.4	1020.2	853.3	96.6
		Mercia (a.s.)	1036.9	1408.2	1222.6	92.9
		Mercia (b.s.)†	2923.7	3076.1	2801.4	62.8
		Sherwood†	3076.1	3265.6	2972.4	64.0
Melville	73/7-1	U K Chalk	883.7	1272.9	1078.3	87.3
		Greensand/Gault	1359.1	1386.5	1372.8	92.0
		Wealden	1386.5	1484.1	1435.3	93.2
		Mercia (b.s.)	1488.4	2117.8	1803.1	79.6
		Sherwood	2117.8	2228.4	2173.1	69.7
Melville	73/8-1	U K Chalk	637.9	1118.0	878.0	92.3
		Greensand/Gault	1119.5	1150.6	1135.1	104.1
		Mercia (b.s.)	1150.6	1637.0	1393.8	87.0
		Sherwood	1637.1	1756.6	1696.8	77.7
Melville	73/12-1A	U K Chalk	1073.8	1425.9	1249.8	85.7
		Mercia (b.s.)	1473.1	1646.8	1559.9	85.5
		Sherwood	1646.8	1915.1	1781.0	78.1
Melville	73/13-1	Danian Chalk	1029.3	1089.7	1059.5	87.9
		U K Chalk	1118.9	1486.2	1302.6	82.4
		Greensand/Gault	1502.1	1522.5	1512.3	99.6
		Mercia (a.s.)	2055.3	2265.9	2160.6	74.4
		Mercia (b.s.)	2265.9	2358.9	2312.4	68.4
		Sherwood	2358.9	2466.1	2412.5	73.7
Melville	73/14-1	Danian Chalk	902.8	957.7	930.3	91.2
		U K Chalk*	957.7	1388.4	1187.7	84.3
		Mercia (a.s.)	1451.2	1771.0	1611.1	84.7
		Mercia (b.s.)	1771.0	1936.4	1853.7	71.1
Melville	74/1-1A	U K Chalk	595.0	952.1	773.6	92.6
		Greensand/Gault	952.2	1004.9	978.6	121.3
		Mercia (b.s.)	1004.9	1274.4	1139.7	92.7
		Sherwood	1274.4	1471.3	1372.8	80.4
Melville	83/24-1	U K Chalk	298.5	643.5	471.0	104.7
		Greensand/Gault	644.5	691.5	668.0	114.2

Basin	Well Name	Unit	Top (mbsb)	Bottom (mbsb)	Mid-point depth (mbsb)	Average Δt (μs/ft)
St. Mary's	85/28-1	U K Chalk	415.2	902.9	659.0	96.5
		Greensand/Gault	912.0	1000.4	956.2	118.8
		Wealden	1000.4	1022.9	1011.6	111.6
		Mercia (b.s.)	1022.9	1052.2	1037.6	102.6
		Sherwood	1052.2	1184.8	1118.5	91.5
St. Mary's	86/17-1	U K Chalk	235.9	501.1	368.5	95.7
		Greensand/Gault	502.3	651.1	576.7	113.1
		Mercia (b.s.)	651.1	844.0	747.5	99.3
		Sherwood	844.0	973.8	908.9	91.4
St. Mary's	86/18-1	U K Chalk	406.0	747.7	576.8	87.7
		Greensand/Gault	754.4	880.9	817.6	105.7
		Wealden	880.9	903.4	892.2	112.7
		Mercia (b.s.)	903.5	1104.3	1003.9	92.6
		Sherwood	1104.3	1113.4	1108.8	85.4
St. Mary's	87/12-1A	U K Chalk	78.2	225.2	151.7	76.5
		Greensand/Gault	225.2	298.2	261.7	111.4
		Wealden	298.2	348.2	323.2	115.8
		Mercia (b.s.)	348.2	578.2	463.2	88.8
		Sherwood	578.2	666.2	622.2	83.1
Plymouth Bay	87/14-1	U K Chalk	255.0	581.0	418.0	89.2
St. Mary's	87/16-1	U K Chalk	123.7	665.7	394.7	93.0
		Greensand/Gault	671.7	708.2	690.0	111.6
		Mercia (b.s.)	715.7	803.7	759.7	94.8
Plymouth Bay	88/2-1	U K Chalk	40.0	113.0	76.5	100.1
		Mercia (a.s.)	687.5	770.0	728.8	93.8
South Celtic Sea	93/2-1	U K Chalk*	165.0	1000.0	580.3	100.7
		Greensand/Gault	1000.0	1052.0	1026.0	79.9
		Wealden	1052.0	1348.0	1200.0	96.2
South Celtic Sea	102/28-1	U K Chalk*	78.1	349.9	208.4	108.5
		Greensand/Gault	350.5	419.1	384.8	97.8
		Wealden	419.1	448.4	433.7	118.7
		Mercia (a.s.)	1081.5	1288.1	1184.8	76.1
		Mercia (b.s.)†	2094.3	2304.6	2052.7	67.8
South Celtic Sea	102/29-1	U K Chalk	305.7	392.2	349.0	90.6
		Greensand/Gault	392.3	474.6	433.4	103.0
		Wealden	474.6	505.7	490.1	107.4
Cardigan Bay	103/2-1B	Mercia (a.s.)	814.8	1269.5	1042.1	83.8
		Mercia (b.s.)†	2093.7	2485.1	2196.3	73.2
		Sherwood†	2485.1	2826.4	2562.5	65.9
South Celtic Sea	103/18-1	Wealden	257.0	268.5	262.7	101.6
		Mercia (a.s.)	1220.1	1387.7	1303.9	74.2
		Mercia (b.s.)†	1799.2	2068.6	1878.5	70.7
		Sherwood†	2068.6	2093.4	2025.6	63.1
South Celtic Sea	103/21-1	U K Chalk	248.5	296.6	272.5	99.0
		Greensand/Gault	296.9	345.4	321.1	112.2
		Mercia (a.s.)	1306.1	1528.6	1417.3	75.9
		Mercia (b.s.)†	1635.3	1688.9	1652.4	89.4
Cardigan Bay	106/24-1	Upper Jurassic	690.7	1989.1	1339.9	98.9
Cardigan Bay	106/24A-2B	Upper Jurassic	648.9	1435.6	1042.3	109.1
Cardigan Bay	106/28-1	Mercia (a.s.)	1278.3	1487.1	1382.7	80.0
		Mercia (b.s.)†	2217.7	2792.6	2390.1	77.0

Basin	Well Name	Unit	Top (mbsb)	Bottom (mbsb)	Mid-point depth (mbsb)	Average Δt (μs/ft)
Cardigan Bay	107/16-1	Upper Jurassic	388.3	668.7	528.5	115.2
Cardigan Bay	107/21-1	Upper Jurassic	410.3	809.0	609.6	114.2
Brittany	Brezell-1	U K Chalk	170.0	321.0	245.5	63.3
		Greensand/Gault	334.0	505.0	419.5	94.7
		Wealden	505.0	1195.0	850.0	88.2
		Upper Jurassic	1195.0	1792.0	1493.5	74.6
Brittany	Garlizenn-1	Danian Chalk	864.0	961.0	912.5	100.4
		U K Chalk	972.0	1485.0	1228.5	85.6
		Greensand/Gault	1487.0	1555.0	1521.0	103.3
Brittany	Glazenn-1	Danian Chalk	579.0	649.0	614.0	105.5
		U K Chalk	649.0	1119.0	884.0	98.0
		Greensand/Gault	1308.0	1489.0	1398.5	84.5
		Wealden	1489.0	2854.0	2171.5	69.0
Brittany	Kerluz-1	U K Chalk	789.6	1067.6	928.6	91.8
Brittany	Krogen-1B	U K Chalk	543.0	1266.0	904.5	100.1
		Greensand/Gault	1356.0	1472.0	1414.0	95.4
		Wealden	1472.0	1874.0	1673.0	83.1
		Upper Jurassic	1874.0	2335.0	2104.5	78.2
South-West Channel	Kulzenn-1	Danian Chalk	211.0	266.0	238.5	97.2
		U K Chalk	266.0	640.0	453.0	95.5
		Mercia (a.s.)	649.0	843.0	746.0	102.2
		Mercia (b.s.)	870.0	1016.0	943.0	81.2
		Sherwood	1056.0	1260.0	1158.0	77.1
South-West Channel	Lennket-1	Wealden	220.0	1380.0	800.0	82.2
		Upper Jurassic	1517.0	2350.0	1933.5	64.4
Brittany	Levneg-1	Wealden	163.0	530.0	346.5	97.6
		Upper Jurassic	530.0	839.0	684.5	71.3
Brittany	Lizenn-1	U K Chalk	151.1	715.1	433.1	78.1
		Greensand/Gault	743.1	1316.1	1029.6	102.2
		Wealden	1316.1	1831.1	1573.6	92.8
		Upper Jurassic	1831.1	2731.1	2281.1	69.5
Amorican Shelf	Penma-1	Danian Chalk	852.0	915.0	883.5	89.9
		U K Chalk	915.0	1278.0	1096.5	84.1
		Greensand/Gault	1278.0	1439.0	1358.5	94.4
Brittany	Rea Gwenn-1	U K Chalk	953.0	1520.0	1236.5	79.6
		Greensand/Gault	1550.0	1644.0	1597.0	96.8
		Mercia (a.s.)	2063.0	2355.0	2209.0	73.8
Brittany	Travank-1	Greensand/Gault	206.0	233.0	219.5	122.3
		Wealden	233.0	424.0	328.5	111.9
		Upper Jurassic	424.0	635.0	529.5	103.9
Brittany	Yar Vor-1	U K Chalk	185.0	288.0	236.5	78.2
		Greensand/Gault	289.0	407.0	348.0	105.8
		Wealden	407.0	1138.0	772.5	99.0
		Upper Jurassic	1138.0	2014.0	1576.0	75.9

* Mid-point depth/mean Δt weighted for missing or poor data. † Mid-point depth adjusted for salt thickness.

Appendix II

Apparent exhumation results (in kilometres)

Well number	Danian Chalk	Upper Cretaceous Chalk	Greensand / Gault Clay	Wealden	Upper Jurassic mudstone	Mercia (above salt)	Mercia (below salt)	Sherwood Sandstone	Mean (no Wealden/ UJ)	Mean (all units)
33/17-1							1.25	1.08	1.17	1.17
33/21-1								1.22	1.22	1.22
42/12-1							1.49	1.31	1.40	1.40
42/16-1						1.47	1.76	1.71	1.65	1.65
42/17-1							1.66	2.35	2.01	2.01
42/21-1					1.54					1.54
47/29-1		0.76	0.99	0.66	0.91				0.87	0.83
48/19-1		0.92	0.92	0.49	0.00				0.92	0.58
48/26-1		1.01	0.91	0.40	0.10				0.96	0.60
48/30-1		0.90	0.82	0.68	0.85	0.12			0.61	0.67
49/9-1		0.58	0.82	0.68					0.70	0.69
49/9-2		0.63	0.90	0.83	1.18				0.77	0.89
49/9-3		0.62	0.99	0.80	0.96				0.81	0.84
49/14-3		0.66	0.91	0.50	0.00				0.79	0.52
49/29-1		0.51	0.79	0.38	1.01	0.00			0.43	0.54
50/3-1					1.66					1.66
50/3-2				0.72	1.25					0.99
50/6-1		0.79	0.83		1.26				0.81	0.96
50/7-1			0.91	0.68	1.27				0.91	0.95
50/12-1			1.09	0.65	0.86				1.09	0.86
50/12-2A		1.14	1.03	0.65	0.63				1.09	0.86
56/14-1		0.61	0.00	0.18	0.78				0.31	0.39
56/18-1		0.28	0.65	0.00					0.46	0.31
57/2-1		0.99	1.04	0.60	0.65				1.02	0.82
57/7-1			1.05	1.01	1.33	0.02			0.53	0.85
58/3-1		0.52	0.69	0.49		0.63	0.46	0.47	0.55	0.54
72/10-1A		0.20				0.52	0.34	0.15	0.30	0.30
73/01-1	0.01	0.00				0.00			0.00	0.00
73/02-1	0.27	0.34	0.22			0.67	0.08	0.00	0.27	0.27
73/04-1		0.42	0.50			0.54			0.49	0.49
73/05-1		0.27	0.23	0.26		0.52	0.68	0.75	0.49	0.45
73/06-1	0.23	0.23				0.63	0.00	0.00	0.22	0.22
73/07-1		0.15	0.35	0.17			0.51	0.55	0.39	0.34
73/08-1		0.27	0.37				0.71	0.67	0.51	0.51
73/12-1A		0.00					0.58	0.57	0.39	0.39
73/13-1	0.00	0.00	0.07			0.13	0.33	0.13	0.11	0.11
73/14-1	0.09	0.09				0.43	0.71		0.33	0.33
74/01-1A		0.37	0.23				0.80	0.88	0.57	0.57
83/24-1		0.49	0.66						0.57	0.57
85/28-1		0.43	0.29	0.15			0.61	0.65	0.49	0.43
86/17-1		0.73	0.77				1.00	0.86	0.84	0.84
86/18-1		0.64	0.66	0.25			0.93	0.92	0.79	0.68
87/12-1A		1.24	1.12	0.74			1.58	1.51	1.36	1.22
87/14-1		0.78							0.78	0.78
87/16-1		0.74	0.68				1.11		0.85	0.85
88/02-1		0.95				1.10			1.03	1.03
93/02-1		0.44	0.91	0.33					0.67	0.56
102/28-1		0.69	1.23	0.57		1.06	0.60		0.90	0.83
102/29-1		0.83	1.09	0.77					0.96	0.90
103/2-1B						1.02	0.30	0.33	0.55	0.55
103/18-1				1.14		0.99	0.69	0.98	0.89	0.95
103/21-1		0.78	1.04			0.84	0.38		0.76	0.76
106/24-1					0.75					0.75
106/24A-2B					0.89					0.89
106/28-1						0.77	0.00		0.39	0.39
107/16-1					1.31					1.31
107/21-1					1.24					1.24

Well number	Danian Chalk	Upper Cretaceous Chalk	Greensand / Gault Clay	Wealden	Upper Jurassic mudstone	Mercia (above salt)	Mercia (below salt)	Sherwood Sandstone	Mean (no Wealden/ UJ)	Mean (all units)
Brezell-1		1.35	1.25	0.87	0.97				1.30	1.11
Garlizenn-1	0.00	0.02	0.00						0.00	0.00
Glazenn-1	0.24	0.18	0.45	0.00					0.29	0.22
Kerluz-1		0.23							0.23	0.23
Krogen-1B		0.13	0.25	0.17	0.31				0.19	0.21
Kulzenn-1	0.71	0.65				0.88	1.33	1.24	0.96	0.96
Lennket-1				1.06	0.69					0.88
Levneg-1				1.15	1.83					1.49
Lizenn-1		0.94	0.51	0.04	0.27				0.72	0.44
Penma-1	0.15	0.18	0.32						0.22	0.22
Rea Gwenn-1		0.11	0.04			0.09			0.08	0.08
Travank-1			0.97	0.83	1.48				0.97	1.09
Yar Vor-1		1.13	1.13	0.69	0.87				1.13	0.96

Appendix III

Exhumation at the time of denudation (assuming Palaeocene or Oligo-Miocene exhumation) and maximum burial-depth for the base Upper Cretaceous

Well Number	Exhumation at the time of denudation (km bsb)		Max. burial-depth (km bsb)
	Palaeocene denudation	Oligo-Miocene denudation	base Upper Cretaceous
33/17-1	1.45	1.45	
33/21-1	1.35	1.35	
42/12-1	1.52	1.52	
42/16-1	1.80	1.80	
42/17-1	2.06	2.06	
42/21-1	1.71	1.71	
47/29-1	0.99	0.99	1.72
48/19-1	0.60	0.60	2.20
48/26-1	0.60	0.60	2.75
48/30-1	0.67	0.67	2.26
49/9-1	1.03	1.03	1.46
49/9-2	0.94	0.94	1.85
49/9-3	0.89	0.89	1.95
49/14-3	0.55	0.55	2.13
49/29-1	0.82	0.82	1.83
50/3-1	1.66	1.66	
50/3-2	0.99	0.99	1.35
50/6-1	0.96	0.96	1.47
50/7-1	0.95	0.95	1.44
50/12-1	0.86	0.86	1.99
50/12-2A	0.86	0.86	1.73
56/14-1	0.83	0.68	1.72
56/18-1	1.09	0.82	1.90
57/2-1	0.88	0.88	2.58
57/7-1	0.94	0.94	1.84
58/3-1	0.54	0.54	1.62
72/10-1A	1.14	0.75	1.57
73/01-1	0.87	0.50	1.44
73/02-1	0.81	0.60	1.32
73/04-1	0.78	0.71	1.37
73/05-1	1.14	0.54	1.80
73/06-1	0.85	0.64	1.25
73/07-1	1.22	0.72	1.83
73/08-1	1.12	0.78	1.66
73/12-1A	1.41	0.84	1.86
73/13-1	1.14	0.48	1.63
73/14-1	1.23	0.69	1.74
74/01-1A	1.16	0.83	1.57
83/24-1	0.84	0.66	1.27
85/28-1	0.85	0.51	1.45
86/17-1	1.07	0.84	1.49
86/18-1	0.95	0.68	1.58
87/12-1A	1.24	1.24	1.58
87/14-1	0.87	0.78	1.36
87/16-1	0.97	0.85	1.56
88/02-1	1.03	1.03	1.14
93/02-1	0.72	0.61	1.91
102/28-1	0.90	0.90	1.28
102/29-1	1.00	1.00	1.40
103/2-1B	0.65	0.65	
103/18-1	0.95	0.95	1.35
103/21-1	0.76	0.76	1.10
106/24-1	1.44	0.90	

Well Number	Exhumation at the time of denudation (km bsb)		Max. burial-depth (km bsb)
	Palaeocene denudation	Oligo-Miocene denudation	base Upper Cretaceous
106/24A-2B	1.54	0.89	
106/28-1	1.19	0.44	
107/16-1	1.44	1.44	
107/21-1	1.65	1.27	
Brezell-1	1.11	1.11	2.31
Garlizenn-1	0.87	0.61	1.56
Glazenn-1	0.74	0.38	
Krogen-1	0.74	0.37	2.09
Kulzenn-1	1.17	0.96	1.61
Lennket-1	0.88	0.88	2.39
Levneg-1	1.51	1.51	2.02
Lizenn-1	0.44	0.44	2.24
Penma-1	1.07	0.62	1.66
Rea Gwenn-1	1.03	0.59	1.72
Travank-1	1.09	1.09	1.52
Yar Vor-1	1.02	1.02	2.09

References

Asquith, G. & Gibson, C. 1982. *Basic Well Log Analysis for Geologists*. American Association of Petroleum Geologists, Tulsa, 216p.

Badley, M. E., Price, J. D., Rambeck Dahl, C. & Agdenstein, T. 1987. The structural evolution of the northern Viking Graben and its bearing upon extensional modes of basin formation. *Journal of the Geological Society, London*, **144**, 455-472.

Beaumont, C., Keen, C. E. & Boutilier, R. 1982. On the evolution of rifted continental margins: comparison of models and observations for the Nova Scotian margin. *Geophysical Journal of the Royal Astronomical Society*, **70**, 667-715.

Bois, C., Cazes, M., Gariel, O., Lefort, J. P., Le Gall, B., Pinet, B. & Sibuet, J. C. 1991. Main scientific contribution of the SWAT and WAM surveys to the geology of the Celtic Sea, the English Channel and the Atlantic Margin. *In*: Bois, C., Gariel, O. & Sibuet, J. C. (eds) *Étude de la croute terrestre par sismique profonde: Mer Celtique-Manche et ses Approches Occidentales*. Mémoires de la Société Géologique de France, **159** (1), 185-217.

Bond, G. C. & Kominz, M. A. 1984. Construction of tectonic subsidence curves for the early Palaeozoic miogeocline, southern Canadian Rocky Mountains: implications for subsidence mechanisms, age of breakup, and crustal thinning. *Geological Society of America Bulletin*, **95**, 155-173.

Bray, R. J., Green, P. F. & Duddy, I. R. 1992. Thermal history reconstruction using apatite fission track analysis and vitrinite reflectance: a case study from the UK East Midlands Shelf and Southern North Sea. *In*: Hardman R. F. P. (ed.) *Exploration Britain: Geological insights for the next decade*. Geological Society, London, Special Publication, **67**, 3-25.

Brigaud, F., Vassuer, G. & Caillet, G. 1992. Thermal state in the north Viking Graben (North Sea) determined from oil exploration well data. *Geophysics*, **57**, 69-88.

Brodie, J. & White, N. 1994. Sedimentary basin inversion caused by igneous underplating: Northwest European continental shelf. *Geology*, **22**, 147-150.

Brodie, J. & White, N. 1995. The link between sedimentary basin inversion and igneous underplating. *In*: Buchanan, J. G. & Buchanan, P. G. (eds) *Basin Inversion*. Geological Society, London, Special Publication, **88**, 21-38.

Brooks, M., Trayner, P. M. & Trimble, T. J. 1988. Mesozoic reactivation of Variscan thrusting in the Bristol Channel area, UK. *Journal of the Geological Society, London*, **145**, 439-444.

Brown, R. W. 1991. Backstacking apatite fission-track 'stratigraphy': a method for resolving the erosional and isostatic rebound components of tectonic uplift histories. *Geology*, **19**, 74-77.

Buchanan, J. G. & Buchanan, P. G. (eds) 1995. *Basin Inversion*. Geological Society, London, Special Publication, **88**, 596p.

Bulat, J. & Stoker, S. J. 1987. Uplift determination from interval velocity studies, UK southern North Sea. *In*: Brooks, J. & Glennie, K. (eds) *Petroleum Geology of North West Europe*. Graham & Trotman, London, 293-305.

Cameron, T. D. J., Crosby, A., Balson, P. S., Jeffery, D. H., Lott, G. K., Bulat, J. & Harrison, D. J. 1992. *United Kingdom offshore regional report: the geology of the southern North Sea*. HMSO for the British Geological Survey, London, 152p.

Chadwick, R. A., Kirby, G. A. & Baily, H. E. 1994. The post-Triassic structural evolution of north-west England and adjacent parts of the East Irish Sea. *Proceedings of the Yorkshire Geological Society*, **50**, 91-102.

Chapman, T. J. 1989. The Permian to Cretaceous structural evolution of the Western Approaches Basin (Melville sub-basin), UK. *In*: Cooper, M. A. & Williams, G. D. (eds) *Inversion Tectonics*. Geological Society, London, Special Publication, **44**, 177-200.

Cheadle, M. J., McGeary, S., Warner, M. R. & Matthews, D. H. 1987. Extensional structures on the western UK continental shelf: a review of evidence from deep seismic profiling. *In*: Coward, M. P., Dewey, J. F. & Hancock, P. L. (eds) *Continental Extensional Tectonics*. Geological Society, London, Special Publication, **28**, 445-465.

Chen, Y., Zentilli, M. A., Clark, A. H., Farrar, E., Grist, A. M. & Willis-Richards, J. 1996. Geochronological evidence for post-Variscan cooling and uplift of the Carnmenellis granite, SW England. *Journal of the Geological Society, London*, **153**, 191-195.

Cochran, J. R. 1983. Effects of finite rifting times on the development of sedimentary basins. *Earth and Planetary Science Letters*, **66**, 289-302.

Cooper, M. A. & Williams, G. D. (eds) 1989. *Inversion Tectonics*. Geological Society, London, Special Publication, **44**, 375p.

Cornford, C. 1986. The Bristol Channel Graben: organic geochemical limits on subsidence and speculation on the origin of inversion. *Proceedings of the Ussher Society*, **6**, 360-367.

Coward, M. P. 1990. The Precambrian, Caledonian, and Variscan framework to NW Europe. *In*: Hardman, R. F. P. & Brooks, J. (eds) *Tectonic events responsible for Britain's oil and gas reserves*. Geological Society, London, Special Publication, **55**, 1-34.

Croker, P. F. & Shannon, P. M. (eds) 1995. *The Petroleum Geology of Ireland's Offshore Basins*. Geological Society, London, Special Publication, **93**, 498p.

Dewey, J. F. 1982. Plate tectonics and the evolution of the British Isles. *Journal of the Geological Society, London*, **139**, 371-412.

Dobson, M. R. & Whittington, R. J. 1987. The geology of Cardigan Bay. *Proceedings of the Geologists' Association*, **98**, 331-353.

Draper, N. R. & Smith, H. 1981. *Applied regression analysis*, 2nd edition. John Wiley & Sons, Toronto, 709p.

Dyment, J. 1991. Subsidence analysis and deep seismic data: geodynamic implications on the formation and evolution of the Celtic Sea basins. *In*: Bois, C., Gariel, O. & Sibuet, J. C. (eds) *Étude de la croute terrestre par sismique profonde: Mer Celtique-Manche et ses Approches Occidentales*. Mémoires de la Société Géologique de France, **159** (1), 67-81.

Emerson, D. W. 1990. Notes on mass properties of rocks- density, porosity, permeability. *Exploration Geophysics*, **21**, 209-216.

England, P. & Molnar, P. 1990. Surface uplift, uplift of rocks, and exhumation of rocks. *Geology*, **18**, 1173-1177.

Evans, C. D. R. 1990. *United Kingdom offshore regional report: The geology of the western English Channel and its western approaches.* British Geological Survey, London, HMSO for the British Geological Survey, 107p.

Garfunkel, Z. 1988. Relation between continental

rifting and uplifting: evidence from the Suez rift and northern Red Sea. *Tectonophysics*, **150**, 33-49.

Giltner, J. P. 1987. Application of extensional models to the Northern Viking Graben. *Norsk Geologisk Tidsskrift*, **67**, 339-352.

Green, P. F. 1989. Thermal and tectonic history of the East Midlands shelf (onshore UK) and surrounding regions assessed by apatite fission track analysis. *Journal of the Geological Society, London*, **146**, 755-773.

Green, P. F., Duddy, I. R., Bray, R. J. & Lewis, C. L. E. 1993. Elevated palaeotemperatures prior to Early Tertiary cooling throughout the UK region: implications for hydrocarbon generation. *In*: Parker, J. R. (ed.) *Petroleum Geology of Northwest Europe: Proceedings of the 4th Conference*. Geological Society, London, 1067-1074.

Green, P. F., Duddy, I. R. & Bray, R. J. 1995. Further discussion on Mesozoic cover over northern England: interpretation of apatite fission track data. *Journal of the Geological Society, London*, **152**, 416.

Hansen, S. 1996. A compaction trend for Cretaceous and Tertiary shales on the Norwegian Shelf based on sonic transit times. *Petroleum Geoscience*, **2**, 159-166.

Haq, B. U., Hardenbol, J. & Vail, P. R. 1988. Mesozoic and Cenozoic chronostratigraphy and cycles of sea-level change. *In*: Wilgus, C. K., Hastings, B. S., Ross, C. A., Posamentier, H. W., Van Wagoner, J. & Kendall, C. G. St. C. (eds)*Sea Level Changes: an integrated approach*. Society of Economic Palaeontologists and Mineralogists, Special Publication, **42**, 71-109.

Harland, W. B., Armstrong, R. L., Cox, A. V., Craig, L. E., Smith, A. G. & Smith, D. G. 1989. *A Geologic Time Scale 1989*. Cambridge University Press, Cambridge, 263p.

Harvey, M. J., Stewart, S. A., Wilkinson, J. J., Ruffell, A. H. & Shail, R. K. 1994. Tectonic evolution of the Plymouth Bay Basin. *Proceedings of the Ussher Society*, **8**, 271-278.

Hauser, F., O'Reilly, B. M., Jacob, A. W. B., Shannon, P. M., Makris, J. & Vogt, U. 1995. The crustal structure of the Rockall Trough: differential stretching without underplating. *Journal of Geophysical Research*, **B100**, 4097-4116.

Hayward, A. B. & Graham, R. H. 1989. Some geometrical characteristics of inversion. *In*: Cooper, M. A. & Williams, G. D. (eds) *Inversion Tectonics*. Geological Society, London, Special Publication, **44**, 17-39.

Hegarty, K. A., Weissel, J. K. & Mutter, J. C. 1988. Subsidence history of Australia's southern margin: constraints on basin models. *American Association of Petroleum Geologists Bulletin*, **72**, 615-633.

Hellinger, S. J. & Sclater, J. G. 1983. Some comments on two-layer extensional models for the evolution of sedimentary basins. *Journal of Geophysical Research*, **B88**, 8251-8269.

Hellinger, S. J., Sclater, J. G. & Giltner, J. P. 1989. Mid-Jurassic through mid-Cretaceous extension in the Central Graben of the North Sea, Part 1. Estimates from subsidence. *Basin Research*, **1**, 191-200.

Hemingway, J. E. & Riddler, G. P. 1982. Basin inversion in North Yorkshire. *Transactions of the Institute of Mining and Metallurgy*, Section B **91**, B175-186.

Hillis, R. R. 1988. The geology and tectonic evolution of the Western Approaches Trough. Unpublished PhD thesis, University of Edinburgh.

Hillis, R. R. 1991. Chalk porosity and Tertiary

uplift, Western Approaches Trough, SW UK and NW French continental shelves. *Journal of the Geological Society, London,* **148**, 669-679.

Hillis, R. R. 1992*a*. A two-layer lithospheric compressional model for the Tertiary uplift of the southern United Kingdom. *Geophysical Research Letters*, **19**, 573-576.

Hillis, R. R. 1992*b*. Evidence for Pliocene erosion at Ashmore Reef (Timor Sea) from the sonic velocities of Neogene limestone formations. *Exploration Geophysics*, **23**, 489-495.

Hillis, R. R. 1993. Tertiary erosion magnitudes in the East Midlands Shelf, onshore UK. *Journal of the Geological Society, London*, **150**, 1047-1050.

Hillis, R. R. 1994. Discussion on the amount of Tertiary erosion in the UK estimated using sonic velocity analysis (reply). *Journal of the Geological Society, London*, **151**, 1041-1044.

Hillis, R. R. 1995*a*. Regional Tertiary exhumation in and around the United Kingdom. *In*: Buchanan, J. G. & Buchanan, P. G. (eds) *Basin Inversion.* Geological Society, London, Special Publication, **88**, 167-190.

Hillis, R. R. 1995*b*. Quantification of Tertiary exhumation in the United Kingdom Southern North Sea using sonic velocity data. *American Association of Petroleum Geologists Bulletin,* **79**, 130-152.

Hillis, R. R. & Chapman, T. J. 1992. Variscan structure and its influence on post-Carboniferous basin development, Western Approaches Basin, SW UK Continental Shelf. *Journal of the Geological Society, London*, **149**, 413-417.

Hillis, R. R., Thomson, K. & Underhill, J. R. 1994. Quantification of Tertiary erosion in the Inner Moray Firth using sonic velocity data from the Chalk and Kimmeridge Clay. *Marine and Petroleum Geology,* **11**, 283-293.

Holliday, D. W. 1993. Mesozoic cover over northern England: interpretation of apatite fission track data. *Journal of the Geological Society, London*, **150**, 657-660.

Holliday, D. W. 1994. Discussion on Mesozoic cover over northern England: interpretation of apatite fission track data (reply). *Journal of the Geological Society, London*, **151**, 735-736.

Howell, T. J. & Griffiths, P. 1995. A study of the hydrocarbon distribution and Lower Cretaceous Greensand prospectivity in Blocks 48/15, 48/17, 48/18 and 48/19, North Celtic Sea Basin. *In*: Croker, P. F. & Shannon, P. M. (eds) *The Petroleum Geology of Ireland's Offshore Basins.* Geological Society, London, Special Publication, **93**, 261-275.

Issler, D. R. 1992. A new approach to shale compaction and stratigraphic restoration, Beaufort-Mackenzie Basin and Mackenzie Corridor, Northern Canada. *American Association of Petroleum Geologists Bulletin*, **76**, 1170-1189.

Jankowsky, W. 1962. Diagenesis and oil accumulation as aids in the analysis of the structural history of the north-western German Basin. *Zeitschrift der Deutscher Geologischer Gesellschaft*, **114**, 452-460.

Japsen, P. 1993. Influence of lithology and Neogene uplift on seismic velocities in Denmark: implications for depth conversion of maps. *American Association of Petroleum Geologists Bulletin,* **77**, 194-211.

Jarvis, G. T. & McKenzie, D. P. 1980. Sedimentary basin formation with finite extension rates. *Earth and Planetary Science Letters*, **48**, 42-52.

Karner, G. D., Lake, S. D. & Dewey, J. F. 1987. The thermal and mechanical development of the Wessex Basin, southern England. *In*: Coward,

M. P., Dewey, J. F. & Hancock, P. L. (eds) *Continental Extensional Tectonics*. Geological Society, London, Special Publication, **28**, 517-536.

Keeley, M. L., Lewis, C. L. E., Sevastopulo, G. D., Clayton, G. & Blackmore, R. 1993. Apatite fission track data from southeast Ireland: implications for post-Variscan burial-history. *Geological Magazine*, **130**, 171-176.

Keen, C. E. & Dehler, S. A. 1993. Stretching and subsidence: rifting of conjugate margins in the North Atlantic region. *Tectonics*, **12**, 1209-1229.

Keen, C. E., Boutilier, R., De Voogd, B., Mudford, B. & Enachescu, M. E. 1987. Crustal geometry and extensional models for the Grand Banks, eastern Canada: constraints from deep seismic data. *In*: Beaumont, C. & Tankard, A. J. (eds) *Sedimentary Basins and Basin-forming Mechanisms*. Canadian Society of Petroleum Geologists Memoir, **12**, 101-115.

Kendall, C. G. St. C. & Lerche, I. 1988. The rise and fall of eustacy. *In*: Wilgus, C. K., Hastings, B. S., Ross, C. A., Posamentier, H. W., Van Wagoner, J. & Kendall, C. G. St. C. (eds)*Sea Level Changes: an integrated approach*. Society of Economic Palaeontologists and Mineralogists, Special Publication, **42**, 3-17.

Kent, P. E. 1980. Subsidence and uplift in East Yorkshire and Lincolnshire: a double inversion. *Proceedings of the Yorkshire Geological Society*, **42**, 505-524.

Kusznir, N. J. & Egan, S. S. 1989. Simple-shear and pure-shear models of extensional sedimentary basin formation: application to the Jeanne d'Arc Basin, Grand Banks of Newfoundland. *In*: Tankard, A. J. & Balkwill, H. R. (eds) *Extensional Tectonics and Stratigraphy of the North Atlantic Margins*. American Association of Petroleum Geologists Memoir, **46**, 305-322.

Kusznir, N. J., Karner, G. D. & Egan, S. 1987. Geometric thermal and isostatic consequences of detachments in continental lithosphere extension and basin formation. *In*: Beaumont, C. & Tankard, A. J. (eds) *Sedimentary Basins and Basin-forming Mechanisms*. Canadian Society of Petroleum Geologists Memoir, **12**, 185-203.

Kusznir, N. J., Marsden, G. & Egan, S. S. 1991. A flexural-cantilever simple-shear/pure-shear model of continental lithosphere extension: applications to the Jeanne d'Arc Basin, Grand Banks and Viking Graben, North Sea. *In*: Roberts, A. M., Yielding, G. & Freeman, B. (eds) *The Geometry of Normal Faults*. Geological Society, London, Special Publication, **56**, 41-60.

Kusznir, N. J., Roberts, A. M. & Morley, C. K. 1995. Forward and reverse modelling of rift basin formation. *In*: Lambiase, J. J. (ed.) *Hydrocarbon Habitat in Rift Basins*. Geological Society, London, Special Publication, **80**, 33-56.

Lake, S. D. & Karner, G. D. 1987. The structure and evolution of the Wessex Basin, southern England: an example of inversion tectonics. *In*: Ziegler, P. A. (ed.) Compressional Intra-Plate Deformations in the Alpine Foreland. *Tectonophysics*, **137**, 347-378.

Lang, W. H. 1978. The determination of prior depth of burial (uplift and erosion) using interval transit time. *Society of Professional Well Log Analysts Nineteenth Annual Logging Symposium*, June 13-16, 1978, Paper B.

Le Pichon, X. & Sibuet, J-C. 1981. Passive margins; a model of formation. *Journal of Geophysical Research*, **86**, 3708-3720.

Lewis, C. L. E., Green, P. F., Carter, A. & Hurford, A. J. 1992. Elevated K/T palaeotemperatures throughout Northwest England: three kilometres of Tertiary erosion? *Earth and Planetary Science Letters*, **112**, 131-145.

Lippard, S. & Liu, G. 1992. Tectonic modelling of the northern North Sea using program RIFT. *In*: Larsen, R. M., Brekke, H., Larsen, B. T. & Talleraas, E. (eds) *Structural and Tectonic Modelling and its Application to Petroleum Geology*. Elsevier, Amsterdam, Norwegian Petroleum Society Special Publication, **1**, 43-54.

Liu, G. & Roaldset, R. 1994. A new decompaction model and its application to the northern North Sea. *First Break*, **12**, 81-89.

McCulloch, A. A. 1994. Discussion on Mesozoic cover over northern England: interpretation of apatite fission track data. *Journal of the Geological Society, London*, **151**, 735-736.

McKenzie, D. 1978. Some remarks on the development of sedimentary basins. *Earth and Planetary Science Letters*, **40**, 25-32.

Maddox, S. J., Blow, R. & Hardman, M. 1995. Hydrocarbon prospectivity of the Central Irish Sea Basin with reference to Block 42/12, offshore Ireland. *In*: Croker, P. F. & Shannon, P. M. (eds) *The Petroleum Geology of Ireland's Offshore Basins*. Geological Society, London, Special Publication, **93**, 59-77.

Magara, K. 1976. Thickness of removed sedimentary rock, paleopore pressure, and paleotemperature, southwestern part of Western Canada Basin. *American Association of Petroleum Geologists Bulletin*, **60**, 554-565.

Marie, J. P. P. 1975. Rotliegendes stratigraphy and diagenesis. *In*: Woodland, A. W. (ed.) *Petroleum and the Continental Shelf of North-west Europe, Volume 1, Geology*. Applied Science Publishers, London, 205-211.

Masson, D. G. & Parson, L. M. 1983. Eocene deformation on the continental margin SW of the British Isles. *Journal of the Geological Society, London*, **140**, 913-920.

Merkel, R. H. 1981. *Well Log Formation Evaluation*. American Association of Petroleum Geologists Course Note Series, **14**.

Murdoch, L. M., Musgrove, F. W. & Perry, J. S. 1995. Tertiary uplift and inversion history in the North Celtic Sea Basin and its influence on source rock maturity. *In*: Croker, P. F. & Shannon, P. M. (eds) *The Petroleum Geology of Ireland's Offshore Basins*. Geological Society, London, Special Publication, **93**, 297-319.

Murphy, N. J., Sauer, M. J. & Armstrong, J. P. 1995. Toarcian source rock potential in the North Celtic Sea Basin, offshore Ireland. *In*: Croker, P. F. & Shannon, P. M. (eds) *The Petroleum Geology of Ireland's Offshore Basins*. Geological Society, London, Special Publication, **93**, 193-207.

Musgrove, F. W., Murdoch, L. M. & Lenehan, T. 1995. The Variscan fold-thrust belt of southeast Ireland and its control on early Mesozoic extension and deposition: a method to predict the Sherwood Sandstone. *In*: Croker, P. F. & Shannon, P. M. (eds) *The Petroleum Geology of Ireland's Offshore Basins*. Geological Society, London, Special Publication, **93**, 81-100.

Naylor, D., Haughey, N., Clayton, G. & Graham, J. R. 1993. The Kish Bank Basin, offshore Ireland. *In*: Parker, J. R. (ed.) *Petroleum Geology of Northwest Europe: Proceedings of the 4th Conference*. Geological Society, London, 845-855.

Odling, N. E. 1992. RIFT, a model of sedimentary basin evolution by finite rate, non-uniform, pure shear extension of the lithosphere. *In*: Larsen, R. M., Brekke, H., Larsen, B. T. & Talleraas, E. (eds) *Structural and Tectonic Modelling and its Application to Petroleum Geology*. Elsevier, Amsterdam, Norwegian Petroleum Society Special Publication, **1**, 457-467.

O'Reilly, B. M., Shannon, P. M. & Vogt, U. 1991. Seismic studies in the North Celtic Sea Basin: implications for basin development. *Journal of the Geological Society, London*, **148**, 191-195.

Petrie, S. H., Brown, J. R., Granger, P. J. & Lovell, J. P. B. 1989. Mesozoic history of the Celtic Sea basins. *In*: Tankard, A. J. & Balkwill, H. R. (eds) *Extensional Tectonics and Stratigraphy of the North Atlantic Margins*. American Association of Petroleum Geologists Memoir, **46**, 433-444.

Raiga-Clemenceau, J., Martin, J. P. & Nicoletis, S. 1988. The concept of acoustic formation factor for more accurate porosity determination from sonic transit time data. *The Log Analyst*, January-February, 54-59.

Rawson, P. F. & Wright, J. K. 1992. *The Yorkshire Coast*. Geologists Association Guide, **34**, 117p.

Raymer, L. L., Hunt, E. R. & Gardner, J. S. 1980. An improved sonic transit time-to-porosity transform. *Society of Professional Well Log Analysts Twenty-First Annual Logging Symposium*, July 8-11, 1980, Paper P.

Roberts, A. M., Yielding, G., Kusznir, N. J., Walker, I. M. & Dorn-Lopez, D. 1995. Quantitative analysis of Triassic extension in the northern Viking Graben. *Journal of the Geological Society, London*, **152**, 15-26.

Roberts, D. G. 1989. Basin inversion in and around the British Isles. *In*: Cooper, M. A. & Williams, G. D. (eds) *Inversion Tectonics*. Geological Society, London, Special Publication, **44**, 131-150.

Robinson, K. W., Shannon, P. M. & Young, D. G. 1981. The Fastnet Basin: an integrated analysis. *In*: Illing, L. V. & Hobson, G. D. (eds) *Petroleum Geology of the Continental Shelf of North-West Europe*. Heyden, London, 444-454.

Rollin, K. E. 1995. A simple heat-flow quality function and appraisal of heat-flow measurements and heat-flow estimates from the UK Geothermal Catalogue. *Tectonophysics*, **244**, 185-196.

Royden, L. & Keen, C. E. 1980. Rifting processes and thermal evolution of the continental margin of eastern Canada determined from subsidence curves. *Earth and Planetary Science Letters*, **51**, 343-361.

Schlumberger, 1974. *Well Evaluation Conference North Sea*. Services Techniques Schlumberger, France.

Schlumberger, 1987. *Log Interpretation Principles/Applications*. Schlumberger Educational Services, Houston, Texas.

Schlumberger, 1989. *Log Interpretation Charts*. Schlumberger Educational Services, Houston, Texas.

Schneider, F., Bouteca, M. & Vasseur, G. 1994. Validity of the porosity/effective-stress concept in sedimentary basin modelling. *First Break*, **12**, 321-326.

Scholle, P. A. 1977. Chalk diagenesis and its relation to petroleum exploration: oil from chalks, a modern miracle? *American Association of Petroleum Geologists Bulletin*, **61**, 982-1009.

Sclater, J. G. & Christie, P. A. F. 1980. Continental stretching: An explanation of the post-mid-Cretaceous subsidence of the Central North Sea Basin. *Journal of Geophysical Research*, **B85**, 3711-3739.

Sclater, J. G., Royden, L., Horvath, F., Burchfiel, B. C., Semken, S. & Stegena, L. 1980. The formation of the intra-Carpathian basins as determined from subsidence data. *Earth and Planetary Science Letters*, **51**, 139-162.

Scotchman, I. C. 1994. Maturity and burial history of the Kimmeridge Clay Formation, onshore UK: a biomarker study. *First Break*, **12**, 193-202.

Selley, R. C. 1988. *Applied Sedimentology*. Academic Press, London, 446p.

Shannon, P. M. 1995. Permo-Triassic development of the Celtic Sea region, offshore Ireland. *In*: Boldy, S. A. R. (ed.) *Permian and Triassic Rifting in Northwest Europe*. Geological Society, London, Special Publication, **91**, 215-237.

Sibuet, J-C., Dyment, J., Bois, C., Pinet, B. & Ondreas, H. 1990. Crustal structure of the Celtic Sea and Western Approaches from gravity data and deep seismic profiles: constraints on the formation of continental basins. *Journal of Geophysical Research*, **B95**, 10999-11020.

Simpson, I. R., Gravestock, M., Ham, D., Leach, H. & Thompson, S. D. 1989. Notes and cross-sections illustrating inversion tectonics in the Wessex Basin. *In*: Cooper, M. A. & Williams, G. D. (eds) *Inversion Tectonics*. Geological Society, London, Special Publication, **44**, 123-129.

Skagen, J. I. 1992. Methodology applied to uplift and erosion. *Norsk Geologisk Tidsskrift*, **72**, 307-311.

Sleep, N. H. 1971. Thermal effects of the formation of Atlantic continental margins by continental break-up. *Geophysical Journal of the Royal Astronomical Society*, **24**, 325-350.

Smith, K., Gatliff, R. W. & Smith, N. J. P. 1994. Discussion on the amount of Tertiary erosion in the UK estimated using sonic velocity analysis. *Journal of the Geological Society, London*, **151**, 1041-1044.

Steckler, M. S. & Watts, A. B. 1978. Subsidence of the Atlantic-type continental margin off New York. *Earth and Planetary Science Letters*, **41**, 1-13.

Stewart, S. A. & Bailey, H. W. 1996. The Flamborough Tertiary outlier, UK southern North Sea. *Journal of the Geological Society, London*, **153**, 163-173.

Tappin, D. R., Chadwick, R. A., Jackson, A. A., Wingfield, R. T. R. & Smith, N. J. P. 1994. *United Kingdom offshore regional report: The geology of Cardigan Bay and the Bristol Channel*. British Geological Survey, London, HMSO for the British Geological Survey, 107p.

Tucker, R. M. & Arter, G. 1987. The tectonic evolution of the North Celtic Sea and Cardigan Bay basins with special reference to basin inversion. *In*: Ziegler, P. A. (ed.) Compressional Intra-Plate Deformations in the Alpine Foreland. *Tectonophysics*, **137**, 291-307.

Vail, P. R., Mitchum, R. M., Todd, R. G., Widmier, J. M., Thompson, S., III, Sangree, J. B., Bubb, J. N. & Hatlelid, W. G. 1977. Seismic stratigraphy and global changes in sea level. *In*: Payton, C. E. (ed.) *Seismic Stratigraphy - Applications to Hydrocarbon Exploration*. American Association of Petroleum Geologists Memoir, **26**, 49-212.

Van Hoorn, B. 1987. The South Celtic Sea/Bristol Channel Basin: origin, deformation and inversion history. *In*: Ziegler, P. A. (ed.) Compressional Intra-Plate Deformations in the Alpine Foreland. *Tectonophysics*, **137**, 309-334.

Watts, A. B., Karner, G. D. & Steckler, M. S. 1982. Lithospheric flexure and the evolution of sedimentary basins. *Philosophical Transactions of the Royal Society of London*, **A305**, 249-281.

Wells, P. E. 1990. Porosities and seismic velocities of mudstones from Wairarapa and oil wells of North Island, New Zealand, and their use in determining burial history. *New Zealand Journal of Geology and Geophysics*, **33**, 29-39.

Wernicke, B. 1985. Uniform-sense normal simple shear of the continental lithosphere. *Canadian Journal of Earth Science*, **22**, 108-125.

White, N. 1990. Does the uniform stretching model work in the North Sea? *In*: Blundell, D. J. & Gibbs, A. D. (eds) *Tectonic Evolution of the North Sea Rifts*. Oxford Science Publications,

Oxford, 217-239.

White, N. & Latin, D. 1993. Subsidence analyses from the North Sea 'triple-junction'. *Journal of the Geological Society, London*, **150**, 473-488.

White, N. & McKenzie, D. 1988. Formation of the "steer's head" geometry of sedimentary basins by differential stretching of the crust and mantle. *Geology*, **16**, 250-253.

White, R. & McKenzie, D. 1989. Magmatism at rift zones: the generation of volcanic continental margins and flood basalts. *Journal of Geophysical Research*, **B94**, 7685-7729.

Whittaker, A., Holliday, D. W. & Penn, I. E. 1985. *Geophysical logs in British Stratigraphy*. Geological Society, London, Special Report, **18**, 74p.

Williams, G. D., Powell, C. M. & Cooper, M. A. 1989. Geometry and kinematics of inversion tectonics. *In*: Cooper, M. A. & Williams, G. D. (eds) *Inversion Tectonics*. Geological Society, London, Special Publication, **44**, 3-15.

Wood, R. J. 1981. The subsidence history of Conoco well 15/30-1, central North Sea. *Earth and Planetary Science Letters*, **54**, 306-312.

Wyllie, M. R. J., Gregory, A. R. & Gardner, L. W. 1956. Theory of propagation of elastic waves in a fluid saturated porous solid. *Journal of the Acoustical Society of America*, **28**, 168-191.

Ziegler, P. A. (ed.) 1987*a*. Compressional Intra-Plate Deformations in the Alpine Foreland. *Tectonophysics*, **137**.

Ziegler, P. A. 1987*b*. Celtic Sea - Western Approaches area: an overview. *In*: Ziegler, P. A. (ed.) Compressional Intra-Plate Deformations in the Alpine Foreland. *Tectonophysics*, **137**, 309-334.

Ziegler, P. A. 1990. *Geological Atlas of Western and Central Europe*. Netherlands, Shell Internationale Petroleum Maatschappij B.V., 233p.

Menpes, R.J., and Hillis, R.R., (1996) Determining apparent exhumation from chalk outcrop samples, Cleveland Basin/East Midlands Shelf.
Geological Magazine, v. 133 (6), pp. 751-762.

Menpes, R.J., and Hillis, R.R., (1995) Quantification of tertiary exhumation from sonic velocity data, Celtic Sea/South-Western approaches.
Geological Society Special Publications, v. 88, pp. 191-207.

Menpes, R.J., and Hillis, R.R., (1995) Quantification of tertiary exhumation from sonic velocity data, Celtic Sea/Southwestern approaches.
Geological Society Special Publications, v. 93, pp. 321-322..